CHARACTERISATION OF Mg, Sr, and Zn CONTAINING FLUORO-ALUMINOSILICATE GLASSES AND THEIR GLASS POLYALKENOATE CEMENTS

Hiroko Kusumoto

A thesis submitted in partial fulfilment of the requirements for the degree of

Doctor of Philosophy

And the Diploma of Imperial College London

Supervised by Professor Robert G. Hill and Dr. Rob V. Law

Department of Materials
Imperial College London
London SW7 2AZ
United Kingdom

December 2009

Abstract

The glass polyalkenoate cements (GPCs) are formed by the acid-base reaction between fluoro-aluminosilicate glasses and polycarboxylic acid in the presence of water. Three series of glasses were produced by modifiying glass LG26 [32.1SiO_2. 21.4Al_2O_3. 10.7P_2O_5. 21.4CaO. 14.3CaF_2] (mole %). In the first series, calcium was substituted by magnesium, and in the second series, calcium in the first series was substituted by strontium. The last series were zinc substitution for calcium in LG26. These glasses were characterised by X-ray diffraction (XRD), magic angle spinning nuclear magnetic resonance (MAS-NMR) spectroscopy and differential scanning calorimetry (DSC). The gradual substitution of calcium by magnesium resulted in the formation of F-Mg(n) species and a disappearance of Al-F species on the ^{19}F MAS-NMR. The ^{31}P and ^{27}Al MAS-NMR showed that all glasses contained Q^1 pyrophosphate Al-O-PO_3^{3-} species. In addition, the fully magnesium substituted glass showed the possible formation of magnesium pyrophosphate, $Mg_2P_2O_7$. The fully zinc substituted glass, however, showed only Al-O-PO_3^{3-} species charge balanced by Zn^{2+}. An increase in Al(V) species was observed on the ^{27}Al MAS-NMR with the fully magnesium and zinc substituted glasses. The presence of magnesium also increased the number of bridging oxygen on SiO_4 tetrahedra, but the presence of zinc affected the Q structure of the aluminosilicate network less. GPCs with these glasses were formed with poly (acrylic acid) (PAA) and L-(+)-tartaric acid. The setting reaction of selected cements was studied by ^{19}F, ^{31}P and ^{27}Al MAS-NMR spectroscopy. F-Ca(n) species were clearly shown to be consumed for cement formulation, and F-Mg(n) species were still present in the ^{19}F MAS-NMR spectra of the magnesium containing cements. The Al-O-PO_3^{3-} species were present in the cement. The conversion to Al(VI) from Al(IV) and Al(V) was observed by deconvoluting the ^{27}Al MAS-NMR spectra. The experimental ratio of Al(VI):Al(IV)+Al(V) was higher than the theoretical ratio which may have resulted from the possibility of L-(+)-tartaric acid being involved in the Al conversion during the setting reaction. The working and setting times increased with magnesium substitution, but did not change with zinc substitution for calcium. The compressive strengths decreased with magnesium substitution, possibly resulting from the preferential crosslinking between Mg^{2+} and COO^-. The highest release of fluoride was observed from the fully magnesium substituted cements.

Another series of glasses [34.0SiO_2. 22.6Al_2O_3. 5.7P_2O_5. (22.6-x)SrO. xZnO. 15.1SrF_2] (mole %) was produced for formulating GPCs with poly (γ-glutamic acid), PgGA. All the glasses have Al-O-PO_3^{3-} species with no change in the phosphorus environment with zinc substitution for strontium. Al(IV) was found to be the major aluminium species with a small presence of Al(V) and Al(VI). The Q structures of all the glasses were found to be a mixture of Q^4(4Al) and Q^3(3Al). Similarly, DSC showed a negligible change with zinc substitution for strontium. For cement formulations with PgGA, a co-polymer of PAA and poly (but-3-ene 1,2,4-tricarboxylic acid) was used due to the lower reactivity of PgGA than PAA, and cements with different proportions of PgGA and the co-polymer were formed. The working and setting times increased with PgGA content and zinc substitution. On the contrary, the compressive strengths decreased with PgGA content. The highest zinc containing cements in the series showed the highest compressive strength. A long-term fluoride release measurement showed the highest release from the highest PgGA containing cements, possibly resulting from the cements being less crosslinked. There was a slight increase in the adhesion to dentine.

Declaration

This research was carried out at Imperial College London between October 2006 and September 2009. This is my own work and has not been previously submitted to any university for any award.

Hiroko Kusumoto

December 2009

Acknowledgement

Last three years have been challenging, and it would not have been possible to complete the research without the help from so many people.

Firstly, I would like to express my great gratitude to Professor Robert G. Hill and Dr. Rob V. Law for helpful guidance and advice for the research. Also, this study would not have been possible without the contribution from the Department of Technology and Industry, UK, as well as Dr. Barry Woodfine, Dr. Iza Radecka, and Dr. Gopal Kedia who were also involved in this project.

I also would like to thank all members of Robert's group, especially Dr. Natalia Karpukhina for her technical assistance in MAS-NMR spectroscopy and the valuable discussion on the analysis of the spectra, and Dr. Delia Brauer for her support in the research. Also, I would like to thank Dr. Eileen Gentleman for performing biocompatibility tests on the cements.

Finally, special thanks go to my family in Japan and UK for all their support.

Table of Contents

Abstract……ii

Declaration……...iii

Acknowledgement……...…iv

List of Figures……...x

List of Tables……xvii

List of Equations……..….xix

List of Abbreviations……xx

1. Introduction……....1

1.1. Significance of the Study…… 3

1.2. Objectives of the Study…….. 6

2. Literature Review…… 7

2.1. Structure of Glass…….. 7

2.1.1. Goldschmidt's Rule …… 7

2.1.2. Zachariasen's Rule ……... 7

2.1.3. Loewenstein's Rule …….. 9

2.2. Kinetics of Glass Formation…….. 9

2.2.1. Nucleation ……9

2.2.2. Crystal Growth ……10

2.2.3. General Kinetic Conditions for Glass Formation ……10

2.3. General Principles of MAS-NMR Spectroscopy……..……11

2.3.1. Glass Characterisation by MAS-NMR Spectroscopy …….. 13

A. ^{19}F MAS-NMR Spectroscopy …….. 14

B. ^{31}P MAS-NMR Spectroscopy …….. 14

C. ^{27}Al MAS-NMR Spectroscopy …… 14

D. ^{29}Si MAS-NMR Spectroscopy …… 15

2.4. Glass Polyalkenoate (Ionomer) Cements…… 15

2.4.1. Setting Reaction of GPCs …… 15

2.4.2. Factors Affecting the Mechanical Properties of GPCs ……17

A. Glass Compositions 17
B. Glass Volume, Concentration and Molecular Weight of PAA 18
C. Aging Time 19
2.5. Poly (γ-glutamic acid) 20
2.5.1. Stereochemistry of PgGA 21

3. Experimental Design and Rationale 22
3.1. Glass Design 22
3.1.1. Fluoro-Aluminosilicate Glasses for PAA Cements 23
A. Ca-Mg Series:
[$4.5SiO_2$. $3.0Al_2O_3$. $1.5\ P_2O_5$. $(3.0\text{-}x)CaO$. $xMgO$. $(2.0\text{-}y)CaF_2$. $yMgF_2$] .. 23
B. Sr-Mg Series:
[$4.5SiO_2$. $3.0Al_2O_3$. $1.5\ P_2O_5$. $(3.0\text{-}x)SrO$. $xMgO$. $(2.0\text{-}y)SrF_2$. $yMgF_2$] ... 24
C. Ca-Zn Series:
[$4.5SiO_2$. $3.0Al_2O_3$. $1.5\ P_2O_5$. $(3.0\text{-}x)CaO$. $xZnO$. $(2.0\text{-}y)CaF_2$. $yZnF_2$] ... 25
D. Fluoro-Aluminosilicate Glasses from Schott AG (Germany) 25
3.1.2. Fluoro-Aluminosilicate Glass for PgGA Cements 26
3.2. Cement Design 27
3.2.1. GPCs with PAA 27
3.2.2. GPCs with PgGA 29

4. Materials and Methods 32
4.1. Materials 32
4.2. Methods 32
4.2.1. Glass Synthesis 32
4.2.2. Glass Characterisation 33
A. X-ray Powder Diffraction 33
B. MAS-NMR Spectroscopy 33
C. Differential Scanning Calorimetry 33
4.2.3. Synthesis of GPCs 34
4.2.4. Characterisation of GPCs 34
A. Aging Study 34
B. Working and Setting Time 35

C. Radiopacity …….. 36
D. Compressive Strength …….. 36
E. Fluoride Release ……... 37
F. Adhesion (PgGA cements only) …….. 37

5. Results and Discussion …….. 39

Part I. Characterisation of Mg, Sr, and Zn containing Fluoro-Aluminosilicate Glasses ……. 39

5.1. XRD Analysis …….. 39

5.1.1. Ca-Mg Series

[4.5SiO_2. 3.0Al_2O_3. 1.5P_2O_5. (3.0-x)CaO. xMgO. (2.0-y)CaF_2. yMgF_2] ... 39

5.1.2. Sr-Mg Series

[4.5SiO_2. 3.0Al_2O_3. 1.5P_2O_5. (3.0-x)SrO. xMgO. (2.0-y)SrF_2. yMgF_2] … 41

5.1.3. Ca-Zn Series

[4.5SiO_2. 3.0Al_2O_3. 1.5P_2O_5. (3.0-x)CaO. xZnO. (2.0-y)CaF_2. yZnF_2] … 42

5.2. ^{19}F MAS-NMR Spectroscopy …… 43

5.2.1. Ca-Mg Series

[4.5SiO_2. 3.0Al_2O_3. 1.5P_2O_5. (3.0-x)CaO. xMgO. (2.0-y)CaF_2. yMgF_2] ... 43

5.2.2. Sr-Mg Series

[4.5SiO_2. 3.0Al_2O_3. 1.5P_2O_5. (3.0-x)SrO. xMgO. (2.0-y)SrF_2. yMgF_2] … 46

5.2.3. Ca-Zn Series

[4.5SiO_2. 3.0Al_2O_3. 1.5P_2O_5. (3.0-x)CaO. xZnO. (2.0-y)CaF_2. yZnF_2] … 49

5.3. ^{31}P MAS-NMR Spectroscopy …… 52

5.3.1. Ca-Mg Series

[4.5SiO_2. 3.0Al_2O_3. 1.5P_2O_5. (3.0-x)CaO. xMgO. (2.0-y)CaF_2. yMgF_2] .. 52

5.3.2. Sr-Mg Series

[4.5SiO_2. 3.0Al_2O_3. 1.5P_2O_5. (3.0-x)SrO. xMgO. (2.0-y)SrF_2. yMgF_2] … 57

5.3.3. Ca-Zn Series

[4.5SiO_2. 3.0Al_2O_3. 1.5P_2O_5. (3.0-x)CaO. xZnO. (2.0-y)CaF_2. yZnF_2] … 59

5.4. ^{27}Al MAS-NMR Spectroscopy …….. 63

5.4.1. Ca-Mg Series

[4.5SiO_2. 3.0Al_2O_3. 1.5P_2O_5. (3.0-x)CaO. xMgO. (2.0-y)CaF_2. yMgF_2] .. 63

5.4.2. Sr-Mg Series

[4.5SiO_2. 3.0Al_2O_3. 1.5P_2O_5. (3.0-x)SrO. xMgO. (2.0-y)SrF_2. yMgF_2] … 66

5.4.3. Ca-Zn Series

[4.5SiO_2. 3.0Al_2O_3. 1.5P_2O_5. (3.0-x)CaO. xZnO. (2.0-y)CaF_2. yZnF_2] …. 69

5.5. ^{29}Si MAS-NMR Spectroscopy ……... 71

5.5.1. Ca-Mg Series

[4.5SiO_2. 3.0Al_2O_3. 1.5P_2O_5. (3.0-x)CaO. xMgO. (2.0-y)CaF_2. yMgF_2] .. 71

5.5.2. Sr-Mg Series

[4.5SiO_2. 3.0Al_2O_3. 1.5P_2O_5. (3.0-x)SrO. xMgO. (2.0-y)SrF_2. yMgF_2] … 74

5.5.3. Ca-Zn Series

[4.5SiO_2. 3.0Al_2O_3. 1.5P_2O_5. (3.0-x)CaO. xZnO. (2.0-y)CaF_2. yZnF_2] … 76

5.6. DSC Analysis …….. 79

5.6.1. Ca-Mg Series

[4.5SiO_2. 3.0Al_2O_3. 1.5P_2O_5. (3.0-x)CaO. xMgO. (2.0-y)CaF_2. yMgF_2] .. 79

5.6.2. Sr-Mg Series

[4.5SiO_2. 3.0Al_2O_3. 1.5P_2O_5. (3.0-x)SrO. xMgO. (2.0-y)SrF_2. yMgF_2] … 84

5.6.3. Ca-Zn Series

[4.5SiO_2. 3.0Al_2O_3. 1.5P_2O_5. (3.0-x)CaO. xZnO. (2.0-y)CaF_2. yZnF_2] … 87

5.7. Fluoro-Aluminosilicate Glasses from Schott AG (Germany) …… 90

5.7.1. ^{19}F MAS-NMR Spectroscopy …….. 90

5.7.2. ^{27}Al MAS-NMR Spectroscopy …… 92

5.7.3. ^{31}P MAS-NMR Spectroscopy …….. 95

5.7.4. ^{29}Si MAS-NMR Spectroscopy ……. 97

5.7.5. DSC Analysis ……... 98

Part II. Characterisation of GPCs with Mg, Sr, and Zn containing Fluoro-Aluminosilicate Glasses ……. 99

5.8. MAS-NMR Studies on the Setting Reaction of GPCs …… 99

5.8.1. ^{19}F MAS-NMR Spectroscopy ……. 100

5.8.2. ^{31}P MAS-NMR Spectroscopy ……. 108

5.8.3. ^{27}Al MAS-NMR Spectroscopy …… 117

5.9. Working and Setting Time …… 133

5.10. Radiopacity ……. 137

5.11. Compressive Strength …… 139

5.12. Fluoride Release ……. 147

Part III. Characterisation of Fluoro-Aluminosilicate Glasses containing Sr, Zn, and Lower Phosphate …… 152
5.13. XRD Analysis ……. 153
5.14. ^{31}P MAS-NMR Spectroscopy …… 153
5.15. ^{27}Al MAS-NMR Spectroscopy …….. 155
5.16. ^{29}Si MAS-NMR Spectroscopy ……... 157
5.17. DSC Analysis …….. 159

Part IV. Characterisation of GPCs with PgGA and Fluoro-Aluminosilicate Glasses containing Sr, Zn, and Lower Phosphate …….. 161
5.18. Working and Setting Time …… 162
5.19. Compressive Strength …… 164
5.20. Fluoride Release ……. 167
5.21. Adhesion …….. 173

6. Conclusion ……. 179
6.1. Characterisation of Mg, Sr, and Zn containing Fluoro-Aluminosilicate Glasses ……. 179
6.2. Characterisation of GPCs with Mg, Sr, and Zn containing Fluoro-Aluminosilicate Glasses ……. 180
6.3. Characterisation of Fluoro-Aluminosilicate Glasses containing Sr, Zn, and Lower Phosphate …… 183
6.4. Characterisation of GPCs with PgGA and Fluoro-Aluminosilicate Glasses containing Sr, Zn, and Lower Phosphate …… 183
6.5. Recommendations for Future Work …… 184

References …… 186

Appendices ……... 193

List of Figures

Figure 1.1. Poly (γ-glutamic acid)……..4

Figure 2.1. Two dimensional representation of soda-silica glass……...8

Figure 2.2. Variations of the rate of nucleation *I* and the rate of growth *u* as a function of the temperature……...10

Figure 2.3. Schematic showing the Zeeman effect with a spin number ½ ……..12

Figure 2.4. Schematic showing the spinning of sample at magic angle, θ, with respect to the magnetic field ……..13

Figure 2.5. Schematic of Al^{3+} charge compensated by P^{5+} by the formation of Al-O-P bonds…….18

Figure 2.6. Schematic showing the reconstruction of the silicate network…….....20

Figure 4.1. Schematic of an oscillating rheometer (left) and a typical trace of the oscillating rheometer (right)……..…….35

Figure 4.2. Apparatus for adhesion measurement ……...38

Figure 5.1. XRD patterns for the glasses in the Ca-Mg series [$4.5SiO_2$. $3.0Al_2O_3$. $1.5P_2O_5$. (3.0-x)CaO. xMgO. (2.0-y)CaF_2. yMgF_2].....40

Figure 5.2. XRD patterns for the glasses in the Sr-Mg series [$4.5SiO_2$. $3.0Al_2O_3$. $1.5P_2O_5$. (3.0-x)SrO. xMgO. (2.0-y)SrF_2. yMgF_2]……..41

Figure 5.3. XRD patterns for the glasses in Ca-Zn series [$4.5SiO_2$. $3.0Al_2O_3$. $1.5P_2O_5$. (3.0-x)CaO. xZnO. (2.0-y)CaF_2. yZnF_2]……..42

Figure 5.4. ^{19}F MAS-NMR spectra for the glasses in the Ca-Mg series [$4.5SiO_2$. $3.0Al_2O_3$. $1.5P_2O_5$. (3.0-x)CaO. xMgO. (2.0-y)CaF_2. yMgF_2].....44

Figure 5.5. ^{19}F MAS-NMR spectra for the glasses in the Sr-Mg series [$4.5SiO_2$. $3.0Al_2O_3$. $1.5P_2O_5$. (3.0-x)SrO. xMgO. (2.0-y)SrF_2. yMgF_2]……..47

Figure 5.6. Schematic of F attached to Al in Al-O-PO_3^{3-} species ……...48

Figure 5.7. ^{19}F MAS-NMR spectra for the glasses in the Ca-Zn series [$4.5SiO_2$. $3.0Al_2O_3$. $1.5P_2O_5$. (3.0-x)CaO. xZnO. (2.0-y)CaF_2. yZnF_2]……..….50

Figure 5.8. ^{31}P MAS-NMR spectra for the glasses in the Ca-Mg series [$4.5SiO_2$. $3.0Al_2O_3$. $1.5P_2O_5$. (3.0-x)CaO. xMgO. (2.0-y)CaF_2. yMgF_2].....53

Figure 5.9. Chemical shift in ^{31}P MAS-NMR spectra against Mg content in mol% for the glasses in the Ca-Mg series [$4.5SiO_2$. $3.0Al_2O_3$. $1.5P_2O_5$. (3.0-x)CaO. xMgO. (2.0-y)CaF_2. yMgF_2].....55

Figure 5.10. Schematic of magnesium pyrophosphate…….56

Figure 5.11. ^{31}P MAS-NMR spectra for the glasses in the Sr-Mg series [$4.5SiO_2$. $3.0Al_2O_3$. $1.5P_2O_5$. (3.0-x)SrO. xMgO. (2.0-y)SrF_2. yMgF_2]……...57

Figure 5.12. Chemical shift in ^{31}P MAS-NMR spectra against Mg content in mol% for the glasses in the Sr-Mg series [$4.5SiO_2$. $3.0Al_2O_3$. $1.5P_2O_5$. (3.0-x)SrO. xMgO. (2.0-y)SrF_2. yMgF_2]……...59

Figure 5.13. ^{31}P MAS-NMR spectra for the glasses in the Ca-Zn series [$4.5SiO_2$. $3.0Al_2O_3$. $1.5P_2O_5$. (3.0-x)CaO. xZnO. (2.0-y)CaF_2. yZnF_2]……...60

Figure 5.14. Chemical shift in ^{31}P MAS-NMR spectra against Zn content in mol% for the glasses in the Ca-Zn series [$4.5SiO_2$. $3.0Al_2O_3$. $1.5P_2O_5$. (3.0-x)CaO. xZnO. (2.0-y)CaF_2. yZnF_2]……61

Figure 5.15. Schematics of Q^1 pyrophosphate Al-O-PO_3^{3-} species charge balanced by Ca^{2+} (left) and Zn^{2+} (right)……...62

Figure 5.16. ^{27}Al MAS-NMR spectra for the glasses in the Ca-Mg series [$4.5SiO_2$. $3.0Al_2O_3$. $1.5P_2O_5$. (3.0-x)CaO. xMgO. (2.0-y)CaF_2. yMgF_2]……..64

Figure 5.17. ^{27}Al MAS-NMR spectra for the glasses in the Sr-Mg series [$4.5SiO_2$. $3.0Al_2O_3$. $1.5P_2O_5$. (3.0-x)SrO. xMgO. (2.0-y)SrF_2. yMgF_2]……...67

Figure 5.18. ^{27}Al MAS-NMR spectra for the glasses in the Ca-Zn series [$4.5SiO_2$. $3.0Al_2O_3$. $1.5P_2O_5$. (3.0-x)CaO. xZnO. (2.0-y)CaF_2. yZnF_2]……69

Figure 5.19. ^{29}Si MAS-NMR spectra for the glasses in the Ca-Mg series [$4.5SiO_2$. $3.0Al_2O_3$. $1.5P_2O_5$. (3.0-x)CaO. xMgO. (2.0-y)CaF_2. yMgF_2]……..72

Figure 5.20. ^{29}Si MAS-NMR spectra for the glasses in the Sr-Mg series [$4.5SiO_2$. $3.0Al_2O_3$. $1.5P_2O_5$. (3.0-x)SrO. xMgO. (2.0-y)SrF_2. yMgF_2]……...75

Figure 5.21. ^{29}Si MAS-NMR spectra for the glasses in the Ca-Zn series [$4.5SiO_2$. $3.0Al_2O_3$. $1.5P_2O_5$. (3.0-x)CaO. xZnO. (2.0-y)CaF_2. yZnF_2]……77

Figure 5.22. Glass transition temperature against Mg content in mol% for the glasses in the Ca-Mg series [$4.5SiO_2$. $3.0Al_2O_3$. $1.5P_2O_5$. (3.0-x)CaO. xMgO. (2.0-y)CaF_2.yMgF_2].....79

Figure 5.23. First and second crystallisation temperatures, T_{c1} and T_{c2}, against Mg content in mol% for the glasses in the Ca-Mg series [$4.5SiO_2$. $3.0Al_2O_3$. $1.5P_2O_5$. (3.0-x)CaO. xMgO. (2.0-y)CaF_2. yMgF_2]……82

Figure 5.24. Glass transition temperature against Mg content in mol% for the glasses in the Sr-Mg series [$4.5SiO_2$. $3.0Al_2O_3$. $1.5P_2O_5$. (3.0-x)SrO. xMgO. (2.0-y)SrF_2.yMgF_2]…….84

Figure 5.25. First and second crystallisation temperatures, T_{c1} and T_{c2}, against Mg content in mol% for the glasses in the Sr-Mg series [4.5SiO_2. 3.0Al_2O_3. 1.5P_2O_5. (3.0-x)SrO. xMgO. (2.0-y)SrF_2. yMgF_2].....85

Figure 5.26. Glass transition temperature against Zn content in mol% for the Ca-Zn series [4.5SiO_2. 3.0Al_2O_3. 1.5P_2O_5. (3.0-x)CaO. xZnO. (2.0-y)CaF_2. yZnF_2]…….…….87

Figure 5.27. First and second crystallisation temperatures, T_{c1} and T_{c2}, against Zn content in mol% for the glasses in the Ca-Zn series [4.5SiO_2. 3.0Al_2O_3. 1.5P_2O_5. (3.0-x)CaO. xZnO. (2.0-y)CaF_2. yZnF_2]……..88

Figure 5.28. ^{19}F MAS-NMR spectra for Schott glasses……...90

Figure 5.29. ^{27}Al MAS-NMR spectra for Schott glasses…….92

Figure 5.30. Schematic of metaphosphate species forming P-O-P bonds……...…94

Figure 5.31. ^{31}P MAS-NMR spectra for Schott glasses……...95

Figure 5.32. ^{29}Si MAS-NMR spectra for Schott glasses…….97

Figure 5.33. ^{19}F MAS-NMR spectra for glass LG26 [4.5SiO_2. 3.0Al_2O_3. 1.5P_2O_5. 3.0CaO. 2.0CaF_2] and its cements…….100

Figure 5.34. ^{19}F MAS-NMR spectra for glass ICHK04 [4.5SiO_2. 3.0Al_2O_3. 1.5P_2O_5. 3.0CaO. 2.0MgF_2] and its cements……....101

Figure 5.35. ^{19}F MAS-NMR spectra for glass LG26Mg [4.5SiO_2. 3.0Al_2O_3. 1.5P_2O_5. 3.0MgO. 2.0MgF_2] and its cements……...103

Figure 5.36. ^{19}F MAS-NMR spectra for glass ICHK10 [4.5SiO_2. 3.0Al_2O_3. 1.5P_2O_5. 3.0SrO. 2.0MgF_2] and its cements…….105

Figure 5.37. ^{19}F MAS-NMR spectra for glass LG26Sr [4.5SiO_2. 3.0Al_2O_3. 1.5P_2O_5. 3.0SrO. 2.0SrF_2] and its cements……...106

Figure 5.38. ^{31}P MAS-NMR spectra for glass LG26 [4.5SiO_2. 3.0Al_2O_3. 1.5P_2O_5. 3.0CaO. 2.0CaF_2] and its cements…….…108

Figure 5.39. ^{31}P MAS-NMR spectra for glass ICHK04 [4.5SiO_2. 3.0Al_2O_3. 1.5P_2O_5. 3.0CaO. 2.0MgF_2] and its cements……109

Figure 5.40. ^{31}P MAS-NMR spectra for glass LG26Mg [4.5SiO_2. 3.0Al_2O_3. 1.5P_2O_5. 3.0MgO. 2.0MgF_2] and its cements…….…..111

Figure 5.41. ^{31}P MAS-NMR spectra for glass ICHK10 [4.5SiO_2. 3.0Al_2O_3. 1.5P_2O_5. 3.0SrO. 2.0MgF_2] and its cements…….……114

Figure 5.42. ^{31}P MAS-NMR spectra for glass LG26Sr [4.5SiO_2. 3.0Al_2O_3. 1.5P_2O_5. 3.0SrO. 2.0SrF_2] and its cements……..115

Figure 5.43. ^{27}Al MAS-NMR spectra of glass LG26 [$4.5SiO_2$. $3.0Al_2O_3$. $1.5P_2O_5$. 3.0CaO. $2.0CaF_2$] and its cements…….117
Figure 5.44. ^{27}Al MAS-NMR spectra of glass ICHK04 [$4.5SiO_2$. $3.0Al_2O_3$. $1.5P_2O_5$. 3.0CaO. $2.0MgF_2$] and its cements……118
Figure 5.45. ^{27}Al MAS-NMR spectra of glass LG26Mg [$4.5SiO_2$. $3.0Al_2O_3$. $1.5P_2O_5$. 3.0MgO. $2.0MgF_2$] and its cements……...119
Figure 5.46. ^{27}Al MAS-NMR spectra of glass ICHK10 [$4.5SiO_2$. $3.0Al_2O_3$. $1.5P_2O_5$. 3.0SrO. $2.0MgF_2$] and its cements…….120
Figure 5.47. ^{27}Al MAS-NMR spectra of glass LG26Sr [$4.5SiO_2$. $3.0Al_2O_3$. $1.5P_2O_5$. 3.0SrO. $2.0SrF_2$] and its cements……...121
Figure 5.48. Al(VI):Al(IV)+Al(V) ratio plotted against log time in seconds for glass LG26 and its cements……124
Figure 5.49. Al(VI):Al(IV)+Al(V) ratio plotted against log time in seconds for glass ICHK04 and its cements……125
Figure 5.50. Al(VI):Al(IV)+Al(V) ratio plotted against log time in seconds for glass LG26Mg and its cements……...125
Figure 5.51. Al(VI):Al(IV)+Al(V) ratio plotted against log time in seconds for glass ICHK10 and its cements……126
Figure 5.52. Al(VI):Al(IV)+Al(V) ratio plotted against log time in seconds for glass LG26Sr and its cements…….126
Figure 5.53. Al(VI):Al(IV)+Al(V) ratio plotted against log time in seconds for all glasses and cements……...127
Figure 5.54. Percentages of Al(IV) species calculated by deconvoluting the ^{27}Al MAS-NMR spectra of LG26 (○) and LG26Mg (□) cements……130
Figure 5.55. Percentages of Al(V) species calculated by deconvoluting the ^{27}Al MAS-NMR spectra of LG26 (○) and LG26Mg (□) cements……..130
Figure 5.56. Percentages of Al(VI) species calculated by deconvoluting the ^{27}Al MAS-NMR spectra of LG26 (○) and LG26Mg (□) cements……131
Figure 5.57. Working (top) and setting times (bottom) of the cements made with glasses in the Ca-Mg series [$4.5SiO_2$. $3.0Al_2O_3$. $1.5P_2O_5$. (3.0-x)CaO. xMgO. (2.0-y)CaF_2. yMgF_2] and the Sr-Mg series [$4.5SiO_2$. $3.0Al_2O_3$. $1.5P_2O_5$. (3.0-x)SrO. xMgO. (2.0-y)SrF_2. yMgF_2]……133
Figure 5.58. Working (top) and setting times (bottom) of the cements made with glasses in the Ca-Zn series [$4.5SiO_2$. $3.0Al_2O_3$. $1.5P_2O_5$. (3.0-x)CaO.

xZnO. (2.0-y)CaF_2. yZnF_2] plotted with the cements in the Ca-Mg series [4.5SiO_2. 3.0Al_2O_3. 1.5P_2O_5. (3.0-x)CaO. xMgO. (2.0-y)CaF_2. yMgF_2]……...135

Figure 5.59. Radiopacity of the cements formed using the glasses in the Ca-Mg (○) series and the Sr-Mg (●) series…….……138

Figure 5.60. Radiopacity of the cements formed using the glasses in the Ca-Zn series. ……...138

Figure 5.61. Compressive strengths of the cements formed using the glasses in the Ca-Mg series [4.5SiO_2. 3.0Al_2O_3. 1.5P_2O_5. (3.0-x)CaO. xMgO. (2.0-y)CaF_2. yMgF_2] measured at 1 and 7 days……140

Figure 5.62. Compressive strengths of the cements formed using the glasses in the Sr-Mg series [4.5SiO_2. 3.0Al_2O_3. 1.5P_2O_5. (3.0-x)SrO. xMgO. (2.0-y)SrF_2. yMgF_2] measured at 1 and 7 days…….140

Figure 5.63. Compressive strengths of the cements formed using the glasses in the Ca-Mg [4.5SiO_2. 3.0Al_2O_3. 1.5P_2O_5. (3.0-x)CaO. xMgO. (2.0-y)CaF_2. yMgF_2] and the Sr-Mg series [4.5SiO_2. 3.0Al_2O_3. 1.5P_2O_5. (3.0-x)SrO. xMgO. (2.0-y)SrF_2. yMgF_2] measured at 1 day……143

Figure 5.64. Compressive strengths of the cements formed using the glasses in the Ca-Mg [4.5SiO_2. 3.0Al_2O_3. 1.5P_2O_5. (3.0-x)CaO. xMgO. (2.0-y)CaF_2. yMgF_2] and the Sr-Mg series [4.5SiO_2. 3.0Al_2O_3. 1.5P_2O_5. (3.0-x)SrO. xMgO. (2.0-y)SrF_2. yMgF_2] measured at 7 days……...143

Figure 5.65. Compressive strengths of the cements formed using the glasses in the Ca-Zn series [4.5SiO_2. 3.0Al_2O_3. 1.5P_2O_5. (3.0-x)CaO. xZnO. (2.0-y)CaF_2. yZnF_2] measured at 1 and 7 days…….144

Figure 5.66. Compressive strengths of the cements formed using the glasses in the Ca-Mg [4.5SiO_2. 3.0Al_2O_3. 1.5P_2O_5. (3.0-x)CaO. xMgO. (2.0-y)CaF_2. yMgF_2] and the Ca-Zn series [4.5SiO_2. 3.0Al_2O_3. 1.5P_2O_5. (3.0-x)CaO. xZnO. (2.0-y)CaF_2. yZnF_2] measured at 1 day…….145

Figure 5.67. Compressive strengths of the cements formed using the glasses in the Ca-Mg [4.5SiO_2. 3.0Al_2O_3. 1.5P_2O_5. (3.0-x)CaO. xMgO. (2.0-y)CaF_2. yMgF_2] and the Ca-Zn series [4.5SiO_2. 3.0Al_2O_3. 1.5P_2O_5. (3.0-x)CaO. xZnO. (2.0-y)CaF_2. yZnF_2] measured at 7 days……146

Figure 5.68. Cumulative fluoride release against time for the cements made with glasses in the Ca-Mg series [4.5SiO_2. 3.0Al_2O_3. 1.5P_2O_5. (3.0-x)CaO. xMgO. (2.0-y)CaF_2. yMgF_2]…….147

Figure 5.69. Cumulative fluoride release against time for the cements made with glasses in the Sr-Mg series [4.5SiO_2. 3.0Al_2O_3. 1.5P_2O_5. (3.0-x)SrO. xMgO. (2.0-y)SrF_2. yMgF_2]……..148

Figure 5.70. Cumulative fluoride release against square root of time for the cements made with glasses in the Ca-Mg series [4.5SiO_2. 3.0Al_2O_3. 1.5P_2O_5. (3.0-x)CaO. xMgO. (2.0-y)CaF_2. yMgF_2]…….149

Figure 5.71. Cumulative fluoride release against square root of time for the cements made with glasses in the Sr-Mg series [4.5SiO_2. 3.0Al_2O_3. 1.5P_2O_5. (3.0-x)SrO. xMgO. (2.0-y)SrF_2. yMgF_2]……..149

Figure 5.72. XRD patterns for the glasses in the Sr-Zn series [4.5SiO_2. 3.0Al_2O_3. 0.75 P_2O_5. (3.0-x)SrO. xZnO. 2.0SrF_2]…….153

Figure 5.73. ^{31}P MAS-NMR spectra for the glasses in the Sr-Zn series [4.5SiO_2. 3.0Al_2O_3. 0.75P_2O_5. (3.0-x)SrO. xZnO. 2.0SrF_2]……..154

Figure 5.74. ^{27}Al MAS-NMR spectra for the glasses in the Sr-Zn series [4.5SiO_2. 3.0Al_2O_3. 0.75P_2O_5. (3.0-x)SrO. xZnO. 2.0SrF_2]……..156

Figure 5.75. ^{29}Si MAS-NMR spectra for the glasses in the Sr-Zn series [4.5SiO_2. 3.0Al_2O_3. 0.75P_2O_5. (3.0-x)SrO. xZnO. 2.0SrF_2]……..158

Figure 5.76. Working time of the PgGA-TCA/PAA hybrid cements for the glasses in the Sr-Zn series [4.5SiO_2. 3.0Al_2O_3. 0.75P_2O_5. (3.0-x)SrO. xZnO. 2.0SrF_2]……..162

Figure 5.77. Setting time of the PgGA-TCA/PAA hybrid cements for the glasses in the Sr-Zn series [4.5SiO_2. 3.0Al_2O_3. 0.75P_2O_5. (3.0-x)SrO. xZnO. 2.0SrF_2]……..163

Figure 5.78. Compressive strengths of the cements formed with the glasses in the Sr-Zn series [4.5SiO_2. 3.0Al_2O_3. 0.75P_2O_5. (3.0-x)SrO. xZnO. 2.0SrF_2]. No PgGA was used……..164

Figure 5.79. Compressive strengths of the cements formed with the glasses in the Sr-Zn series [4.5SiO_2. 3.0Al_2O_3. 0.75P_2O_5. (3.0-x)SrO. xZnO. 2.0SrF_2]. A hybrid of 25wt% PgGA and 75wt% TCA/PAA co-polymer was used. 165

Figure 5.80. Compressive strengths of the cements formed with the glasses in the Sr-Zn series [4.5SiO_2. 3.0Al_2O_3. 0.75P_2O_5. (3.0-x)SrO. xZnO. 2.0SrF_2]. A hybrid of 50wt% PgGA and 50wt% TCA/PAA co-polymer was used. ……...……166

Figure 5.81. Fluoride release profile of the cements containing no PgGA and the glasses in the Sr-Zn series [4.5SiO_2. 3.0Al_2O_3. 0.75P_2O_5. (3.0-x)SrO. xZnO. 2.0SrF_2]……..168

Figure 5.82. Fluoride release profile of the cements containing 25wt% PgGA and the glasses in the Sr-Zn series [4.5SiO_2. 3.0Al_2O_3. 0.75P_2O_5. (3.0-x)SrO. xZnO. 2.0SrF_2]…….….168

Figure 5.83. Fluoride release profile of the cements containing 50wt% PgGA and the glasses in the Sr-Zn series [4.5SiO_2. 3.0Al_2O_3. 0.75P_2O_5. (3.0-x)SrO. xZnO. 2.0SrF_2]……..169

Figure 5.84. Fluoride release profile of the cements containing no PgGA and the glasses in the Sr-Zn series [4.5SiO_2. 3.0Al_2O_3. 0.75P_2O_5. (3.0-x)SrO. xZnO. 2.0SrF_2]……..170

Figure 5.85. Fluoride release profile of the cements containing 25wt% PgGA and the glasses in the Sr-Zn series [4.5SiO_2. 3.0Al_2O_3. 0.75P_2O_5. (3.0-x)SrO. xZnO. 2.0SrF_2]……..170

Figure 5.86. Fluoride release profile of the cements containing 50wt% PgGA and the glasses in the Sr-Zn series [4.5SiO_2. 3.0Al_2O_3. 0.75P_2O_5. (3.0-x)SrO. xZnO. 2.0SrF_2]……..171

Figure 5.87. Fluoride release profile of the cements containing 0wt% PgGA, 25wt% PgGA, and 50wt% PgGA and the glasses in the Sr-Zn series [4.5SiO_2. 3.0Al_2O_3. 0.75P_2O_5. (3.0-x)SrO. xZnO. 2.0SrF_2]……..172

Figure 5.88. Tensile bond strengths to bovine dentine measured 1 day after mixing. ……...173

Figure 5.89. Tensile bond strength to bovine enamel measured 1 day after mixing. ……...175

Figure 5.90. Tensile bond strength to stainless steel measured 1 day after mixing. ……...176

List of Tables

Table 2.1. Nuclei with their natural abundance and spin quantum number……12

Table 3.1. Glass compositions in the Ca-Mg series [4.5SiO_2. 3.0Al_2O_3. 1.5P_2O_5. (3.0-x)CaO. xMgO. (2.0-y)CaF_2. yMgF_2] …….23

Table 3.2. Glass compositions in the Sr-Mg series [4.5SiO_2. 3.0Al_2O_3. 1.5 P_2O_5. (3.0-x)SrO. xMgO. (2.0-y)SrF_2. yMgF_2] ……..…….....24

Table 3.3. Glass compositions in the Ca-Zn series [4.5SiO_2. 3.0Al_2O_3. 1.5 P_2O_5. (3.0-x)CaO. xZnO. (2.0-y)CaF_2. yZnF_2] ……..…….....25

Table 3.4. Glass compositions of three fluoro-aluminosilicate glasses obtained from Schott AG (Germany) in mole percentages……25

Table 3.5. Glass compositions in the Sr-Zn series [4.5SiO_2. 3.0Al_2O_3. 0.75P_2O_5. (3.0-x)SrO. xZnO. 2.0SrF_2] ……..…….26

Table 5.1. Al coordination states and their percentages for the glasses in the Ca-Mg series [4.5SiO_2. 3.0Al_2O_3. 1.5P_2O_5. (3.0-x)CaO. xMgO. (2.0-y)CaF_2. yMgF_2]……65

Table 5.2. Al coordination states and their percentages for the glasses in the Sr-Mg series [4.5SiO_2. 3.0Al_2O_3. 1.5P_2O_5. (3.0-x)SrO. xMgO. (2.0-y)SrF_2. yMgF_2]……68

Table 5.3. Al coordination states and their percentages for the glasses in the Ca-Zn series [4.5SiO_2. 3.0Al_2O_3. 1.5P_2O_5. (3.0-x)CaO. xZnO. (2.0-y)CaF_2. yZnF_2]……..71

Table 5.4. Glass transition temperatures, T_g, measured with particle size <38μm, and first and second crystallisation temperatures, T_{c1} and T_{c2}, with different particle sizes for the glasses in the Ca-Mg series [4.5SiO_2. 3.0Al_2O_3. 1.5P_2O_5. (3.0-x)CaO. xMgO. (2.0-y)CaF_2. yMgF_2]……..…...……...83

Table 5.5. Glass transition temperatures, T_g, measured with particle size <38μm, and first and second crystallisation temperatures, T_{c1} and T_{c2}, with different particle sizes for the glasses in the Sr-Mg series [4.5SiO_2. 3.0Al_2O_3. 1.5P_2O_5. (3.0-x)SrO. xMgO. (2.0-y)SrF_2. yMgF_2]……..86

Table 5.6. Glass transition temperatures, T_g, measured with particle size <38μm, and first and second crystallisation temperatures, T_{c1} and T_{c2}, with different particle sizes for the glasses in the Ca-Zn series [4.5SiO_2. 3.0Al_2O_3. 1.5P_2O_5. (3.0-x)CaO. xZnO. (2.0-y)CaF_2. yZnF_2]…….……...……..89

Table 5.7. Half-width values of the peaks observed in ^{31}P MAS-NMR spectra for glasses LG26, ICHK04, LG26Mg, ICHK10, and LG26Sr and their cements, in Hz……..……113

Table 5.8. Chemical shift and percentages of Al species in glasses LG26, ICHK04, LG26Mg, ICHK10 and LG26Sr and their cements at 4 months aging time……123

Table 5.9. Glass transition temperatures, T_g, and first crystallisation temperatures of the glasses, T_{c1}, measured with particle sizes <38μm and >38μm, in the Sr-Zn series [$4.5SiO_2$. $3.0Al_2O_3$. $0.75P_2O_5$. (3.0-x)SrO. xZnO. $2.0SrF_2$]…..159

List of Equations

Equation 1.1. Formation of fluoroapatite…….1

List of Abbreviations

GPCs	Glass polyalkenoate cements
PAA	Poly (acrylic acid)
PgGA	Poly (γ-glutamic acid)
Mw	Weight average molecular weight
XRD	X-ray diffraction
MAS-NMR	Magic angle spinning nuclear magnetic resonance
DSC	Differential scanning calorimetry
BOs	Bridging oxygens
NBOs	Non-bridging oxygens
FTIR	Fourier transform infrared
TCA	Poly (but-3-ene 1,2,4-tricarboxylic acid)
T_m	Melting temperature
T_g	Glass transition temperature
T_{c1}	First crystallisation temperature
T_{c2}	Second crystallisation temperature
TISAB	Total ionic strength adjustment buffer
s.d.	Standard deviation
AHL	Luting cement from Advanced Healthcare Ltd (UK)
CPMAS	Cross-polarisation magic angle spinning

1. Introduction

The glass (ionomer) polyalkenoate cements, GPCs, were first introduced by Wilson and Kent in 1970's. GPCs are formed by the acid-base reaction between a fluoro-aluminosilicate glass and polymeric acid, usually poly (acrylic acid), PAA. The acid attacks the glass releasing metal cations, such as Ca^{2+} and Al^{3+}, which will then crosslink with the carboxylate groups of the polymeric acid [1].

Before GPCs were invented, amalgams were most commonly used for the restoration of the posterior teeth. The amalgams are alloy made with mercury which may contain silver, tin, copper, and zinc. Problem arises if mercury is heated above $80^{o}C$ at which point toxic mercury vapour is released [2]. On the contrary, GPCs are non-toxic and biocompatible [1]. Initially, the application of GPCs was for dentistry as adhesives and restorative cements. One of the advantages with GPCs for dental application is fluoride release over a period of time, and this fluoride release is known to inhibit the formation of secondary caries by forming a more chemically and thermodynamically stable fluoroapatite phase in the tooth apatite (Equation 1.1).

$$Ca_{10}(PO_4)_6(OH)_2 + 2F^- \rightarrow Ca_{10}(PO_4)_6F_2 + 2OH^-$$

Equation 1.1. Formation of fluoroapatite.

More recently, strontium and zinc have been incorporated in the glass compositions for GPCs in addition to the fluoride. These also provide bactericidal effect inhibiting the formation of secondary caries [3, 4]. Moreover, they can form radiopaque cements which are very useful for clinicians to identify the cements once they are placed. The

radiopacity of cements depends on the atomic number of the glass components, and therefore the radiopacity can be easily controlled [1].

Another advantage with GPCs for dentistry is their aesthetic nature. The translucency of the cements usually matches with that of tooth. This is very important, especially if the cement is used for restoration of the anterior teeth [1].

GPCs are known to be more adhesive to enamel and dentine under wet conditions than amalgams, and the adhesion occurs *via* chemical bonds between the cement and the dental apatite. The adhesion to the enamel is better as there is a higher proportion of apatite in the enamel than the dentine. In the adhesion process, free carboxylate groups in the cements will form hydrogen bonding with the apatite, followed by the ionic bonding between the carboxylates from the cements and the cations from the teeth. Therefore, GPCs can seal the cavities and prevent the formation of secondary caries. The better sealing of GPCs is also due to the minimal shrinkage of the material as no polymerisation reaction occurs during the setting reaction [1].

Finally, the setting properties of GPCs are carefully controlled so that the cements will set fast enough for a specific application at body temperature when they are in use [1].

A major disadvantage with GPCs, however, is the toughness. Compared to amalgams, GPCs are relatively weak in toughness although they show a high compressive strength [1].

1.1. Significance of the Study

Several studies have looked at the influence of glass compositions on the mechanical properties of the GPCs. Griffin and Hill [5] investigated the effect of the Al:Si ratio and concluded that this ratio has no significant influence on the mechanical properties of the GPCs. De Barra and Hill [6] found that the addition of fluorite content increases the compressive strength and the Young's modulus, but not fracture toughness. Fluoride can increase the reactivity of the glass by disrupting the glass network efficiently. Moreover, decreasing the phosphate content has been found to increase the compressive strength significantly [7]. Al^{3+} in fluoro-aluminosilicate glasses containing phosphate is charge compensated by P^{5+} by forming Al-O-P bonds [8], and these Al-O-P bonds are not susceptible to acid attack. Therefore, Al in the Al-O-P bonds is not released for cement formation. Hence, by reducing the phosphate content, the number of Al^{3+} charge compensated by P^{5+} is reduced, increasing the number of Al^{3+} ions available to be released for crosslinking with polymeric acid. Originally, Wilson [9] postulated a mechanism for the acid hydrolysis of the Al-O-Si bonds as the polarisation of the Al-O-Si bonds. However, the reaction model by Loewenstein [10] for the acid hydrolysis of aluminosilicate minerals envisaged that the first step in the acid hydrolysis is the exchange of the charge balancing cations for Al^{3+} from the glass for H^{+} from the polymeric acid, followed by the subsequent hydrolysis. Furthermore, the Wilson's model does not explain the reduced reactivity of the glasses with a lower Al:P ratio whilst the Loewenstein's model does.

The mechanical properties are strongly related to how well the carboxylate groups of the polymeric acids form crosslinkages with the metal cations from the glass. Therefore, it was proposed that by substituting calcium by magnesium in the

commercially used glass composition, LG26 [$4.5SiO_2$. $3.0Al_2O_3$. $1.5P_2O_5$. 3.0CaO. $2.0CaF_2$], the crosslinking process would improve and polymer chains would be brought closer together as Mg^{2+} is a smaller cation than Ca^{2+} and should crosslink the polycarboxylate chains more efficiently. Apart from possible improvement in the mechanical properties of GPCs, this study is very useful as it will also study the role of Mg^{2+} in the glass structure. The role of Mg^{2+}, whether it is network forming cation, network modifying cation, or intermediate cation, has been controversial and varies depending on the glass compositions. It has been shown that Mg^{2+} acts as network modifying cation in magnesium phosphate glasses [11] and as network forming cation in aluminosilicate glasses [12, 13]. Moreover, the charge to size ratio of Mg^{2+} and Zn^{2+} is quite similar, and the effect of zinc substitution into glass LG26 will also be studied and compared with magnesium containing glasses.

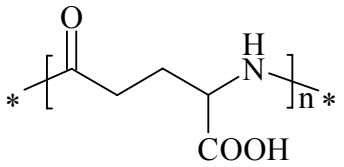


Figure 1.1. Poly (γ-glutamic acid)

The second part of this study will look at poly (γ-glutamic acid), PgGA, (Figure 1.1) as an alternative to PAA for the GPC formation. PgGA has an amide linkage between α-amino and γ-carboxylic acid groups, and this amine group could provide hydrogen bonding to the collagen phase of teeth increasing the adhesive property of the cements. Also, PgGA is biodegradable, edible and non-toxic to human and environment [14]. Ledezma-Perez and co-workers [15] have made GPCs using PgGA and a fluoro-aluminosilicate glass and achieved relatively high compressive strength. However,

their glass composition seems to contain insufficient amount of network modifying cations to maintain aluminium in a tetrahedral coordination. As a result, the glass could have undergone crystallisation, incomplete melting, and/or amorphous phase separation, reducing the reactivity of the glass. The fact that they had to use very small average particle sizes of 1μm, 3μm, 8μm, shows that their glass was not reactive. In this study, the glass compositions will be carefully designed to make GPCs with PgGA as well as PAA. The carboxylate content per PgGA monomer is less than PAA, and therefore, the reactivity of the glasses will be increased to compensate the reduced reactivity of the acid by decreasing the phosphate content in the glass compositions to increase the number of Al^{3+} to be released for crosslinking process.

1.2. Objectives of the Study

The objectives of the study were to produce magnesium containing fluoro-aluminosilicate glasses:

1. To understand the role of Mg^{2+} in the glass structures by using XRD, ^{19}F, ^{31}P, ^{27}Al, and ^{29}Si MAS-NMR spectroscopy and DSC.
2. To study the setting chemistry of the magnesium containing GPCs with PAA using ^{19}F, ^{31}P, ^{27}Al MAS-NMR spectroscopy.
3. To make cements with magnesium and zinc containing fluoro-aluminosilicate glasses and PAA, and determine the effect of the substitution on working and setting times, radiopacity, compressive strengths, and fluoride release.

Then another series of glasses, containing strontium, zinc and a lower amount of phosphate, was produced, and the objectives were:

4. To understand the effect of reducing the phosphate content and incorporating strontium and zinc on the glass structures by using XRD, ^{31}P, ^{27}Al, and ^{29}Si MAS-NMR spectroscopy and DSC.
5. To make cements with PgGA, and determine the effect of substitution on working and setting times, compressive strengths, fluoride release, and adhesion.

2. Literature Review

2.1. Structure of Glass

A glass can be simply defined as a non-crystalline solid. One of the ways to form a glass is melting followed by fast quenching. The structure and the kinetics affect the glass formation. However, no structural theories can describe the glass formation in all systems.

2.1.1. Goldschmidt's Rule

In the early 1920's, Goldschmidt proposed a rule for the formation of a glass based on the knowledge about glass forming oxides, such as SiO_2. He stated that if an oxide is expressed as A_mO_n, the ratio of the ionic radii of the atom A and the atom O, rA/rO, needs to be between 0.2 and 0.4 for glass formation. This implies the tetrahedral coordination of the glass forming cation [16].

2.1.2. Zachariasen's Rule

The Goldschmidt's rule was not applicable to all oxides. For example, BeO satisfies the Goldschmidt's rule but cannot form a glass. The anomalies led Zachariasen to form a new rule for the glass formation, known as the random network theory.

Zachariasen categorised different oxides participating in glass formation. Firstly, those which form the glass network are called glass formers. The oxides which do not participate in the glass network but modify it by terminating bridging anions are known as glass modifying oxides. For example, Na^+ is a network modifying cation and hence can disrupt the network (Figure 2.1). Lastly, there are intermediate oxides,

such as Al_2O_3, which can go into the network, like the network forming oxides, but cannot form the network on its own, and depending on the glass composition, the intermediate oxide can act as a network modifying oxide. The glass forming oxides must satisfy following criteria [16].

1. The number of oxygens around the cations must be small, either 3 or 4.
2. The oxygen polyhedra can only be connected only at the corners.
3. No oxygen can be linked to more than two network cations.
4. The network can only be three-dimensional if the oxygen polyhedron shares at least three corners.

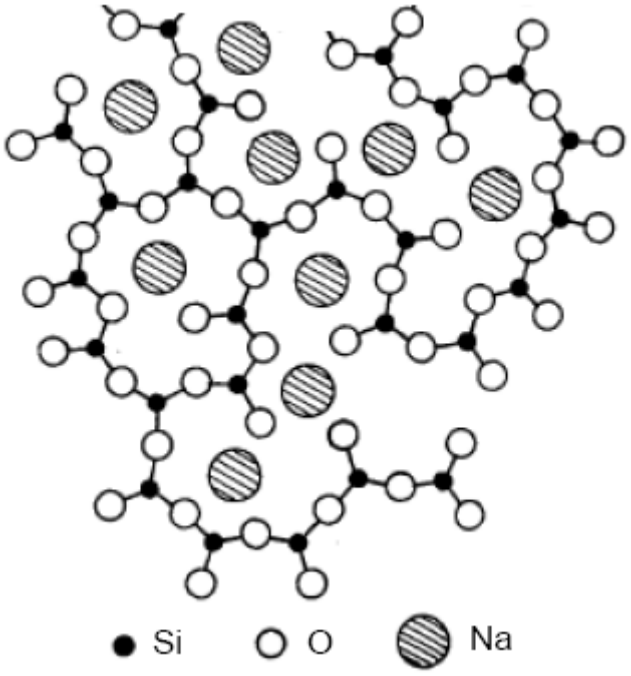


Figure 2.1. Two dimensional representation of soda-silica glass, after Zarzycki [16].

2.1.3. Loewenstein's Rule

Loewenstein's rule states that AlO_4^- tetrahedra cannot be next to each other: the AlO_4^- tetrahedra need to be attached to a small ion with electrovalence of more than three, such as silicon and phosphorus. This will ensure Al to be in a four coordination state. If two AlO_4^- tetrahedra are next to each other, one of the Al needs to be in a higher coordination state than four, which is not favourable for glass formation. In order to meet the Loewenstein's rule, the Al:(Si+P) and the P:Al ratios must be less than one to avoid amorphous phase separation.

2.2. Kinetics of Glass Formation

In order to understand the kinetics of glass formation, one needs to understand that of crystallisation. The nucleation and crystal growth are the two processes which are involved in crystallisation, and these need to be avoided for glass formation [16].

2.2.1. Nucleation

Crystallisation can only occur if there is a nucleus above a critical size, which can serve as a starting point for crystallisation. There are two types of nucleation processes: the homogeneous and the heterogeneous nucleation. In the homogeneous nucleation, all the elements of the initial phase are structurally, chemically, and energetically identical. The nuclei are formed with the equal probability throughout the melt, and the homogeneous nuclei are formed spontaneously from the melt. On the contrary, the heterogeneous nucleation is formed at a pre-existing surface, such as an impurity or a crucible wall [16].

2.2.2. Crystal Growth

Once the nucleation process takes place, the nucleus can grow by the successive addition of atoms from the liquid phase leading to the formation of crystalline phases. If there is no nuclei formed, then there will be no crystal growth and hence a glass is formed. A glass can also be formed with a presence of nuclei, but this only happens if the size and the volume of nuclei are small [16].

2.2.3. General Kinetic Conditions for Glass Formation

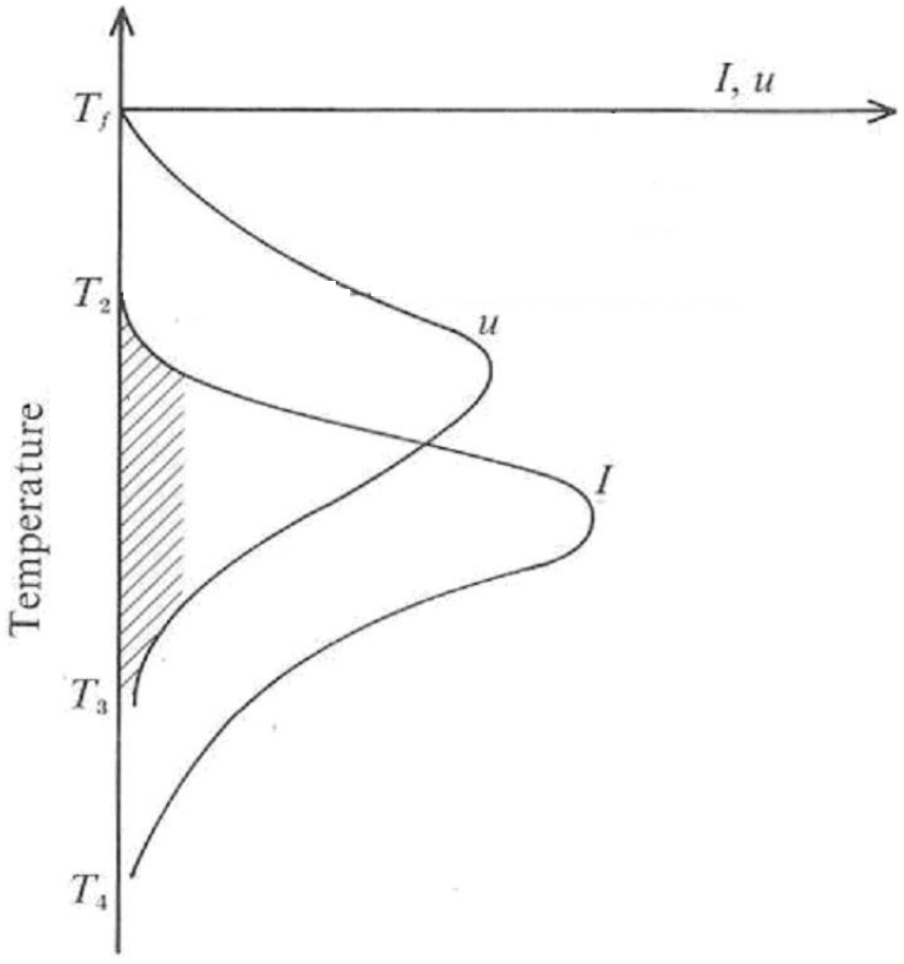


Figure 2.2. Variations of the rate of nucleation *I* and the rate of growth *u* as a function of the temperature, after Zarzycki [16].

I is the number of nuclei produced in a unit volume per unit time and is temperature dependent, and *u* is the rate at which these nuclei grow (Figure 2.2). T_f is the temperature of fusion, and above this temperature, the stable phase is liquid. Crystal growth is possible between T_f and T_3. However, the initial formation of nuclei occurs between T_2 and T_4. Therefore, the important temperature range is between T_2 and T_3. In this region, if *I* and *u* are small, then crystallisation is unlikely to take place and a glass will be formed. On the contrary, if *I* and *u* are both high, then crystallisation cannot be avoided. If *I* is high and *u* is low, then a glass with a small number of crystals will be formed, and if *I* is low and *u* is high, then crystalline material with fine grains will be formed. In practical terms, this region would be between 800^{o}C and 1400^{o}C. Therefore, the molten liquid needs to be cooled very quickly and pass through this region to avoid crystallisation [16].

2.3. General Principles of MAS-NMR Spectroscopy

A nuclear magnetic resonance, NMR, spectroscopy is a technique used to study the structure of materials. When an atom is exposed to a magnetic field, the energy level in the atom splits into several substates, known as the Zeeman effect (Figure 2.3), and this splitting occurs as a result of the radiation, called resonance frequency. The number of energy states is given by $2I+1$, where *I* is the spin quantum number, and spin quantum number is highly dependent on the number of unpaired protons and neutrons in the atom. For an atom with a spin quantum number ½, there will be 2 energy states after Zeeman effect [17].

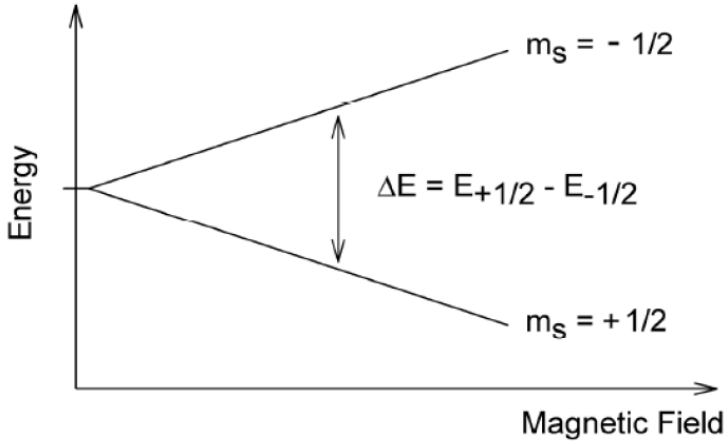


Figure 2.3. Schematic showing the Zeeman effect with a spin number ½, after McKenzie and Smith [18].

In order for a nucleus to be detected on the NMR, the nucleus needs to have a natural abundance high enough. Table 2.1 shows the natural abundance and the spin quantum number of the nuclei which will be investigated in this study.

Table 2.1. Nuclei with their natural abundance and spin quantum number [18].

Isotopes	^{19}F	^{27}Al	^{31}P	^{29}Si
Natural abundance /%	100	100	100	4.7
Spin quantum number (*I*)	1/2	5/2	1/2	1/2

The magnetic nuclei spread according to the Boltzmann distribution in the allowed energy states. In the NMR experiment, a short and an intense burst of radiofrequency radiation is applied to the sample. This will excite the magnetic nuclei, and the nuclei in the lower energy level excite to the higher energy level. An NMR spectrum can be recorded if the difference in the energy states is the same as the applied frequency [17].

The materials that are in interest in this study are in powder form, and therefore, it is necessary to perform NMR in the solid state. A magic angle spinning nuclear magnetic resonance, MAS-NMR, spectroscopy is used for solid state materials. In the solid state, there are interactions within the material, such as chemical shielding, dipole-dipole coupling, and quadrupole coupling, and these interactions cause the spectrum to broaden. These interactions have a $3\cos^2\theta$-1 angular dependency and can be averaged out when this $3\cos^2\theta$-1 terms is zeroed by spinning the sample at $\theta = 54.7$ degrees with respect to the direction of the magnetic field (Figure 2.4).

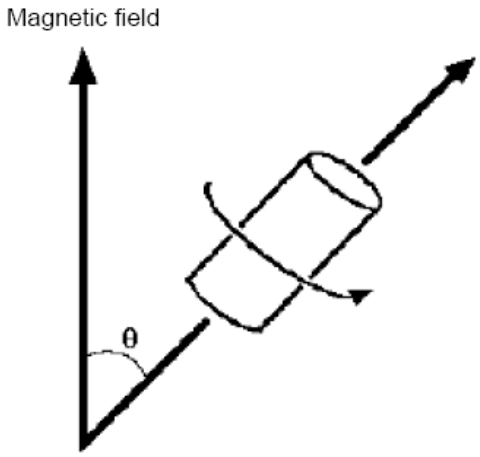


Figure 2.4. Schematic showing the spinning of sample at magic angle, θ, with respect to the magnetic field, after Zainuddin [19].

2.3.1. Glass Characterisation by MAS-NMR Spectroscopy

The MAS-NMR spectroscopy can probe a short range order characteristic of a glass and has been used extensively to study the structures of glasses used for GPCs [20-23]. The basic glass composition used in this study is called LG26 [$4.5SiO_2$. $3.0Al_2O_3$. $1.5P_2O_5$. 3.0CaO. $2.0CaF_2$], and there have been numerous studies performed on the

characterisation of this glass. The environment around ^{19}F, ^{31}P, ^{27}Al, and ^{29}Si nuclei in glass LG26 and the related glasses are discussed in detail here.

A. ^{19}F MAS-NMR Spectroscopy

The ^{19}F MAS-NMR spectrum of glass LG26 contains two peaks. The first peak is at around -100ppm for F-Ca(n) species where F is primarily attached to Ca, and the other peak is at around -150ppm for Al-F-Ca(n) species where F is close to both Al and Ca [20, 21, 23-26]. The relative proportions of Al-F-Ca(n) and F-Ca(n) species increase with the increase in fluorine content of the glass [20, 26].

B. ^{31}P MAS-NMR Spectroscopy

The ^{31}P MAS-NMR spectrum of glass LG26 shows a large symmetrical peak at around -5ppm, which has been assigned to Q^1 pyrophosphate Al-O-PO_3^{3-} species. This assignment is supported by the ^{27}Al MAS-NMR spectrum with the evidence of Al-O-P bonds [23-25].

C. ^{27}Al MAS-NMR Spectroscopy

The ^{27}Al MAS-NMR spectrum for glass LG26 shows a broad peak at around 50ppm, and this peak is assigned to Al in a tetrahedral coordination, Al(IV) [23-25]. This is lower than the chemical shift for Al(IV) for a simple calcium aluminosilicate glass, around 60ppm [20]. This reduction in chemical shift is because of P_2O_5 which forms Al-O-P bonds in LG26, and P^{5+} can charge compensate the AlO_4^- complexes in the glass network. The chemical shift is reduced as P is more electronegative than Si [23-25].

Matsuya and co-workers [25] found that Al in LG26 and related glasses can also be present in higher coordination states: pentahedral Al(V) and octahedral Al(VI). They suggested that Al(V) and Al(VI) are promoted by the presence of fluorine. Stebbins and co-workers [27] also found the presence of Al(V) and Al(VI) in fluorine containing aluminosilicate glasses.

D. ^{29}Si MAS-NMR Spectroscopy

The expression, $Si(OSi)_{m-n}(OAl^-)_n(O^-)_{4-m}$, has been used to describe the structure of aluminosilicate glasses, where *m* is the number of bridging oxygens, BOs, per SiO_4 unit and *n* is the number of Al next to each SiO_4 unit. The chemical shift increases as *m* is decreased or *n* is increased [28]. The ^{29}Si MAS-NMR spectrum of LG26 exhibits a peak at around -90ppm indicating a mixture of Q^4 (4Al) and Q^3(3Al) species [24].

2.4. Glass Polyalkenoate (Ionomer) Cements

The glass polyalkenoate (ionomer) cements, GPCs, were first introduced by Wilson and Kent in the 1970's [1]. GPCs are formed by the acid-base reaction between the aluminosilicate glass and the aqueous solution of polyalkenoic acid, usually poly (acrylic acid), PAA. The glass acts as a proton acceptor and the polymeric acid as the proton donor [29]. The main components in the glasses used for the GPCs are silica, SiO_2, alumina, Al_2O_3, and calcium fluoride, CaF_2.

2.4.1. Setting Reaction of GPCs

The ions, such as Ca^{2+} and Al^{3+}, leach from the glass network as soon as the acid-base reaction occurs, and these ions will form insoluble salts by binding to carboxylate groups in the polymeric acid [1]. The setting reaction has been studied using Fourier

transform infrared, FTIR, spectroscopy [30] and MAS-NMR spectroscopy [31-33]. Crisp and co-workers [30] used FTIR and argued that the formation of calcium salts occurs before the formation of aluminium salts, but these salts were found to be in equal amount when cements are completely set. They stated that the delay in the formation of the two insoluble salts occurs as a result of PAA preferentially binding to divalent cations, Ca^{2+}. This leads to a formation of calcium salts entropically more favoured and would be faster than the formation of aluminium salts, which requires three carboxylic acid groups per Al^{3+}. Furthermore, since Al^{3+} is smaller and therefore tends to be more hydrated than Ca^{2+}, Al^{3+} has a lower mobility than Ca^{2+}. The statement by Crisp and co-workers seems logical, but there are some problems with their study. Firstly, they used glass G200 which is an aluminosilicate glass containing high sodium content. It has been shown that glasses with high sodium content can induce amorphous phase separation [34]. Secondly, they used FTIR and measured the absorption of C=O bond vibrations, but the difference in the vibrations from either Al^{3+} or Ca^{2+} species in carboxylate salts would be very subtle and hard to distinguish. Matsuya and co-workers [31] used more advanced techniques, MAS-NMR spectroscopy, to study the setting reaction of cements. They observed the ^{27}Al MAS-NMR of GPCs formed from aluminosilicate glasses and found that a peak at around 0ppm starts to appear after 6 minutes of mixing. They assigned this peak to the octahedrally coordinated Al, Al(VI), resulting from the release of Al^{3+} ions from the glass network. This peak may arise from the Al^{3+} ions crosslinking to the carboxylate groups of the polymeric acid or free hydrated Al^{3+} ions. The authors have pointed out that ^{27}Al MAS-NMR cannot distinguish the two different Al^{3+} environments. Stamboulis and co-workers [33] found a similar result that the intensity of the Al(VI) peak increased with aging time. They also found that the peak maxima for Al(IV)

increased slightly with aging time and concluded that this was due to the increase in the Si:Al ratio as a result of the Al^{3+} ions being released from the glass network. More recently, Zainuddin and co-workers [35] performed a long-term study on the aging cements using ^{27}Al MAS-NMR spectroscopy. They deconvoluted the area under Al(IV), Al(V), and Al(VI) peaks and calculated the Al(VI):Al(IV)+Al(V) ratio to determine the extent of the aging reaction. It was concluded that the aging process was highly dependent on the glass composition.

2.4.2. Factors Affecting the Mechanical Properties of GPCs

Some of the factors which can affect the mechanical properties of GPCs include glass compositions, glass volume fraction, concentration and molecular weight of polymeric acid, and the aging time.

A. Glass Compositions

Griffin and Hill [5] studied the effect of the Si:Al ratio on compressive strength and found that the ratio does not affect the mechanical property. Instead, they found that the P_2O_5 content was far more important than the Si:Al ratio, and later published a study on the effect of phosphate content on mechanical properties [7]. They studied the glass compositions [$4.5SiO_2$. $3.0Al_2O_3$. $(1.5+x)P_2O_5$. $(3.0-x)CaO$. $2.0CaF_2$], and the highest compressive strength was achieved with the lowest phosphate containing glass, x=0. They argued that the phosphates may compete with carboxylate groups to crosslink with cations. However, this is not the case. Phosphorus is known to charge compensate the AlO_4^- tetrahedra forming Al-O-P bonds [8, 23]. This can maintain aluminium in a tetrahedral coordination. The NBOs on PO_4^{3-} can be charge balanced by divalent cations, such as Ca^{2+} (Figure2.5) as well as Al(VI). The Al^{3+} charge

compensated by P^{5+} is not released as readily as Al^{3+} complexes which are charge balanced by network modifying cations, such as Ca^{2+}.

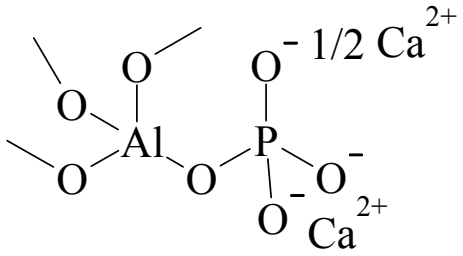


Figure 2.5. Schematic of Al^{3+} charge compensated by P^{5+} by the formation of Al-O-P bonds.

Another component in glass compositions which can affect the mechanical properties is fluoride, F^-. F^- can replace BOs forming non-bridging F^-, which disrupt the network more efficiently [6, 36-39]. Several studies have shown that the addition of fluoride increases the reactivity of the glass. This consequently decreases the working and setting times and increases the mechanical properties of GPCs [6, 37].

B. Glass volume, Concentration and Molecular Weight of PAA

The effect of glass volume fraction, the concentration and molecular weight of PAA, have been studied extensively, and the increase in these components can improve the mechanical properties of GPCs [5, 6, 34, 37, 40, 41]. For example, Hill and co-workers [42] suggested that increasing the crosslinking process between the cations from the glass and the carboxylate groups of the polymer can increase the compressive strength and the Young's modulus of the cements.

Wilson and co-workers [43] found an increase in fracture toughness with an increase in the molecular weight of PAA. Hill and co-workers [42] related GPCs to

thermoplastic polymers and used reputation model to explain the effect of molecular weight on the cement fracture as the crack propagates through the polymer matrix rather than the glassy matrix. In a thermoplastic polymer, chains are entangled, and before the chain scission or the fracture to occur, these chains need to be stretched. As the molecular weight is increased, the chain entanglement will increase constricting the chain movement. However, if the molecular weight is too high, the energy to pull out a chain from its entanglement becomes higher than the energy required chain scission in the polymer, and the fracture property will become independent of the molecular weight of a polymer. An increase in the molecular weight of the polymer can also increase the viscosity of the cement paste, which would make the mixing process of glass and acid more difficult as well.

C. Aging Time

It has been shown that the mechanical properties can increase with aging time of the cements due to the continued reaction of the cements [40, 41]. Crisp and co-workers [44] suggested that the increased mechanical properties with time is due to the continued crosslinking process. Wasson and Nicholson [45] found a secondary reaction contributing to the increased mechanical properties. They postulated that a hydrated silicate matrix is formed as a result of the silica component being released from the glass.

The ^{29}Si MAS-NMR spectroscopy has been used extensively to study the setting reaction of GPCs. Matsuya and co-workers [31] performed the ^{29}Si MAS-NMR analysis on the cements and found the broadening of the peak indicating the reconstruction of the silicate network (Figure 2.6). They concluded that the

continuous increase in the mechanical properties could be due to this reconstruction of the silicate network.

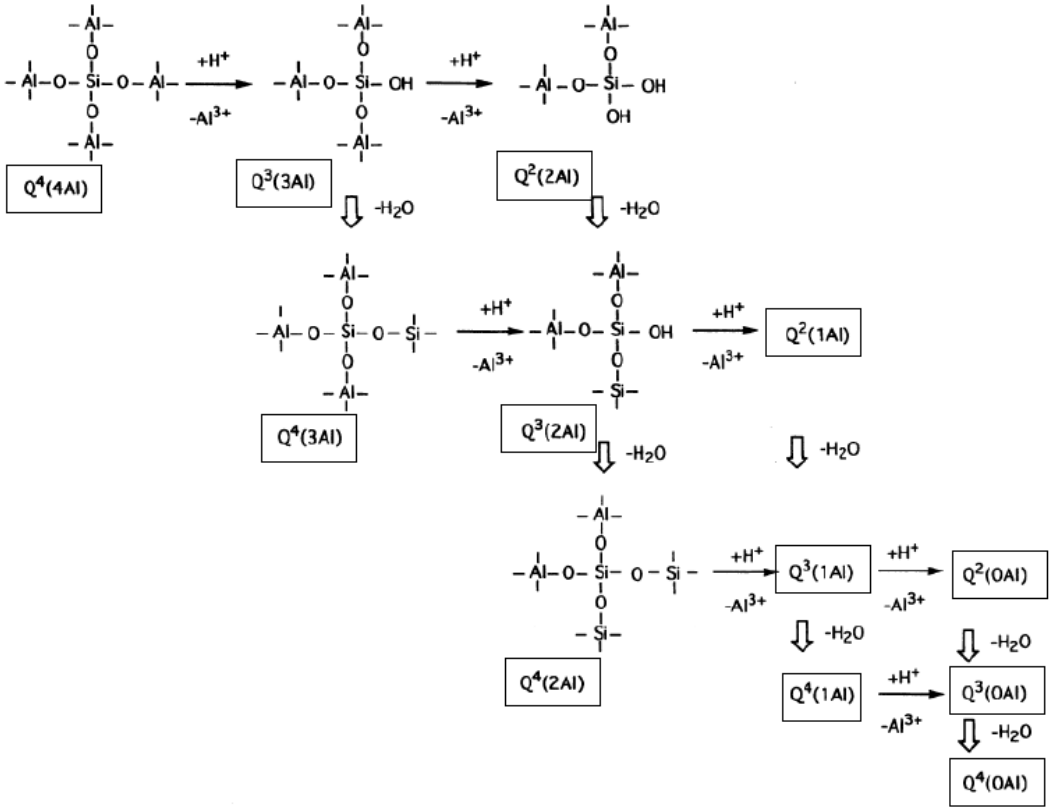


Figure 2.6. Schematic showing the reconstruction of the silicate network, after Matsuya and co-workers [31].

Stamboulis and co-workers [33] have also found similar results which suggested the reconstruction of the silicate network as the cements aged. They observed the chemical shift in the ^{29}Si MAS-NMR spectra moving towards a more negative value as well as the peaks becoming more asymmetrical with time.

2.5. Poly (γ-glutamic acid)

Poly (γ-glutamic acid), PgGA, is a poly-anionic biopolymer with γ-linkages between α-amino and γ-carboxyl groups (Figure 1.1). It is known to be biodegradable and non-

toxic to humans and environment. Hence it has been used in various areas, such as water treatment and cosmetics. Moreover, PgGA is found in a traditional Japanese food, natto, and is therefore edible [14].

PgGA was first discovered in the capsular of *Bacillus anthracis* in the early 1940's [46]. Since then, various bacterium have been found to produce PgGA. The two most commonly known and studied are *Bacillus subtilis* and *Bacillus licheniformis* [46, 47].

2.5.1. Stereochemistry of PgGA

The stereochemistry of PgGA depends highly on the type of bacteria and the synthesis conditions. *Bacillus anthracis* produces PgGA containing only D-glutamic acid [46]. On the contrary, a pure poly (γ-L-glutamic acid) is produced from *Bacillus halodurans* [47]. A mixture of D- and L-isomers is produced from *Bacillus licheniformis* and *Bacillus subtilis* [48, 49]. The amount of D-isomer is found to be influenced by the concentration of Mn^{2+} in the culture medium [50]. In this study, PgGA was produced using *Bacillus licheniformis*, and therefore, the stereochemistry of the polymer is highly likely to be a mixture of D- and L- isomers.

3. Experimental Design and Rationale

3.1. Glass Design

Three series of fluoro-aluminosilicate glasses for PAA based cements and one series of glasses for PgGA based cements were synthesised. In addition, three fluoro-aluminosilicate glasses were obtained from Schott AG (Germany) for structural analysis. The structures of all these glasses were characterised by XRD, ^{19}F, ^{31}P, ^{27}Al and ^{29}Si MAS-NMR spectroscopy, and DSC.

3.1.1. Fluoro-Aluminosilicate Glasses for PAA cements

Three series of glasses were produced. The base glass composition for all these series is LG26 [$4.5SiO_2$. $3.0Al_2O_3$. $1.5P_2O_5$. 3.0CaO. $2.0CaF_2$].

A. Ca-Mg Series:

[$4.5SiO_2$. $3.0Al_2O_3$. $1.5P_2O_5$. (3.0-x)CaO. xMgO. (2.0-y)CaF_2. yMgF_2]

In this series, calcium in glass LG26 was gradually substituted by magnesium [$4.5SiO_2$. $3.0Al_2O_3$. $1.5P_2O_5$. (3.0-x)CaO. xMgO. (2.0-y)CaF_2. yMgF_2]. The glass compositions and their melting temperatures, T_m, are shown (Table 3.1).

Table 3.1. Glass compositions in the Ca-Mg series [$4.5SiO_2$. $3.0Al_2O_3$. $1.5P_2O_5$. (3.0-x)CaO. xMgO. (2.0-y)CaF_2. yMgF_2] in mole fractions, mole percentages and T_m.

Glass	x	y	SiO_2	Al_2O_3	P_2O_5	CaO	MgO	CaF_2	MgF_2	T_m /°C
LG26	0.0	0.0	32.1	21.4	10.7	21.4	---	14.3	---	1420
ICHK02	0.75	0.0	32.1	21.4	10.7	16.1	5.4	14.3	---	1440
ICHK03	1.5	0.0	32.1	21.4	10.7	10.7	10.7	14.3	---	1440
ICHK04	0.0	2.0	32.1	21.4	10.7	21.4	---	---	14.3	1440
ICHK05	3.0	0.0	32.1	21.4	10.7	---	21.4	14.3	---	1440
ICHK06	1.5	2.0	32.1	21.4	10.7	10.7	10.7	---	14.3	1455
LG26Mg	3.0	2.0	32.1	21.4	10.7	---	21.4	---	14.3	1475

B. Sr-Mg Series:

[4.5SiO_2. 3.0Al_2O_3. 1.5P_2O_5. (3.0-x)SrO. xMgO. (2.0-y)SrF_2. yMgF_2]

Calcium in the Ca-Mg series was substituted by strontium. The glass compositions and their T_m are shown (Table 3.2).

Table 3.2. Glass compositions in the Sr-Mg series [4.5SiO_2. 3.0Al_2O_3. 1.5P_2O_5. (3.0-x)SrO. xMgO. (2.0-y)SrF_2. yMgF_2] in mole fractions, mole percentages and T_m.

Glass	x	y	SiO_2	Al_2O_3	P_2O_5	SrO	MgO	SrF_2	MgF_2	T_m /°C
LG26Sr	0.0	0.0	32.1	21.4	10.7	21.4	---	14.3	---	1420
ICHK08	0.75	0.0	32.1	21.4	10.7	16.1	5.4	14.3	---	1440
ICHK09	1.5	0.0	32.1	21.4	10.7	10.7	10.7	14.3	---	1440
ICHK10	0.0	2.0	32.1	21.4	10.7	21.4	---	---	14.3	1440
ICHK11	3.0	0.0	32.1	21.4	10.7	---	21.4	14.3	---	1440
ICHK12	1.5	2.0	32.1	21.4	10.7	10.7	10.7	---	14.3	1455
LG26Mg	3.0	2.0	32.1	21.4	10.7	---	21.4	---	14.3	1475

C. Ca-Zn Series:

[4.5SiO_2. 3.0Al_2O_3. 1.5P_2O_5. (3.0-x)CaO. xZnO. (2.0-y)CaF_2. yZnF_2]

In this series, calcium was gradually substituted by zinc. The glass compositions and their T_m are shown (Table 3.3).

Table 3.3. Glass compositions in the Ca-Zn series [4.5SiO_2. 3.0Al_2O_3. 1.5P_2O_5. (3.0-x)CaO. xZnO. (2.0-y)CaF_2. yZnF_2] in mole fractions, mole percentages and T_m.

Glass	x	y	SiO_2	Al_2O_3	P_2O_5	CaO	ZnO	CaF_2	ZnF_2	T_m /^oC
LG26	0.0	0.0	32.1	21.4	10.7	21.4	---	14.3	---	1420
ICHK14	1.5	0.0	32.1	21.4	10.7	10.7	10.7	14.3	---	1450
ICHK15	3.0	0.0	32.1	21.4	10.7	---	21.4	14.3	---	1450
LG26Zn	3.0	2.0	32.1	21.4	10.7	---	21.4	---	14.3	1470

D. Fluoro-Aluminosilicate Glasses from Schott AG (Germany)

The elemental analysis on the fluoro-aluminosilicate glasses obtained from Schott AG (Germany) was performed by Ceram (UK).

Table 3.4. Glass compositions of three fluoro-aluminosilicate glasses obtained from Schott AG (Germany) in mole percentages.

Glass	SiO_2	Al_2O_3	P_2O_5	CaO	Na_2O	SrO	ZnO	F
GM35429	23.7	14.5	2.9	9.5	7.7	---	---	41.7
G018-090	26.4	12.9	1.6	---	2.0	12.1	6.5	38.4
G018-117	29.8	12.2	1.6	---	2.2	12.9	6.2	35.0

3.1.2. Fluoro-Aluminosilicate Glasses for PgGA Cements

A series of fluoro-aluminosilicate glasses containing strontium and zinc, the Sr-Zn series [$4.5SiO_2$. $3.0Al_2O_3$. $0.75P_2O_5$. (3.0-x)SrO. xZnO. $2.0SrF_2$], was produced for PgGA based cements. These glasses contain a half amount of phosphates, P_2O_5, compared to the glasses used for the PAA based cements (the Ca-Mg, the Sr-Mg, and the Ca-Zn series) to increase the reactivity of glasses. The glass compositions and their T_m are shown (Table 3.5).

Table 3.5. Glass compositions in the Sr-Zn series [$4.5SiO_2$. $3.0Al_2O_3$. $0.75P_2O_5$. (3.0-x)SrO. xZnO. $2.0SrF_2$] in mole fractions, mole percentages and T_m.

Glass	x	SiO_2	Al_2O_3	P_2O_5	SrO	ZnO	SrF_2	T_m /^oC
LPLG26Sr	0.0	34.0	22.6	5.7	22.6	---	15.1	1480
ICHK18	1.0	34.0	22.6	5.7	15.1	7.6	15.1	1500
ICHK19	2.0	34.0	22.6	5.7	7.6	15.1	15.1	1520

3.2. Cement Design

The glasses, which have been structurally characterised, were then used for making GPCs. Only PAA was used for the PAA based cements. For the PgGA based cements, a co-polymer of poly (but-3-ene 1,2,4-tricarboxylic acid), TCA, and PAA was also used along with PgGA. This was because cements with only PgGA were first tried, but it was impossible to make water stable cements. Therefore, in order to increase the water stability of the cements, the co-polymer of TCA and PAA, which is used in commercially available dental cements, was incorporated.

3.2.1. GPCs with PAA

The glasses in the Ca-Mg, the Sr-Mg, and the Ca-Zn series were used to make GPCs with PAA. The Ca-Mg series will determine the effect of substituting calcium by magnesium on cement formation. The glasses in the Sr-Mg series are strontium substituted glasses of the Ca-Mg series, and therefore, the effect of having strontium on GPC formation will be studied. In the Ca-Zn series, zinc has been incorporated into the glass compositions, and its effect on the cement formation will be investigated.

In order to fully understand the relationships between the glass composition and the cement properties, the ratio between the cations from the glass and the number of carboxylate groups in the polymeric acids was kept constant in all the series. The following assumptions have been made to perform the necessary calculations [19].

1) A simple acid-base reaction between the glass and PAA.

2) No preferential release of Al^{3+} relative to divalent cations, $Mg^{2+}/Ca^{2+}/Sr^{2+}/Zn^{2+}$.

3) A complete neutralisation in the acid-base reaction.

4) No five- and six-coordinated aluminium for simplification.

5) Al(IV) in Al-O-PO_3^{3-} and CaF_2 not involved in the acid-base reaction.

In addition to the above, it was assumed that Mg^{2+} and Zn^{2+} will behave similarly to Ca^{2+} and Sr^{2+} in the cement reaction when the calculation and the cement preparation were performed.

An example of the calculation is shown below.

LG26 cement is made with the (glass powder + PAA powder):water ratio of 6:1, with glass powder:PAA powder of 5:1. Both ratios are in terms of weight, and the PAA concentration was 50wt%.

Glass LG26 is $4.5SiO_2$. $3.0Al_2O_3$. $1.5P_2O_5$. 3.0CaO. $2.0CaF_2$.

Therefore,

LG26 molecular weight = (4.5 x 60.09) + (3 x 101.96) + (1.5 x 141.94)
+ (3 x 56.08) + (2 x 78.08)
= 1113.60

The positive charges available from glass LG26 for the acid-base reaction are:

3CaO: 3.0 x 1(Ca) x 2 (charge of Ca^{2+}) = 6

$1.5Al_2O_3$ is charge balanced by $1.5P_2O_5$, and therefore $1.5Al_2O_3$ is available for setting reaction: 1.5 x 2 (Al) x 3 (charge of Al^{3+}) = 9

Therefore, the total number of charges available for the setting reaction is 15.

The molecular weight of a PAA monomer is 72, and there is one carboxylate group in each monomer. Since the glass:PAA ratio is 5:1,

A number of positive charge = (15/1113.15) * 5 = 0.0674

A number of negative charge = (1/72) * 1 = 0.0139

Therefore, the charge ratio, which is the ratio of the cations from the glass and the carboxylate groups of the polymer, for the acid-base reaction = 0.0139/(0.0674-0.0139) = 0.26

3.2.2. GPCs with PgGA

The glasses in the Sr-Zn series were used for the hybrid PgGA-TCA/PAA cements. The same charge ratio, 0.26, used for the PAA based cements, was used. A co-polymer of TCA/PAA was used together with PgGA as it was impossible to form water stable cements when only PgGA was used. The co-polymer of TCA/PAA contained 45wt% TCA and 55wt% PAA. The amount of PgGA and the TCA/PAA co-polymer was varied, and an example of the calculation for glass LPLG26Sr [$4.5SiO_2$. $3.0Al_2O_3$. $0.75P_2O_5$. 3.0SrO. $2.0SrF_2$] is shown below.

Before calculating the required amount of PgGA and the TCA/PAA co-polymer, the amount of the glass and the equivalent amount of PAA, if it was to be used for the PAA cements, had to be calculated. This is because the charge ratio is based on LG26 cements produced with PAA, and glass LG26 contains twice more phosphates than the glasses used for the PgGA cements.

Glass LPLG26Sr is $4.5SiO_2$. $3.0Al_2O_3$. $0.75P_2O_5$. 3.0SrO. $2.0SrF_2$.

Therefore,

LPLG26Sr molecular weight = (4.5 x 60.09) + (3 x 101.96) + (0.75 x 141.94)
+ (3 x 103.62) + (2 x 125.62)
= 1244.84

The positive charges available from glass LPLG26Sr for the acid-base reaction are:

3SrO: 3.0 x 1(Sr) x 2 (charge of Sr^{2+}) = 6

$0.75Al_2O_3$ is charge compensated by $0.75P_2O_5$, and therefore $2.25Al_2O_3$ is available for setting reaction: 2.25 x 2 (Al) x 3 (charge of Al^{3+}) = 13.5

Therefore, the total number of charges available for the setting reaction is 19.5.

The ratio between glasses LG26 and LPLG26Sr for the charge per weight of each glass are (15 / 1113.60) / (19.5 / 1244.84) = 0.86.

Therefore, in order to make 0.6g of the cement, 0.113g of PAA is required for 0.487g of glass LPLG26Sr if it was to be used for the PAA cements. The number of COOH groups in a 0.113g PAA = (1/72) * 0.113 = 1.569 * 10^{-3}.

Molecular weight of a PgGA monomer = 129 (one COOH group per monomer)

Molecular weight of a TCA monomer = 188 (three COOH groups per monomer)

Molecular weight of a PAA monomer = 72 (one COOH group per monomer)

X = amount of TCA/PAA co-polymer in aqueous solution

Y = amount of PgGA

$(Y/125) + [0.45(3X/188) + 0.55(X/72)] = 1.569 * 10^{-3}$

The percentages of the X and Y were varied, and X and Y for each variation were calculated accordingly.

4. Materials and Methods

4.1. Materials

The analytical grade reagents of silica (SiO_2), alumina (Al_2O_3), phosphorus pentoxide (P_2O_5), calcium carbonate ($CaCO_3$), magnesium oxide (MgO), strontium carbonate ($SrCO_3$), zinc oxide (ZnO), calcium fluoride (CaF_2), magnesium fluoride (MgF_2), strontium fluoride (SrF_2), and zinc fluoride (ZnF_2) were obtained from Sigma-Aldrich (UK) and were used for glass making.

The medical grade PAA and the TCA/PAA co-polymer were provided by Advanced Healthcare Ltd (UK) and were used for cement formulation. The weight average molecular weight, Mw, of PAA and the TCA/PAA co-polymer were both around 60,000-80,000 given by the company data sheets using gel permeation chromatography. Distilled water and L-(+)-tartaric acid were also used for cement formulation. Ethanol was used to dehydrate cements. PgGA was bacterially synthesised at the University of Wolverhampton (UK) using *Bacillus licheniformis*. The molecular weight of PgGA was 433,000. Mw was characterised by Smithers Rapra Technology Ltd (UK) using gel permeation chromatography.

4.2. Methods

4.2.1. Glass Synthesis

The reagents were weighed and mixed in a plastic container. The mixed powder was melted in platinum/rhodium crucible in furnace at required temperatures for 1.5 hours. The melt was then poured rapidly into water to prevent crystallisation and amorphous phase separation. The resulting frit was dried overnight in an oven at 100^{o}C, and 100g

of the dried frit was ground for 14 minutes using Gyro Mill (Glen Creston Gyro Mill, UK). The ground powder was sieved through 38μm sieve to remove any large particles for cement formulation.

4.2.2. Glass Characterisation

A. X-ray Powder Diffraction

Each glass composition was studied using X-ray powder diffractometer (Philips PW1700 series Automated Powder Diffractometer, UK) using Cu K alpha radiation at 40KV / 40mA with a secondary graphite crystal monochromater. The pattern was taken in the 2θ range of 10° to 80° with a step size of 0.04°.

B. MAS-NMR Spectroscopy

The MAS-NMR analysis was performed on the ^{19}F, ^{31}P, ^{27}Al, and ^{29}Si nuclei using MAS-NMR spectrometer: 200MHz for ^{19}F, ^{31}P, and ^{29}Si, and 600MHz for ^{27}Al. The resonance frequencies were 188.3MHz, 80.9MHz, 156.3MHz, and 39.8MHz, and the spinning rates were 11-12kHz, 5kHz, 15kHz, and 4-5kHz for ^{19}F, ^{31}P, ^{27}Al, and ^{29}Si nuclei respectively. The recycle times were 10, 2, 1, and 2 seconds for ^{19}F, ^{31}P, ^{27}Al and ^{29}Si respectively. A 4mm zirconia rotor was used.

C. Differential Scanning Calorimetry

The glass transition temperatures, T_g, and the first and the second crystallisation temperatures, T_{c1} and T_{c2} respectively, of each glass produced were determined by using differential scanning calorimetry, DSC (Polymer Laboratories Thermal Sciences, Main Package V.4.30, UK). Platinum crucibles were used, and alumina was

the reference material. The measurements were performed up to 1350^{o}C with a heating rate of 10^{o}C minute^{-1}, and particle sizes <38μm and >38μm were analysed on DSC to determine the mechanism of nucleation, either surface or bulk nucleation.

4.2.3. Synthesis of GPCs

GPCs were produced by mixing the required amount of glass, acid, and distilled water with 10wt% L-(+)-tartaric acid. The acid concentration was 50% in all the cements studied.

4.2.4. Characterisation of GPCs

A. Aging Study

GPCs were prepared by mixing the required amount of glass, PAA, and distilled water with 10wt% L-(+)-tartaric acid. The cements with setting time less than 1 hour were put into a 37^{o}C oven for a required time and were quenched with liquid nitrogen and dehydrated with ethanol [31]. The cements with setting times longer than 1 hour were left in the 37^{o}C oven for 1 hour and then were stored in distilled water at 37^{o}C for a required amount of setting time. The termination of the setting reaction was, again, by dehydration with ethanol. The cements were ground using Gyro Mill to fine powder for MAS-NMR analysis. ^{19}F, ^{31}P, and ^{27}Al MAS-NMR were run on the aging cements using the same procedure as the characterisation of glasses by MAS-NMR spectroscopy.

B. Working and Setting Times

The working and the setting times of cements were determined by using an oscillating rheometer at 37^{o}C +/-3^{o}C. There are two plates in the oscillating rheometer, one oscillating and one fixed. As soon as the glass, PAA and water were mixed together, the oscillating rheometer was switched on. When the mixing was complete, the cement was transferred to between the two plates. As the setting of the cement proceeds, the movement of the oscillating plate will gradually slow down until it stops (Figure 4.1, left)

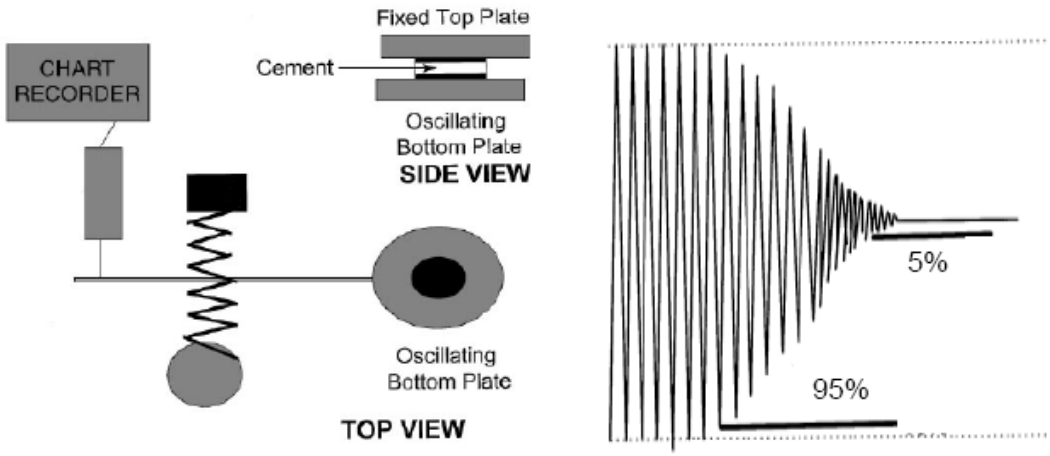


Figure 4.1. Schematic of an oscillating rheometer (left) and a typical trace of the oscillating rheometer (right), after Griffin and Hill [5].

The working and the setting times were taken as the time it takes for the amplitude of the oscillation to fall to 95% and 5%, respectively, of the original value (Figure 4.1, right)

C. Radiopacity

The thoroughly hand mixed cements were placed into the mould and were put into an oven at 37^{o}C for 1 hour. The cement disks were placed onto the X-ray film with an aluminium step wedge with equally spaced steps of 0.5mm (0.5mm-2.5mm) and were radiated with 70KVp X-rays with the exposure time of 0.7 second. After irradiation, the film was developed using an X-ray film processor (Velopex Intra-X). The films were then scanned, and with imaging software (Adobe Photoshop version 9.0), the mean luminosity values for each thickness of the aluminium step wedge were evaluated and used to calibrate the luminosity values for the cement disks. The radiopacity of the cement disks was determined in terms of the thickness of the aluminium step wedge.

D. Compressive Strength

The cement mixture was packed into a PMMA mould with 6mm height and 4mm diameter. The cement was allowed to set in an oven at 37^{o}C for 1 hour. After 1 hour, the cement was transferred into distilled water and stored in an oven at 37^{o}C for 1 and 7 days for compressive strength measurement. The measurement was performed using Zwick Roell Z010 (Zwick Roell AG, Germany) with a 10kN load cell. The test was run with no preload, and eight specimens were run for each composition. The maximum value for the stress was taken as the compressive strength of the specimen.

E. Fluoride Release

A required amount of glass, polymeric acid, and distilled water with 10wt% L-(+)-tartaric acid were mixed and poured into PMMA moulds with 6mm height by 4mm diameter. Four cylinders for each composition were produced for statistical analysis. The moulds with cement mix were stored in the 37^{o}C oven for 1 hour. Each cylinder was put into 10ml deionised water in a plastic container and was kept in the 37^{o}C oven until the measurement. The measurements were done at 1, 3, 7, 14, 21, 28, 42, and 56 days. For measurement, 5ml deionised water from the plastic container was mixed with 5ml total ionic strength adjustment buffer, TISAB, solution to de-complex any fluoride attached to aluminium. The concentration of F^- was measured with fluoride electrode.

F. Adhesion (PgGA cements only)

The weighed amount of glass powder, PgGA, the TCA/PAA co-polymer, and distilled water with 10wt% L-(+)-tartaric acid, were mixed for 30 seconds. Then the mixture was transferred onto a specimen, either bovine enamel, bovine dentine, or stainless steel, and an orthodontic bracket was put onto the cement. A 100g weight was put onto the bracket for 1.5 minutes, and the specimen was put into the 37^{o}C oven for 1 hour. Then, the specimen was stored in distilled water at the 37^{o}C oven for further 23 hours prior to testing. All brackets and stainless steel were polished with silicon carbide paper with 600 grit paper and were cleaned with acetone for de-greasing beforehand. The specimen was clamped with a nylon thread going through the orthodontic bracket, and the nylon thread was pulled off using the Instron 5567

(Instron Ltd, UK) with a speed of 5mm min^{-1} and a 100N load cell to measure the tensile bond strength (Figure 4.2).

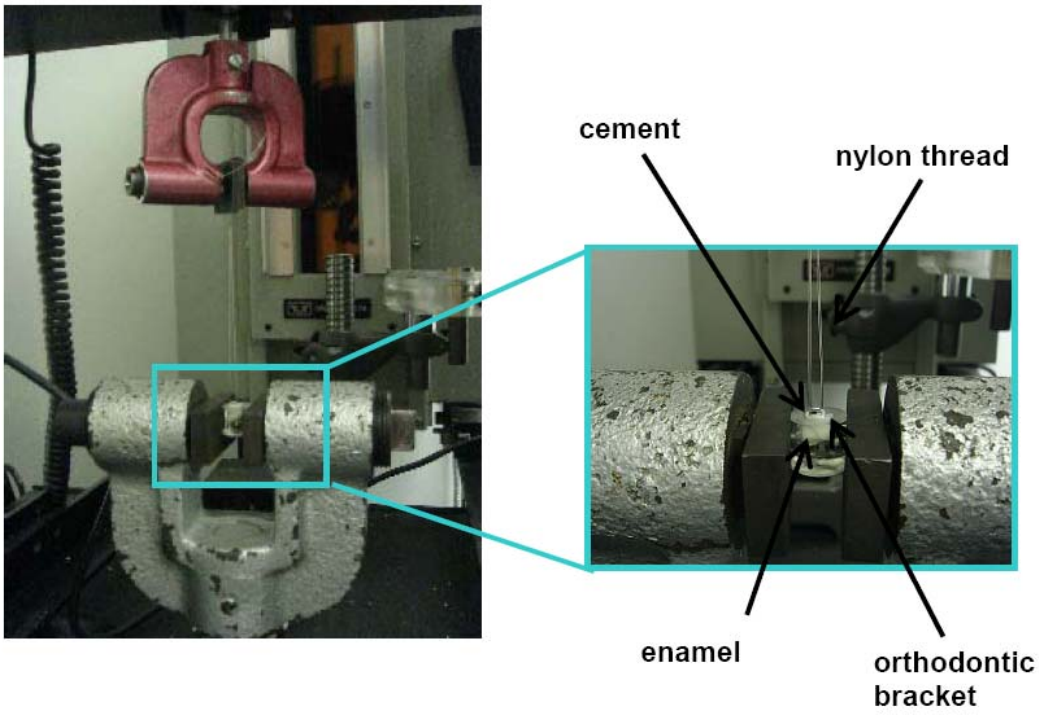


Figure 4.2. Apparatus for adhesion measurement.

5. Results and Discussion

Part I. Characterisation of Mg, Sr, and Zn containing Fluoro-Aluminosilicate Glasses

5.1. XRD Analysis

5.1.1. Ca-Mg Series

[$4.5SiO_2$. $3.0Al_2O_3$. $1.5P_2O_5$. $(3.0-x)CaO$. $xMgO$. $(2.0-y)CaF_2$. $yMgF_2$]

Amorphous structure of all glasses in the Ca-Mg series was confirmed by XRD as all glasses showed typical amorphous halo (Figure 5.1). The amorphous halo shifted towards lower 2θ value as calcium was substituted by magnesium. The Bragg's equation, $n\lambda=2d\sin\theta$, where n is an integer, λ is the wavelength of the radiation, d is the distance between the inter-atomic planes, and θ is the diffracted angle, describes the relationship between the distance between the inter-atomic plane and the diffracted angle [51]. Therefore, a decrease in the distance between the inter-atomic planes should increase the angle of diffraction. The ionic radius of Mg^{2+} is smaller than that of Ca^{2+}, 0.78Å for Mg^{2+} and 1.06Å for Ca^{2+} [52], and therefore, it was expected that the diffracted angle would increase with magnesium substitution. However, results show that the average distance has increased, and the largest change was seen for the fully magnesium substituted glass ICHK07 (Figure 5.1). Although the cause of this phenomenon needs further investigation, the expansion of the network with magnesium substitution may be related to the preferential formation of F-Mg(n) species shown on the ^{19}F MAS-NMR (Figure 5.4). These F-Mg(n) species

are not part of the glass network and hence may contribute to the increase in the distance between the inter-atomic planes.

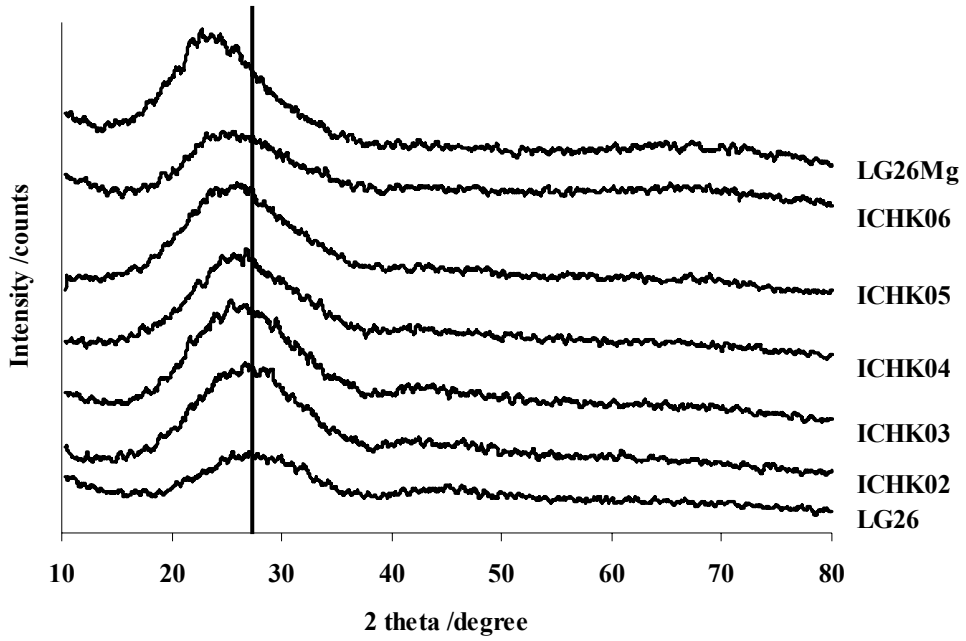


Figure 5.1. XRD patterns for the glasses in the Ca-Mg series [4.5SiO_2. 3.0Al_2O_3. 1.5P_2O_5. (3.0-x)CaO. xMgO. (2.0-y)CaF_2. yMgF_2]. The vertical line is a guide to eye only.

5.1.2. Sr-Mg Series

[4.5SiO_2. 3.0Al_2O_3. 1.5P_2O_5. (3.0-x)SrO. xMgO. (2.0-y)SrF_2. yMgF_2]

All the glasses in the Sr-Mg series were found to be amorphous by XRD (Figure 5.2). Similar to the glasses in the Ca-Mg series, the substitution of strontium by magnesium resulted in a shift of the amorphous halo towards lower 2θ values, indicating an increase in the distance between inter-atomic planes. Again, Mg^{2+} is a smaller cation, and therefore the distance between the inter-atomic planes was expected to decrease. Again, this increase in the distance between the inter-atomic plane may be related to the preferential formation of F-Mg(n) species with magnesium substitution for strontium shown on the ^{19}F MAS-NMR (Figure 5.5).

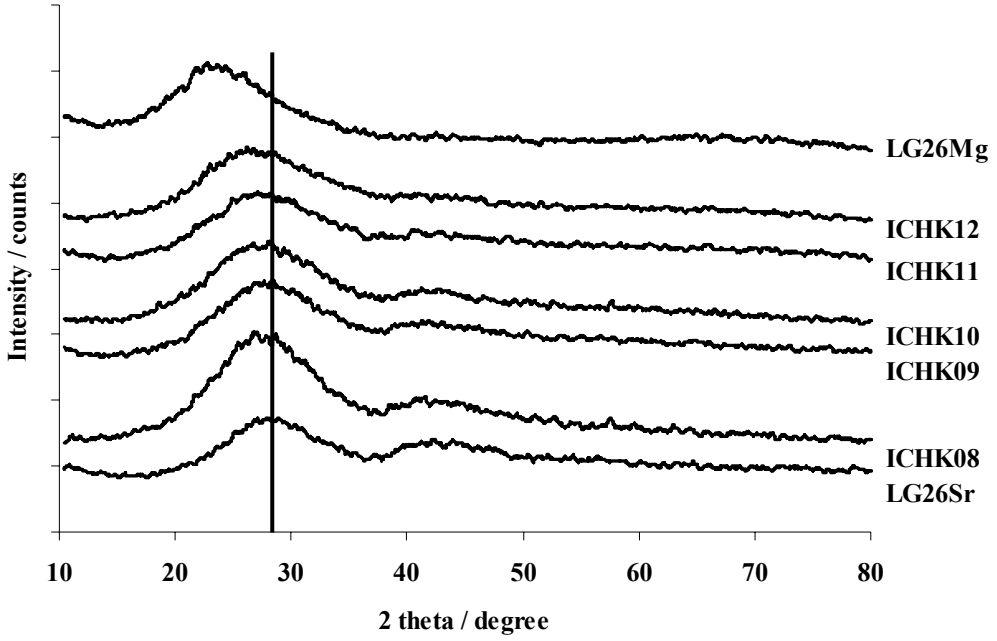


Figure 5.2. XRD patterns for the glasses in the Sr-Mg series [4.5SiO_2. 3.0Al_2O_3. 1.5P_2O_5. (3.0-x)SrO. xMgO. (2.0-y)SrF_2. yMgF_2]. The vertical line is a guide to eye only.

5.1.3. Ca-Zn Series

[4.5SiO_2. 3.0Al_2O_3. 1.5P_2O_5. (3.0-x)CaO. xZnO. (2.0-y)CaF_2. yZnF_2]

All the glasses, apart from LG26Zn, in the Ca-Zn series, were determined to be amorphous by XRD (Figure 5.3). There is a slight shift of the amorphous halo towards lower 2θ values as zinc is substituted for calcium in the Ca-Zn series, but the shift is not as pronounced as for the Ca-Mg and the Sr-Mg series. Glass LG26Zn was shown to contain some crystalline region by XRD, but it was not possible to identify the crystal phases as there are few possibilities. However, ^{27}Al MAS-NMR for glass LG26Zn (Figure 5.17), which will be discussed in more details in the Section 5.4.3, exhibited a very sharp peak at around 15ppm, and this peak on the ^{27}Al MAS-NMR may result from the crystalline nature shown on the XRD (Figure 5.3) indicating that the crystalline region is rich in aluminium.

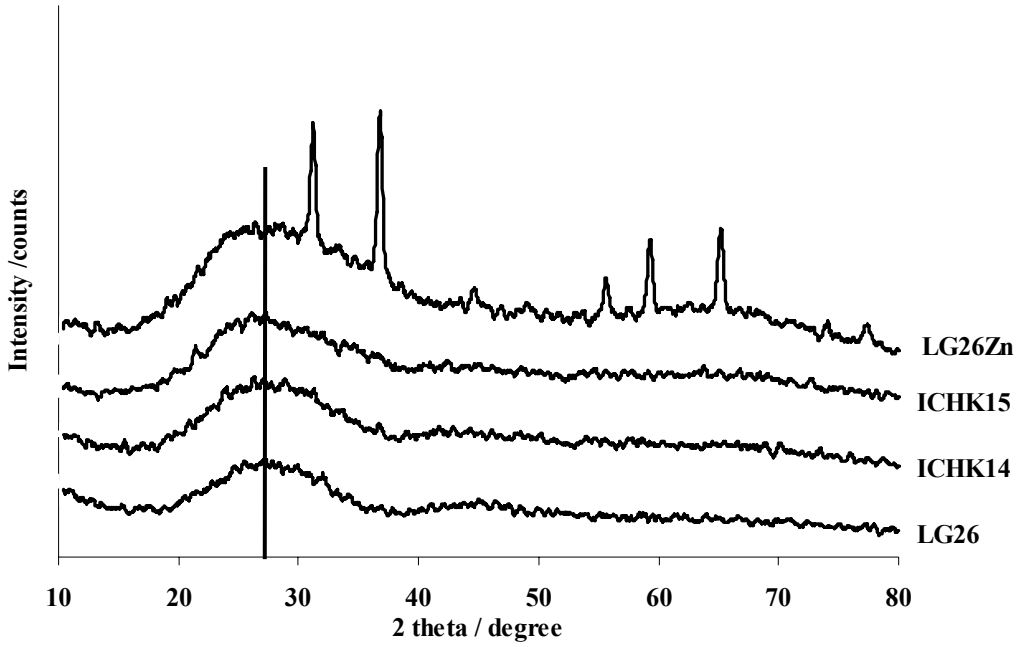


Figure 5.3. XRD patterns for the glasses in Ca-Zn series [4.5SiO_2. 3.0Al_2O_3. 1.5P_2O_5. (3.0-x)CaO. xZnO. (2.0-y)CaF_2. yZnF_2]. The vertical line is a guide to eye only.

5.2. ^{19}F MAS-NMR Spectroscopy

5.2.1. Ca-Mg Series

[4.5SiO_2. 3.0Al_2O_3. 1.5P_2O_5. (3.0-x)CaO. xMgO. (2.0-y)CaF_2. yMgF_2]

^{19}F MAS-NMR spectra for the glasses in the Ca-Mg series are shown (Figure 5.4). Glass LG26 exhibited two peaks approximately at -98ppm and -159ppm which have been assigned to F-Ca(n) and Al-F-Ca(n) species respectively: F-Ca(n) species contains fluorine in a close proximity to calcium and is not part of the glass network, and fluorine in Al-F-Ca(n) species is attached to Al in the glass network and is in a close proximity to calcium as well [20, 26]. The F-Ca(n) peak starts to disappear with glass ICHK03 containing 10.7mol% Mg, and ^{19}F MAS-NMR spectra for higher magnesium substituted glasses start to consist of only one peak. The peak for glasses ICHK03 and ICHK04 is found at around -160ppm, which have been assigned to Al-F-Ca(n) species. This peak is asymmetrical and contains a shoulder at around -180ppm. In the higher magnesium substituted glasses, the large peak moves to a more negative chemical shift, away from 0ppm, to around -180ppm. In the LG26-based glasses [4.5SiO_2. 3.0Al_2O_3. 1.5P_2O_5. (3.0-x)CaO. xMgO. (2.0-y)CaF_2. yMgF_2], there are 6mol of Al^{3+} and 3mol of P^{5+}. These form three Al-O-PO_3^{3-} species to compensate the charge deficient Al^{3+} ions by P^{5+} ions [20] leaving 3mol Al^{3+} which need to be charge balanced by available Ca^{2+} or Mg^{2+} ions. Each Al-O-PO_3^{3-} species will require 1.5 divalent cations to charge balance the NBOs on phosphorus, and each Al^{3+} will require 0.5 divalent cations. When these are taken into consideration, there are enough Ca^{2+} ions in the glass ICHK03 and just enough in the glass ICHK04 to form Al-F-Ca(n) species.

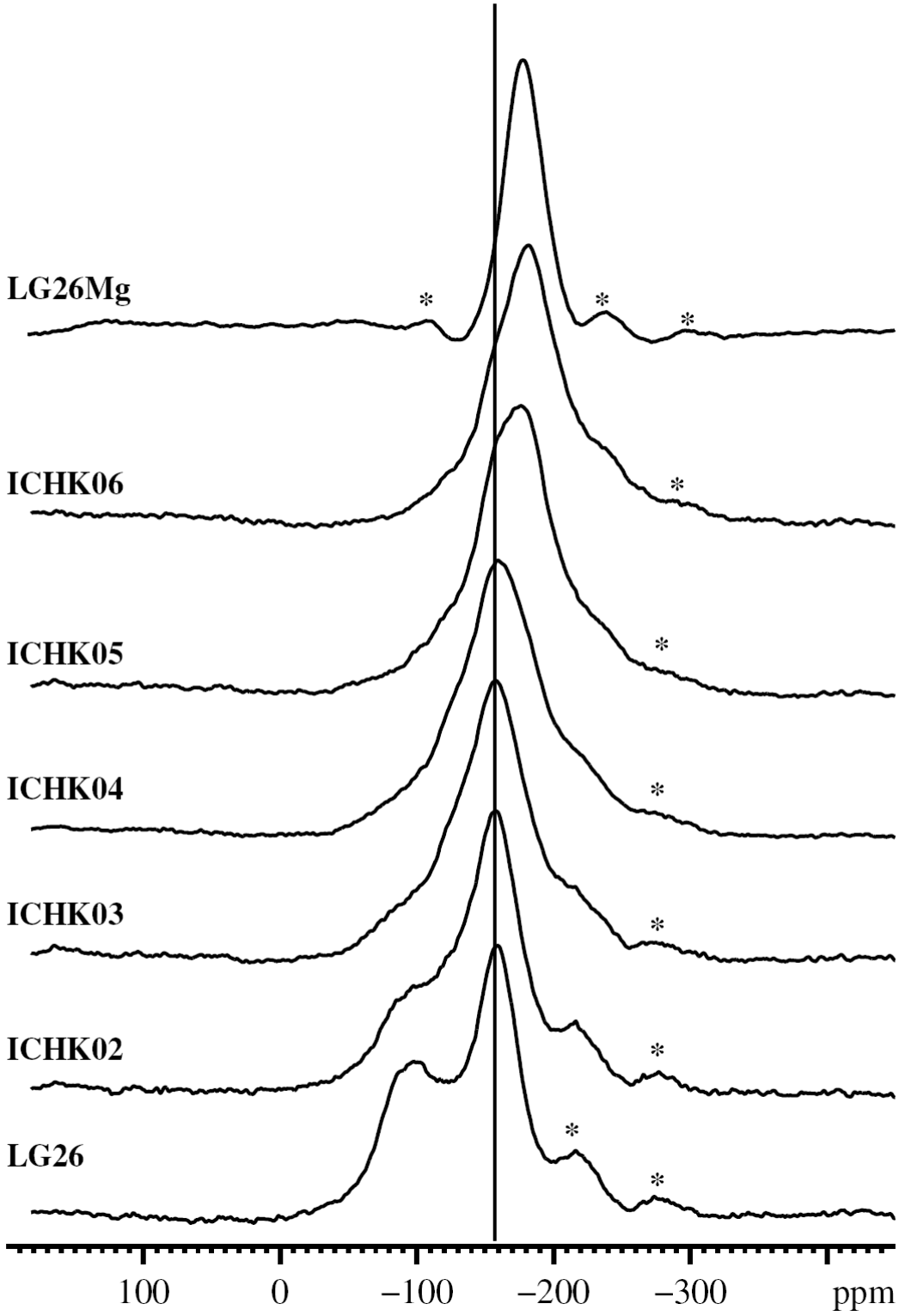


Figure 5.4. ^{19}F MAS-NMR spectra for the glasses in the Ca-Mg series [$4.5SiO_2$. $3.0Al_2O_3$. $1.5P_2O_5$. (3.0-x)CaO. xMgO. (2.0-y)CaF_2. yMgF_2]. Spinning sidebands are marked by asterisks, and the vertical line is a guide to eye only.

The largest transition in chemical shift occurs between glasses ICHK04 and ICHK05, from around -160ppm to -176ppm (Figure 5.4). This clearly indicates a structural change. The peak at around -176ppm has been assigned to F-Mg(n) species, with n close to three, showing that there are possibly three Mg surrounding F with the octahedral coordination of magnesium [53, 54]. F-Mg(n) species are not part of the glass network, and therefore, it is very unlikely that the magnesium coordination will be less than six. If magnesium forms a glass network, such as SiO_2, then, the coordination number of magnesium will be four. However, ^{19}F MAS-NMR of magnesium containing fluoro-aluminosilicate glasses (Figure 5.4) have shown a preferential formation of F-Mg(n) species, especially with the fully magnesium substituted glass. Therefore, for the glasses studied here, it is very unlikely that magnesium coordination becomes less than six. The F-Mg(n) peaks for both ICHK05 and ICHK06 contain shoulder which may result from the Al-F-Ca(n) species. The fact that F-Mg(n) species are solely formed may indicate that F^- attaches preferentially to Mg^{2+} rather than Al, and similar observation was reported by Labouriau [55]. F-Mg(n) species are probably favoured by the higher charge to size ratio of Mg^{2+} relative to Ca^{2+} as Stebbins and Zeng [56] suggested that fluorine preferentially attaches to cations of the highest charge to size ratio.

5.2.2. Sr-Mg Series

[4.5SiO_2. 3.0Al_2O_3. 1.5P_2O_5. (3.0-x)SrO. xMgO. (2.0-y)SrF_2. yMgF_2]

Glass LG26Sr showed two peaks approximately at -62ppm and -156ppm (Figure 5.5), and these peaks have been assigned to F-Sr(n) and Al-F-Sr(n) species, respectively [20]. The chemical shift for F-Sr(n) species in the fully strontium substituted glass LG26Sr is less negative than for F-Ca(n) species, -98ppm (Figure 5.4) in the fully calcium substituted glass LG26. According to Bureau and co-workers [57], the increase in the chemical shift from F-Ca(n) to F-Sr(n) species is due to an increase in the distance between the divalent cation and F^-, and the chemical shift generally increases down Groups I and II in the periodic table. Therefore, Sr^{2+} being slightly larger has resulted in the chemical shift for F-Sr(n) species being shifted to a more positive value.

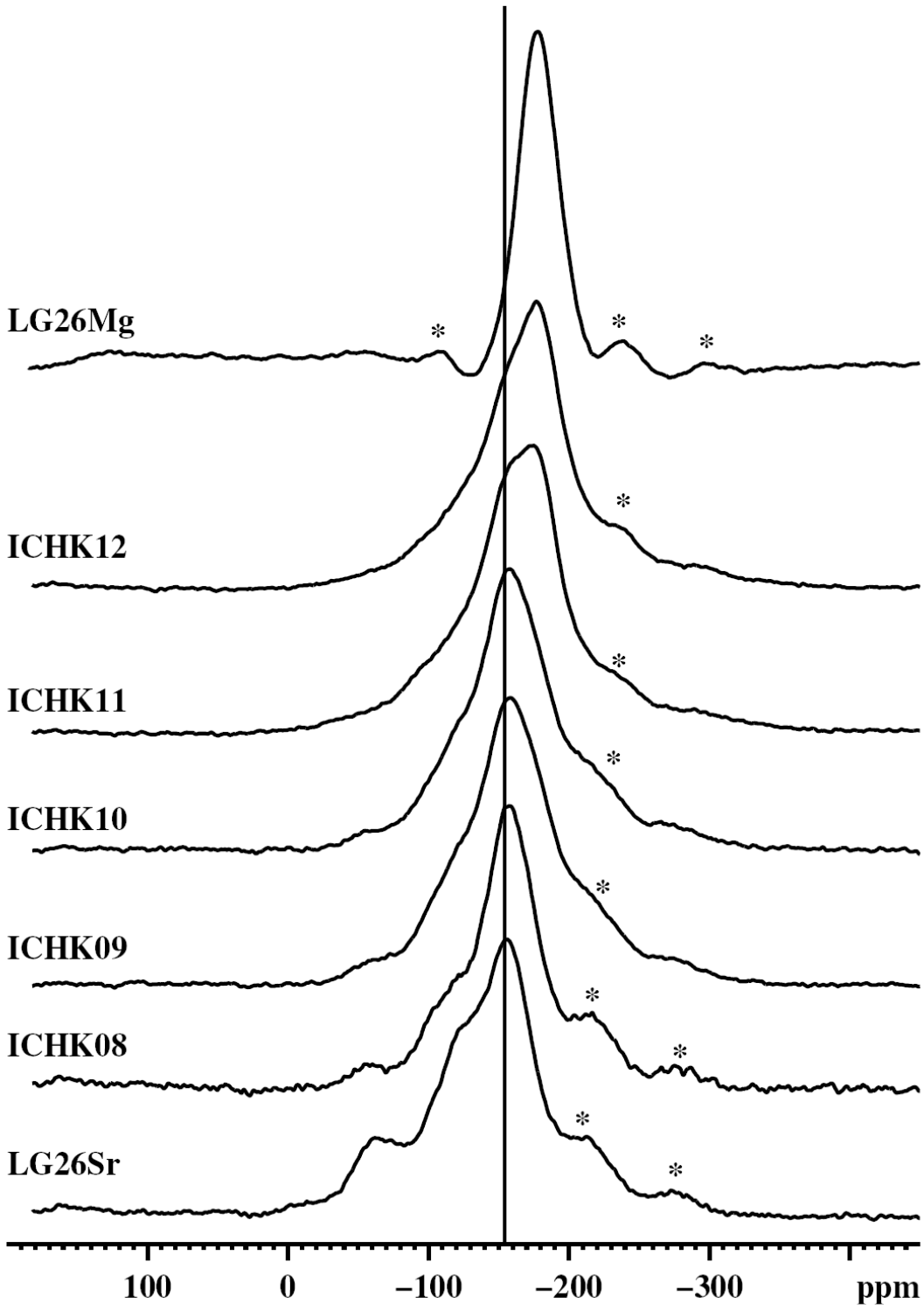


Figure 5.5. ^{19}F MAS-NMR spectra for the glasses in the Sr-Mg series [4.5SiO_2. 3.0Al_2O_3. 1.5P_2O_5. (3.0-x)SrO. xMgO. (2.0-y)SrF_2. yMgF_2]. Spinning sidebands are marked by asterisks, and the vertical line is a guide to eye only.

The F-Sr(n) peak starts to disappear as soon as the magnesium substitution for strontium occurs with glass ICHK08. Glass ICHK02 in the Ca-Mg series and glass ICHK08 in the Sr-Mg series both contain the same amount of magnesium. However, the F-Sr(n) peak for ICHK08 (Figure 5.5) is much smaller than the F-Ca(n) peak for ICHK02 (Figure 5.4). This suggests that Mg^{2+} takes F^- away from Sr^{2+} in the Sr-Mg series more efficiently than Ca^{2+} in the Ca-Mg series, which may be due to Sr^{2+} being a larger cation than Ca^{2+} and having a lower charge to size ratio.

Once the F-Sr(n) peak disappears upon the magnesium substitution, the Al-F-Sr(n) peak dominates the ^{19}F MAS-NMR spectra up to glass ICHK10 (Figure 5.5). This trend is quite similar to the glasses in the Ca-Mg series (Figure 5.4): the largest shift seems to occur when the magnesium content increases from 14.3mol% (ICHK10) to 21.4mol% (ICHK11). The dominant peaks for glasses ICHK11, ICHK12, and LG26Mg, all at around -175ppm/-179ppm, have been assigned to F-Mg(n) species with the number of Mg around F close to three [54, 57]. These results show that calcium and strontium behave similarly in fluoro-aluminosilicate glasses.

Especially with LG26Sr, there is a shoulder at around -130ppm. This peak has been observed in other studies and has been attributed to F attached to Al in Al-O-PO_3^{3-} species (Figure 5.6) [58].

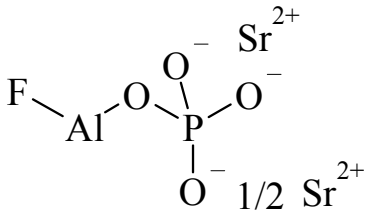


Figure 5.6. Schematic of F attached to Al in Al-O-PO_3^{3-} species.

5.2.3. Ca-Zn Series

[4.5SiO_2. 3.0Al_2O_3. 1.5P_2O_5. (3.0-x)CaO. xZnO. (2.0-y)CaF_2. yZnF_2]

As mentioned previously, glass LG26 showed two peaks in the ^{19}F MAS-NMR spectrum (Figure 5.4, Figure 5.7): -99ppm for F-Ca(n) and -156ppm for Al-F-Ca(n) species. The substitution of zinc for calcium seems to have resulted in a slightly less intense peak for F-Ca(n) species, especially when LG26 and ICHK15 are compared (Figure 5.7). This reduction in F-Ca(n) species was also seen for glasses in the Ca-Mg series (Figure 5.4). Therefore, in both Ca-Mg and Ca-Zn series, F-Ca(n) species becomes reduced as soon as calcium is substituted by other divalent cations, Mg^{2+} and Zn^{2+}. The charge to size ratio of Zn^{2+} and Mg^{2+} is quite similar having similar ionic radii: 0.78Å for Mg^{2+} and 0.83Å for Zn^{2+} [52]. Both Zn^{2+} and Mg^{2+} seem to take F^- away from Ca^{2+} very efficiently.

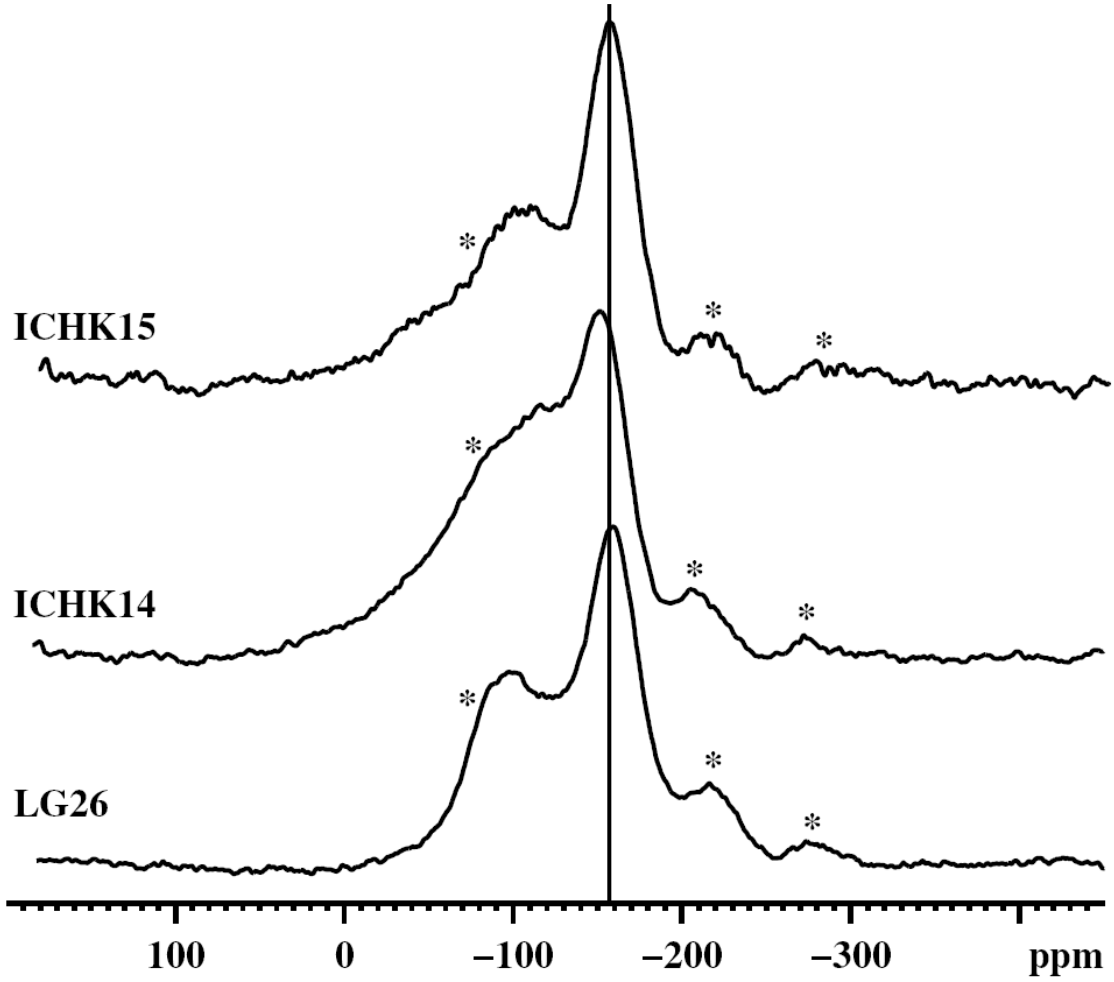


Figure 5.7. ^{19}F MAS-NMR spectra for the glasses in the Ca-Zn series [4.5SiO_2. 3.0Al_2O_3. 1.5P_2O_5. (3.0-x)CaO. xZnO. (2.0-y)CaF_2. yZnF_2]. Spinning sidebands are marked by asterisks, and the vertical line is a guide to eye only.

The zinc substitution for calcium does not seem to have much influence on Al-F-Ca(n) species (Figure 5.7). The chemical shift becomes slightly less negative as the substitution proceeds, -152ppm for ICHK14 and -153ppm for ICHK15, but the difference in the chemical shift is too small to suggest any structural changes upon the substitution. However, glass ICHK05 in the Ca-Mg series, which has the same magnesium content as the zinc content in glass ICHK15, exhibited only one peak at -176ppm assigned to F-Mg(n) species (Figure 5.4). The chemical shift for F-Zn(n)

species has been shown to occur at -196ppm [57], and neither ICHK14 nor ICHK15 exhibited a peak with this chemical shift value. Therefore, this clearly suggests that magnesium and zinc behave differently in glass compositions although they have quite similar charge to size ratio.

5.3. ^{31}P MAS-NMR Spectroscopy

5.3.1. Ca-Mg Series

[4.5SiO_2.3.0Al_2O_3. 1.5P_2O_5. (3.0-x)CaO. xMgO. (2.0-y)CaF_2. yMgF_2]

Glass LG26 gave a single peak approximately at -8ppm (Figure 5.8), which has been assigned to Q^1 pyrophosphate Al-O-PO_3^{3-} species, and NBOs on phosphorus are charge balanced by Ca^{2+} [23-25].

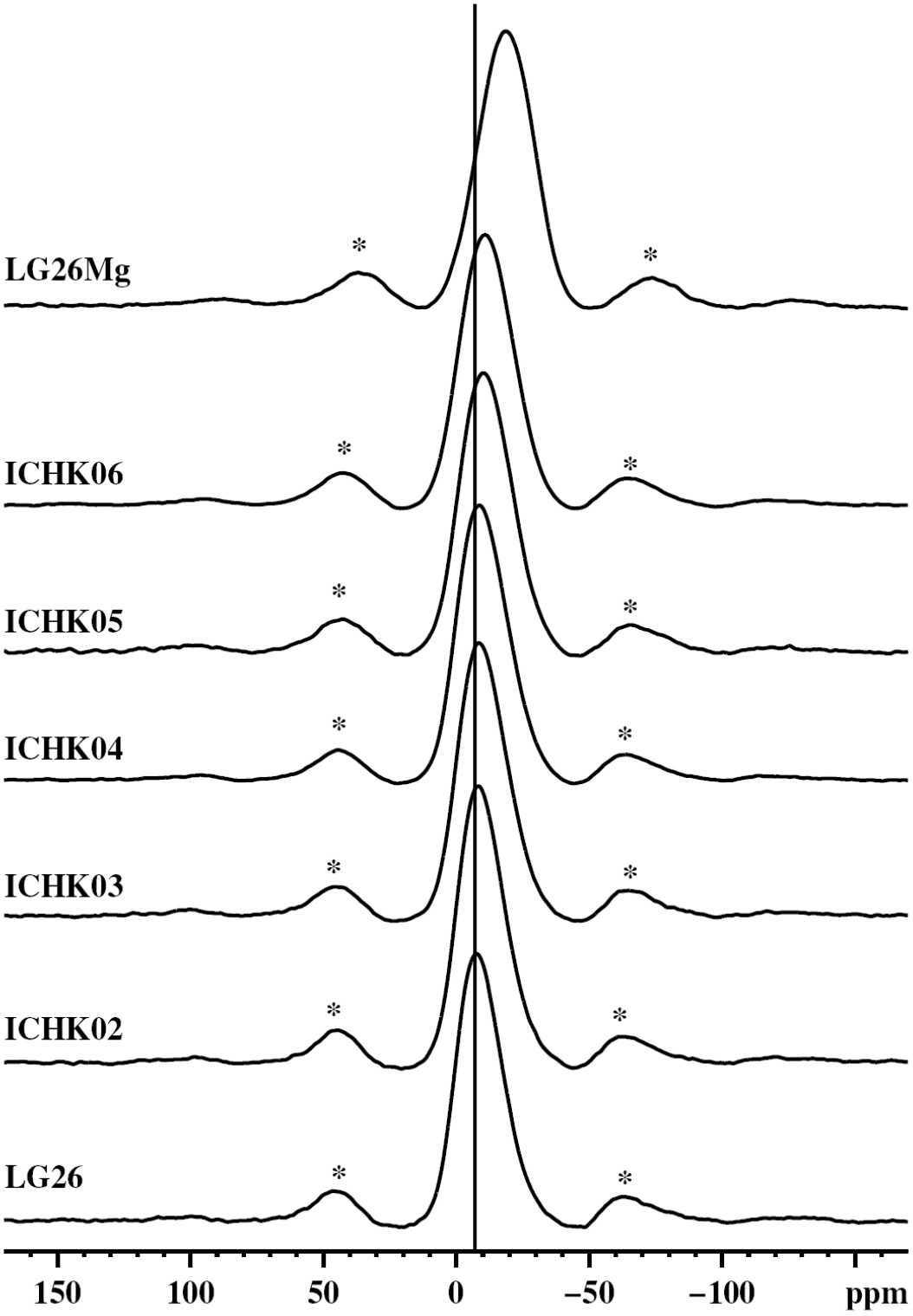


Figure 5.8. ^{31}P MAS-NMR spectra for the glasses in the Ca-Mg series [4.5SiO_2. 3.0Al_2O_3. 1.5P_2O_5. (3.0-x)CaO. xMgO. (2.0-y)CaF_2. yMgF_2]. Spinning sidebands are marked by asterisks, and the vertical line is a guide to eye only.

As calcium is substituted by magnesium, the chemical shift becomes more negative, moving away from 0ppm (Figure 5.8). Brow and co-workers [59] measured the ^{31}P chemical shift for calcium metaphosphate, $Ca(PO_3)_2$, and magnesium metaphosphate, $Mg(PO_3)_2$, and the difference in the chemical shift between the two phosphate species is around 5ppm. The value indicated by a circle (○) in Figure 5.9 was calculated for glass LG26Mg using this value, assuming that the effects of Mg^{2+} and Ca^{2+} ions on the chemical shift of pyrophosphate and metaphosphate species are similar. The diamonds (♦) indicate the experimental chemical shift. If this calculated chemical shift is taken into consideration, for glass LG26, rather than the experimental value, there is a linear relationship between the magnesium content and ^{31}P chemical shift (Figure 5.9). This could indicate that when both Mg^{2+} and Ca^{2+} ions are present in the glass composition, both ions charge balance NBOs on phosphorus in Al-O-PO_3^{3-} species.

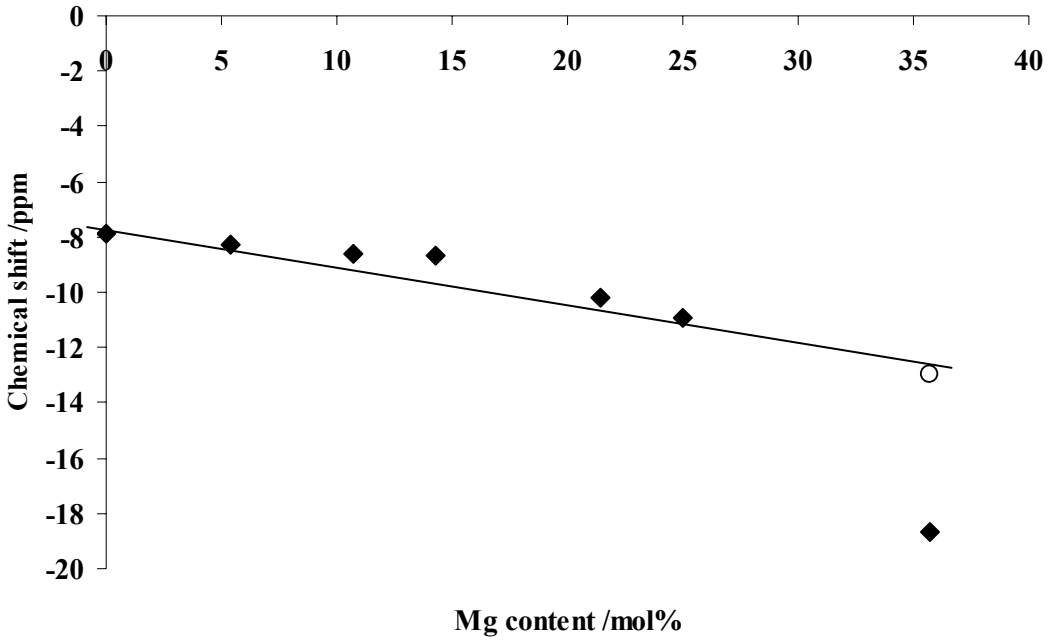


Figure 5.9. Chemical shift in ^{31}P MAS-NMR spectra against Mg content in mol% for the glasses in the Ca-Mg series [4.5SiO_2. 3.0Al_2O_3. 1.5P_2O_5. (3.0-x)CaO. xMgO. (2.0-y)CaF_2. yMgF_2]. The diamond (♦) is the experimental chemical shift, and the circle (○) is the calculated chemical shift for glass LG26Mg. The line is a guide to eye only.

However, the chemical shift of glass LG26Mg was observed at -19ppm, outside of the linear relationship between the chemical shift and magnesium content, and it is too negative for Q^1 pyrophosphate Al-O-PO_3^{3-} species charge balanced by Mg^{2+}: the calculated chemical shift for Al-O-PO_3^{3-} species charge balanced solely by Mg^{2+} is around -13ppm. Moreover, the peak width increases with magnesium substitution with glass LG26Mg having the widest peak in the series (Figure 5.8). It is possible that when magnesium fully substituted calcium in glass LG26Mg, magnesium pyrophosphate, $Mg_2P_2O_7$, is formed (Figure 5.10). It has been shown that there are two phosphorus sites in crystalline α-$Mg_2P_2O_7$ [60], and these sites have chemical shifts at -13ppm and -20ppm in ^{31}P MAS-NMR [18]. The chemical shift for

amorphous α-$Mg_2P_2O_7$ is less negative, at -12ppm and -19ppm [61]. Therefore, the observed chemical shift at -19ppm for glass LG26Mg is in good agreement with published studies.

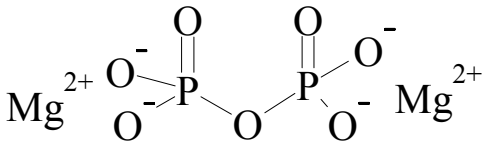


Figure 5.10. Schematic of magnesium pyrophosphate.

Moreover, the fact that glass LG26Mg exhibited a broader peak than the other glasses could indicate the presence of mixed species, such as a mixture of Q^1 pyrophosphate Al-O-PO_3^{3-} species charge balanced by Mg^{2+} and magnesium pyrophosphate, $Mg_2P_2O_7$.

Alternatively, there could be a formation of P-O-Mg bonds implying that magnesium is part of the glass network. It has been shown that phosphorus can take the charge balancing cations from silicon in glasses which contain phosphorus and silicon and no aluminium. This will increase the polymerisation of the silicate network as no charge balancing cations will be available to form NBOs on Si [62]. The formation of P-O-Mg is less likely compared to the formation of magnesium pyrophosphate (Figure 5.10) as glass LG26Mg contains aluminium, and P^{5+} is known to compensate the charge deficiency of Al^{3+}. However, ^{29}Si MAS-NMR, which will be discussed in more details in Section 5.5, have shown an increased polymerisation with LG26Mg, and therefore, the formation of P-O-Mg is a possibility.

5.3.2. Sr-Mg Series

[4.5SiO_2. 3.0Al_2O_3. 1.5P_2O_5. (3.0-x)SrO. xMgO. (2.0-y)SrF_2. yMgF_2]

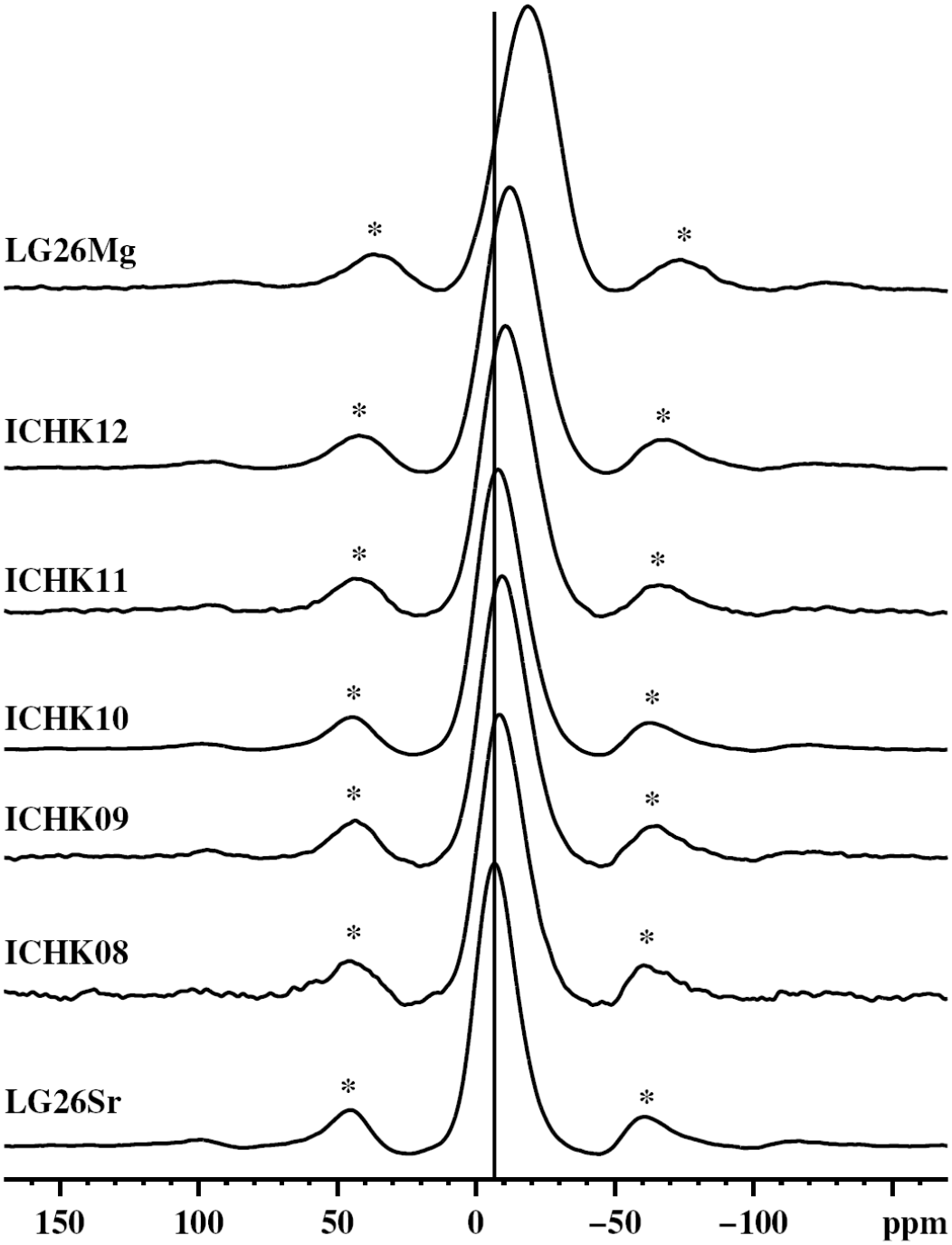


Figure 5.11. ^{31}P MAS-NMR spectra for the glasses in the Sr-Mg series [4.5SiO_2. 3.0Al_2O_3. 1.5P_2O_5. (3.0-x)SrO. xMgO. (2.0-y)SrF_2. yMgF_2]. Spinning sidebands are marked by asterisks, and the vertical line is a guide to eye only.

Glass LG26Sr exhibited a peak at -7ppm (Figure 5.11), and this peak has been assigned to Q^1 pyrophosphate Al-O-PO_3^{3-} species with NBOs on phosphorus charge balanced by Sr^{2+} [20]. This chemical shift is more positive than the calcium only glass, LG26, at -8ppm (Figure 5.8). Hill and co-workers [20] studied the same compositions and did not observe any change in the chemical shift with strontium substitution for calcium. However, a more recent study by Zainuddin [19] showed the chemical shift for LG26Sr being slightly more positive, towards 0ppm, than LG26. She suggested that this may be because of slight differences in the field strengths of Sr^{2+} and Ca^{2+}.

The chemical shift gradually moves to a more negative value, away from 0ppm, as substitution proceeds in the Sr-Mg series (Figure 5.11). This trend is quite similar to the Ca-Mg series (Figure 5.8). The circle (○) in Figure 5.12 indicates the chemical shift for LG26Mg, calculated using the difference in chemical shift between strontium metaphosphate and magnesium metaphosphate determined by Brow and co-workers [59]. When this calculated chemical shift is taken into account, there is a linear relationship between chemical shift and Mg content, which suggests that both Sr^{2+} and Mg^{2+} are present in charge balancing the NBOs on phosphorus in Al-O-PO_3^{3-} species, as was found in the Ca-Mg series.

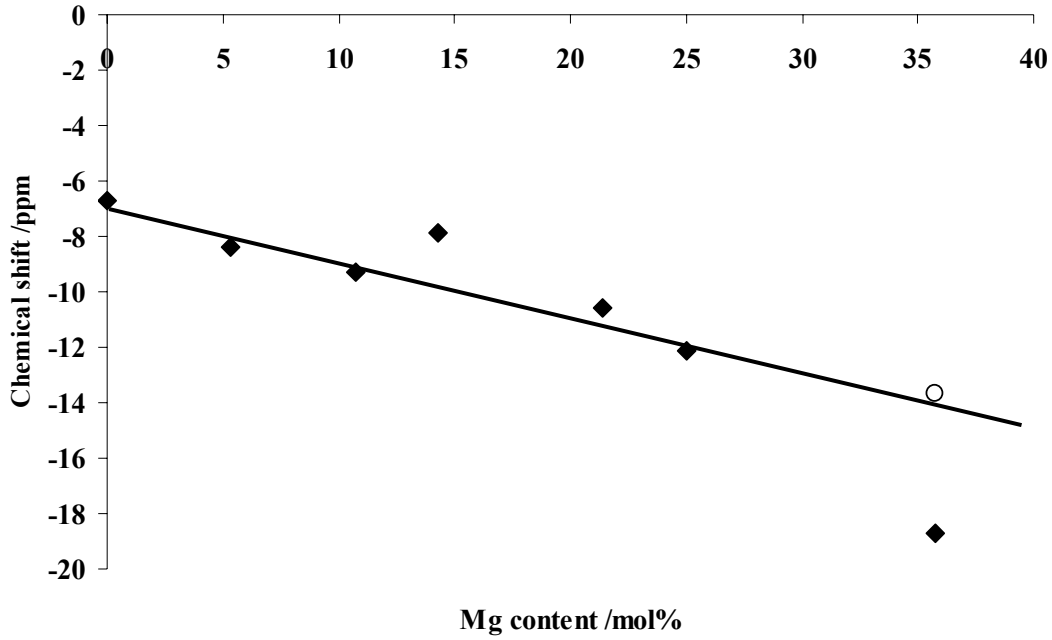


Figure 5.12. Chemical shift in ^{31}P MAS-NMR spectra against Mg content in mol% for the glasses in the Sr-Mg series [4.5SiO_2. 3.0Al_2O_3. 1.5P_2O_5. (3.0-x)SrO. xMgO. (2.0-y)SrF_2. yMgF_2]. The diamond (♦) is the experimental chemical shift, and the circle (○) is the calculated chemical shift for glass LG26Mg. The line is a guide to eye only.

5.3.3. Ca-Zn Series

[4.5SiO_2. 3.0Al_2O_3. 1.5P_2O_5. (3.0-x)CaO. xZnO. (2.0-y)CaF_2. yZnF_2]

The chemical shifts for glasses LG26 and LG26Zn were observed at -8ppm and -15ppm respectively (Figure 5.13). This suggests that the substitution of zinc for calcium in the Ca-Zn series resulted in a more negative chemical shift. This trend is similar to the Ca-Mg series (Figure 5.8). However, different phosphate species may be formed with the fully zinc substituted glass LG26Zn compared to the fully magnesium substituted glass LG26Mg, as discussed in more details below.

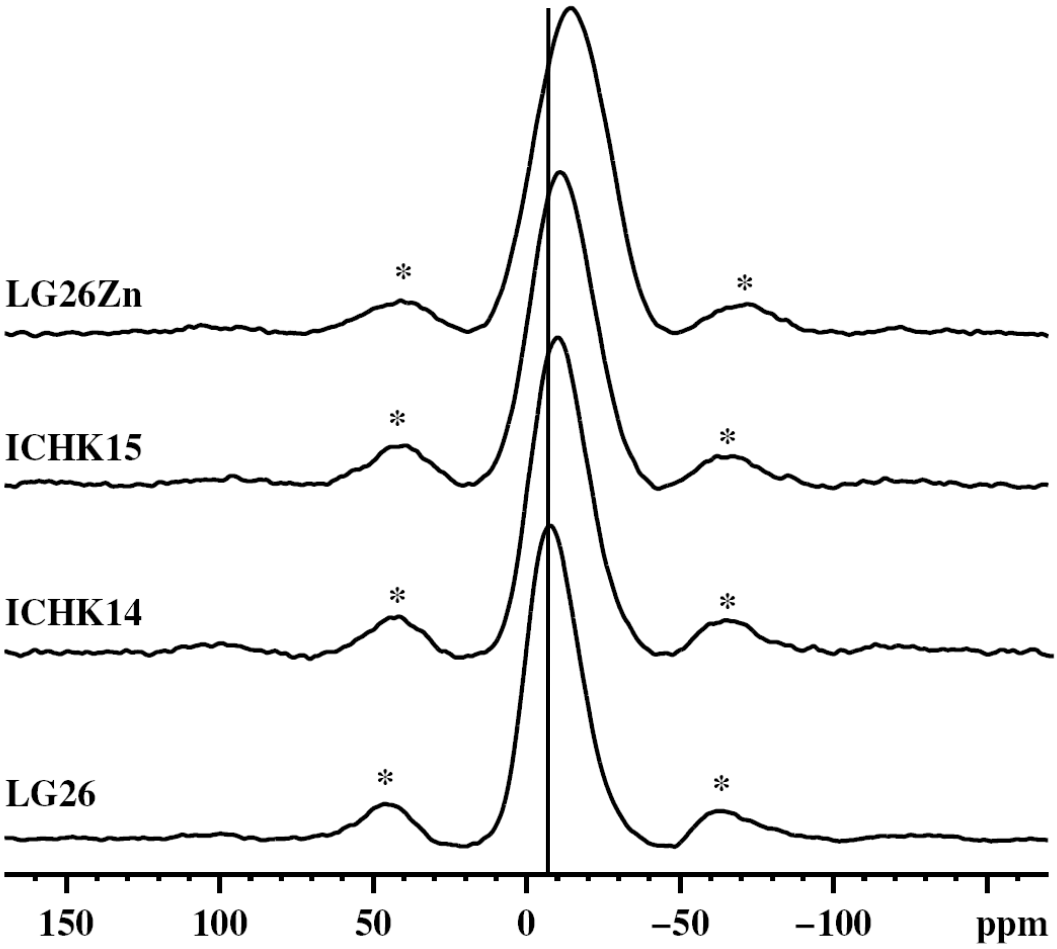


Figure 5.13. ^{31}P MAS-NMR spectra for the glasses in the Ca-Zn series [4.5SiO_2. 3.0Al_2O_3. 1.5P_2O_5. (3.0-x)CaO. xZnO. (2.0-y)CaF_2. yZnF_2]. Spinning sidebands are marked by asterisks, and the vertical line is a guide to eye only.

The chemical shifts in the ^{31}P MAS-NMR spectra and zinc content in mol% have a linear relationship to each other (Figure 5.14) unlike the glasses in the Ca-Mg series (Figure 5.9). Brow and co-workers [59] have shown that the differences in ^{31}P chemical shift for calcium metaphosphate and zinc metaphosphate is about 6ppm. Assuming the influence of different cations on metaphosphate and pyrophosphate species is similar, the chemical shift of LG26Zn was calculated as -14ppm, which is quite similar to the experimental chemical shift, -15ppm. Therefore, these findings may suggest that Zn^{2+} replaces Ca^{2+} in charge balancing Al-O-PO_3^{3-} species (Figure

5.15). In addition to Q^1 pyrophosphate Al-O-PO_3^{3-} species charge balanced by Zn^{2+}, it is possible that there could be a formation of zinc pyrophosphate, $Zn_2P_2O_7$, whose ^{31}P chemical shift has been shown to occur at around -11ppm by Kirkpatrick and Brow [62]. They suggested that if P_2O_5 can take away charge balancing cations from Si to form depolymerised phosphate species increasing the polymerisation of silicate network. ^{29}Si MAS-NMR, which will be discussed in more details in Section 5.5.3, has shown an increased polymerisation of silicate network with zinc substitution.

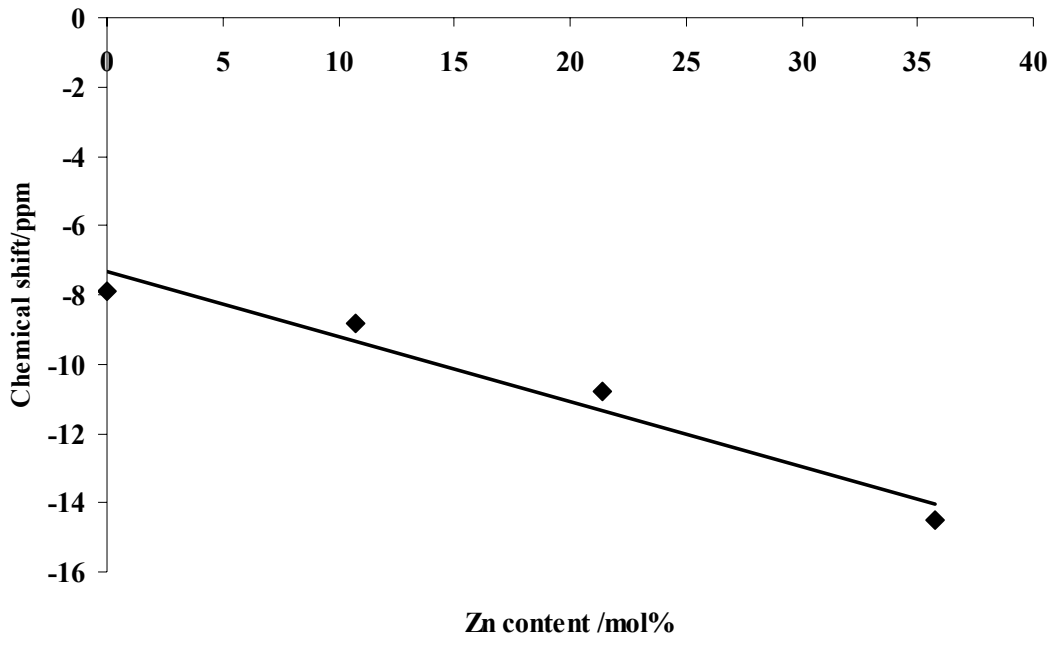


Figure 5.14. Chemical shift in ^{31}P MAS-NMR spectra against Zn content in mol% for the glasses in the Ca-Zn series [$4.5SiO_2$. $3.0Al_2O_3$. $1.5P_2O_5$. (3.0-x)CaO. xZnO. (2.0-y)CaF_2. yZnF_2]. The line is a guide to eye only.

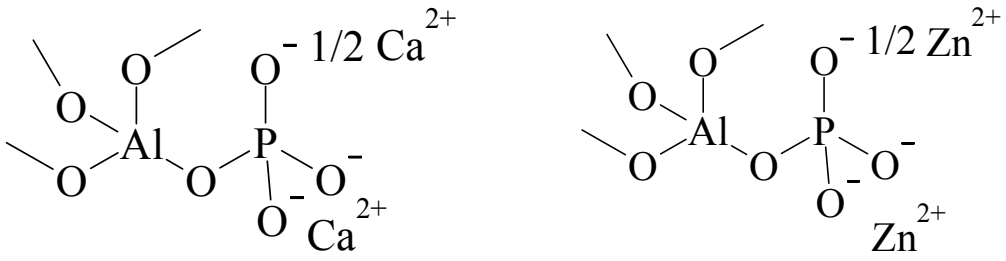


Figure 5.15. Schematics of Q^1 pyrophosphate Al-O-PO_3^{3-} species charge balanced by Ca^{2+} (left) and Zn^{2+} (right).

5.4. ^{27}Al MAS-NMR Spectroscopy

5.4.1. Ca-Mg Series

[4.5SiO_2. 3.0Al_2O_3. 1.5P_2O_5. (3.0-x)CaO. xMgO. (2.0-y)CaF_2. yMgF_2]

The ^{27}Al MAS-NMR spectrum for glass LG26 showed a broad single peak at 51ppm (Figure 5.16), and this peak has been assigned to Al in tetrahedral coordination, Al(IV) [23-25]. In a simple aluminosilicate glass, the chemical shift for Al(IV) is found at 60ppm. When P_2O_5 is introduced to a glass composition, this peak moves to a more negative value, towards 0ppm, as a result of P^{5+} locally charge balancing Al^{3+} forming Al-O-P linkages [24]. These Al-O-P linkages have also been shown on the ^{31}P MAS-NMR spectra (Figure 5.8). The substitution of calcium by magnesium seems to result in a decrease in chemical shift for Al(IV) and a widening of the peak, also observed in published studies [63, 64].

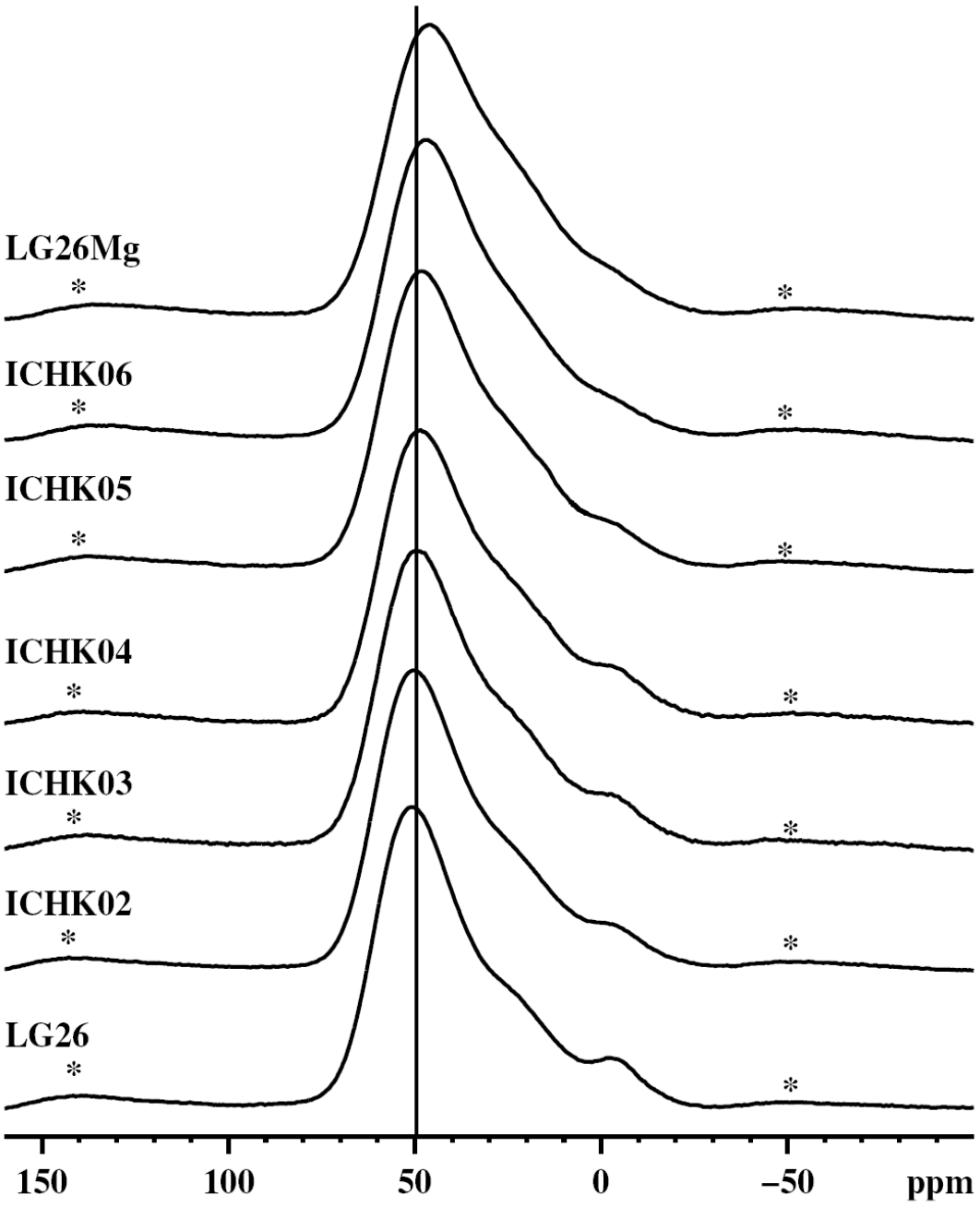


Figure 5.16. ^{27}Al MAS-NMR spectra for the glasses in the Ca-Mg series [4.5SiO_2. 3.0Al_2O_3. 1.5P_2O_5. (3.0-x)CaO. xMgO. (2.0-y)CaF_2. yMgF_2]. Spinning sidebands are marked by asterisks, and the vertical line is a guide to eye only.

All glasses showed a shoulder on the Al(IV) peak at around 20-25ppm and a small peak at around -5ppm (Figure 5.16). These have been assigned to Al(V) and Al(VI) respectively [65]. ^{27}Al MAS-NMR spectra were deconvoluted using *dmfit* Cz software [66] to determine the amount of Al(IV), Al(V), and Al(VI) species in each

glasses in the series. There is an increase in Al(V) species when magnesium fully substitutes calcium in LG26Mg (Figure 5.16, Table 5.1). The increase in Al(V) species with magnesium containing aluminosilicate glasses has also been found in various studies and has been suggested to be due to the higher cation field strength of Mg^{2+} than Ca^{2+} [63, 67]. The increase in Al(V) species could have resulted in a shift of the Al(IV) peak for LG26Mg to a less positive value by superposition of the Al(IV) peak onto the Al(V) peak. It is worth to point out that the glass compositions in the Ca-Mg series have been carefully designed to fulfil the Loewenstein's rule [16], and therefore these glasses should only contain Al(IV). However, ^{27}Al MAS-NMR have revealed a small presence of Al(V) and Al(VI) species. As Neuville and co-workers [68] have pointed out, the role of Al(V) and Al(VI), whether they act network forming or modifying, is not clarified. There is no evidence of Al(V) and Al(VI) acting as either network forming or modifying. Also, reasons behind the formation of Al(V) and Al(VI) in charge balanced glasses have not been determined yet.

Table 5.1. Al coordination states and their percentages for the glasses in the Ca-Mg series [$4.5SiO_2$. $3.0Al_2O_3$. $1.5P_2O_5$. $(3.0-x)CaO$. $xMgO$. $(2.0-y)CaF_2$. $yMgF_2$]. Fitting was performed using *dmfit* software.

Glass	Mg content /mol%	Al(IV) /%	Al(V) /%	Al(VI) /%
LG26	0.0	72	22	6
ICHK02	5.4	71	24	5
ICHK03	10.7	68	26	6
ICHK04	14.3	67	27	6
ICHK05	21.4	68	27	5
ICHK06	25.0	68	27	5
LG26Mg	35.7	65	29	6

5.4.2. Sr-Mg Series

[4.5SiO_2. 3.0Al_2O_3. 1.5P_2O_5. (3.0-x)SrO. xMgO. (2.0-y)SrF_2. yMgF_2]

Glass LG26Sr showed a chemical shift at 52ppm (Figure 5.17) for Al(IV) [24], and similar to LG26, this chemical shift is lower than for a simple aluminosilicate glass, usually found at around 60ppm. This is, again, due to the formation of Al-O-P linkages, also shown in ^{31}P MAS-NMR spectra (Figure 5.10) [24]. There is a slight increase in the chemical shift compared to LG26, 51ppm (Figure 5.16), but the difference is quite small. It has been shown that the strontium substitution for calcium does not affect the Al environment [20]. However, as magnesium substitutes strontium in the Sr-Mg series, the chemical shift for Al(IV) decreases, moving towards 0ppm (Figure 5.17), and this trend was also seen with the glasses in the Ca-Mg series (Figure 5.16).

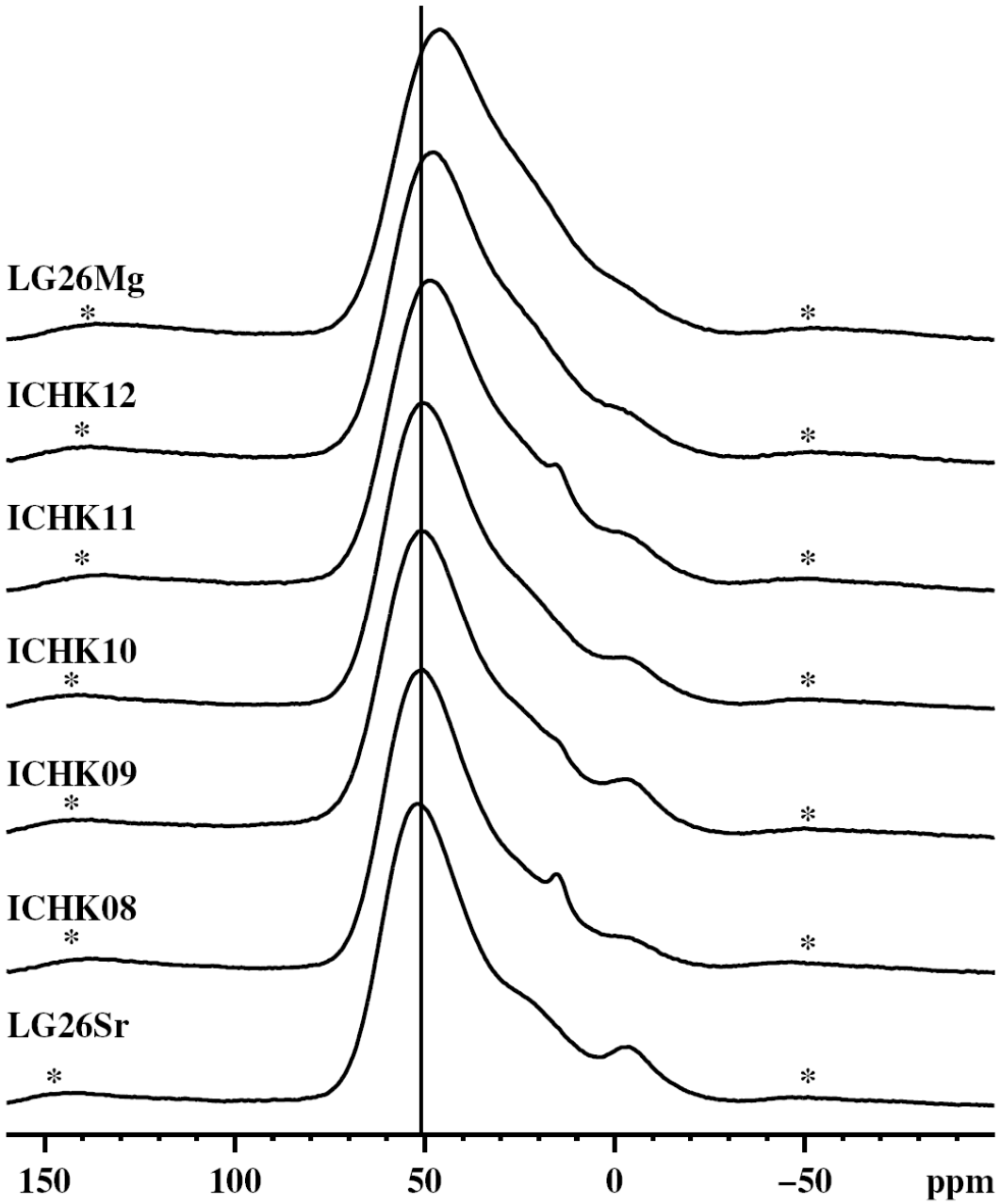


Figure 5.17. ^{27}Al MAS-NMR spectra for the glasses in the Sr-Mg series [4.5SiO_2. 3.0Al_2O_3. 1.5P_2O_5. (3.0-x)SrO. xMgO. (2.0-y)SrF_2. yMgF_2]. Spinning sidebands are marked by asterisks, and the vertical line is a guide to eye only.

All the glasses in the Sr-Mg series showed a shoulder at around 20-25ppm and a small peak at around -5ppm (Figure 5.17). These have been assigned to Al in pentahedral coordination, Al(V), and octahedral coordination, Al(VI), respectively. The deconvolution of the ^{27}Al MAS-NMR spectra showed that there is an increase in

Al(V) species as the magnesium substitution proceeds (Table 5.2). This trend is, again, similar to the Ca-Mg series, indicating that Sr^{2+} and Ca^{2+} behave quite similarly in fluoro-aluminosilicate glasses, and an increase in Al(V) species with magnesium containing aluminosilicate glasses has been reported in published studies [63, 67]. In addition, glasses ICHK08 and ICHK11 exhibited a very small peak at around 15ppm which is an unknown species. Hill and co-workers [20] also observed a peak at around 15ppm with the experimentally produced glass LG35 [$2SiO_2$. Al_2O_3. CaO. CaF_2] and a commercially available glass. O'Dell and co-workers [69] have assigned a peak at around 15ppm for α-Al_2O_3.

Table 5.2. Al coordination states and their percentages for the glasses in the Sr-Mg series [$4.5SiO_2$. $3.0Al_2O_3$. $1.5P_2O_5$. (3.0-x)SrO. xMgO. (2.0-y)SrF_2. yMgF_2]. Fitting was performed using *dmfit* software.

Glass	Mg content /mol%	Al(IV) /%	Al(V) /%	Al(VI) /%
LG26Sr	0.0	72	21	7
ICHK08	5.4	75	21	4
ICHK09	10.7	70	24	6
ICHK10	14.3	71	24	5
ICHK11	21.4	68	27	5
ICHK12	25.0	68	27	5
LG26Mg	35.7	65	29	6

5.4.3. Ca-Zn Series

[4.5SiO_2. 3.0Al_2O_3. 1.5P_2O_5. (3.0-x)CaO. xZnO. (2.0-y)CaF_2. yZnF_2]

Glass LG26 exhibited a chemical shift at 51ppm for Al in a tetrahedral coordination, Al(IV). This chemical shift moved to a less positive value, towards 0ppm, as more zinc was incorporated into the glass composition. Glass LG26Zn showed a chemical shift at 47ppm for Al(IV) (Figure 5.18). All chemical shifts are less positive than for a simple aluminosilicate glass, similar to the Ca-Mg and the Sr-Mg series, and this is, again, due to the formation of Al-O-P linkages which compensate the charge deficient Al^{3+} by P^{5+} [24].

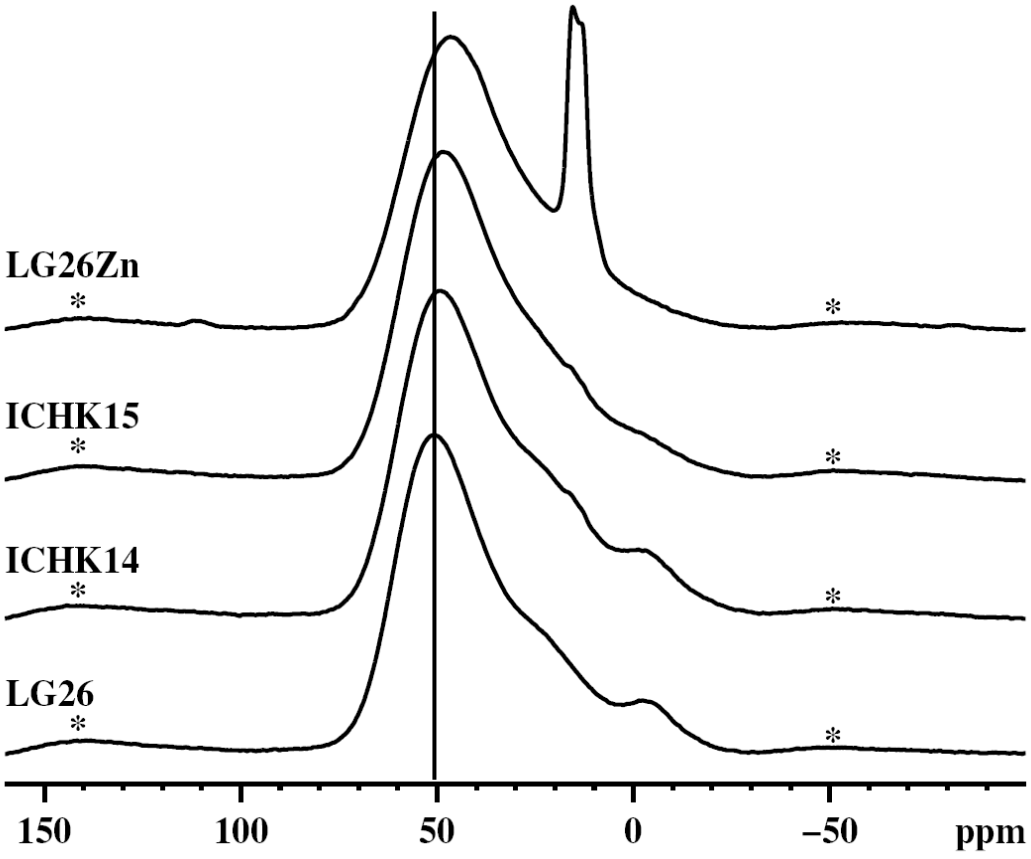


Figure 5.18. ^{27}Al MAS-NMR spectra for the glasses in the Ca-Zn series [4.5SiO_2. 3.0Al_2O_3. 1.5P_2O_5. (3.0-x)CaO. xZnO. (2.0-y)CaF_2. yZnF_2]. Spinning sidebands are marked by asterisks, and the vertical line is a guide to eye only.

Similar to the glasses in the Ca-Mg series, the Al(IV) peak for all the glasses in the Ca-Zn series showed a shoulder at around 20-25ppm and a very small peak at around -5ppm (Figure 5.18). These, again, have been assigned to Al in pentahedral, Al(V), and octahedral coordination, Al(VI), respectively [65]. Moreover, LG26Zn exhibited a sharp peak at around 15ppm which is caused by an unknown species. This peak is quite sharp in LG26Zn, but glasses ICHK14 and ICHK15 also showed a very small peak at around 15ppm. Although the nature of this peak at 15ppm is unknown, a similar peak was observed with glass LG35 by Hill and co-workers [20]. It is possible, however, that this peak is due to the presence of α-Al_2O_3 as suggested by O'Dell and co-workers [69].

The ^{27}Al MAS-NMR spectra were deconvoluted using *dmfit* software to determine the amount of different coordinations of Al (Table 5.3). It needs to be pointed out that deconvolution of LG26Zn was performed taking into account the unknown peak at 15ppm. There is an increase in the Al(V) species as zinc substitutes calcium, and a similar trend was also seen with the Ca-Mg series (Table 5.1). The amount of Al(V) species is also quite similar with the glasses having the same mol% of Mg and Zn: ICHK03 and ICHK14, and ICHK05 and ICHK15. The reduction in chemical shift, therefore, seems to be the result of this increase in Al(V) species that the Al(IV) peak is partly transforming into the Al(V) peak.

A possible reason for an increase in Al(V) species for LG26Zn may be that the charge balancing cation, Zn^{2+}, is consumed in charge balancing NBOs on phosphorus in Al-

$O\text{-}PO_3^{3-}$ species. When ^{19}F MAS-NMR is performed for LG26Zn, it may reveal the insufficient number of Zn^{2+} cations to charge balance Al in tetrahedral coordination.

Table 5.3. Al coordination states and their percentages for the glasses in the Ca-Zn series [$4.5SiO_2$. $3.0Al_2O_3$. $1.5P_2O_5$. (3.0-x)CaO. xZnO. (2.0-y)CaF_2. yZnF_2]. Fitting was performed using *dmfit* software.

Glass	Zn content /mol%	Al(IV) /%	Al(V) /%	Al(VI) /%
LG26	0.0	72	22	6
ICHK14	10.7	67	27	6
ICHK15	21.4	70	25	5
LG26Zn	35.7	52	24	3

5.5. ^{29}Si MAS-NMR Spectroscopy

5.5.1. Ca-Mg Series

[$4.5SiO_2$. $3.0Al_2O_3$. $1.5P_2O_5$. (3.0-x)CaO. xMgO. (2.0-y)CaF_2. yMgF_2]

The chemical shift of glass LG26 was observed to be -89ppm (Figure 5.19), and this suggests that the structure of this glass is a mixture of Q structures, namely Q^4(4Al) and Q^3(3Al) [20, 24, 25].

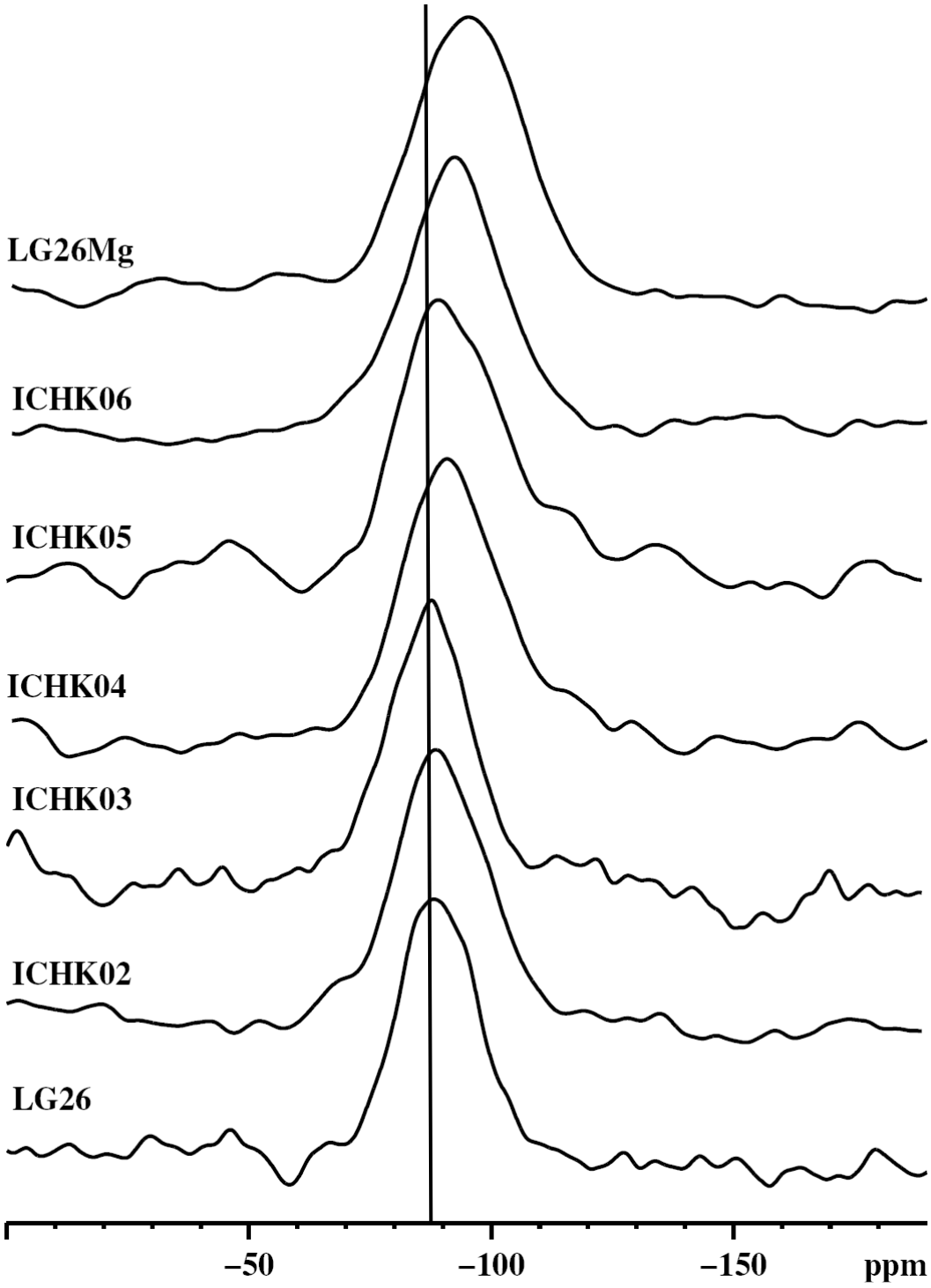


Figure 5.19. ^{29}Si MAS-NMR spectra for the glasses in the Ca-Mg series [4.5SiO_2. 3.0Al_2O_3. 1.5P_2O_5. (3.0-x)CaO. xMgO. (2.0-y)CaF_2. yMgF_2]. The vertical line is a guide to eye only.

When magnesium substituted calcium in the series, the peak shifted slightly towards more negative values, moving away from 0ppm (Figure 5.19), and a similar trend was seen in published studies [64, 70]. The structure of aluminosilicate glasses can be expressed as $Si(OSi)_{m-n}(OAl^-)_n(O^-)_{4-m}$, ($Q^m(n\text{Al})$, $4 \geq m \geq n \geq 0$), where m is the number of BOs per SiO_4 unit and n the number of Al connected by oxygen with SiO_4 unit, and the chemical shift increases as m is decreased or n is increased [28]. As has been discussed for ^{19}F MAS-NMR spectra of the Ca-Mg series (Figure 5.4), Mg^{2+} ions are consumed in forming F-Mg(n) species and are not available for charge balancing NBOs. Moreover, the ^{31}P MAS-NMR spectrum for LG26Mg (Figure 5.8) has shown the possible formation of magnesium pyrophosphate species, $Mg_2P_2O_7$ (Figure 5.10) which will take the available Mg^{2+} ions. Therefore, it is not possible to form any NBOs on Si, and hence the number of BOs increases forming more of Q^4 species. ^{27}Al MAS-NMR spectra of the Ca-Mg series (Figure 5.16) showed that there is an increased amount of Al(V) species and a decreased amount of Al(IV). Therefore, the decrease in the ^{29}Si chemical shift for LG26Mg may also have resulted from the decreased number of Al(IV) next to SiO_4 tetrahedra. Moreover, the substitution of calcium by magnesium seems to result in broadening of peaks in ^{29}Si MAS-NMR spectra (Figure 5.19), and broadening of the peaks has been suggested to be due to the presence of Q^4 species with different number of Al next to SiO_4 [64, 70].

5.5.2. Sr-Mg Series

[4.5SiO_2. 3.0Al_2O_3. 1.5P_2O_5. (3.0-x)SrO. xMgO. (2.0-y)SrF_2. yMgF_2]

Glass LG26Sr exhibited a peak at -90ppm (Figure 5.20), and this shows that this glass contains a mixture of Q structures, namely Q^4(4Al) and Q^3(3Al) [20]. The fully calcium substituted glass, LG26, was also shown to contain a mixture of Q^4(4Al) and Q^3(3Al) (Figure 5.19) suggesting that the Si environment is independent of Sr^{2+}. Hill and co-workers [20] also studied the same glasses and found that the Q structures do not change with strontium content.

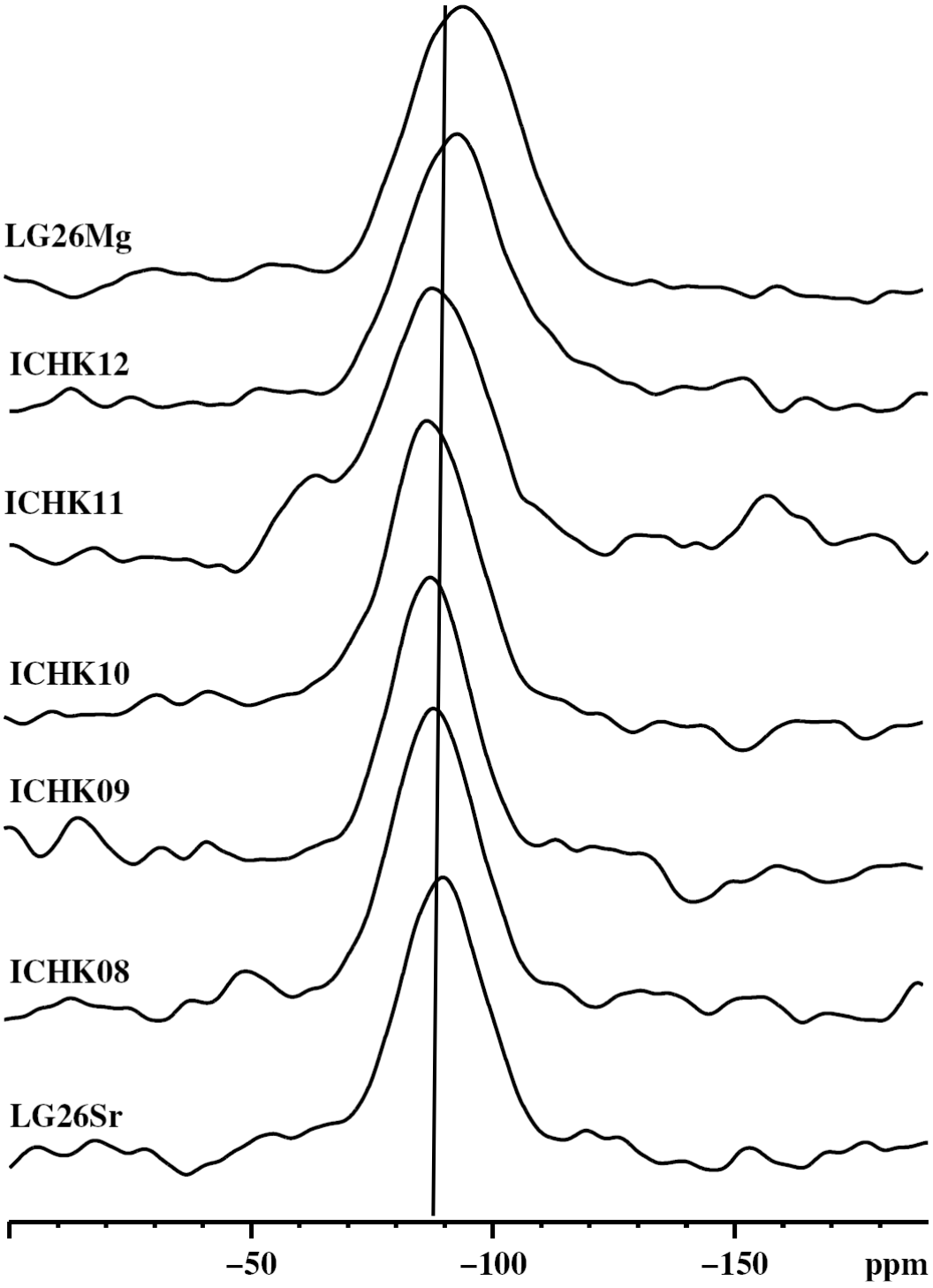


Figure 5.20. ^{29}Si MAS-NMR spectra for the glasses in the Sr-Mg series [4.5SiO_2. 3.0Al_2O_3. 1.5P_2O_5. (3.0-x)SrO. xMgO. (2.0-y)SrF_2. yMgF_2]. The vertical line is a guide to eye only.

The chemical shift moved to more negative values, away from 0ppm, as magnesium substituted strontium (Figure 5.20), and this trend was also seen with the glasses in

the Ca-Mg series (Figure 5.19). The reduction in chemical shift is the result of a) an increase in the number of BOs on Si and/or b) a decrease in the number of Al around SiO_4 tetrahedra [28]. Therefore, LG26Mg is expected to have a Q^4 structure with less than three Al around SiO_4 tetrahedra. As discussed with the glasses in the Ca-Mg series, ^{19}F MAS-NMR spectra for the Sr-Mg series have shown Mg^{2+} is used up by F^- forming F-Mg(n) species (Figure 5.5), and these species will not be available for charge balancing NBOs on Si. Moreover, the ^{31}P MAS-NMR spectrum for LG26Mg (Figure 5.11) showed the possible formation of magnesium pyrophosphate species, $Mg_2P_2O_7$. Therefore, the decrease in the chemical shift indicates a more polymerised glass network.

5.5.3. Ca-Zn Series

[4.5SiO_2. 3.0Al_2O_3. 1.5P_2O_5. (3.0-x)CaO. xZnO. (2.0-y)CaF_2. yZnF_2]

The chemical shift for LG26 was observed at -89ppm showing the presence of a mixture of Q structures, Q^4(4Al) and Q^3(3Al) [20, 24, 25]. There was a slight move in the chemical shift to more negative values, moving away from 0ppm, with zinc substitution, resulting in ICHK14 and ICHK15 both exhibiting a very broad peak at -91ppm (Figure 5.21). This suggests that when both calcium and zinc are present, Q structure of the silicate network is not affected.

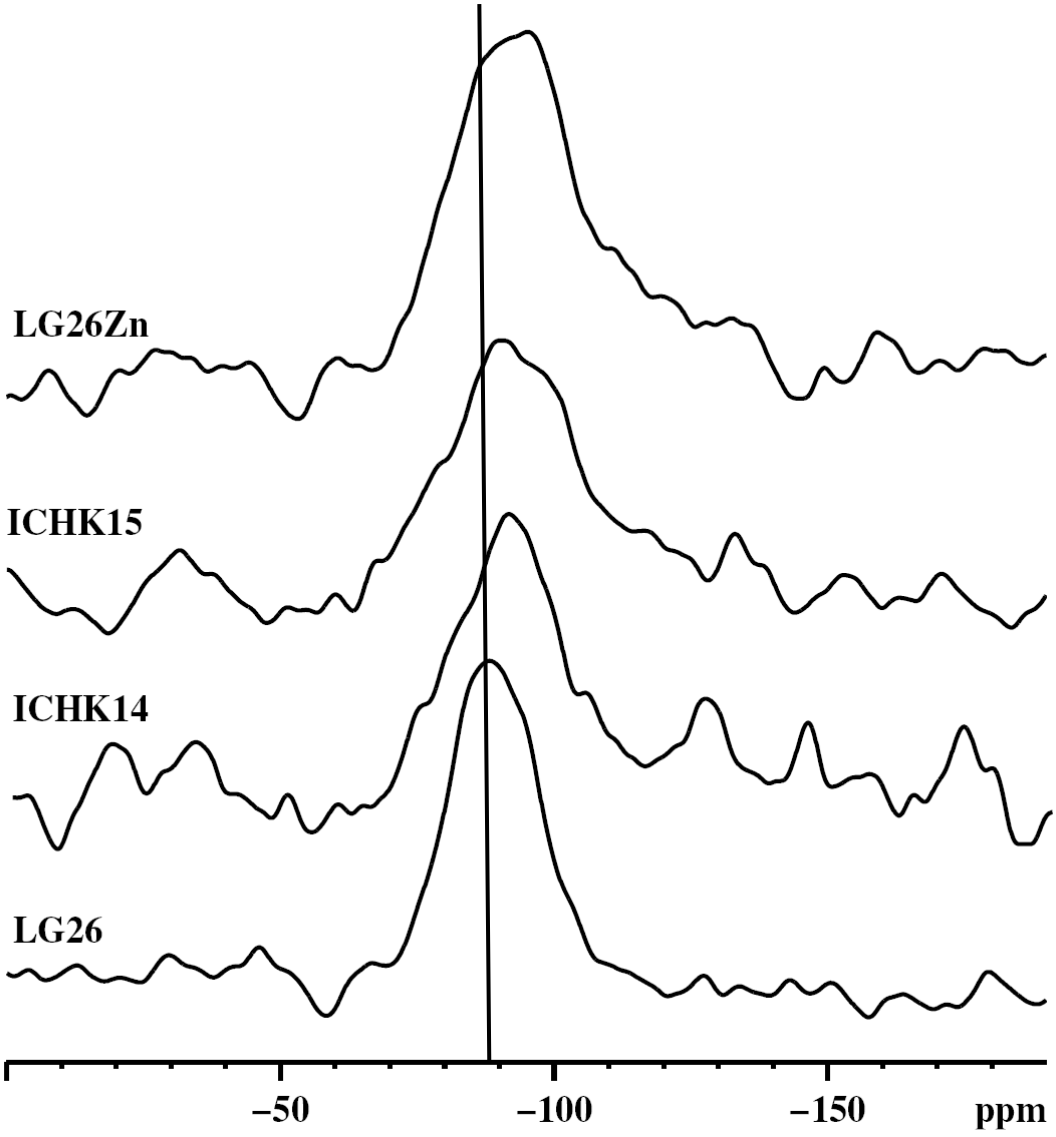


Figure 5.21. ^{29}Si MAS-NMR spectra for the glasses in the Ca-Zn series [4.5SiO_2. 3.0Al_2O_3. 1.5P_2O_5. (3.0-x)CaO. xZnO. (2.0-y)CaF_2. yZnF_2]. The vertical line is a guide to eye only.

However, when all calcium is substituted by zinc in LG26Zn, the chemical shift moves to an even more negative value, to -95ppm (Figure 5.21). As mentioned, the reduction in chemical shift, moving away from 0ppm, suggests that the number of BOs on SiO_4 is increased and/or the number of Al next to SiO_4 tetrahedra is decreased. Similar chemical shifts were observed with LG26Mg which exhibited a chemical shift of -95ppm (Figure 5.19). The increase in BOs next to SiO_4 may have resulted from

the fact that Zn^{2+} is consumed to charge balance NBOs on phosphorus in Al-O-PO_3^{3-} species (Figure 5.15). ^{19}F MAS-NMR analysis for LG26Zn has not been performed, but this might reveal the preferential formation of F-Zn(n) species, which would confirm a deficiency in the charge balancing cations to form NBOs on Si.

Moreover, the peaks in the ^{29}Si MAS-NMR spectra became broader and noisier with zinc substitution (Figure 5.21). Similar findings were observed previously [71, 72], but the cause of the broader and noisier spectra is still under investigation. It may be due to the different coordination states of zinc.

5.6. DSC Analysis

5.6.1. Ca-Mg Series

[4.5SiO_2. 3.0Al_2O_3. 1.5P_2O_5. (3.0-x)CaO. xMgO. (2.0-y)CaF_2. yMgF_2]

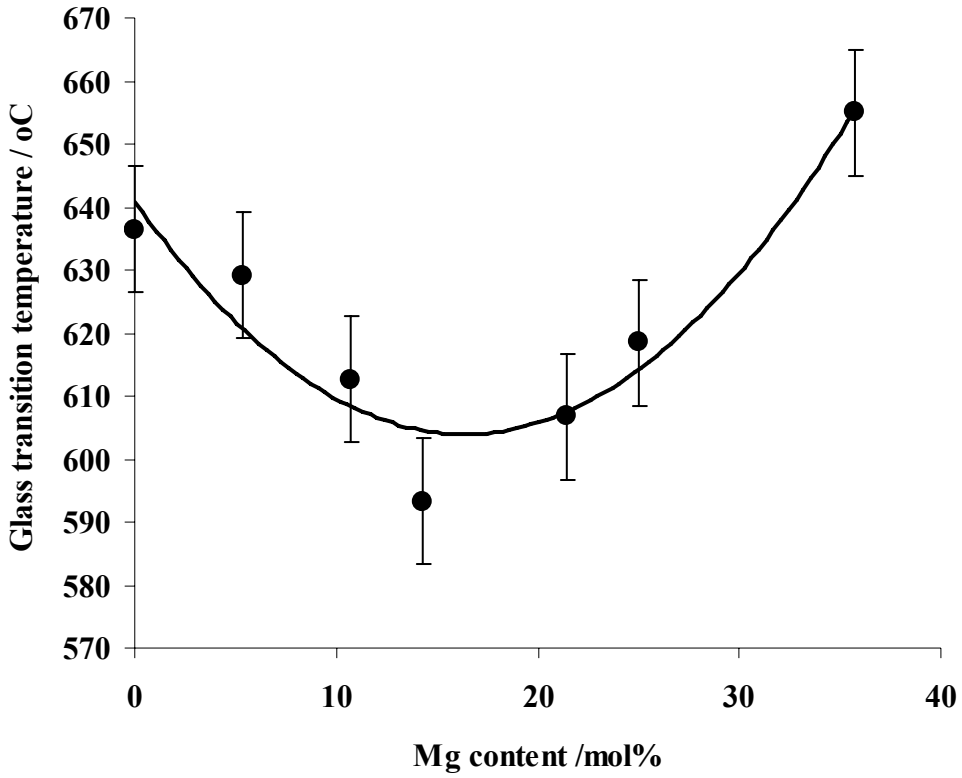


Figure 5.22. Glass transition temperature against Mg content in mol% for the glasses in the Ca-Mg series [4.5SiO_2. 3.0Al_2O_3. 1.5P_2O_5. (3.0-x)CaO. xMgO. (2.0-y)CaF_2. yMgF_2] with particle size <38µm. The line is a guide to eye only. Error bar - 10^oC.

An initial decrease in glass transition temperature, T_g, with magnesium substitution for calcium was observed. Higher magnesium substitution resulted in an increase in T_g (Figure 5.22). Initially, the reduction in T_g was thought to be caused by formation of Si-O-Mg bonds in the glass network, implying that magnesium is acting as a network former. The bond strength of Mg-O is weaker than Si-O or Al-O, and therefore, T_g would decrease. Then, the increase in T_g for higher magnesium

substitution was thought to be due to Mg^{2+} acting as a network modifier cation replacing the BOs and disrupting the glass network. The size of Mg^{2+} is smaller than Ca^{2+}, and therefore the interaction between the NBOs and Mg^{2+} would be stronger than Ca^{2+} resulting in a more compact glass network. Hence, the data from the DSC could have implied that magnesium is an intermediate oxide. However, MAS-NMR results have shown that this is not the case. For example, ^{29}Si MAS-NMR spectra (Figure 5.19) have shown no evidence of Si-O-Mg formation with low magnesium substitution, where a decrease in T_g was observed. Formation of Si-O-Mg would result in the reduction in Al around SiO_4 tetrahedra and hence the chemical shift should decrease, moving away from 0ppm, as magnesium substitution takes place. In the ^{29}Si MAS-NMR spectra for the Ca-Mg series, the shift in peak position appeared for the higher substituted glasses in the series showing an increase in the polymerisation of the silicate network (Figure 5.19). Therefore, it seems that Mg^{2+} is acting like a network modifying oxide. This is different from a study conducted by Bovo and Hill [73]. They studied the effect of magnesium substitution in bioactive glasses and concluded that magnesium switches its role and acts like an intermediate oxide. This difference may result from the presence of Al_2O_3 and P_2O_5 in the glasses studied here which can form the glass network. The glasses studied by Bovo and Hill contained only SiO_2 as a network forming oxide apart from MgO [73].

Therefore, an alternative explanation was considered for the trend in T_g, and this is the mixed cation effect. The mixed cation effect has been studied extensively and occurs if there are two different alkali or alkaline earth ions with constant alkali or alkaline earth content. The mechanisms of the mixed cation effect is yet unknown, but it has been shown that the T_g of a glass containing the same amount of different alkali or

alkaline earth ions is less than the average of the T_g of the single alkali or alkaline earth glasses [60]. Glasses ICHK04 and ICHK05 are in the middle of the Ca-Mg series. Their T_g were determined to be around 590^{o}C and 605^{o}C respectively. T_g for LG26 and LG26Mg, both containing only calcium or magnesium respectively, were 636^{o}C and 654^{o}C (Table 5.4). Therefore, the T_g for the two glasses in the middle of the Ca-Mg series is less than the average of the two glasses at the end of the series. Moreover, T_g generally decreases with the disruption of the glass network. For example, de Barra and Hill [34] have shown that F^- and Na^+ disrupt the glass network and decrease T_g.^{29}Si MAS-NMR of Ca-Mg series (Figure 5.19) have shown that magnesium does not disrupt the glass network. Therefore, T_g was expected to increase with magnesium substitution. However, T_g decreased for the glasses early in the series and increased with higher substituted glasses (Figure 5.22). Therefore, the cause of this trend in T_g is more likely to be due to the mixed cation effect.

DSC was also used to determine the first and the second crystallisation temperatures, T_{c1} and T_{c2} respectively, of the glasses in the Ca-Mg series (Figure 5.23).

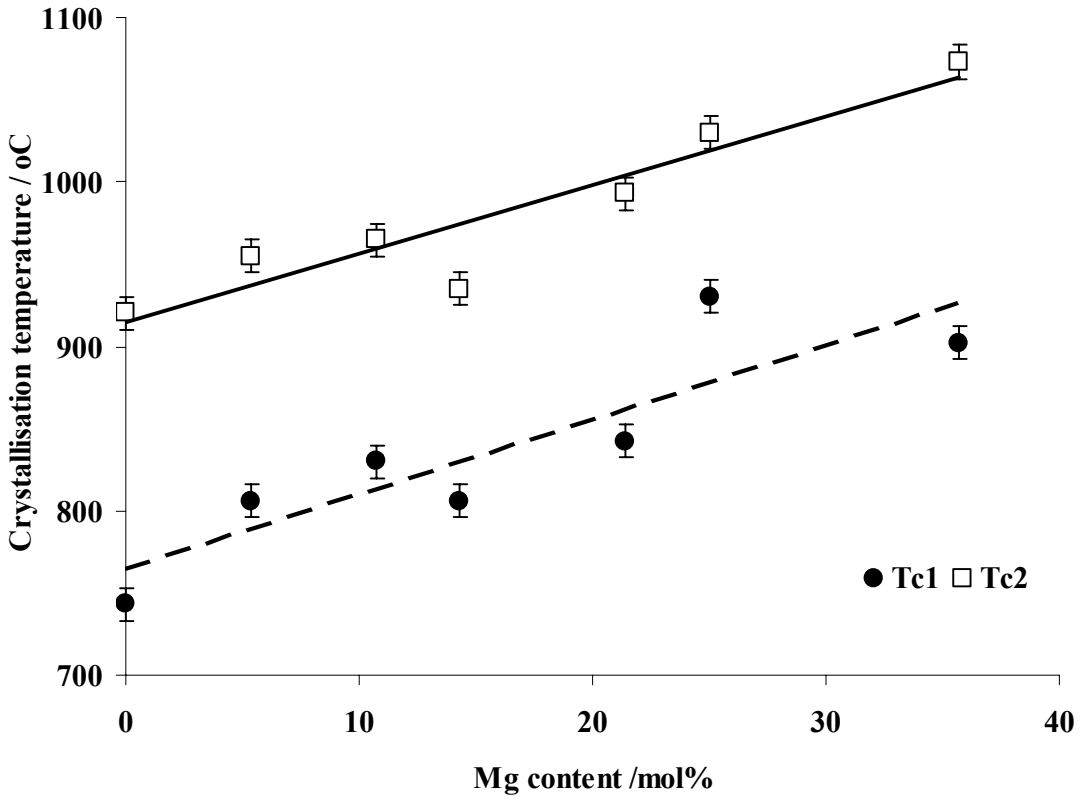


Figure 5.23. First and second crystallisation temperatures, T_{c1} and T_{c2}, against Mg content in mol% for the glasses in the Ca-Mg series [$4.5SiO_2$. $3.0Al_2O_3$. $1.5P_2O_5$. (3.0-x)CaO. xMgO. (2.0-y)CaF_2. yMgF_2] with particle size <38µm. Lines are a guide to eye only. Error bar - 10°C.

T_{c1} and T_{c2} were observed with all the glasses in the Ca-Mg series, and both T_{c1} and T_{c2} increased with magnesium substitution (Figure 5.23). This change in crystallisation temperatures, both in T_{c1} and T_{c2}, may indicate that the crystal phases have changed with the incorporation of magnesium in the glass compositions.

DSC was also performed on coarse particles, >38µm, in order to determine the mechanism of nucleation (Table 5.4). This was to determine if the magnesium substitution for calcium has affected the mechanism of the nucleation.

Table 5.4. Glass transition temperatures, T_g, measured with <38μm, and first and second crystallisation temperatures, T_{c1} and T_{c2}, with different particle sizes for the glasses in the Ca-Mg series [$4.5SiO_2$. $3.0Al_2O_3$. $1.5P_2O_5$. (3.0-x)CaO. xMgO. (2.0-y)CaF_2. yMgF_2]. The error is taken as +/- 10°C.

Glass	Mg content /mol%	T_g / °C	T_{c1} / °C		T_{c2} / °C	
			<38μm	>38μm	<38μm	>38μm
LG26	0.0	636	743	730	920	874
ICHK02	5.4	629	806	816	955	987
ICHK03	10.7	613	830	850	965	971
ICHK04	14.3	593	806	823	935	945
ICHK05	21.4	607	842	864	993	1000
ICHK06	25.0	648	930	943	1030	1044
LG26Mg	35.7	655	902	914	1073	1082

Bulk nucleation occurs if the crystallisation temperature is independent of particle size. On the contrary, surface nucleation is taking place if the crystallisation temperature increases with particle size [16]. The change in the T_{c1} with different particle sizes seems to be small (Table 5.4), and glasses are therefore likely to be bulk nucleating. This is in a good agreement with a study which showed glass LG26 to bulk nucleate [24]. On the contrary, the difference in T_{c2} is rather large (Table 5.4), and therefore glasses are more likely to be surface nucleating. It seems that the magnesium substitution does not affect the mechanism of nucleation.

5.6.2. Sr-Mg Series

[4.5SiO_2. 3.0Al_2O_3. 1.5P_2O_5. (3.0-x)SrO. xMgO. (2.0-y)SrF_2. yMgF_2]

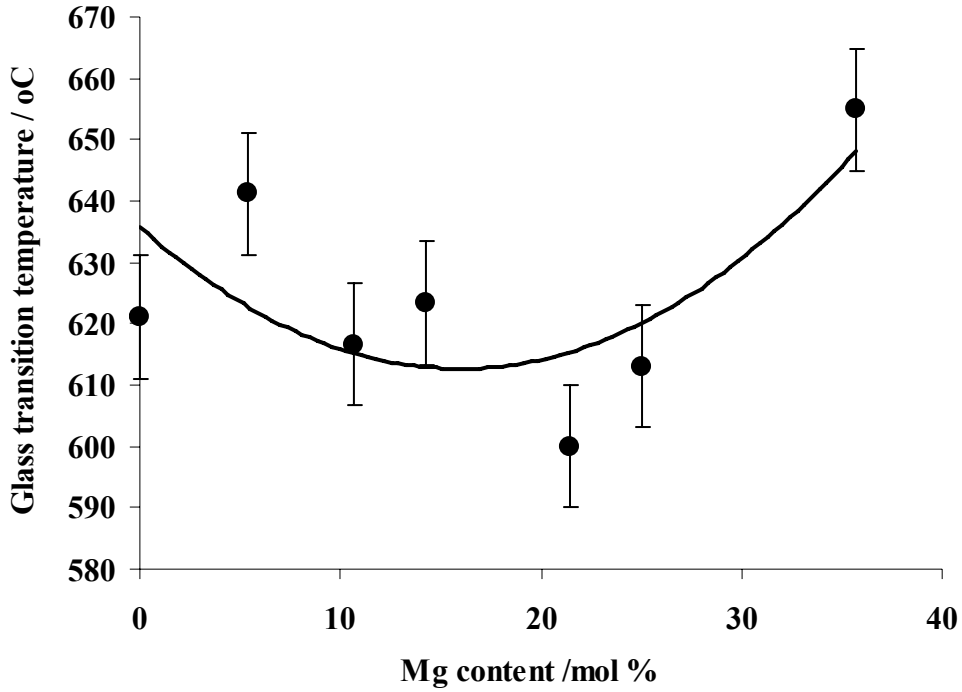


Figure 5.24. Glass transition temperature against Mg content in mol% for the glasses in the Sr-Mg series [4.5SiO_2. 3.0Al_2O_3. 1.5P_2O_5. (3.0-x)SrO. xMgO. (2.0-y)SrF_2. yMgF_2] with particle size <38µm. The line is a guide to eye only. Error bar - 10^oC.

T_g for LG26Sr was around 620^oC (Table 5.5), which is lower than the fully calcium substituted glass LG26, at around 635^oC (Table 5.4). This is because Sr^{2+} is a bigger cation than Ca^{2+}, 1.16Å for Sr^{2+} and 1.00Å for Ca^{2+} [74], and therefore Sr^{2+} is capable of disrupting the glass network more effectively than Ca^{2+}.

Similar to the Ca-Mg series (Figure 5.22), T_g decreases in the beginning of the series and increases towards the end of the series (Figure 5.24), and again, the cause of this trend seems to be due to the mixed cation effect taking into account the NMR results, and Mg^{2+} is acting like a network modifier. Again, this is different from a study

conducted by Bovo and Hill [73], and this difference may result from the presence of Al_2O_3 and P_2O_5 in the glasses studied here which can form the glass network.

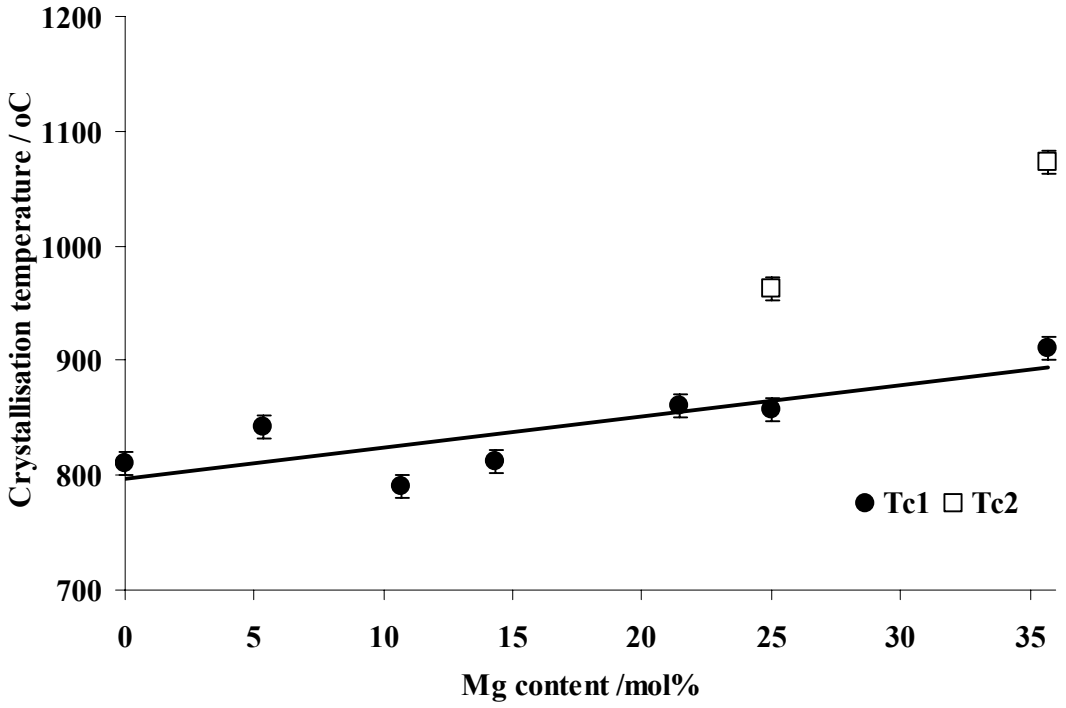


Figure 5.25. First and second crystallisation temperatures, T_{c1} and T_{c2}, against Mg content in mol% for the glasses in the Sr-Mg series [4.5SiO_2. 3.0Al_2O_3. 1.5P_2O_5. (3.0-x)SrO. xMgO. (2.0-y)SrF_2. yMgF_2] with particle size <38µm. The line is a guide to eye only. Error bar - 10°C.

T_{c1} gradually increases with magnesium substitution, and glass ICHK12 was the only mixed Sr-Mg glass exhibiting T_{c2} (Figure 5.25). Once again, the increase in the crystallisation temperature may suggest a formation of different crystal phases.

Table 5.5. Glass transition temperatures, T_g, measured with particle size <38μm, and first and second crystallisation temperatures, T_{c1} and T_{c2}, with different particle sizes for the glasses in the Sr-Mg series [$4.5SiO_2$. $3.0Al_2O_3$. $1.5P_2O_5$. (3.0-x)SrO. xMgO. (2.0-y)SrF_2. yMgF_2]. The error is taken as +/- 10^oC.

Glass	Mg content /mol%	T_g / ^oC	T_{c1} / ^oC		T_{c2} / ^oC	
			<38μm	>38μm	<38μm	>38μm
LG26Sr	0.0	621	810	814	---	---
ICHK08	5.4	641	842	849	---	---
ICHK09	10.7	617	790	784	---	---
ICHK10	14.3	623	813	817	---	---
ICHK11	21.4	600	860	854	---	---
ICHK12	25.0	613	857	861	962	969
LG26Mg	35.7	655	902	914	1073	1082

DSC analysis was also performed using coarse particles, >38μm, to determine the mechanism of nucleation to see if the magnesium substitution for strontium has affected the nucleation mechanism. Similar to the glasses in the Ca-Mg series, the difference in T_{c1} with different particle sizes is quite small (Table 5.5). Therefore, the mechanism of the nucleation is most likely to be bulk nucleation. It is difficult to state the mechanism for T_{c2} as there are only two glasses in the Sr-Mg series showing a T_{c2} (Table 5.5). The mechanism is most likely to be surface nucleation, considering Ca^{2+} and Sr^{2+} behave quite similarly in glass structure. Similar to the Ca-Mg series, the magnesium substitution for strontium does not seem to affect the nucleation mechanism.

5.6.3. Ca-Zn Series

[$4.5SiO_2$. $3.0Al_2O_3$. $1.5P_2O_5$. (3.0-x)CaO. xZnO. (2.0-y)CaF_2. yZnF_2]

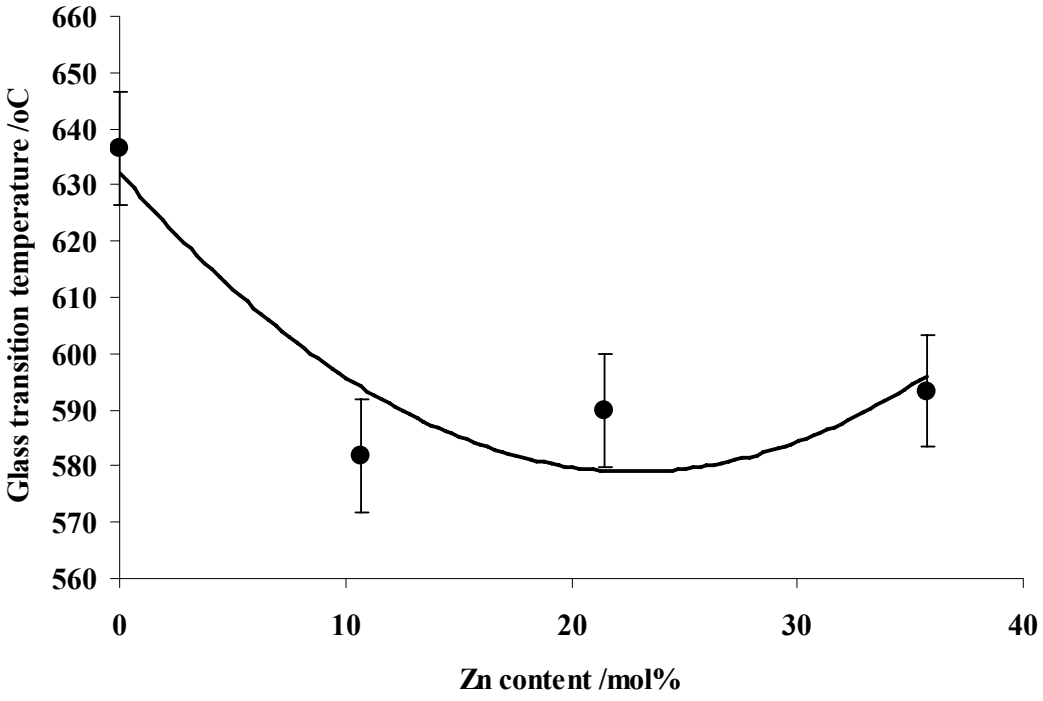


Figure 5.26. Glass transition temperature against Zn content in mol% for the Ca-Zn series [$4.5SiO_2$. $3.0Al_2O_3$. $1.5P_2O_5$. (3.0-x)CaO. xZnO. (2.0-y)CaF_2. yZnF_2] with particle size <38µm. The line is a guide to eye only. Error bar - 10°C.

T_g decreased with zinc substitution in the Ca-Zn series. There is a slight increase in T_g with the fully zinc substituted glass LG26Zn (Figure 5.26), but the increase is small compared to LG26Mg in the Ca-Mg (Figure 5.22) and the Sr-Mg series (Figure 5.24). As with the glasses in the other two series, this trend in T_g may have been caused by a mixed cation effect as NMR results do not suggest that Zn is going into the glass network.

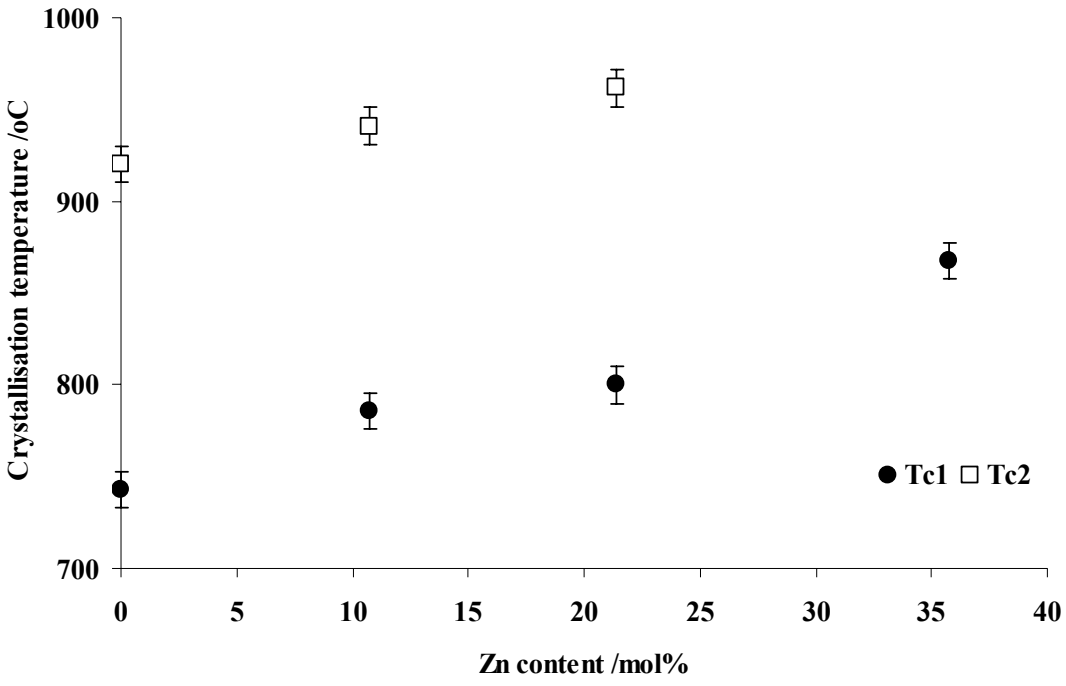


Figure 5.27. First and second crystallisation temperatures, T_{c1} and T_{c2}, against Zn content in mol% for the glasses in the Ca-Zn series [4.5SiO_2. 3.0Al_2O_3. 1.5P_2O_5. (3.0-x)CaO. xZnO. (2.0-y)CaF_2. yZnF_2] with particle size <38µm. Error bar - 10^oC.

Glass LG26Zn exhibited only one crystallisation peak (Figure 5.27). T_{c1} for LG26Zn was higher than for the other three glasses in the series, which can indicate that LG26Zn is forming a different crystal phase. Apart from LG26Zn, T_{c1} for the other three glasses in the Ca-Zn series showed a gradual increase. The same trend was seen for T_{c2} (Figure 5.27).

Table 5.6. Glass transition temperatures, T_g, measured with <38µm, and first and second crystallisation temperatures, T_{c1} and T_{c2}, with different particle sizes for the glasses in the Ca-Zn series [4.5SiO_2. 3.0Al_2O_3. 1.5P_2O_5. (3.0-x)CaO. xZnO. (2.0-y)CaF_2. yZnF_2]. The error is taken as +/- 10°C.

Glass	Zn content /mol%	T_g / °C	T_{c1} / °C		T_{c2} / °C	
			<38µm	>38µm	<38µm	>38µm
LG26	0.0	636	743	730	920	874
ICHK14	10.7	582	786	786	941	946
ICHK15	21.4	590	800	800	962	969
LG26Zn	35.7	593	868	877	n/a	n/a

Both T_{c1} and T_{c2} were measured with different glass particle sizes to determine if the zinc substitution for calcium has affected the mechanism of the nucleation. There seems to be a very small difference in crystallisation temperatures, in both T_{c1} and T_{c2}, with different particle sizes (Table 5.6), which could suggest that the main nucleation mechanism is bulk nucleation.

In conclusion, magnesium seems to act differently from calcium, especially in fluorine environment by a preferential formation of F-Mg(n) species. Also, the magnesium substitution increased the Q^4 species of the silicate network. An increase in the Q^4 species indicates that the glass is more crosslinked, and therefore, the reactivity of the glass is expected to decrease. Hence, the mechanical property of the cement is expected to decrease. This will be discussed in more details in Section 5.11. The strontium substitution for calcium and the zinc substitution for calcium did not affect the glass structure.

5.7. Fluoro-Aluminosilicate Glasses from Schott AG (Germany)

Three glasses, GM35429, G018-090, and G018-117, were obtained from Schott AG (Germany) as they contain zinc. These glasses are commercially used as GPCs, and characterisation of these glasses using MAS-NMR was performed as their structures have not been investigated yet.

5.7.1. ^{19}F MAS-NMR Spectroscopy

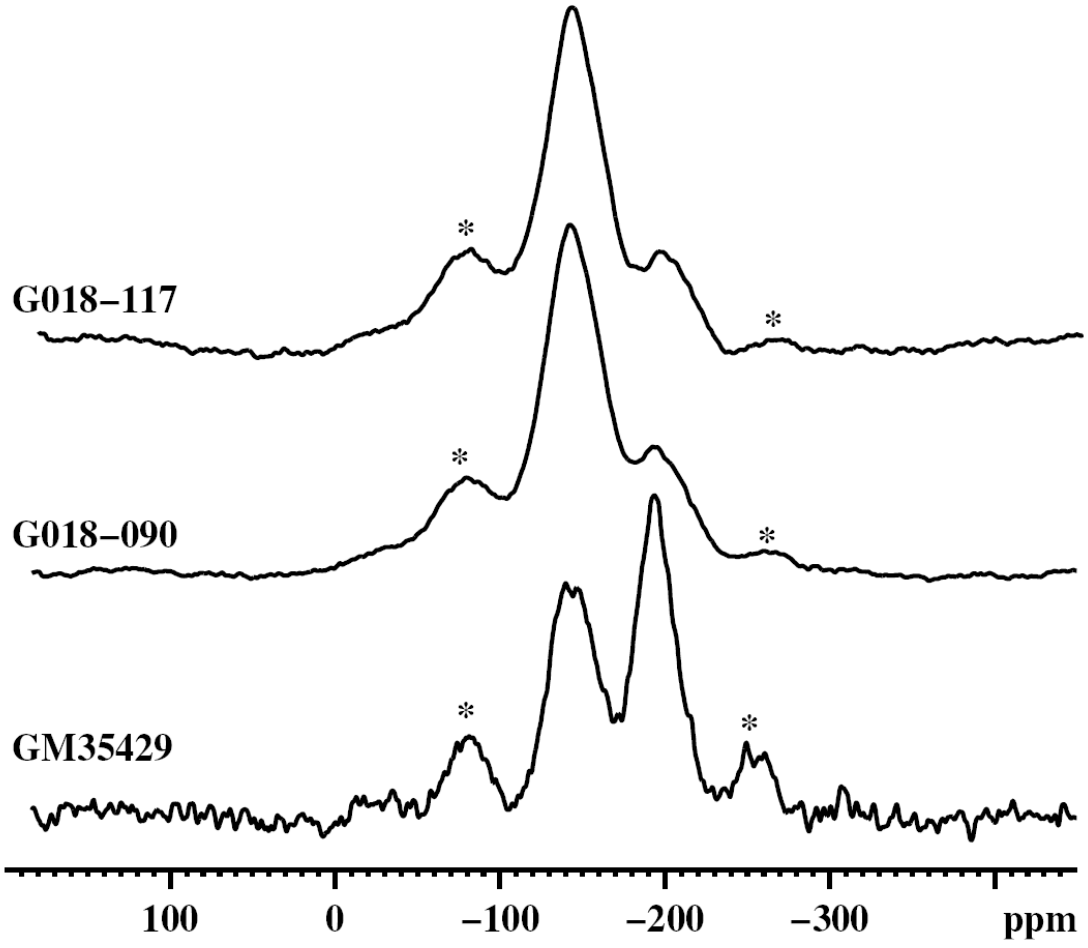


Figure 5.28. ^{19}F MAS-NMR spectra for Schott glasses. Spinning sidebands are marked by asterisks.

Glass GM35429 exhibited mainly two peaks in ^{19}F MAS-NMR spectra at -147ppm and -194ppm (Figure 5.28). As Al possesses the highest cation field strength

compared to the other ions present in this glass, these two peaks are more likely to be due to fluorine bound to Al with a close proximity of Na^+ and Ca^{2+}. Therefore, the peak at -147ppm is for Al-F-Ca(n) species and the peak at -194ppm for Al-F-Na(3) species. Zeng and Stebbins [26] found the chemical shift of these species as -150ppm and -191ppm respectively.

Similarly, ^{19}F MAS-NMR spectra for glasses G018-090 and G018-117 exhibited a broad peak each at -143ppm and -140ppm respectively (Figure 5.28) which are assigned to Al-F-Sr(n) species. However, these peaks are slightly shielded as Al-F-Sr(n) species are known to occur around -150ppm [24].

The peaks at -195ppm and -195ppm for G018-090 and G018-117 (Figure 5.28) have been attributed to Al-F-Na(3) species [26]. These peaks contain a shoulder, which could be due to the presence of F-Zn(4) species whose chemical shift is known to occur at -202ppm [57]. The noticeable difference between the spectrum of GM35429 and those of G018-090 and G018-117 is the intensity of the Al-F-Na(3) peak resulting from GM35429 having more soda content than the other two glasses. Stamboulis and co-workers [22] also saw an intense Al-F-Na(n) peak with their commercial ionomer glasses with high soda content. Similarly, Zainuddin [19] has shown that the intensity of the Al-F-Na(n) peak increased with increasing soda content.

5.7.2. ^{27}Al MAS-NMR Spectroscopy

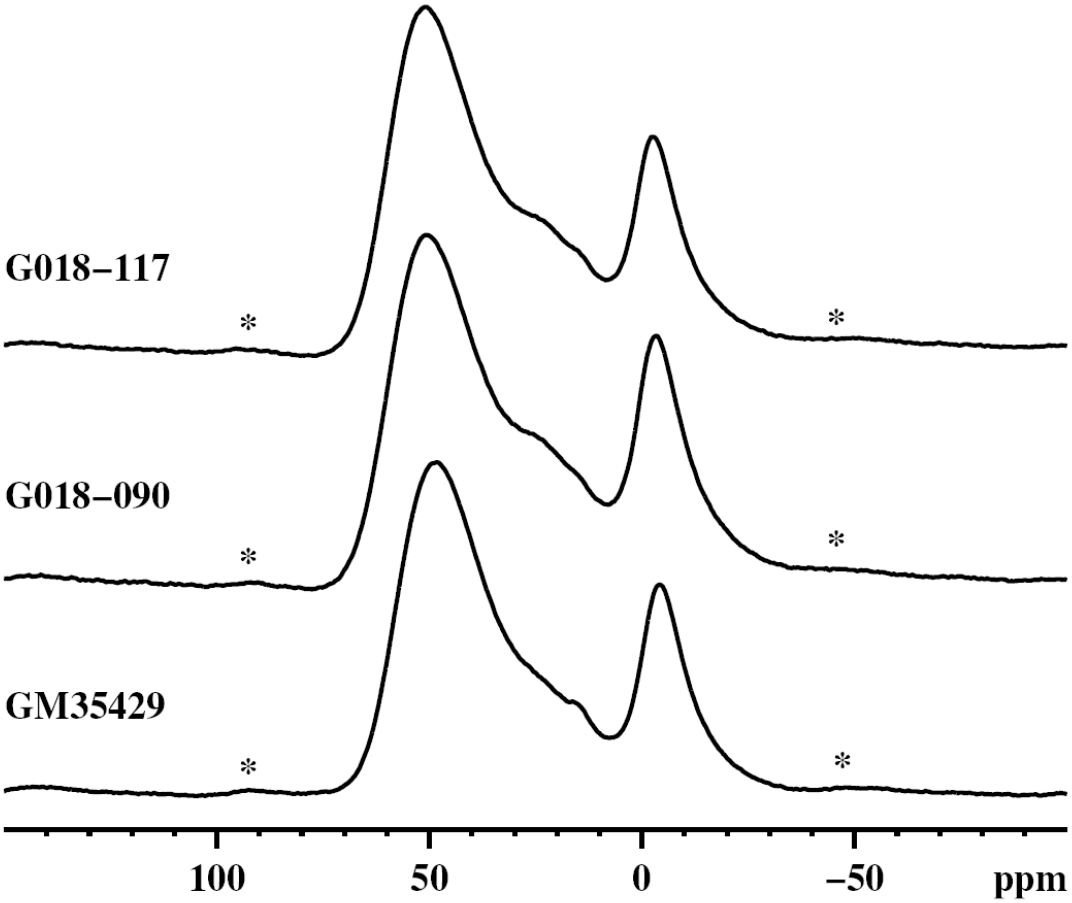


Figure 5.29. ^{27}Al MAS-NMR spectra for Schott glasses. Spinning sidebands are marked by asterisks.

All glasses exhibited predominantly a peak at 48-51ppm attributed to Al in four coordination, Al(IV), and a peak at around -3ppm for Al in six coordination, Al(VI). On the peak for Al(IV), there is a shoulder, which is assigned to Al in five coordination, Al(V) (Figure 5.29). In a simple calcium aluminosilicate glass, SiO_2-Al_2O_3-CaO-CaF_2, the peak for Al(IV) is at 60ppm [21]. This reduction in the chemical shift is due to the formation of Al-O-P bonds as suggested by Stamboulis and co-workers [23]. The Al:P ratio in all the glasses studied here (Appendix III) is much higher than the glasses studied by Stamboulis and co-workers, 2:1 [23], but the chemical shift for Al(IV) is about the same or much lower in the case of glass

GM35429. Therefore, the reduction of this chemical shift is not due to the Al:P ratio but rather due to the decrease in the number of cations to charge balance the NBOs on the phosphorus. ^{19}F MAS-NMR spectra showed that most of the charge balancing cations, Na^{+}, Ca^{2+}, and Sr^{2+}, are consumed forming Al-F-Na/Ca/Sr species (Figure 5.28), decreasing the number of cations available to charge balance NBOs on phosphorus. As a result, there are three possible consequences.

Firstly, there could be more than one Al attached to each PO_4 tetrahedra. The chemical shift at 48ppm for Al(IV) for GM35429 is too high for $AlPO_4$ orthophosphate species having four aluminium around a PO_4 tetrahedra, which occurs at 42.0ppm [8]. Therefore, Al(IV) is more likely to be in a state between $AlPO_4$ orthophosphate and Q^1 pyrophosphate Al-O-PO_3^{3-} species. A similar phenomenon was also observed with one of the commercial glasses studied by Stamboulis and co-workers [22]. Furthermore, the pyrophosphate peak observed on the ^{31}P MAS-NMR for GM35429 (Figure 5.31), which will be discussed later in more details, is not negative enough for $AlPO_4$ orthophosphate species, but too negative for Q^1 pyrophosphate Al-O-PO_3^{3-} species, which would confirm the presence of the species between $AlPO_4$ and Al-O-PO_3^{3-}. The chemical shift of the Al(IV) peak in ^{27}Al MAS-NMR spectra for glasses G018-090 and G018-117 is slightly higher than for GM32459 (Figure 5.29), which could be due to the reduction in phosphate content compared to GM32459. As a result, there will be less Al-O-P bonds formed, and the chemical shift for Al(IV) will increase.

Secondly, one of the oxygens on phosphorus can be bound to another phosphorus, forming P-O-P bonds, due to not enough cations to charge balance the NBOs on

phosphorus. As a result, there could be formation of metaphosphate species (Figure 5.30).

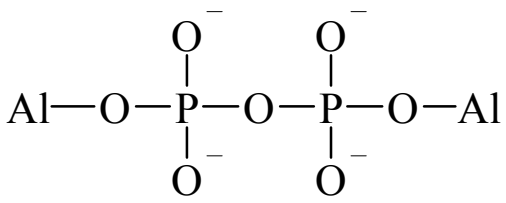


Figure 5.30. A schematic of metaphosphate species forming P-O-P bonds.

The formation of Al-O-P bonds will reduce the chemical shift of Al(IV) to around 50ppm [21]. Generally, the presence of this metaphosphate species, in which the oxygen on phosphorus is charge balanced by Na^+, gives a chemical shift at around -20ppm in ^{31}P MAS-NMR [62]. The three glasses studied here all showed a shoulder at around -20ppm (Figure 5.31). Therefore, this species could be present in all the glasses, but since the Al:P ratio is one in the metaphosphate species, a high content of phosphorus is required. As there is a small amount of phosphorus in all glasses from Schott AG (Germany), the proportion of this species may be quite low.

Lastly, a small number of surplus charge balancing cations can force Al to be in higher coordination states, Al(V) and Al(VI). The Al:(Si+P) ratio (Appendix III) shows that all glass compositions are within the Loewenstein's rule known as the aluminium avoidance principle [10], and therefore, Al is expected to be charge balanced in a four coordination state. However, all the glasses studied here showed a pronounced peak at around -3ppm for Al(VI). It has been suggested that the glass compositions with high fluorine content can have Al in a high coordination, which is associated with Al-F-Na/Ca/Sr species [22, 23, 65], and these species have been observed in ^{19}F MAS-NMR spectra (Figure 5.27). Although all glasses studied here

are within the Loewenstein's aluminium avoidance principle, the number of the charge balancing cations may be insufficient to maintain aluminium in four coordination state.

5.7.3. ^{31}P MAS-NMR Spectroscopy

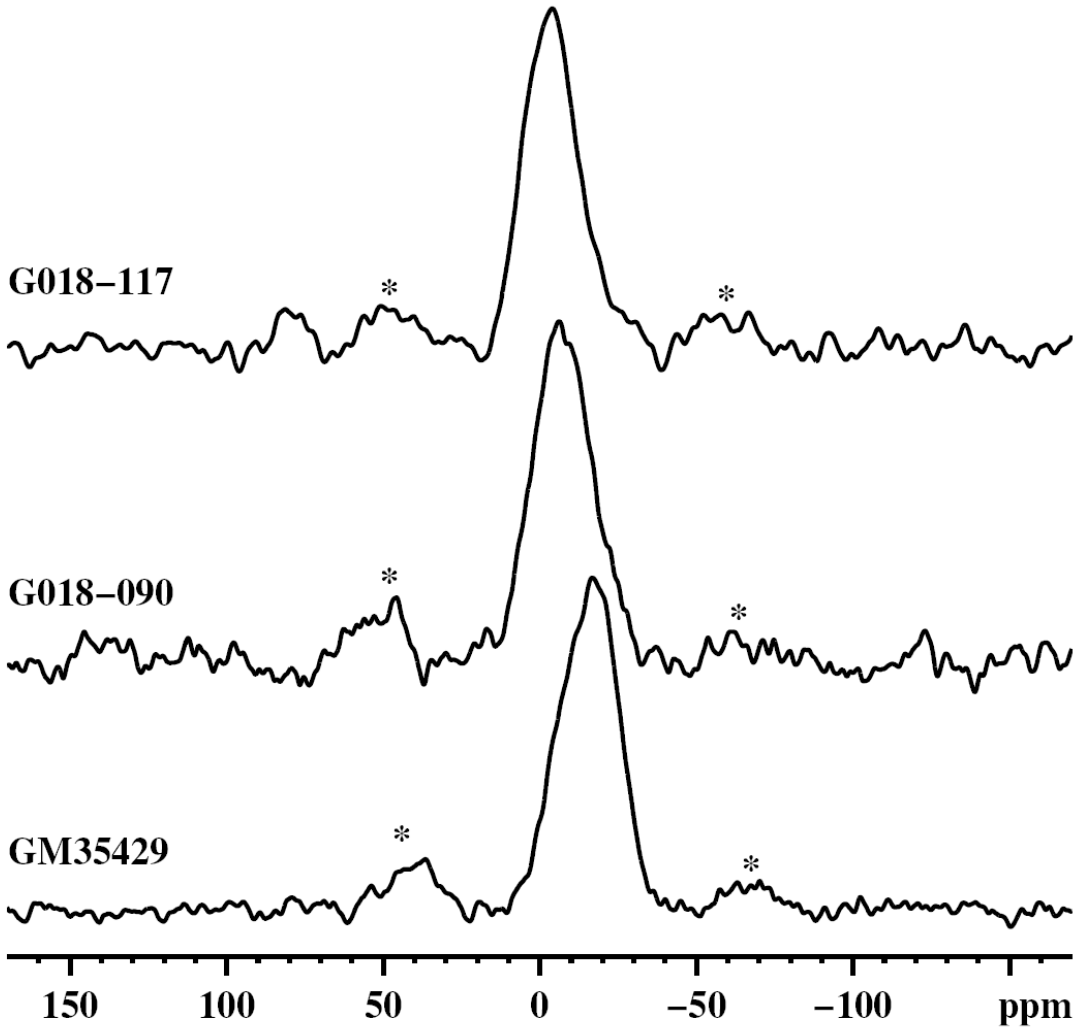


Figure 5.31. ^{31}P MAS-NMR spectra for Schott glasses. Spinning sidebands are marked by asterisks.

Glass GM35429 exhibited an unsymmetrical peak at -17ppm with a shoulder at around -12ppm (Figure 5.31). This is in a region for Q^1 pyrophosphate Al-O-PO_3^{3-} species. The observed chemical shift, however, is too negative to be a simple

pyrophosphate species with one Al surrounding a PO_4 tetrahedron. The chemical shift for $AlPO_4$ is at -27ppm [8]. Therefore, along with its ^{27}Al MAS-NMR spectrum (Figure 5.29), there seems to be more than one Al around each PO_4 tetrahedron. A similar chemical shift was observed by Stamboulis and co-workers [22]. Lang and co-workers [75] also found the chemical shift for phosphorus with two Al attached to each PO_4 tetrahedron at around -12ppm. Therefore, the shoulder observed with glass GM35429 may show the presence of this species.

The chemical shift for metaphosphate species charge balanced by Na^+ occurs at around -20ppm [62], and the chemical shift observed here is quite close to this, although the phosphate content is quite low in GM35429. These possibilities arise due to the lack of Ca^{2+}, Sr^{2+}, Zn^{2+} and Na^+ cations to charge balance the PO_4^{3-} species. GM35429 has the lowest amount of the charge balancing cations for the PO_4^{3-} species (Appendix III) which can force more than one Al to be around a PO_4 tetrahedron.

The chemical shifts for G018-090 and G018-117 are -7ppm and -4ppm, respectively (Figure 5.31). Their chemical shifts are more positive than that of GM35429 because they contain less phosphate. As a result, there will be a reduced number of Al-O-P formed, which was also observed with ^{27}Al MAS-NMR (Figure 5.29). Moreover, these two glass compositions have a higher number of cations per phosphorus (Appendix III). Therefore, more NBOs can be charge balanced by cations than for GM35429.

5.7.4. ^{29}Si MAS-NMR Spectroscopy

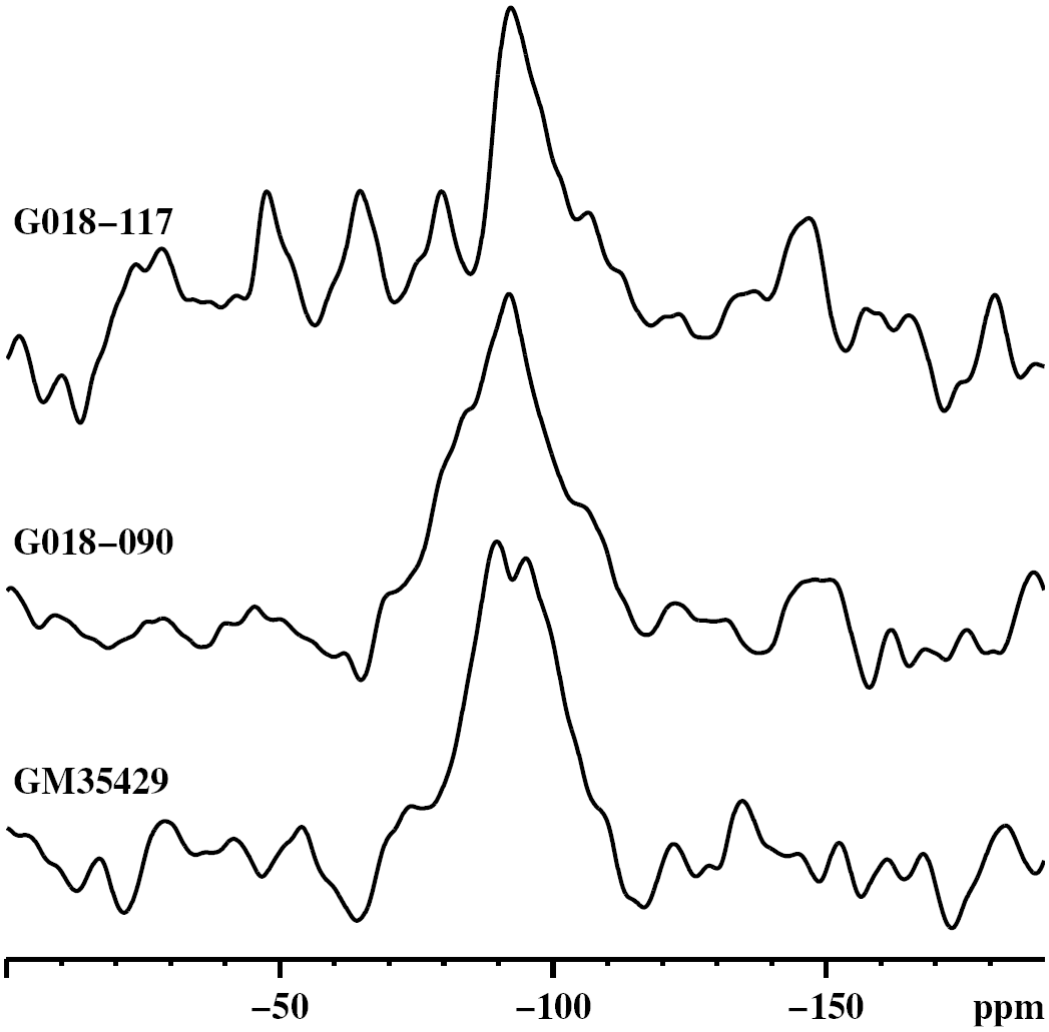


Figure 5.32. ^{29}Si MAS-NMR spectra for Schott glasses.

The ^{29}Si MAS-NMR spectra of glasses GM35429 and G018-090 showed peaks at -92ppm, and G018-117 at -93ppm (Figure 5.32). The change in chemical shift in ^{29}Si MAS-NMR can be described by the formula, $Si(OSi)_{m\text{-}n}$ $(OAl\text{-})_n$ $(O\text{-})_{4\text{-}m}$, where *m* is the number of BOs on Si and *n* the number of next neighbour Al on each SiO_4 tetrahedra. The chemical shift is known to increase if *m* decreases or *n* increases [28].

The Si:Al ratio is the highest for G018-117 (Appendix III), and this glass exhibited the most negative peak position on the ^{29}Si MAS-NMR spectrum (Figure 5.32). This is in accordance with the formula mentioned above. A decrease in the ratio indicates a decrease in the number of next neighbour Al on SiO_4, and therefore the chemical shift becomes more negative. Also, the number of BOs in G018-117 would be the highest due to its lowest fluorine content of the three glasses studied here. It has been shown that fluorine forms Al-F-Na/Ca/Sr species and forms NBOs on Si [21]. Therefore, G018-117 would have the highest number of BOs among the three glasses studied here. This again correlates well with the formula mentioned earlier.

5.7.5. DSC Analysis

The T_g of glass GM35429 is the lowest (Appendix III) simply because this glass composition has the highest amount of fluorine. The decrease in T_g is due to fluorine coordinating preferentially with Ca^{2+} cations forming F-Ca(n) species which can only bridge one NBO. This disrupts the network effectively, and hence T_g decreases [21]. Comparing glasses G018-090 and G018-117, G018-090 has a slightly higher amount of fluorine, which is reflected in its lower T_g than G018-117.

Part II. Characterisation of GPCs with Mg, Sr, and Zn containing Fluoro-Aluminosilicate Glasses

5.8. MAS-NMR Studies on the Setting Reaction of GPCs

This study was conducted to understand the setting chemistry of GPCs formed from fluoro-aluminosilicate glasses containing magnesium. Various studies have been performed on the setting reaction of GPCs [31, 33, 35, 76]. However, the setting reaction of the magnesium containing GPCs has not been studied to date. The two end glass compositions in the Ca-Mg and the Sr-Mg series, LG26, LG26Mg, and LG26Sr, and the middle compositions in each series, ICHK04 and ICHK10, were selected for this study. The setting chemistry of these cements was followed by ^{19}F, ^{31}P, and ^{27}Al MAS-NMR spectroscopy.

5.8.1. ^{19}F MAS-NMR Spectroscopy

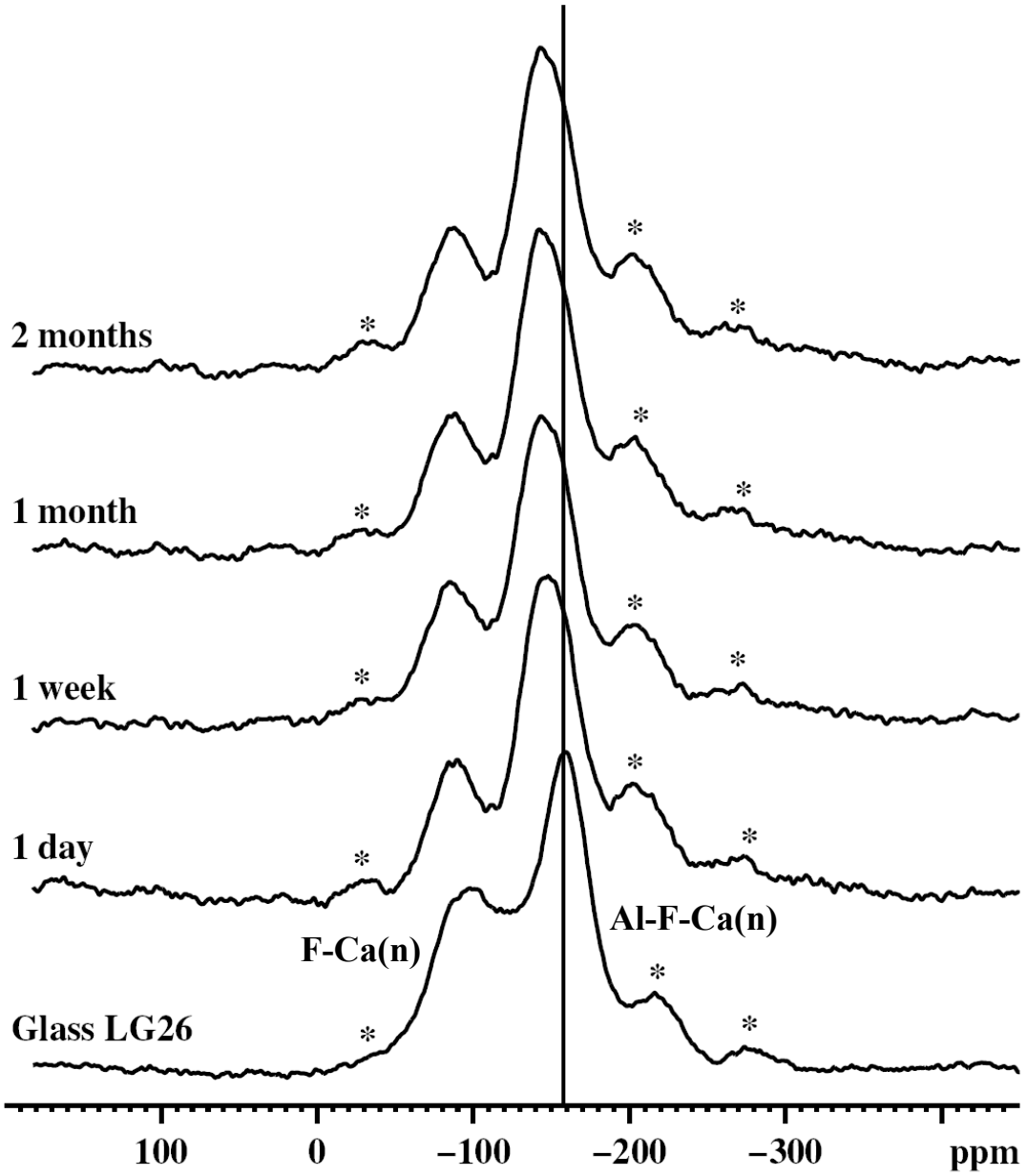


Figure 5.33. ^{19}F MAS-NMR spectra for glass LG26 [$4.5SiO_2$. $3.0Al_2O_3$. $1.5P_2O_5$. $3.0CaO$. $2.0CaF_2$] and its cements. Spinning sidebands are marked by asterisks, and the vertical line is a guide to eye only.

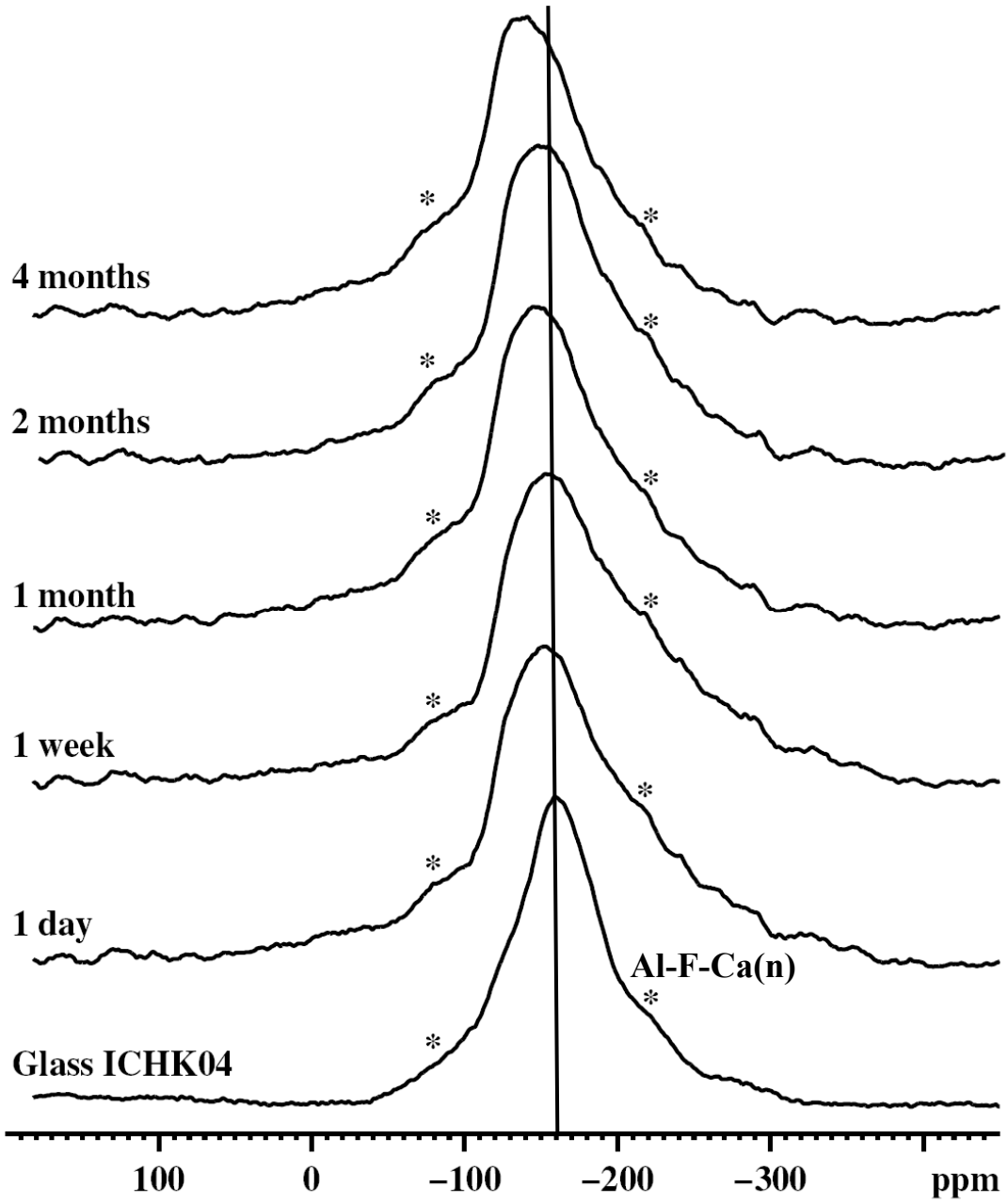


Figure 5.34. ^{19}F MAS-NMR spectra for glass ICHK04 [4.5SiO_2. 3.0Al_2O_3. 1.5P_2O_5. 3.0CaO. 2.0MgF_2] and its cements. Spinning sidebands are marked by asterisks, and the vertical line is a guide to eye only.

Glass LG26 exhibited two major peaks at -98ppm and -159ppm for F-Ca(n) and Al-F-Ca(n) species respectively (Figure 5.33). Glass ICHK04 showed one major peak at -159ppm for Al-F-Ca(n) species with a shoulder at around -180ppm for F-Mg(n) species (Figure 5.34) [20, 26].

The setting reaction seems to result in reduction of the intensity of F-Ca(n) species in LG26 cements (Figure 5.33). The reduction of this peak is difficult to quantify due to the spinning sidebands overlapping with each other. However, the reduction in intensity indicates that F-Ca(n) species are easily released from the glass network when the setting reaction takes place. This may be because F-Ca(n) species are not part of the glass network. Similar results were observed by Zainuddin [19].

The peaks at -159ppm for both LG26 and ICHK04 cements move slightly to a less negative value, towards 0ppm, and the peak also becomes broader (Figure 5.33, Figure 5.34). Zainuddin [19] found that the chemical shift moved to -130ppm in aged cements and suggested that Al in Al-F-Ca(n) species in the glass network is released during cement formation and crosslinks the carboxylate groups of PAA. Then F^- forms a bond to the Al in the cement matrix creating Al-F species with Al at a higher coordination state. Broadening of the Al-F-Ca(n) peaks suggests that there is a possibility of mixed sites, such as Al-F-Ca(n) species in the residual glass matrix and Al-F species in the cement matrix.

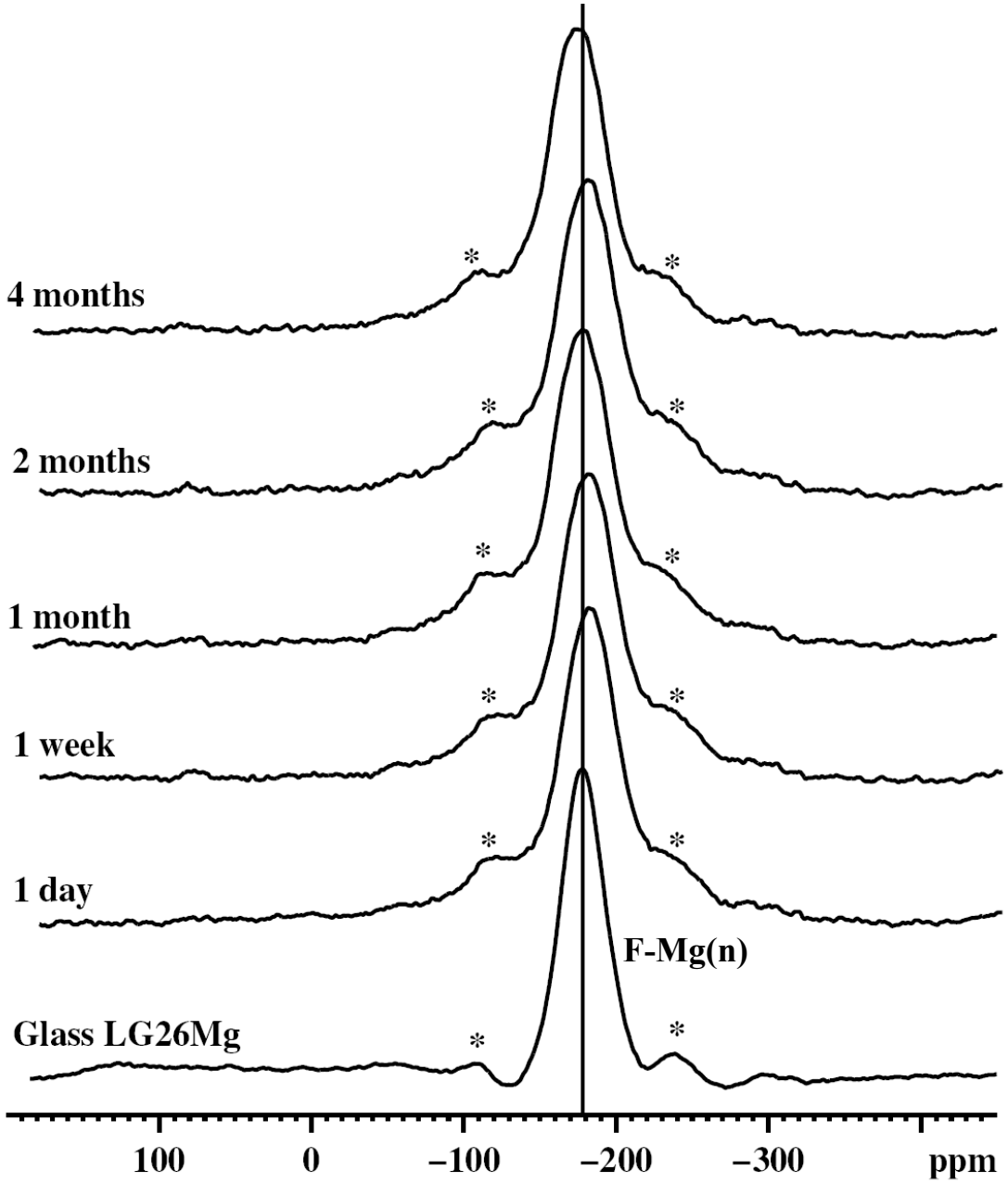


Figure 5.35. ^{19}F MAS-NMR spectra for glass LG26Mg [4.5SiO_2. 3.0Al_2O_3. 1.5P_2O_5. 3.0MgO. 2.0MgF_2] and its cements. Spinning sidebands are marked by asterisks, and the vertical line is a guide to eye only.

The chemical shift for glass LG26Mg was observed at -179ppm (Figure 5.35), which has been assigned to F-Mg(n) species, with the number of Mg around F close to three [54, 57]. It is quite difficult to state whether these F-Mg(n) species participate in the crosslinking process or simply remain unchanged in the glass as there is no other

fluorine species detected on the ^{19}F MAS-NMR spectra to compare with (Figure 5.35). This is very different from LG26 cements. ^{19}F-MAS NMR spectra of the fully calcium substituted glass LG26 [$4.5SiO_2$. $3.0Al_2O_3$. $1.5P_2O_5$. 3.0CaO. $2.0CaF_2$] showed that the peak for F-Ca(n) species became less intense upon setting (Figure 5.33). F-Mg(n) species in glass LG26Mg is not part of the glass network, similar to F-Ca(n) species in glass LG26. Therefore, it is highly possible that these F-Mg(n) species are released during the setting reaction but this is quite difficult to detect due to them being the only fluorine species present in the glass/cement matrix. It is also possible that some of F-Mg(n) species remains in the glass network since there is unreacted glass in the cements.

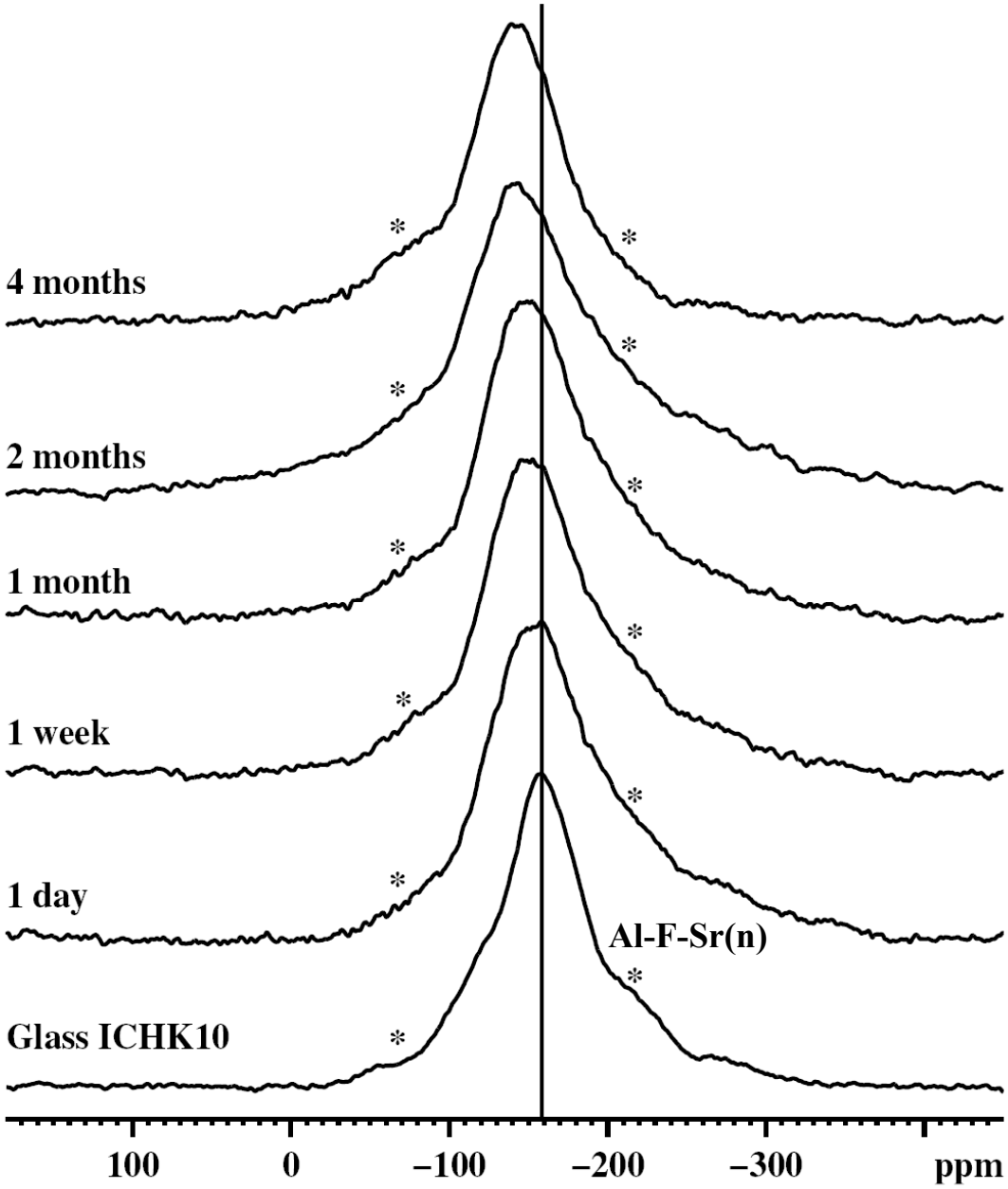


Figure 5.36. ^{19}F MAS-NMR spectra for glass ICHK10 [$4.5SiO_2$. $3.0Al_2O_3$. $1.5P_2O_5$. 3.0SrO. $2.0MgF_2$] and its cements. Spinning sidebands are marked by asterisks, and the vertical line is a guide to eye only.

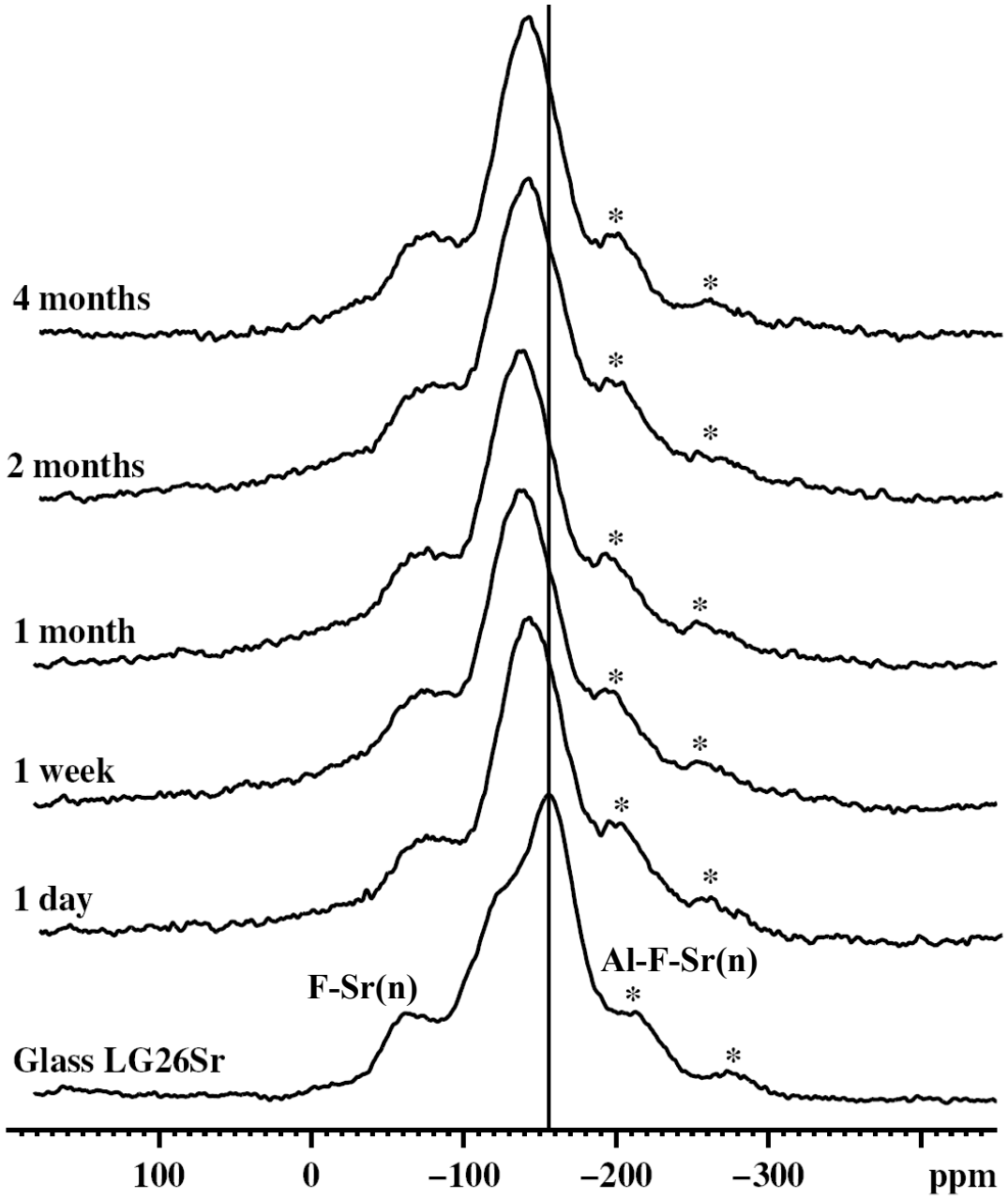


Figure 5.37. ^{19}F MAS-NMR spectra for glass LG26Sr [$4.5SiO_2$. $3.0Al_2O_3$. $1.5P_2O_5$. 3.0SrO. $2.0SrF_2$] and its cements. Spinning sidebands are marked by asterisks, and the vertical line is a guide to eye only.

Glass ICHK10 exhibited a major peak at -158ppm due to Al-F-Sr(n) species (Figure 5.36). There were two peaks observed for glass LG26Sr at -62ppm for F-Sr(n) species and -156ppm for Al-F-Sr(n) species (Figure 5.37) [20]. Similar to Al-F-Ca(n) species in both LG26 and ICHK04 cements, the peaks at -156ppm/-158ppm for glasses

LG26Sr and ICHK10 moved to a less negative value, towards 0ppm with aged cements (Figure 5.36, Figure 5.37). This, again, could have been caused by Al released from the glass and F^- attached to Al in the cement matrix [19]. Moreover, the intensity F-Sr(n) peak for LG26Sr cements reduced slightly during setting (Figure 5.37) although spinning sidebands may overlap with the peak. This reduction in the intensity is quite similar to the F-Ca(n) peak in LG26 cements (Figure 5.33). F-Sr(n) species are not part of the glass network and therefore seem to be released for the crosslinking process with the polycarboxylic acid more readily than Al-F-Sr(n) species. Finally, the peak for Al-F-Sr(n) species in ICHK10 cements (Figure 5.36) seems to move towards 0ppm much more than the peak for Al-F-Ca(n) species in ICHK04 cements (Figure 5.34). This difference may arise from differences in the divalent cations, Ca^{2+} and Sr^{2+}, which was also observed by Zainuddin [19].

The Al-F-Sr(n) peaks in ICHK10 (Figure 5.36) and LG26Sr cements (Figure 5.37) also became broader with aging time. A similar trend was observed for ICHK04 (Figure 5.34) and LG26 cements (Figure 5.33), which contain calcium instead of strontium, and it seems to have resulted from the presence of mixed sites, such as Al-F species with Al in the higher coordination in the cement matrix and Al-F-Sr(n) species in the residual glass.

5.8.2. ^{31}P MAS-NMR Spectroscopy

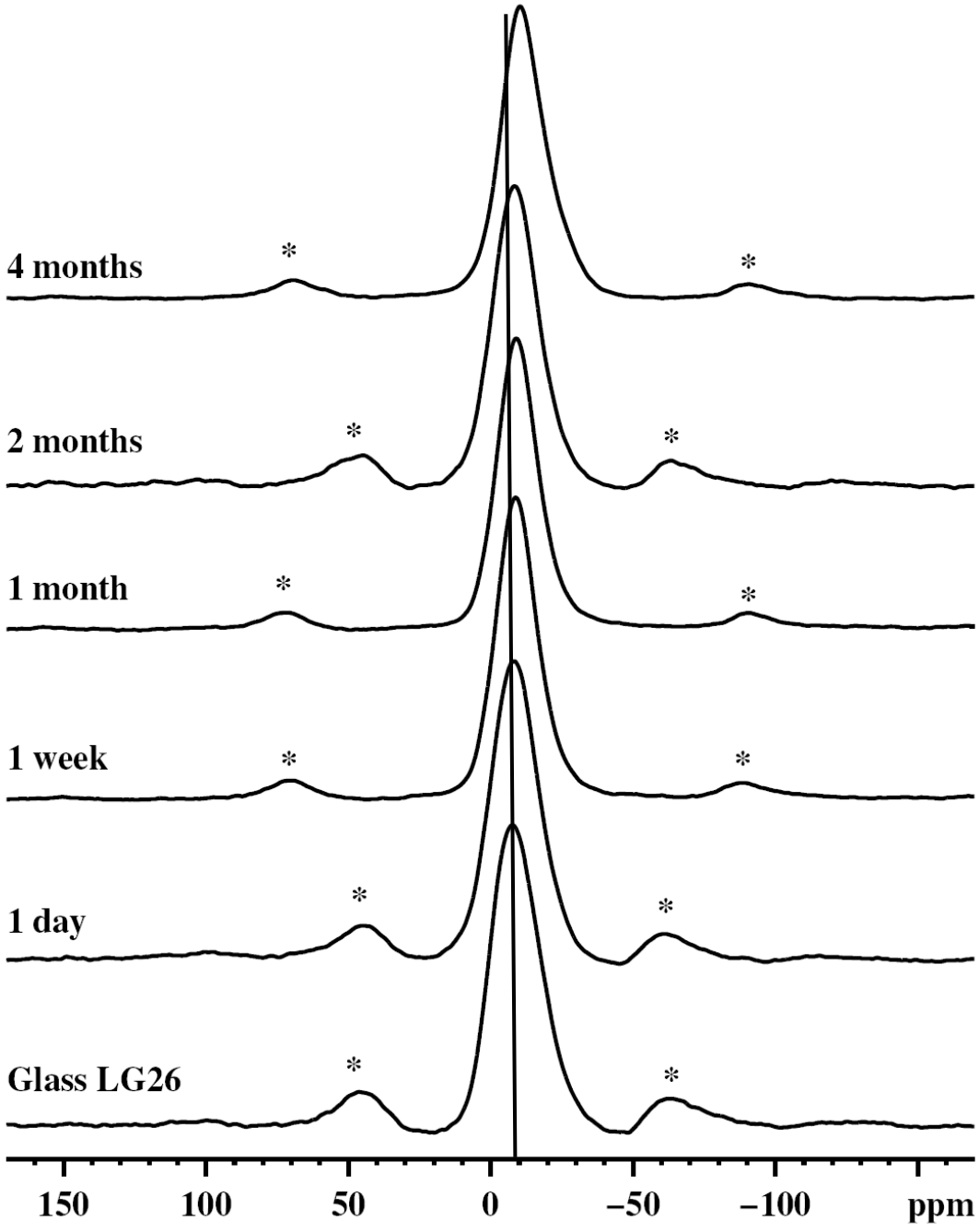


Figure 5.38. ^{31}P MAS-NMR spectra for glass LG26 [4.5SiO_2. 3.0Al_2O_3. 1.5P_2O_5. 3.0CaO. 2.0CaF_2] and its cements. Spinning sidebands are marked by asterisks, and the vertical line is a guide to eye only.

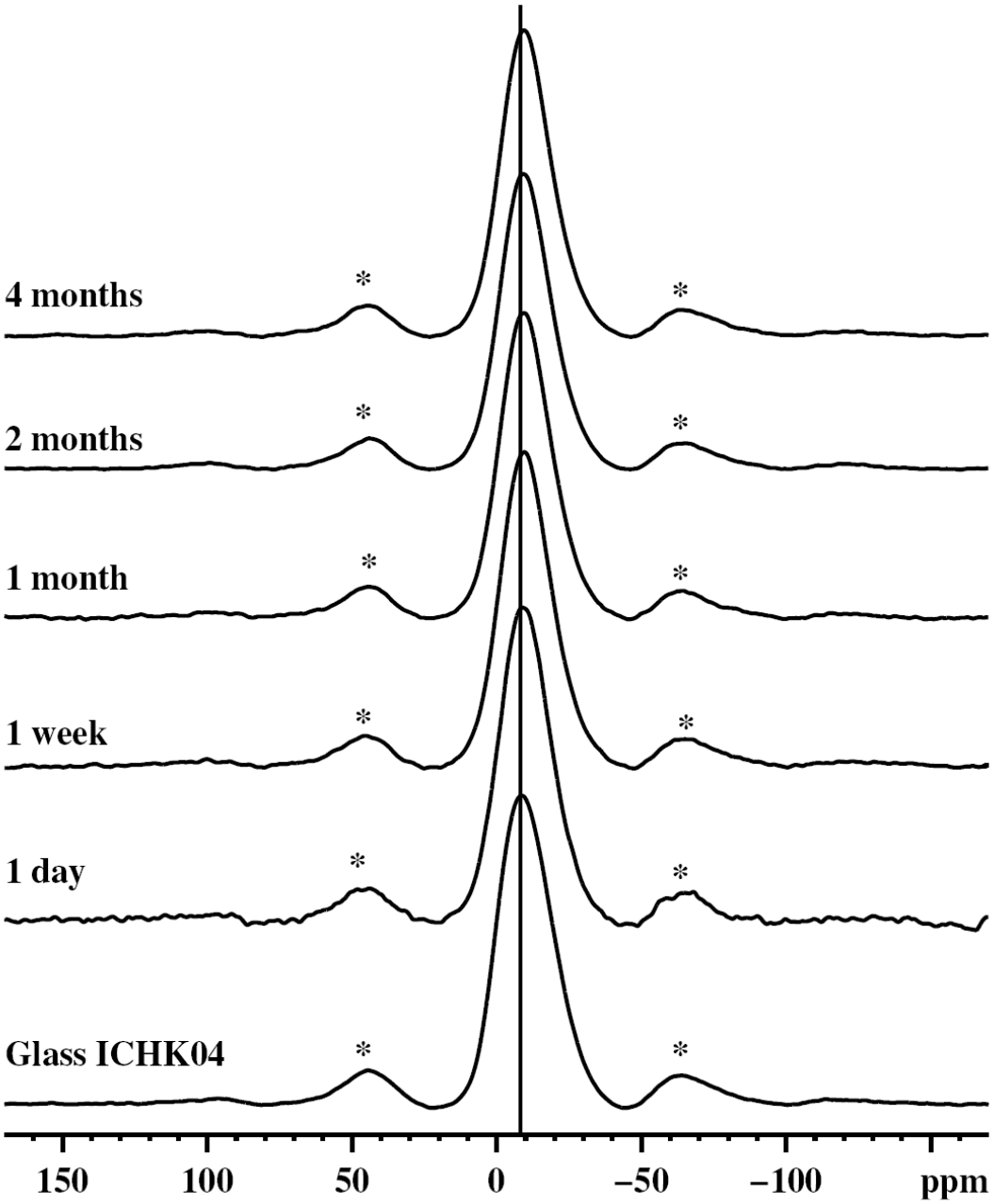


Figure 5.39. ^{31}P MAS-NMR spectra for glass ICHK04 [4.5SiO_2. 3.0Al_2O_3. 1.5P_2O_5. 3.0CaO. 2.0MgF_2] and its cements. Spinning sidebands are marked by asterisks, and the vertical line is a guide to eye only.

Glass LG26 showed a peak at -8ppm assigned to Q^1 pyrophosphate Al-O-PO_3^{3-} species [23, 24, 31]. There is a slight change in the chemical shift, to around -11ppm, when the cement is aged for 4 months, as well as a slight reduction in the peak width (Figure 5.38, Table 5.7).

Glass ICHK04 exhibited a chemical shift at -9ppm for Q^1 pyrophosphate Al-O-PO_3^{3-} species [23, 24, 31]. This peak moved slightly to -9ppm in the cements after 4 months aging time (Figure 5.39). Similar to LG26 cements, the peak width in the ^{31}P MAS-NMR spectra for ICHK04 cements slightly decreased with aging time (Table 5.7).

The change in chemical shift to a more negative value in the ^{31}P MAS-NMR spectra with aging cements was also seen with other studies [33, 76]. Matsuya and co-workers [76] have shown that although their original glasses exhibited a peak between 5ppm and -20ppm, the chemical shift for their cements were all observed at around -10ppm. Similarly, Stamboulis and co-workers [33] found peaks shifting to -10ppm irrespective of the original glass compositions. A chemical shift in the ^{31}P MAS-NMR spectrum generally decreases if the number of Al around PO_4 tetrahedra is increased [8]. Stamboulis and co-workers [33] have therefore suggested that during the setting reaction, the cations charge balancing NBOs on phosphorus in Al-O-PO_3^{3-} species are released preferentially increasing the number of AlO_4 around PO_4 tetrahedra. More recently, Zainuddin [19] studied the setting reaction of GPCs, including LG26 cement, and observed a slight change in the chemical shift moving away from 0ppm, in ^{31}P MAS-NMR spectra of the cements. However, she concluded that this change in the chemical shift was due to the release of the charge balancing cations from the glass or the rearrangement of these cations around the phosphate environment.

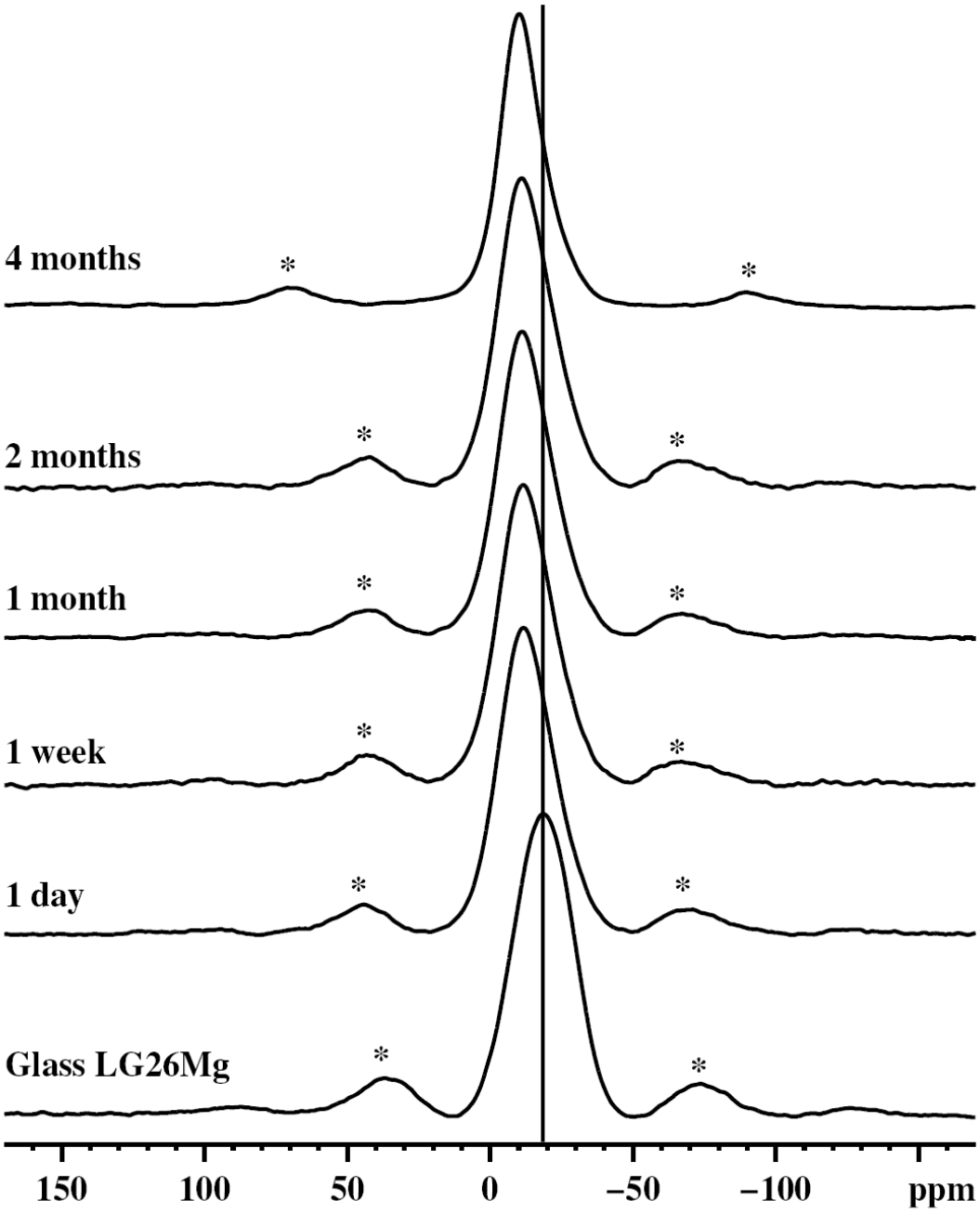


Figure 5.40. ^{31}P MAS-NMR spectra for glass LG26Mg [4.5SiO_2. 3.0Al_2O_3. 1.5P_2O_5. 3.0MgO. 2.0MgF_2] and its cements. Spinning sidebands are marked by asterisks, and the vertical line is a guide to eye only.

The chemical shift for glass LG26Mg was observed at -19ppm (Figure 5.40). This relatively broad peak was assigned to a mixture of magnesium pyrophosphate, $Mg_2P_2O_7$, [18, 61] and Q^1 pyrophosphate Al-O-PO_3^{3-} species [23-25]. At 1 day aging time, this peak moved to a more positive value, around -11ppm. The phosphate species responsible for the chemical shift at -19ppm in the original glass was magnesium pyrophosphate [18, 61]. The change in chemical shift with aging time seems to indicate that these magnesium pyrophosphate species are no longer present in the cement. This absence of magnesium pyrophosphate in the cements can also be seen with the reduction in peak width (Table 5.7). Several studies have shown that L-(+)-tartaric acid holds cations, such as Ca^{2+} and Al^{3+}, from the glass before these cations participate in crosslinking process with the polymeric acid [77, 78]. It is therefore possible that Mg^{2+} from magnesium pyrophosphate is removed by L-(+)-tartaric acid leaving pyrophosphate, $[P_2O_7]^{4-}$, which could be released into storage water, as phosphorus species have been found to be released into water during storage [77]. Alternatively, as it was discussed in Section 5.3.1, there could be a formation of P-O-Mg species in glass LG26Mg. It is possible that this P-O-Mg species is hydrolysed releasing Mg^{2+} and P^{5+} from the glass network, and as a result, this species will no longer be present in the glass/cement matrix.

Moreover, the chemical shifts for LG26Mg cements are quite similar to LG26 and ICHK04 cements. This indicates that the phosphate species present in LG26Mg cements is similar to LG26 and ICHK04 cements although the original glass compositions are quite different.

Table 5.7. Half-width values of the peaks observed in ^{31}P MAS-NMR spectra for glasses LG26, ICHK04, LG26Mg, ICHK10, and LG26Sr and their cements, in Hz.

Aging time	Half-width / Hz				
	LG26	ICHK04	LG26Mg	ICHK10	LG26Sr
0	1652	1736	1959	1608	1374
1 day	1583	1652	1835	1531	1296
1 week	1572	1619	1827	1345	1262
1 month	1557	1630	1798	1230	1257
2 months	1528	1626	1827	1327	1243
4 months	1436	1615	1360	1318	1240

The chemical shift for Q^1 pyrophosphate Al-O-PO_3^{3-} species in glass ICHK10 was observed at -8ppm. This peak shifted to a more negative value, around -10ppm, in the 4 months aged cements (Figure 5.41). This change in chemical shift was also observed with ICHK04 cements (Figure 5.39) which contain the same amount of magnesium in the glass composition, as well as LG26 cements, which have no magnesium in the glass composition (Figure 5.38). This indicates that the phosphorus environment in the cement is similar regardless of the original glass compositions. Also, the peak width became much narrow with aging time (Table 5.7).

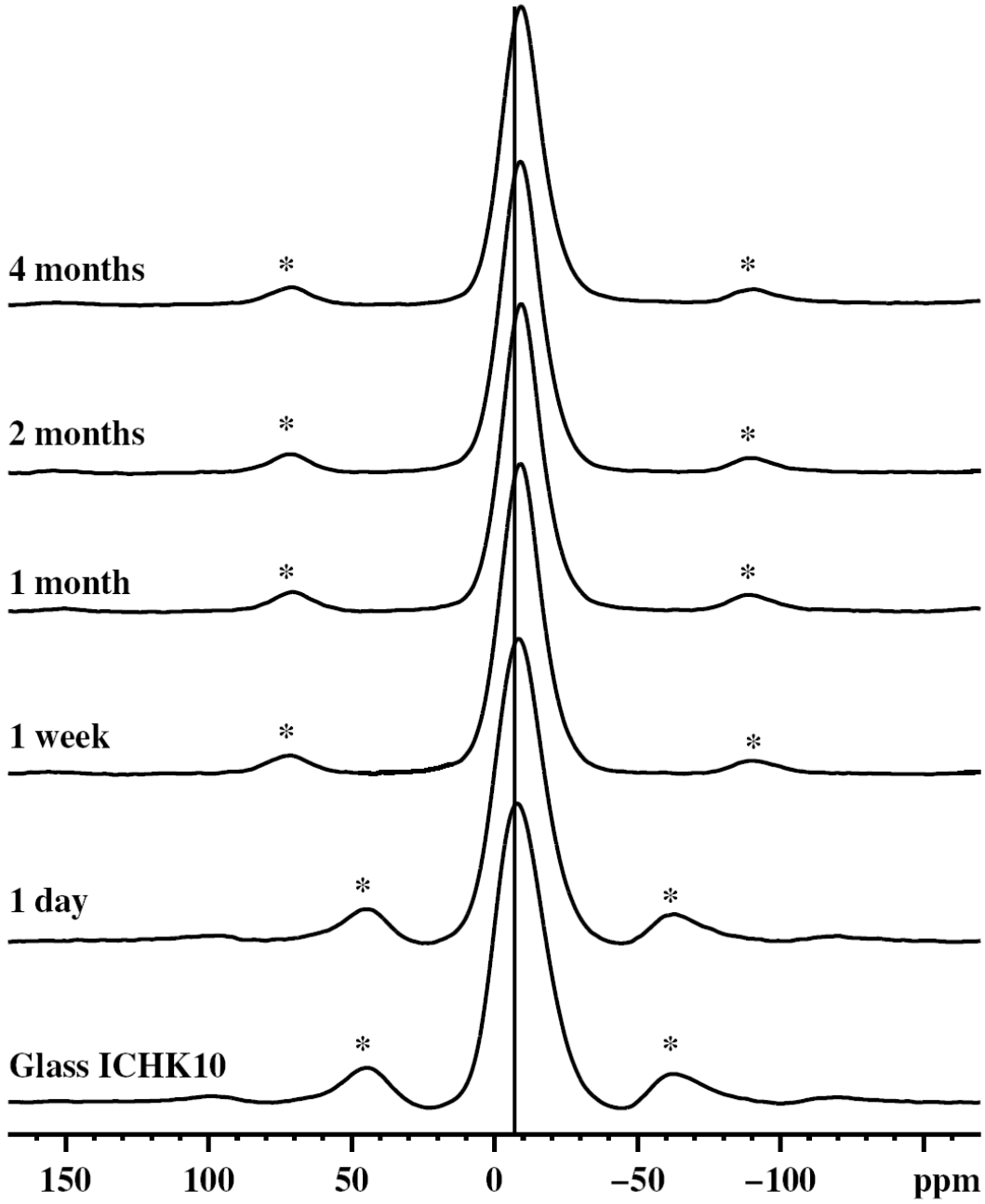


Figure 5.41. ^{31}P MAS-NMR spectra for glass ICHK10 [$4.5SiO_2$. $3.0Al_2O_3$. $1.5P_2O_5$. 3.0SrO. $2.0MgF_2$] and its cements. Spinning sidebands are marked by asterisks, and the vertical line is a guide to eye only.

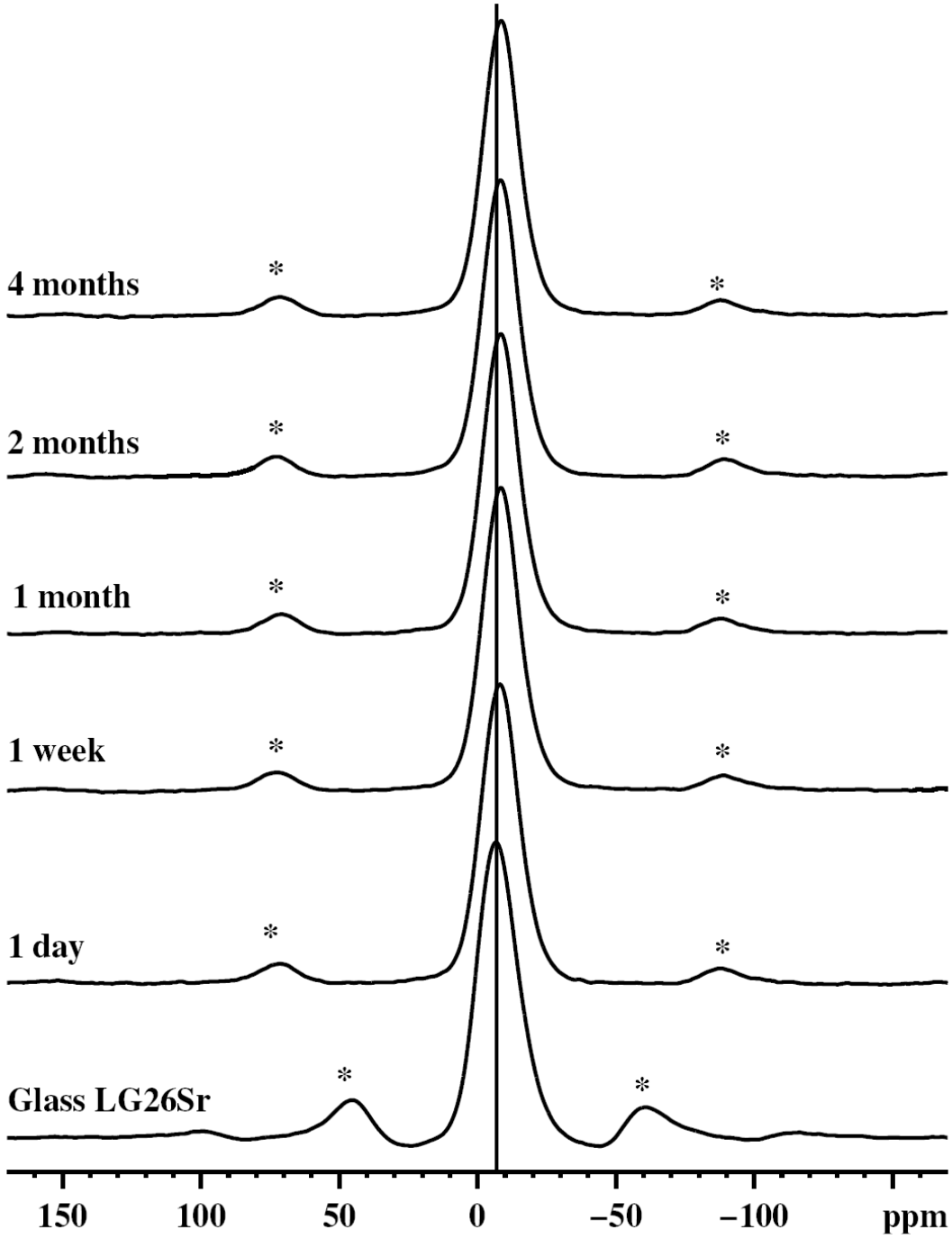


Figure 5.42. ^{31}P MAS-NMR spectra for glass LG26Sr [4.5SiO_2. 3.0Al_2O_3. 1.5P_2O_5. 3.0SrO. 2.0SrF_2] and its cements. Spinning sidebands are marked by asterisks, and the vertical line is a guide to eye only.

Glass LG26Sr exhibited a chemical shift at -7ppm for Q^1 pyrophosphate Al-O-PO_3^{3-} species [23-25]. This peak slightly moved to -8ppm in the 4 months aged cements

(Figure 5.42). The ^{31}P MAS-NMR spectra of LG26, ICHK04, LG26Mg, ICHK10 and LG26Sr cements all showed that the chemical shift of the cements reached around -10ppm although the glass compositions are quite different (Figures 5.38-5.42), indicating that the phosphorus environment in the cement is similar, and the chemical shifts observed with the aged cements correspond to Q^1 pyrophosphate Al-O-PO_3^{3-} species.

Moreover, the width of the peaks in the ^{31}P MAS-NMR spectra for LG26Sr cements slightly decreased with aging time (Table 5.7). The decrease in peak width could indicate that there is a smaller number of mixed phosphorus species present in the cement compared to the glass.

5.8.3. ^{27}Al MAS-NMR Spectroscopy

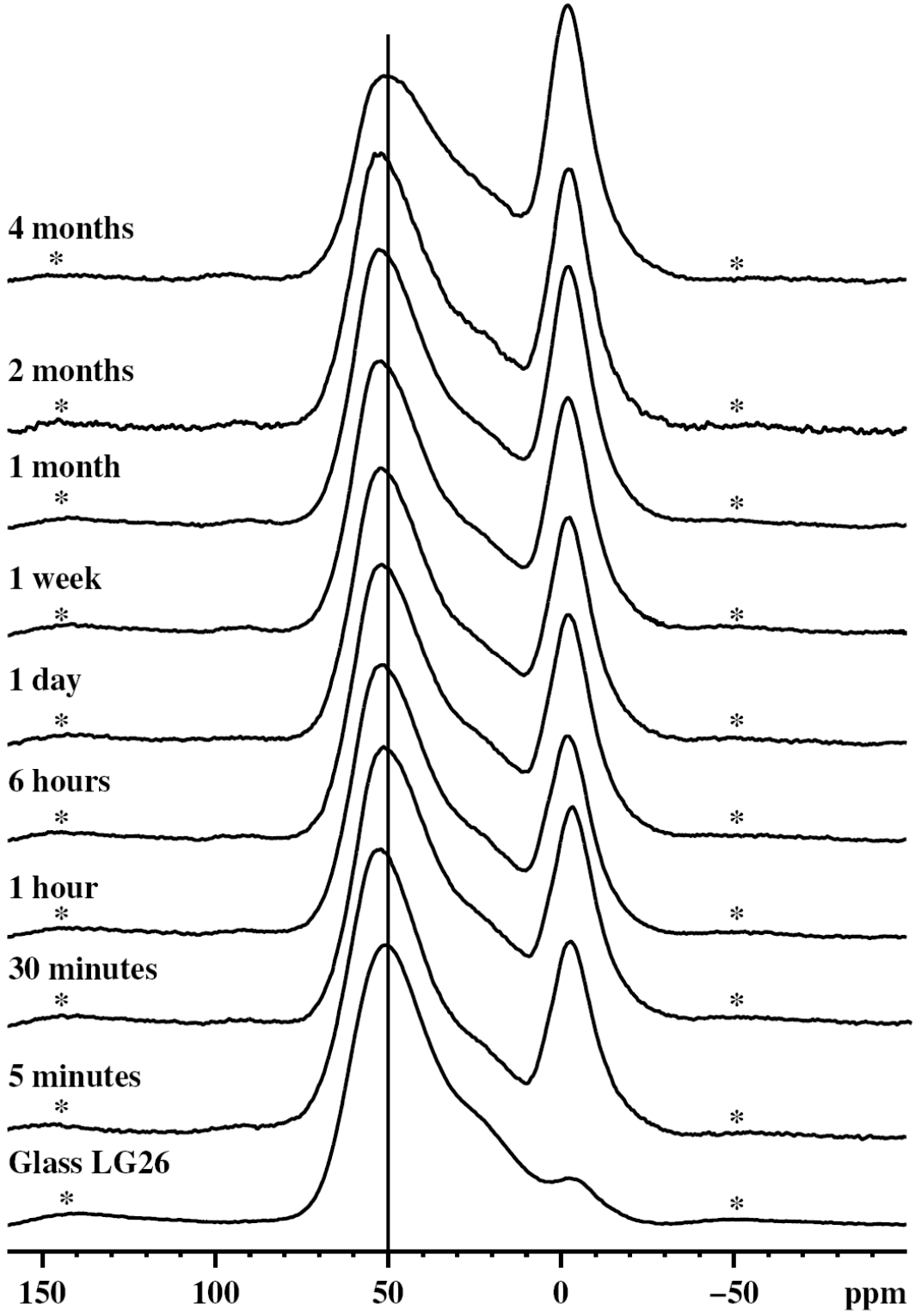


Figure 5.43. ^{27}Al MAS-NMR spectra of glass LG26 [4.5SiO_2. 3.0Al_2O_3. 1.5P_2O_5. 3.0CaO. 2.0CaF_2] and its cements. Spinning sidebands are marked by asterisks, and the vertical line is a guide to eye only.

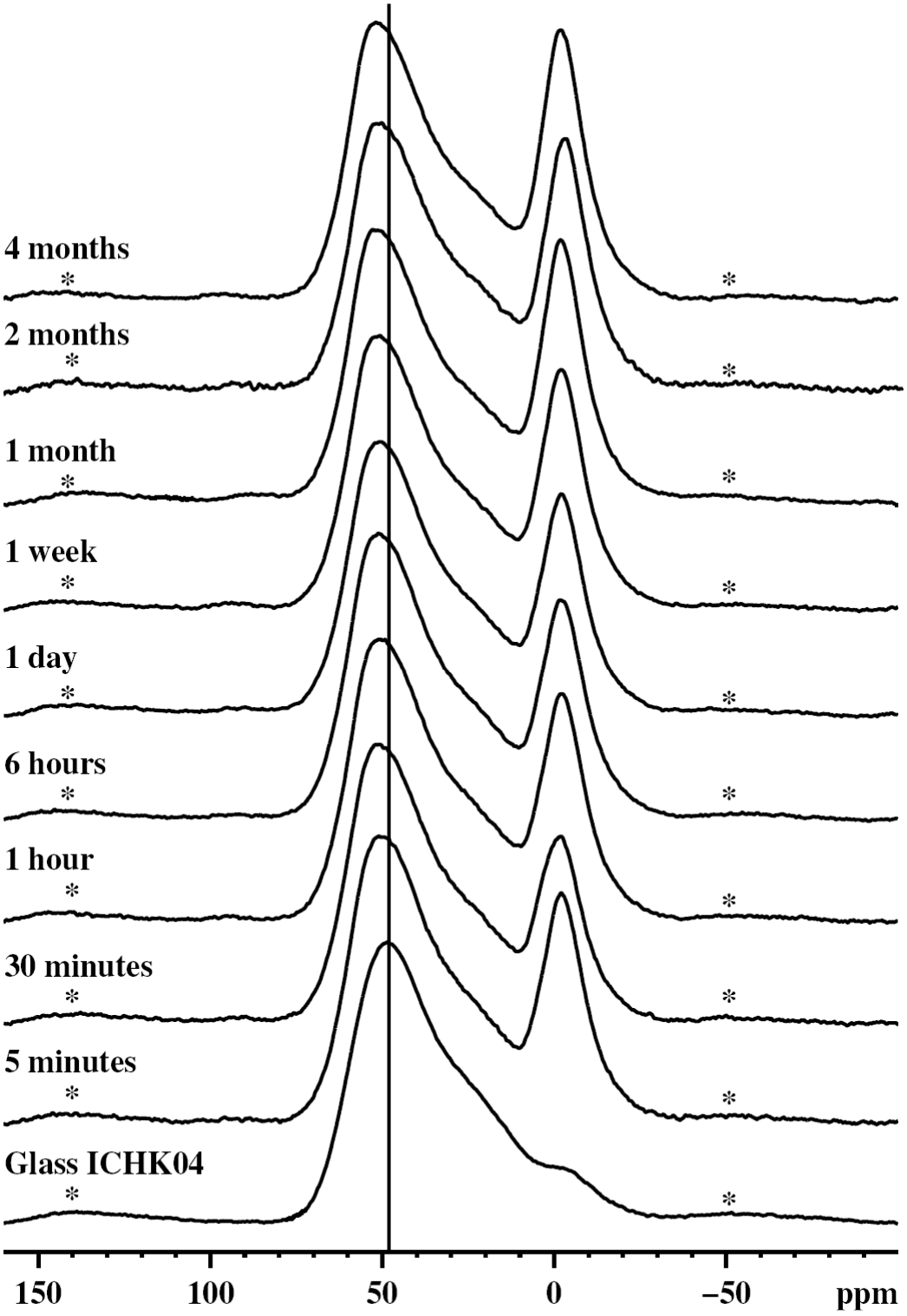


Figure 5.44. ^{27}Al MAS-NMR spectra of glass ICHK04 [$4.5SiO_2$. $3.0Al_2O_3$. $1.5P_2O_5$. 3.0CaO. $2.0MgF_2$] and its cements. Spinning sidebands are marked by asterisks, and the vertical line is a guide to eye only.

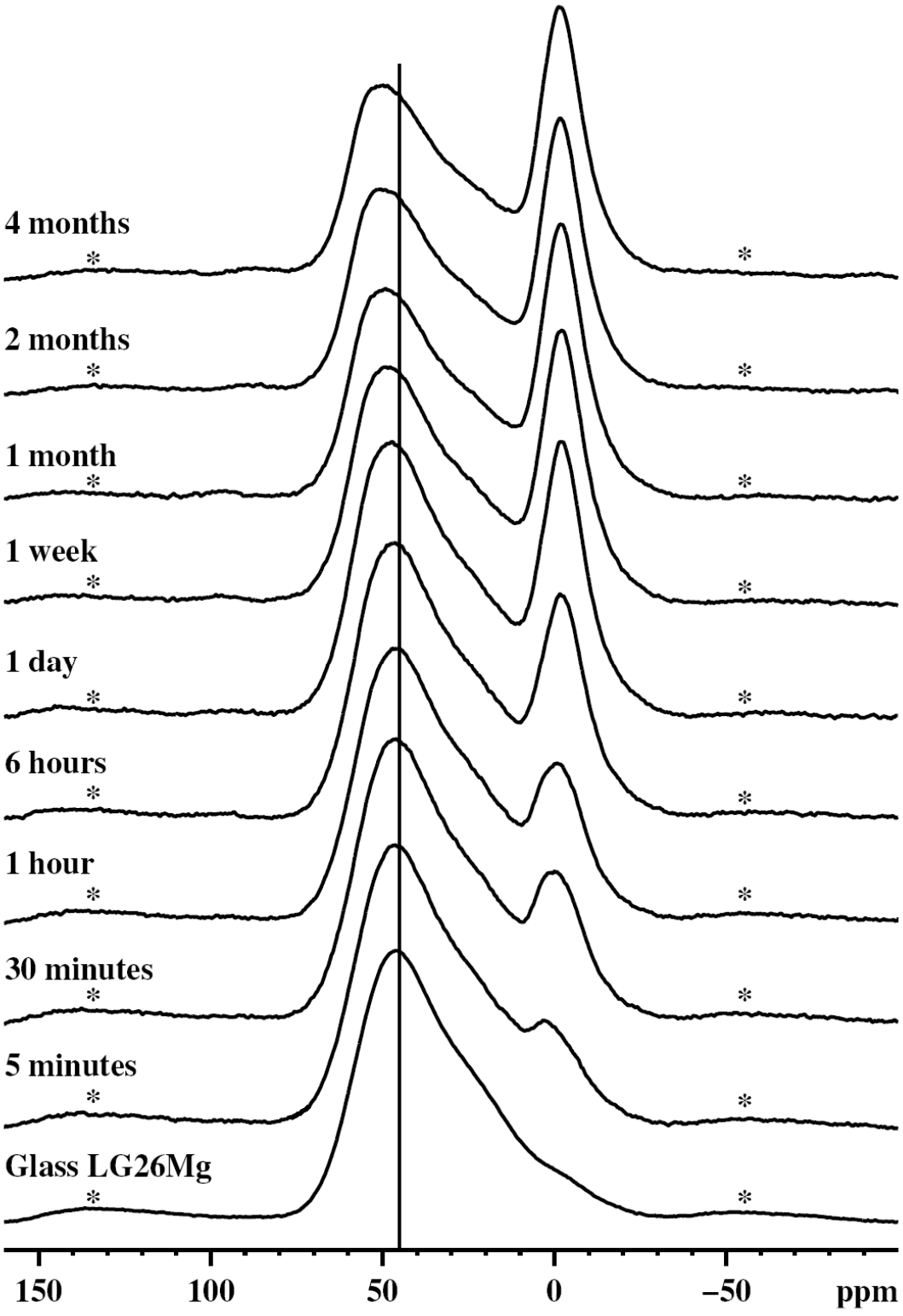


Figure 5.45. ^{27}Al MAS-NMR spectra of glass LG26Mg [4.5SiO_2. 3.0Al_2O_3. 1.5P_2O_5. 3.0MgO. 2.0MgF_2] and its cements. Spinning sidebands are marked by asterisks, and the vertical line is a guide to eye only.

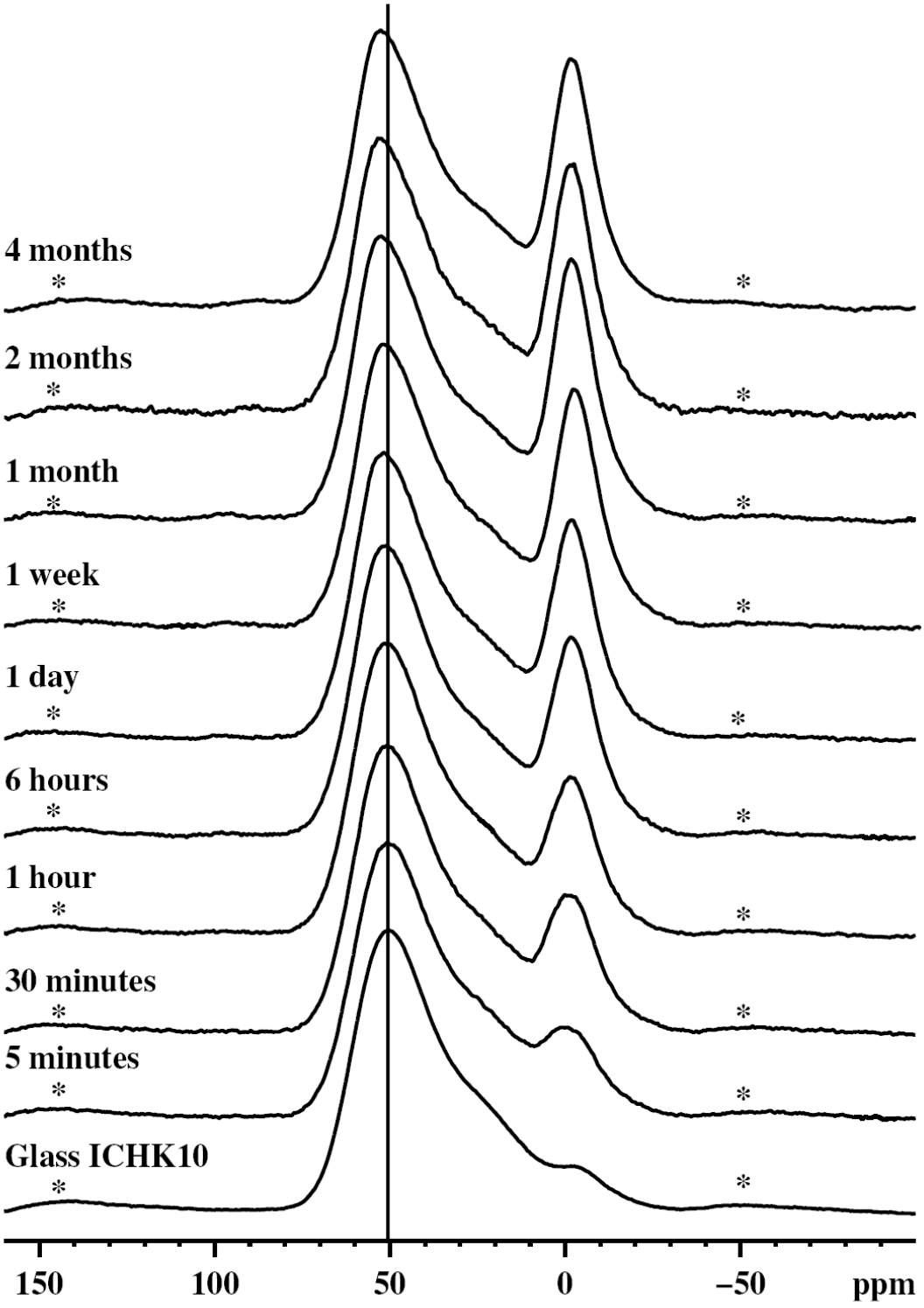


Figure 5.46. ^{27}Al MAS-NMR spectra of glass ICHK10 [4.5SiO_2. 3.0Al_2O_3. 1.5P_2O_5. 3.0SrO. 2.0MgF_2] and its cements. Spinning sidebands are marked by asterisks, and the vertical line is a guide to eye only.

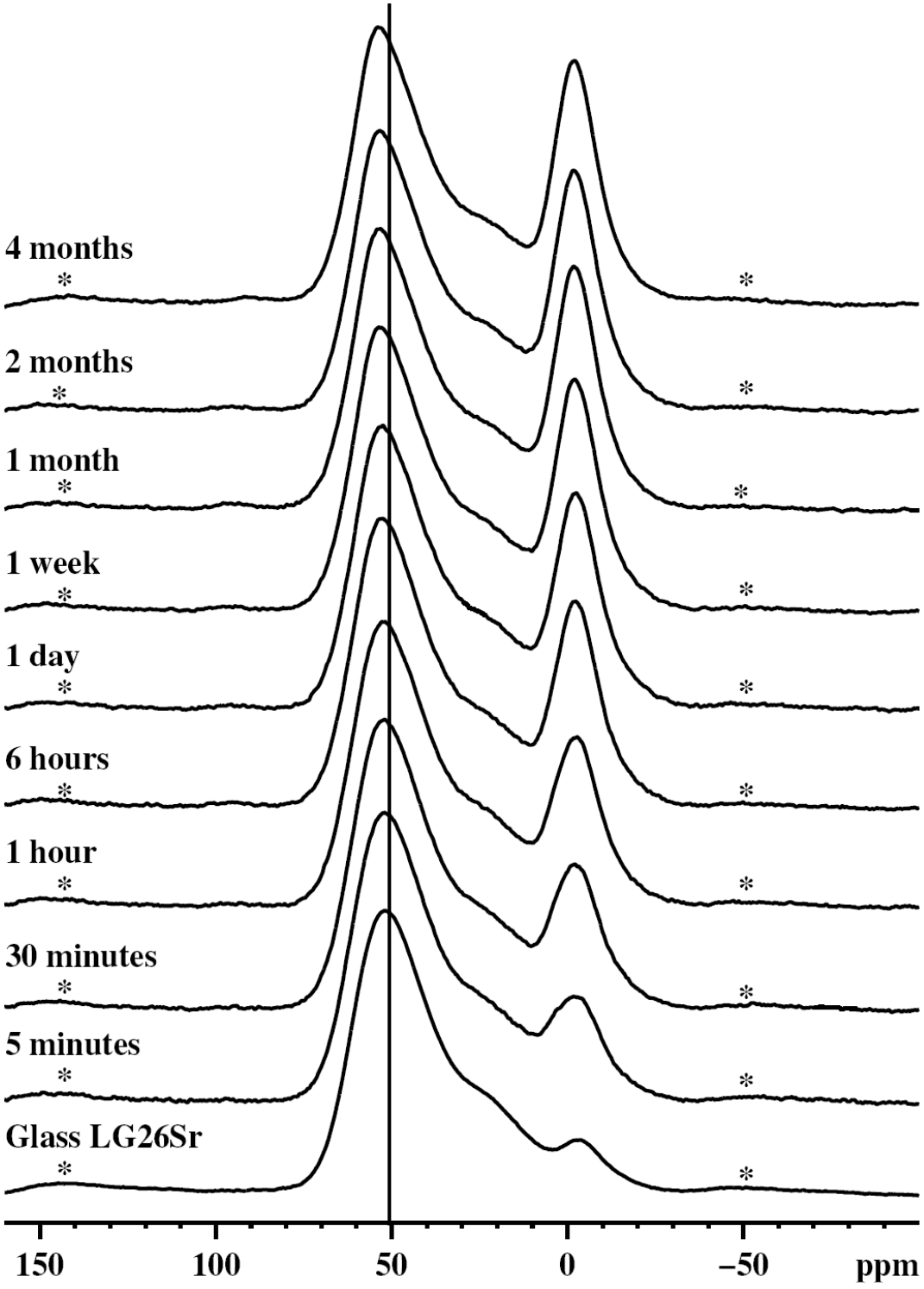


Figure 5.47. ^{27}Al MAS-NMR spectra of glass LG26Sr [4.5SiO_2. 3.0Al_2O_3. 1.5P_2O_5. 3.0SrO. 2.0SrF_2] and its cements. Spinning sidebands are marked by asterisks, and the vertical line is a guide to eye only.

The chemical shifts for glasses LG26, ICHK04, and LG26Mg were observed at 51ppm, 48ppm, and 46ppm respectively (Figure 5.43, Figure 5.44, Figure 5.45), and these peaks have been assigned to Al in the tetrahedral coordination, Al(IV) [23-25]. Similarly, glasses LG26Sr and ICHK10, which contain strontium instead of calcium, exhibited a peak at 52ppm and 50ppm respectively (Figure 5.46, Figure 5.47), and these are assigned to Al(IV) species. All of these glasses had a very small peak at about -5ppm for Al in the octahedral coordination, Al(VI) [23-25, 65]. The shoulder on the Al(IV) peak has been assigned to Al in the pentahedral coordination, Al(V) [65].

With all these cements, the intensity of the Al(VI) peak increased with time, and the chemical shift for Al(IV) increased, moving away from 0ppm, to 50-53ppm at 4 months aging time (Figures 5.43-5.47). This shift to a more positive value was seen despite the differences in the glass compositions. Stamboulis and co-workers [33] observed an opposite effect in chemical shifts with the cements. They observed a decrease in the chemical shift and concluded that the shift was due to an increase in the Si:Al ratio in the glass as Al(IV) converts to Al(VI) and/or Al(V) and is lost from the glass. More recently, however, Zainuddin [19] has also observed a slight movement in the chemical shift to a more positive value in her LG26 cements as well as LG35 cements [2.0SiO_2. 1.0Al_2O_3. 1.0CaO. 1.0CaF_2]. She has suggested that this increase in the chemical shift is because of the release of fluoride ions from Al-F-Ca(n) sites during the setting reaction of the cements. The chemical shift of the Al(IV) peak of her cements containing no fluoride did not increase to higher values.

The proportion of each Al species was quantified by deconvoluting the area under each peak using the *dmfit* Cz software [66]. By doing so, the conversion of Al(IV) to Al(VI) during the setting reaction can be followed. Table 5.8 shows the amount of each Al species in the glass and the 4 months aged cements calculated by deconvoluting the peaks, and Al species present in the cements with shorter aging times are shown in the Appendix V.

Table 5.8. Chemical shift, δ, and percentages of Al species in glasses LG26, ICHK04, LG26Mg, ICHK10 and LG26Sr and their cements at 4 months aging time. The *dmfit* Cz software was used for quantification of Al species.

Glass	Aging time	Al(IV)		Al(V)		Al(VI)	
		Amount /%	δ /ppm	Amount /%	δ /ppm	Amount /ppm	δ /ppm
LG26	0	72	51	22	22	5	-3
	4 months	47	51	18	23	35	-2
ICHK04	0	67	48	26	22	7	-3
	4 months	54	52	17	25	29	-2
LG26Mg	0	65	46	29	20	6	-2
	4 months	46	50	18	25	36	-1
ICHK10	0	71	50	24	23	6	-3
	4 months	56	53	17	23	27	-2
LG26Sr	0	73	52	21	22	7	-4
	4 months	58	54	15	25	27	-2

Table 5.8 clearly shows that in all systems studied here, the amount of Al(IV) species decreased in the cements compared to the original glasses, and the amount of Al(VI)

species increased. For example, glass LG26 originally had 5% Al(VI) which increased to 35% at 4 months aging time. The setting reaction can be followed by calculating the Al(VI):Al(IV)+Al(V) ratio.

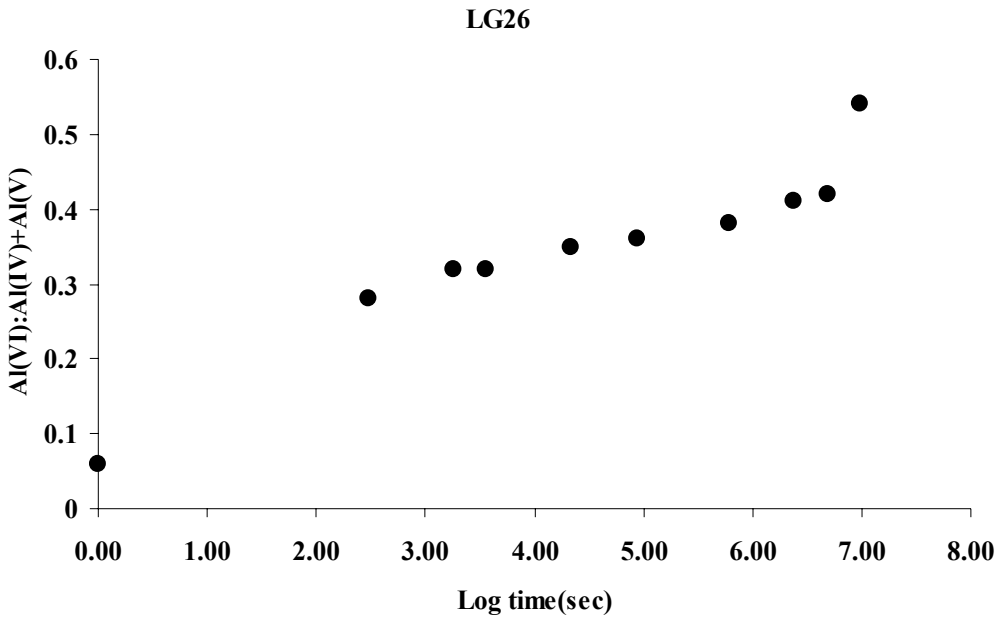


Figure 5.48. Al(VI):Al(IV)+Al(V) ratio plotted against log time in seconds for glass LG26 and its cements.

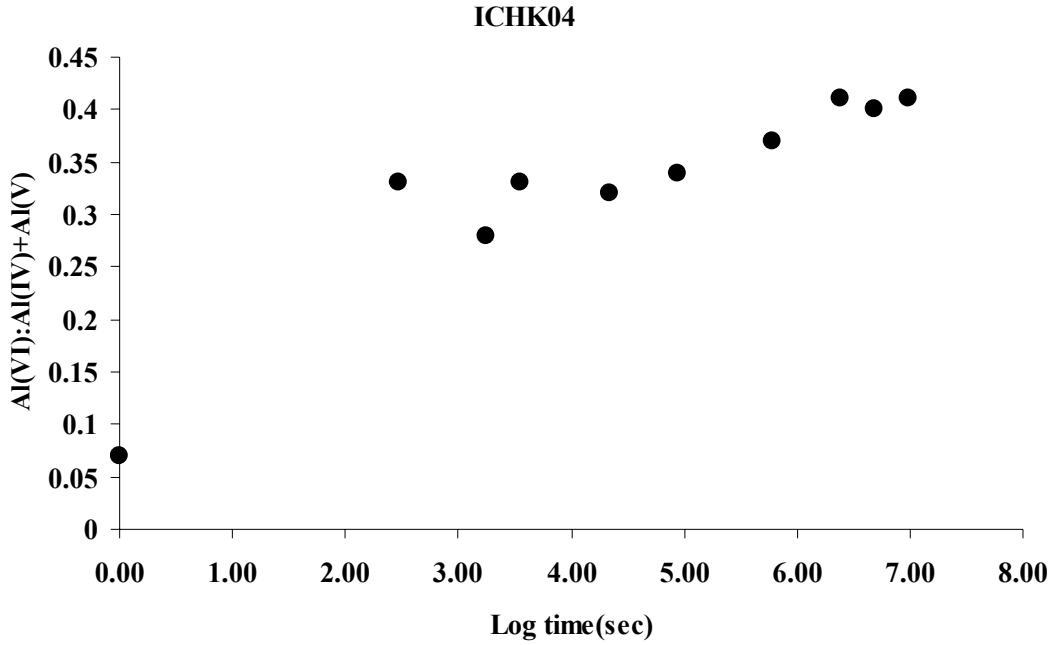


Figure 5.49. Al(VI):Al(IV)+Al(V) ratio plotted against log time in seconds for glass ICHK04 and its cements.

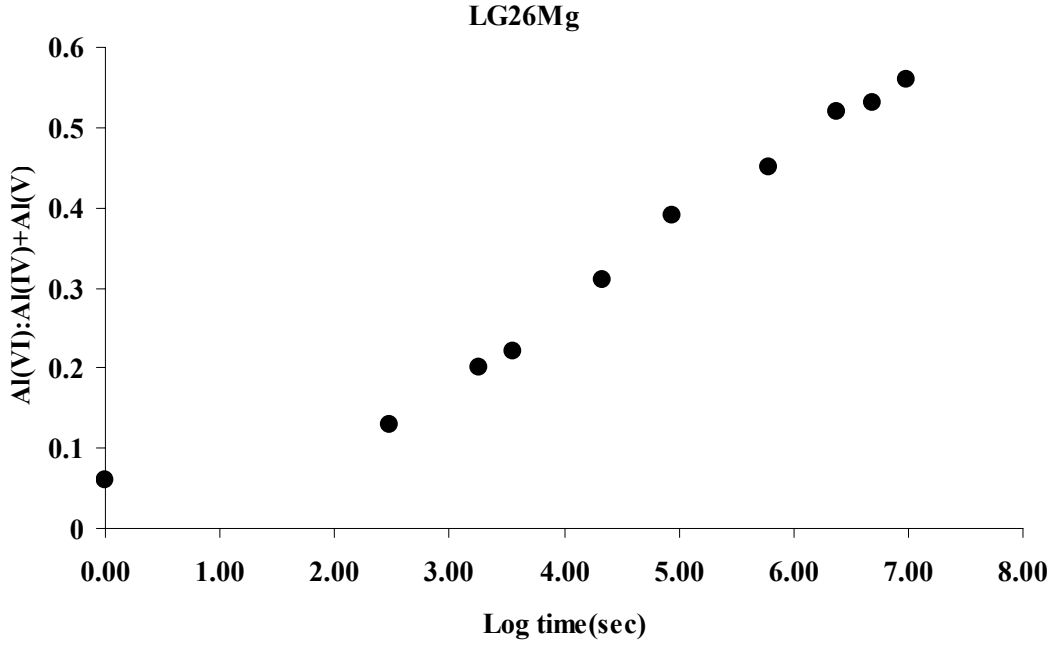


Figure 5.50. Al(VI):Al(IV)+Al(V) ratio plotted against log time in seconds for glass LG26Mg and its cements.

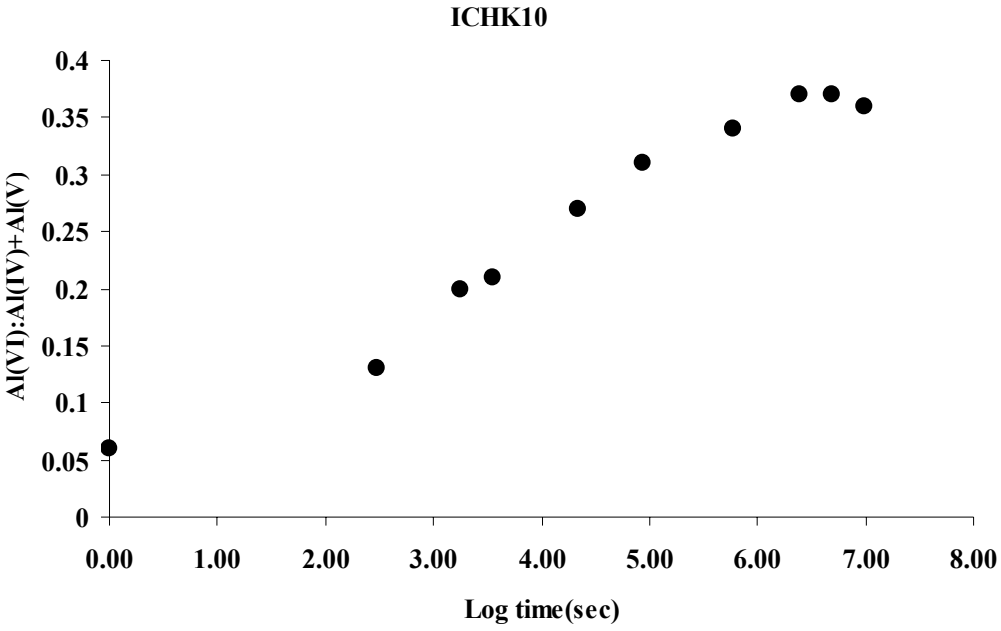


Figure 5.51. Al(VI):Al(IV)+Al(V) ratio plotted against log time in seconds for glass ICHK10 and its cements.

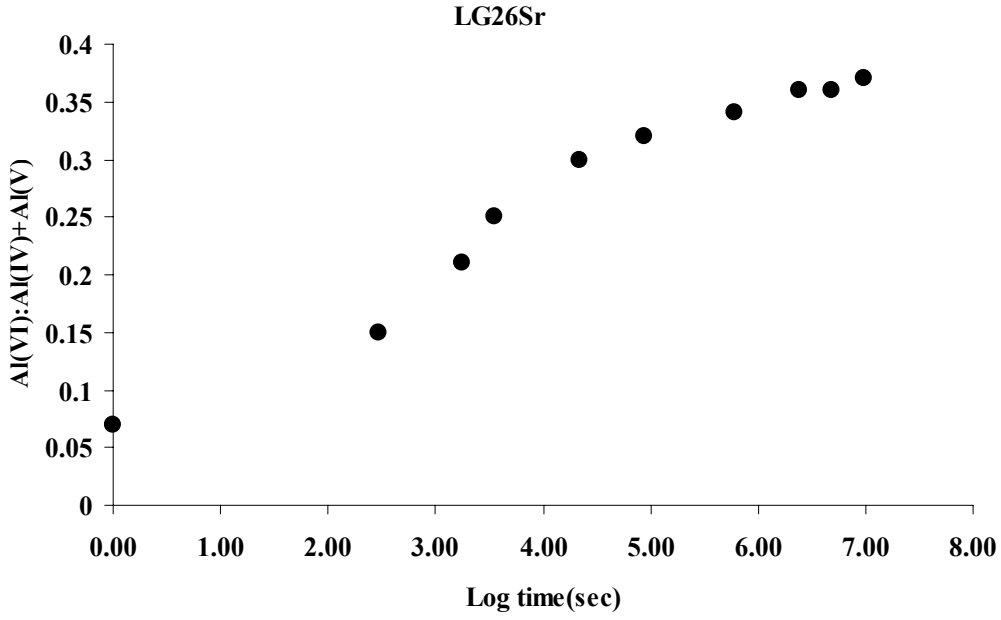


Figure 5.52. Al(VI):Al(IV)+Al(V) ratio plotted against log time in seconds for glass LG26Sr and its cements.

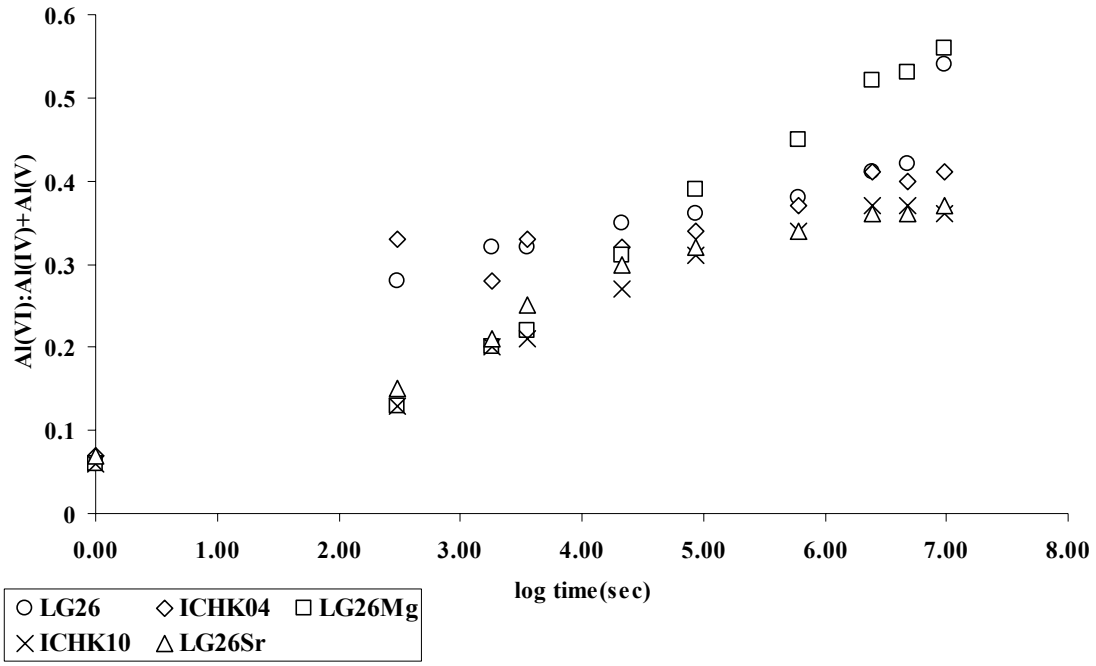


Figure 5.53. Al(VI):Al(IV)+Al(V) ratio plotted against log time in seconds for all glasses and cements.

Figures 5.48-5.52 show the semi-log plot of the Al(VI):Al(IV)+Al(V) ratio against log time in seconds for glasses LG26, ICHK04, LG26Mg, ICHK10, and LG26Sr and their cements. The semi-log plot for LG26 cements (Figure 5.48) and ICHK04 cements (Figure 5.49) look quite similar to each other. In both cases, the Al(VI):Al(IV)+Al(V) ratios become plateau at around 0.4 apart from the 4 months aged LG26 cement, which appears to be anomalous. Similarly, the semi-log plot of the Al(VI):Al(IV)+Al(V) ratio for ICHK10 cements (Figure 5.51) and LG26Sr cements (Figure 5.52) are quite similar to each other and to LG26 and ICHK04 cements as well: the ratio again plateau at around 0.4. On the contrary, the Al(VI):Al(IV)+Al(V) ratio for LG26Mg cements seems to increase linearly with the log time and seems to increase further with time, quite different from the other four cements (Figure 5.50).

For the purpose of the cement preparation, the charge ratio for the acid-base reaction was calculated as 0.26. This ratio was assumed to be the Al(VI):Al(IV)+Al(V) ratio for the setting reaction of the theoretical cements. However, the deconvolution of the ^{27}Al MAS-NMR spectra for the cements have revealed that the experimental Al(VI):Al(IV)+Al(V) ratio is higher, about 0.4 for all cements except LG26Mg (Figure 5.53), than the calculated ratio, 0.26. This is very different from a study conducted by Zainuddin [19] in which similar cement systems were studied. The experimental ratio in her study was about the same or slightly less than the calculated ratio as would be expected if the cement forming reaction has not gone to completion. The amount of PAA used in her cements was much less than this study, and furthermore no L-(+)-tartaric acid was used. The setting reaction of a simple calcium fluoro-aluminosilicate cements with L-(+)-tartaric acid was studied more recently, and the experimental Al(VI):Al(IV)+Al(V) ratio of the cements was also found to be higher [79]. It is therefore possible that L-(+)-tartaric acid provides sites for divalent cations, Ca^{2+}, Sr^{2+}, and Mg^{2+}, and trivalent Al^{3+} ions to ionically bind resulting in a greater conversion of Al(IV) to Al(VI) than the theoretically calculated. Also, the divalent cations, such as Ca^{2+}, Sr^{2+}, and Mg^{2+}, may be released more preferentially than Al^{3+}. By removing these divalent cations from charge balancing Al(IV) in the glass, this Al(IV) could be forced into higher coordination states within the glass. ^{27}Al MAS-NMR spectroscopy cannot distinguish different Al(VI) species and cannot distinguish whether Al is in the polysalt cement matrix or in the glass: Al(VI) could be participating in a crosslinking process with PAA in the cement matrix or is octahedrally coordinated still in the glass network. Zainuddin and co-workers [35] have also pointed out that Al(VI) species shown by ^{27}Al MAS-NMR spectroscopy do not always correlate to the Al^{3+} cations crosslinking to the carboxylate groups of the

polymeric acid. These six coordinate Al(VI) could have different ligands, such as F^-, COO^-, OH^-, attached which may change with time. They suggested that if COO^- ligands attach to Al^{3+} progressively over a long period of time, the mechanical properties would increase consequently.

The Al(VI):Al(IV)+Al(V) ratio of LG26Mg cements increased linearly with log time and may increase further with longer setting times than studied here (Figure 5.50). At 6 hours of aging time, the Al(VI):Al(IV)+Al(V) ratio of all cements studied here is similar to each other, but after this point, the ratio for LG26Mg cements increases while the ratio for the other cements starts to plateau slowly. The plateau in the Al(VI):Al(IV)+Al(V) ratio shows that the setting reaction has almost completed, and the fact that the ratio for LG26Mg cements keeps increasing could indicate that LG26Mg cements have more Al to be converted to Al(VI) than the other four cements. This "extra Al" in LG26Mg cements may arise from the fact that glass LG26Mg has no Al-F species while Al-F-Ca/Sr species are present in the other four glasses whose setting reaction is studied here (Figure 5.4, Figure 5.5). The amount of this "extra Al" in LG26Mg cements was estimated by using the deconvoluted ^{19}F MAS-NMR spectrum of glass LG26 and ^{27}Al MAS-NMR spectra of LG26 and LG26Mg cements. The deconvolution of ^{19}F MAS-NMR spectrum of glass LG26 (Figure 5.4) showed that 55% of fluorine is present as F-Ca(n) and 45% as Al-F-Ca(n) species . The mol% of fluoride in glass LG26 is 14.2mol%, and therefore, the mol% of Al in Al-F-Ca(n) species in glass LG26 can be estimated to be around 6.4mol%. The coordination of Al in Al-F-Ca(n) species is not yet fully determined, and therefore, all possibilities will be considered for the estimation of the "extra Al" in LG26Mg cements.

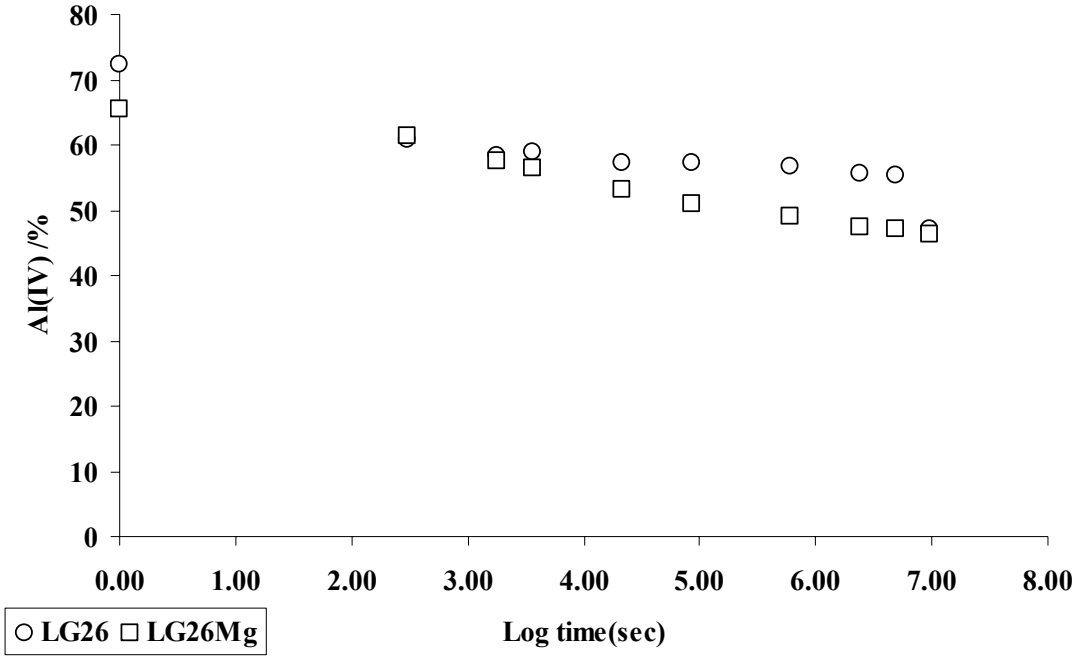


Figure 5.54. Percentages of Al(IV) species calculated by deconvoluting the ^{27}Al MAS-NMR spectra of LG26 (○) and LG26Mg (□) cements.

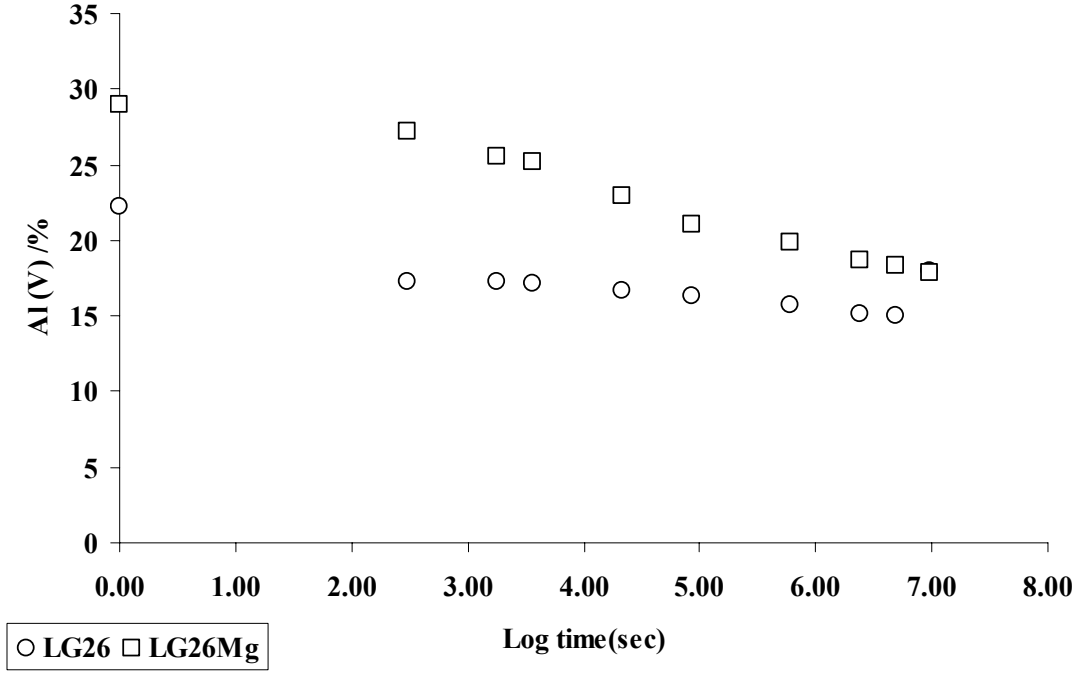


Figure 5.55. Percentages of Al(V) species calculated by deconvoluting the ^{27}Al MAS-NMR spectra of LG26 (○) and LG26Mg (□) cements.

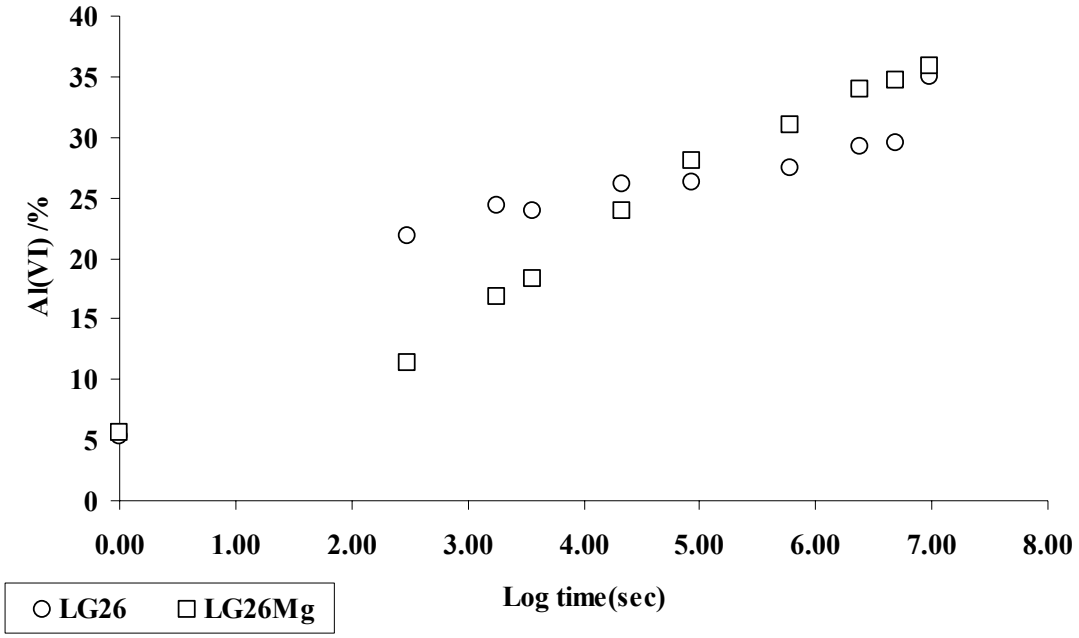


Figure 5.56. Percentages of Al(VI) species calculated by deconvoluting the ^{27}Al MAS-NMR spectra of LG26 (○) and LG26Mg (□) cements.

Figures 5.54-5.56 show each Al species in percentages against log time in seconds. The 4 months aged LG26 cement showed an unexpected behaviour, and therefore, to simplify the calculation, the 2 months aged LG26 and LG26Mg cements are considered here. The Al(V) in LG26Mg cement was about 3% more than LG26 cement (Figure 5.55) and the Al(VI) in LG26Mg cement was about 5% more (Figure 5.56). The sum of the extra Al(V) and Al(VI) in LG26Mg cement is therefore about 8%, which converts to 1.7mol% of aluminium as the Al_2O_3 content in glass LG26Mg is 21.4mol%. This means that LG26Mg cements have "extra Al" compared to other four cements which could come from the absence of Al-F species.

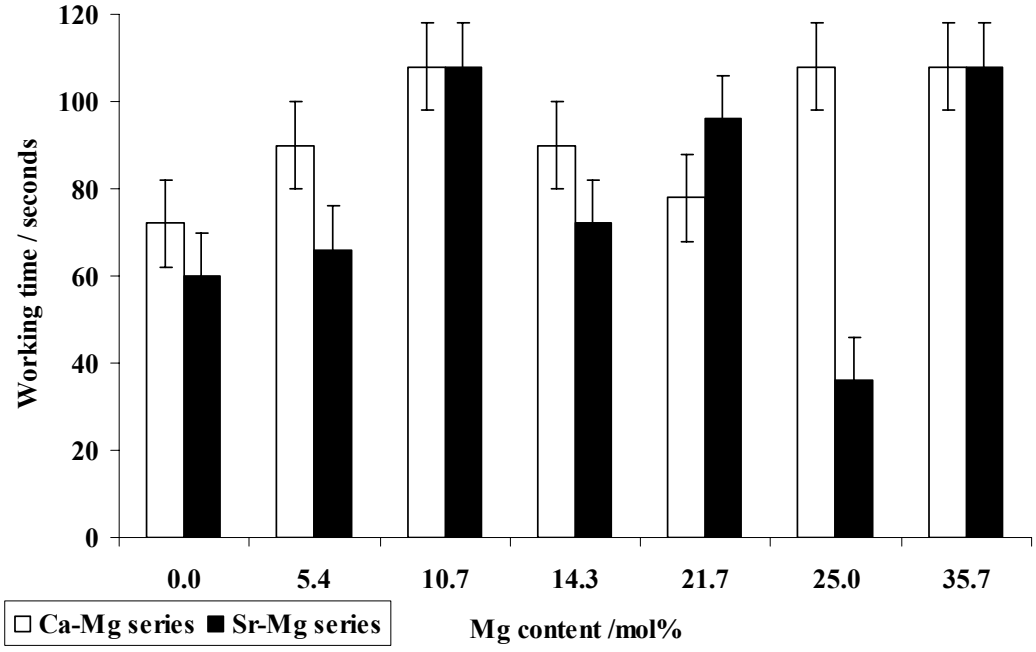
The decrease in the amount of Al(V) in LG26 cements is very rapid in the first 5 minutes, and after this period, the Al(V) content plateaus. However, the amount of

Al(V) in LG26Mg cement decreases constantly throughout the maturation period studied here (Figure 5.55). This constant conversion of Al(V) to Al(VI) could have resulted in the steady increase in the Al(VI):Al(IV)+Al(V) ratio as well.

Alternatively, in glass LG26Mg, there is a possibility of magnesium pyrophosphate species where NBOs on phosphorus are charge balanced by Mg^{2+} (Figure 5.10) or the formation of P-O-Mg bond. This will reduce the number of Al-O-PO_3^{3-} species in which Al^{3+} is charge compensated by P^{5+}. It has been shown that Al in Al-O-PO_3^{3-} species is less readily released as Al-O-P is not acid hydrolysable unlike Si-O-Al bonds. Therefore, due to the possibility of phosphorus occupied by Mg in the formation of magnesium pyrophosphate or P-O-Mg bonds, there would be more Si-O-Al in glass LG26Mg than in the less magnesium substituted glasses, and hence, more Al(IV) can be converted to Al(VI).

This steady increase in the Al(VI):Al(IV)+Al(V) ratio, in LG26Mg cements, may seem to indicate that more aluminium is converted to Al(VI) for crosslinking with polymeric acid. However, as has been mentioned earlier, ^{27}Al MAS-NMR spectroscopy cannot distinguish different Al(VI) species, between Al^{3+} ions crosslinking the polymer chain and the six coordinate Al in the residual glass. If more aluminium is crosslinking with the polymeric acid, then the increase in the mechanical properties is expected. However, this is not the case and will be discussed in more details later.

5.9. Working and Setting Time



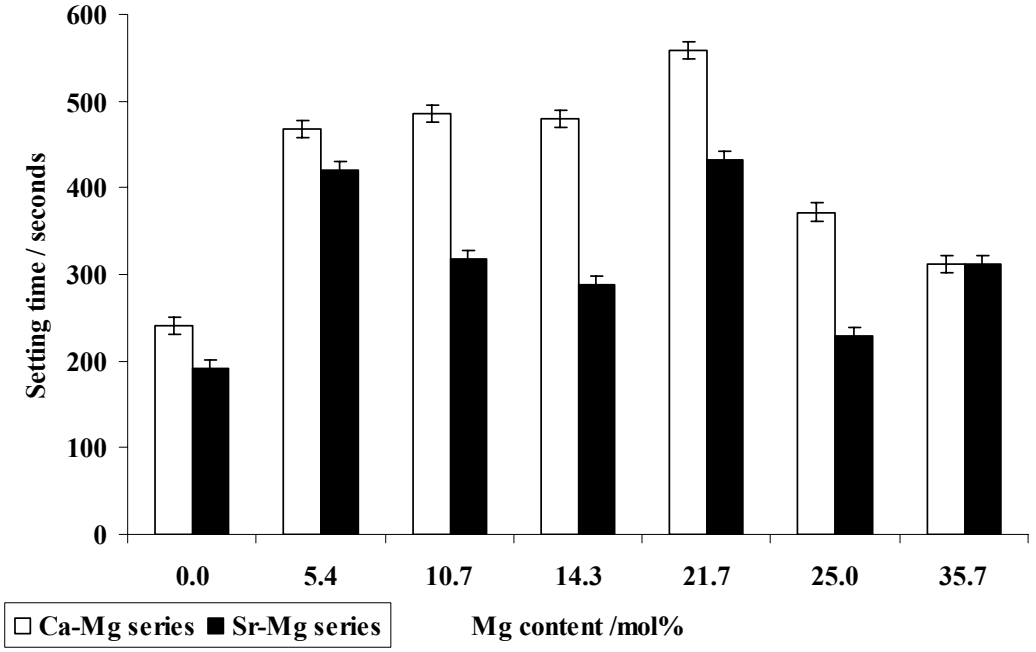
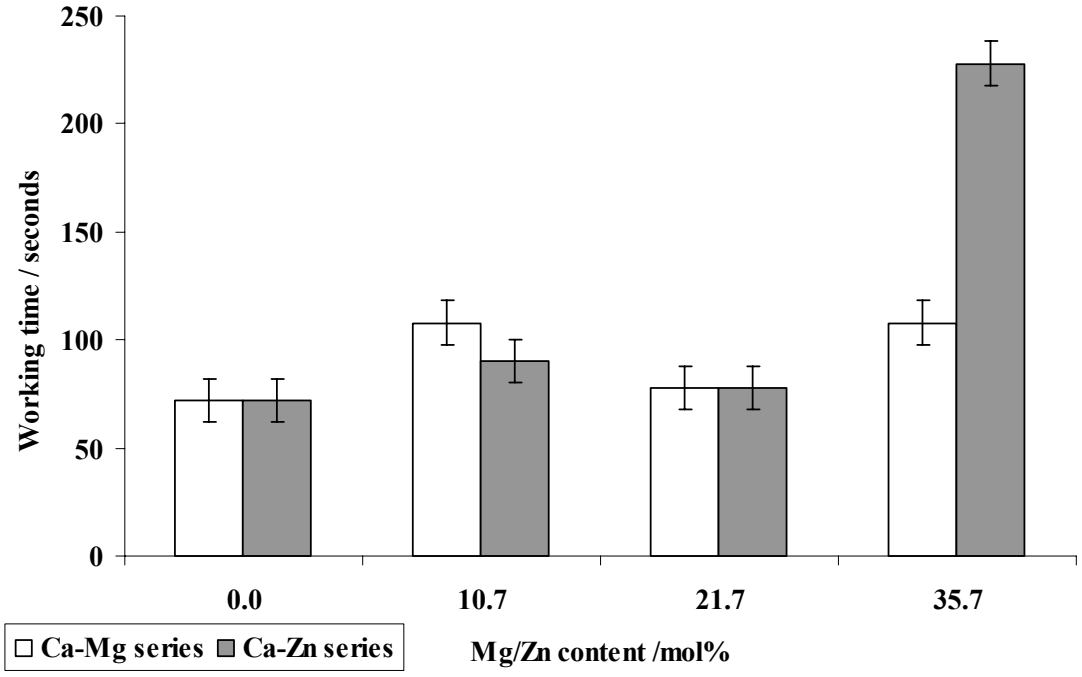


Figure 5.57. Working (top) and setting times (bottom) of the cements made with glasses in the Ca-Mg series [4.5SiO_2. 3.0Al_2O_3. 1.5P_2O_5. (3.0-x)CaO. xMgO. (2.0-y)CaF_2. yMgF_2] and the Sr-Mg series [4.5SiO_2. 3.0Al_2O_3. 1.5P_2O_5. (3.0-x)SrO. xMgO. (2.0-y)SrF_2. yMgF_2]. Error bar – 10 seconds.

It is quite difficult to detect a definite trend in the working and the setting times as calcium and strontium are partially substituted by magnesium since both seem to fluctuate among different glass compositions (Figure 5.57). Slight differences in the particle sizes of the original glasses (Appendix IV) may have affected this variation in the working and setting times which are highly dependent on the particle size of the glasses, particularly the fine particles in the particle size distribution [1]. However, there is an increase in the working and the setting times when calcium and strontium are completely substituted by magnesium, in LG26Mg cements. The ^{29}Si MAS-NMR spectrum of glass LG26Mg (Figure 5.19) has shown an increased number of BOs on Si showing an increased polymerisation in the silicate network. Since a more disrupted less polymerised glass releases cations from their glass network more readily, the reactivity of glass LG26Mg is lower than glass LG26 or the partially magnesium substituted glasses. This reduced reactivity, therefore, may have resulted in the increased working and the setting times of LG26Mg cements.

The working and the setting times of the cements in the Sr-Mg series were found to be, in most of the cases, shorter than the cements in the Ca-Mg series (Figure 5.57). The strontium containing fluoro-aluminosilicate glasses are more reactive than the glasses containing calcium as Sr^{2+} is better at disrupting the glass network than Ca^{2+} [24].



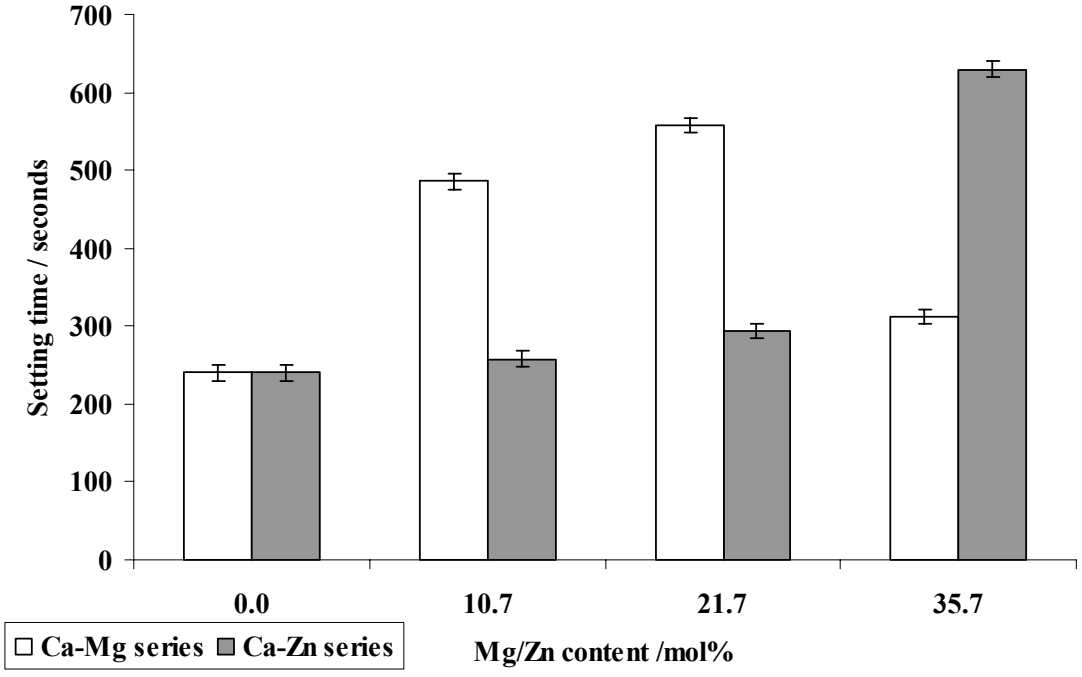


Figure 5.58. Working (top) and setting times (bottom) of the cements made with glasses in the Ca-Zn series [4.5SiO_2. 3.0Al_2O_3. 1.5P_2O_5. (3.0-x)CaO. xZnO. (2.0-y)CaF_2. yZnF_2] plotted with the cements in the Ca-Mg series [4.5SiO_2. 3.0Al_2O_3. 1.5P_2O_5. (3.0-x)CaO. xMgO. (2.0-y)CaF_2. yMgF_2]. Error bar – 10 seconds.

The working and the setting times of cements in the Ca-Zn series do not seem to change much with the zinc substitution for calcium (Figure 5.58). However, once all calcium is substituted by zinc in LG26Zn cements, both working and setting times increase dramatically. This large increase in the working and the setting times may have been caused by the presence of crystalline phase present in glass LG26Zn shown by the XRD analysis (Figure 5.3). The crystalline phase is probably less reactive than the amorphous phase as ions are closely packed together and are not readily released for the cement formulation. Moreover, although the crystalline phase could not be identified, this crystalline phase was picked up in the ^{27}Al MAS-NMR spectrum (Figure 5.18) at around 15ppm, and O'Dell and co-workers [69] have assigned a peak at around 15ppm for Al^{3+} in α-Al_2O_3. It is, therefore, possible that the crystalline phase in glass LG26Zn is α-Al_2O_3, but further work is required. Because of the formation of Al rich crystalline phase, the Al:Si ratio in the glass phase is reduced resulting in a decrease in the number of Al^{3+} ions available for crosslinking with polycarboxylate acids. As a result, the working and the setting times of LG26Zn cement have increased.

The working time seems to vary slightly between the Ca-Mg and the Ca-Zn series apart from the fully magnesium/zinc substituted cements. The large increase in the working time with LG26Zn cements, as has been mentioned, may have resulted from the presence of crystalline phase in glass LG26Zn. However, there is a large difference in the setting time of the cements in the middle of the two series (Figure 5.58). This difference may be related to the differences in their glass structures. The intensity of F-Ca(n) species in ^{19}F MAS-NMR spectra of the Ca-Zn glasses (Figure 5.7) is much higher than the one in the Ca-Mg series (Figure 5.4). Therefore, there are

more F-Ca(n) species in the Ca-Zn glasses, which would be readily released from the glass to crosslink with the polymeric acid during the cement formation. Hence, this additional Ca^{2+} in the Ca-Zn glass may have decreased the setting time by facilitating the crosslinking process.

The ISO standard for the dental restorative materials are a minimum of 60 seconds working time and a maximum of 600 seconds setting time [80]. Therefore, most of the cements in the Ca-Mg, the Sr-Mg, and the Ca-Zn series are well within the ISO standard.

5.10. Radiopacity

In both series, the radiopacity decreased as magnesium substituted calcium in the Ca-Mg series and strontium in the Sr-Mg series (Figure 5.59). The radiopacity decreases with the density of the material. Therefore, since the atomic weight of magnesium is smaller than calcium or strontium, the radiopacity of the cements containing more magnesium is expected to decrease. The ISO standard for the radiopacity of the GPCs is a minimum of 1mm Al thickness for dental application [80]. Therefore, most of the cements in the Sr-Mg series comply with the standard.

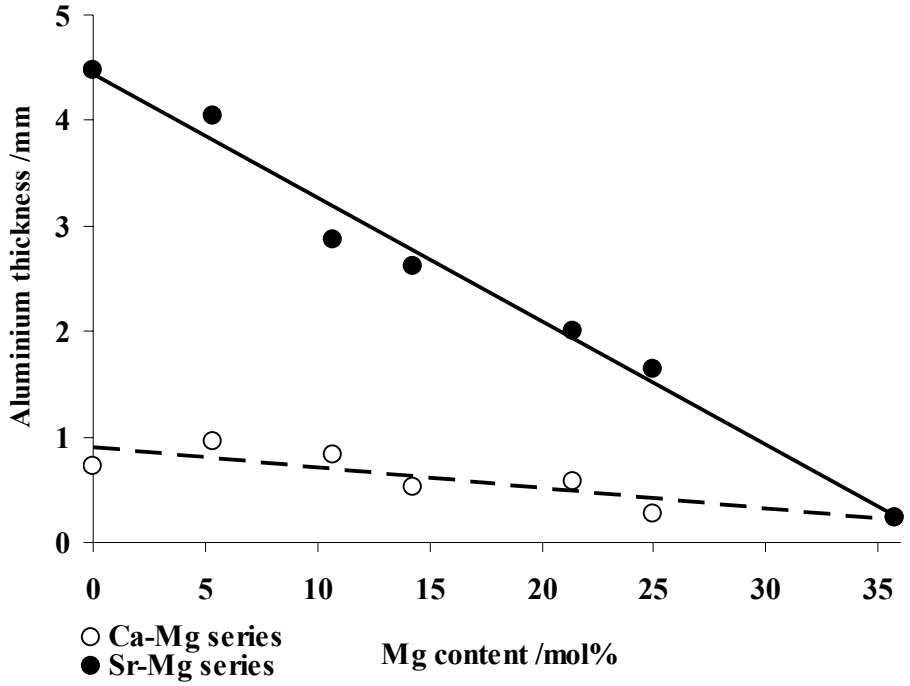


Figure 5.59. Radiopacity of the cements formed using the glasses in the Ca-Mg (○) series and the Sr-Mg (●) series. The line is a guide to eye only.

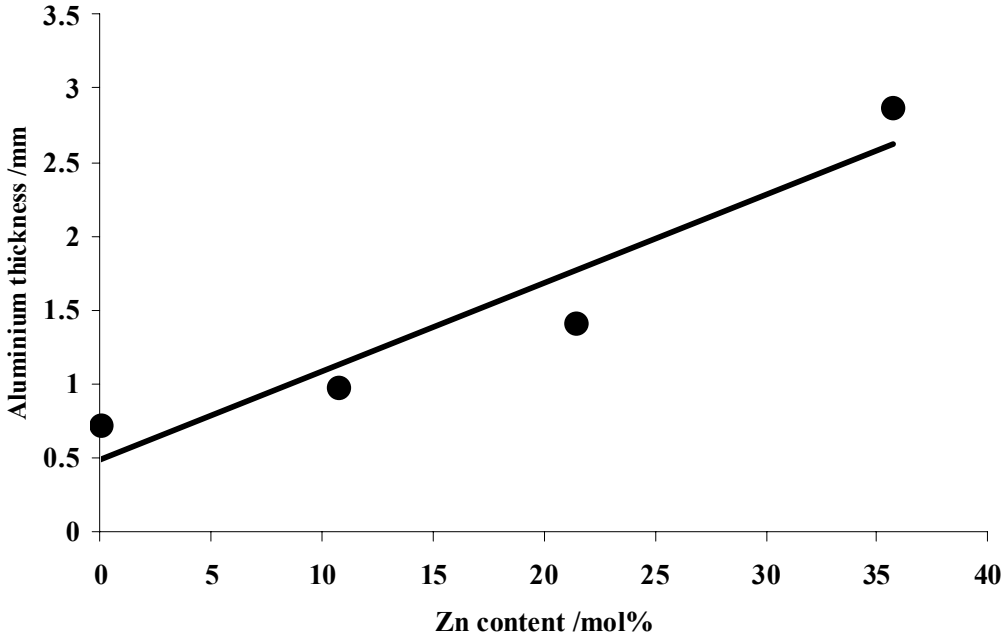


Figure 5.60. Radiopacity of the cements formed using the glasses in the Ca-Zn series. The line is a guide to eye only.

The radiopacity of the cements in the Ca-Zn series increased linearly with zinc substitution (Figure 5.60). This is due to the increase in the atomic number with the zinc substitution. Most of the cements in the Ca-Zn series have shown the radiopacity above the specification of the ISO standard [80]. Therefore, the incorporation of zinc and/or strontium can improve the radiopacity of the cements effectively.

5.11. Compressive Strength

The compressive strengths were measured at 1 and 7 days for the Ca-Mg, the Sr-Mg, and the Ca-Zn series. In both Ca-Mg and Sr-Mg series, the compressive strengths decreased with magnesium substitution (Figure 5.61, Figure 5.62). It was originally thought that the substitution of calcium by magnesium would result in an increase in the compressive strength because of the Mg^{2+} ion being smaller in size which would crosslink the polycarboxylate chains more efficiently.

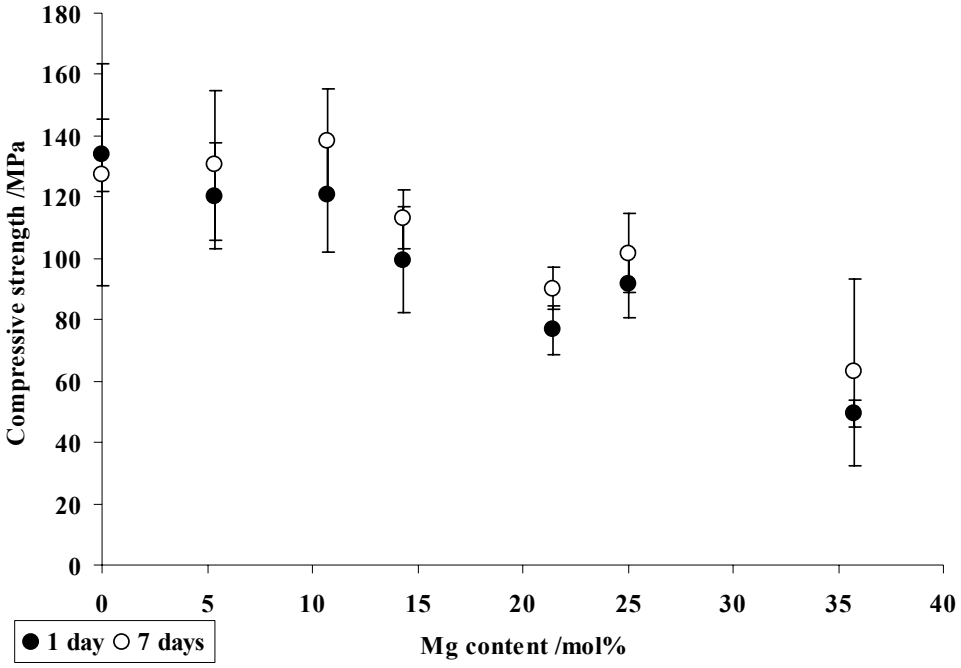


Figure 5.61. Compressive strengths of the cements formed using the glasses in the Ca-Mg series [4.5SiO_2. 3.0Al_2O_3. 1.5P_2O_5. (3.0-x)CaO. xMgO. (2.0-y)CaF_2. yMgF_2] measured at 1 and 7 days. Error bar – 1 s.d.

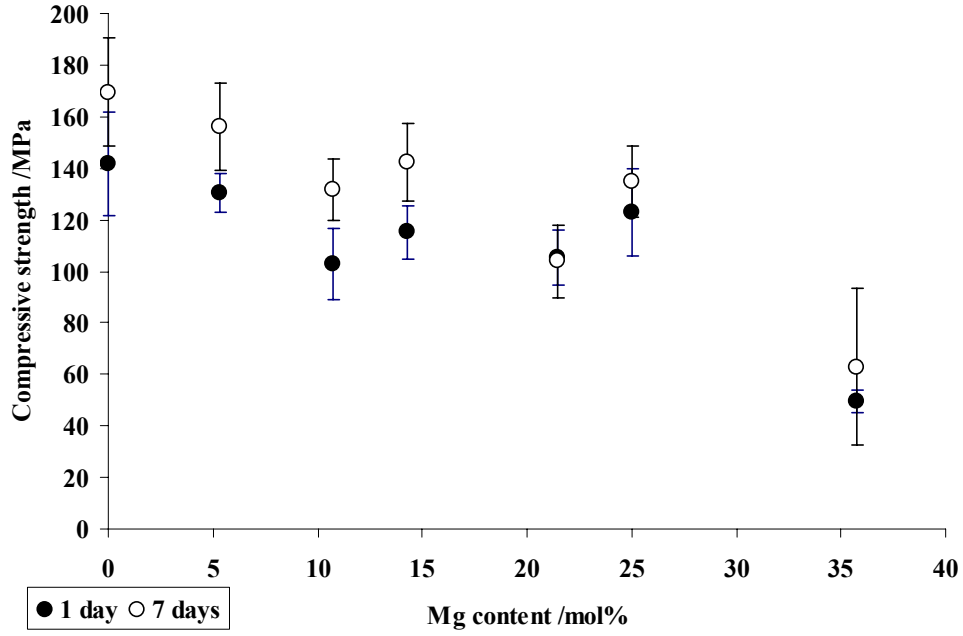


Figure 5.62. Compressive strengths of the cements formed using the glasses in the Sr-Mg series [4.5SiO_2. 3.0Al_2O_3. 1.5P_2O_5. (3.0-x)SrO. xMgO. (2.0-y)SrF_2. yMgF_2] measured at 1 and 7 days. Error bar – 1 s.d.

There are two possible explanations to the decrease in the compressive strength with LG26Mg cements compared to the partially or no magnesium substituted cements. Firstly, although it is quite difficult to say whether F-Mg(n) species actually participate in the cement formation due to them being the only fluorine species in LG26Mg cement/glass (Figure 5.35), considering that F-Mg(n) species are not part of the glass network, these species should be readily released during the cement formation to some extent. Similarly, magnesium pyrophosphate, $Mg_2P_2O_7$, is not part of the glass network and therefore, Mg^{2+} in the magnesium pyrophosphate should also be released from the glass during the crosslinking process. These Mg^{2+} ions may crosslink to the carboxylate groups in PAA in preference to Al^{3+} because both F-Mg(n) and Mg^{2+} in magnesium pyrophosphate species are not part of the glass network and therefore would be easier to be released compared to Al^{3+} which would require a bond breakage in the Si-O-Al bonds *via* acid hydrolysis. As Mg^{2+} is a divalent cation, it can only crosslink two polymeric chains, unlike three chains by trivalent Al^{3+} cation. Therefore, it is more likely that the compressive strengths would decrease.

Secondly, the possible preferential release of Mg^{2+} ions from the glass could also demonstrate that Al(IV) and Al(V), which have been charge balanced by these Mg^{2+} ions, are now forced to be higher coordinated, Al(VI). It is possible that carboxylate groups will be taken up mostly by Mg^{2+} ions, and there are not many carboxylate groups left for the Al^{3+} ions to crosslink. LG26Mg cements required 0.106g PAA, which has 0.00145moles of COOH groups. The magnesium content in glass LG26Mg [$4.5SiO_2$. $3Al_2O_3$. $1.5P_2O_5$. 3MgO. $2MgF_2$] is 35.7mol%. As it is not possible to know,

with certainty, whether F-Mg(n) species are released for cement formation, it is assumed that there would be three Mg^{2+} ions available resulting from 3MgO and no release of F-Mg(n) species. This yields 21.4mol% or 0.106moles of Mg^{2+} in glass LG26Mg used for cement making. As the number of Mg^{2+} ions is larger than the number of carboxylate groups, it is possible that most of carboxylate groups would be taken up by Mg^{2+} ions. The release of Mg^{2+} from the glass, therefore, could result in the insufficient number of charge balancing cations on aluminium which forces Al(IV) and Al(V) to be converted to Al(VI), and these Al(VI) may not be participating in a crosslinking process with PAA, but rather stay in the residual glass as octahedrally coordinated Al.

The cements in both Ca-Mg and Sr-Mg series showed a slight increase in the compressive strengths with aging time (Figure 5.61, Figure 5.62). Several studies found a similar trend [5, 7, 24, 37], and this increase in the compressive strengths over a period of time has been thought to be due to the continuous crosslinking process as well as a possible formation of silica rich layer.

The compressive strengths of the cements in the Sr-Mg series are slightly higher than the cements in the Ca-Mg series (Figure 5.63, Figure 5.64). Hill and co-workers [24] have shown that Sr^{2+} is better at disrupting the glass network than Ca^{2+} due to its slightly larger ionic size. Therefore, Sr^{2+} cations would be more readily released during the setting reaction and crosslink to the carboxylate groups of the polymer more readily.

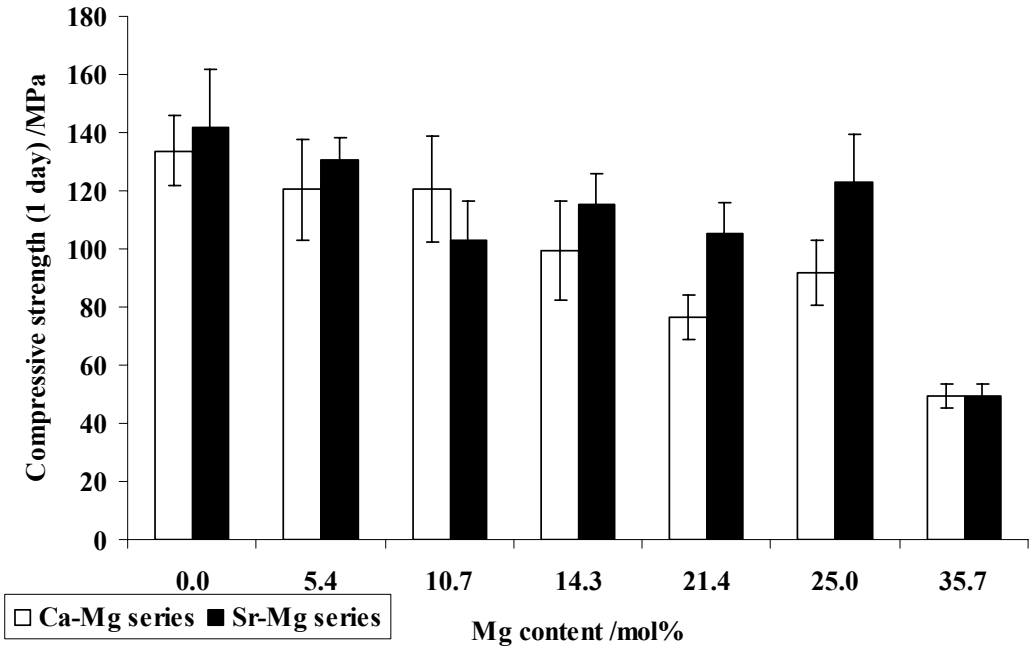


Figure 5.63. Compressive strengths of the cements formed using the glasses in the Ca-Mg [$4.5SiO_2$. $3.0Al_2O_3$. $1.5P_2O_5$. (3.0-x)CaO. xMgO. (2.0-y)CaF_2. yMgF_2] and the Sr-Mg series [$4.5SiO_2$. $3.0Al_2O_3$. $1.5P_2O_5$. (3.0-x)SrO. xMgO. (2.0-y)SrF_2. yMgF_2] measured at 1 day. Error bar – 1 s.d.

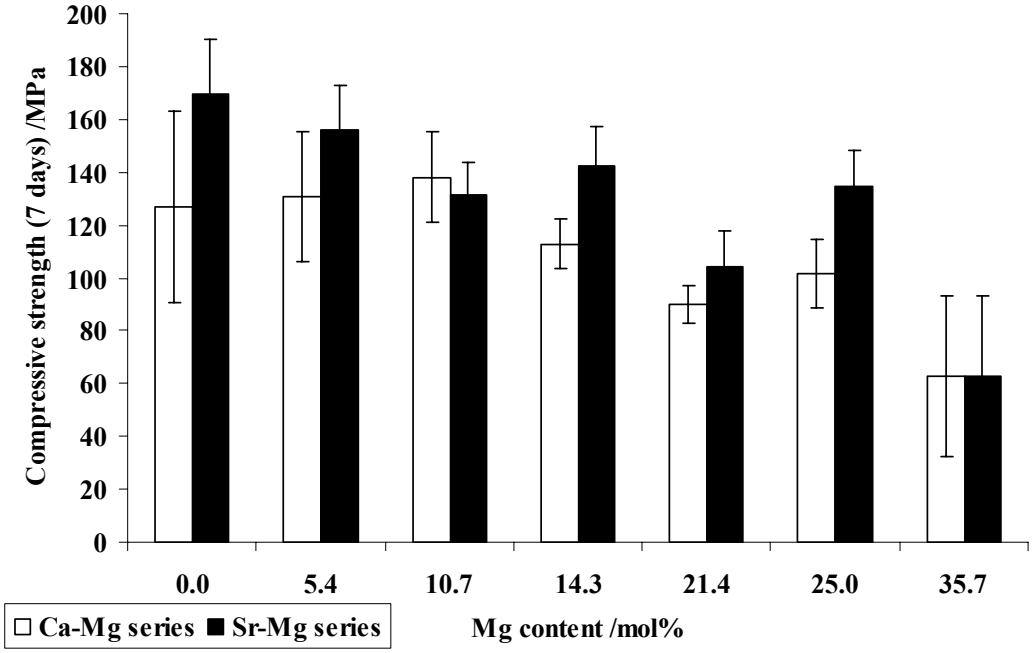


Figure 5.64. Compressive strengths of the cements formed using the glasses in the Ca-Mg [$4.5SiO_2$. $3.0Al_2O_3$. $1.5P_2O_5$. (3.0-x)CaO. xMgO. (2.0-y)CaF_2. yMgF_2] and the Sr-Mg series [$4.5SiO_2$. $3.0Al_2O_3$. $1.5P_2O_5$. (3.0-x)SrO. xMgO. (2.0-y)SrF_2. yMgF_2] measured at 7 days. Error bar – 1 s.d.

There was a slight increase in the compressive strength in the Ca-Zn series as zinc substituted for calcium (Figure 5.65). This may be because Zn^{2+} is slightly smaller than Ca^{2+} so that Zn^{2+} could result in more efficient ionic crosslinking.

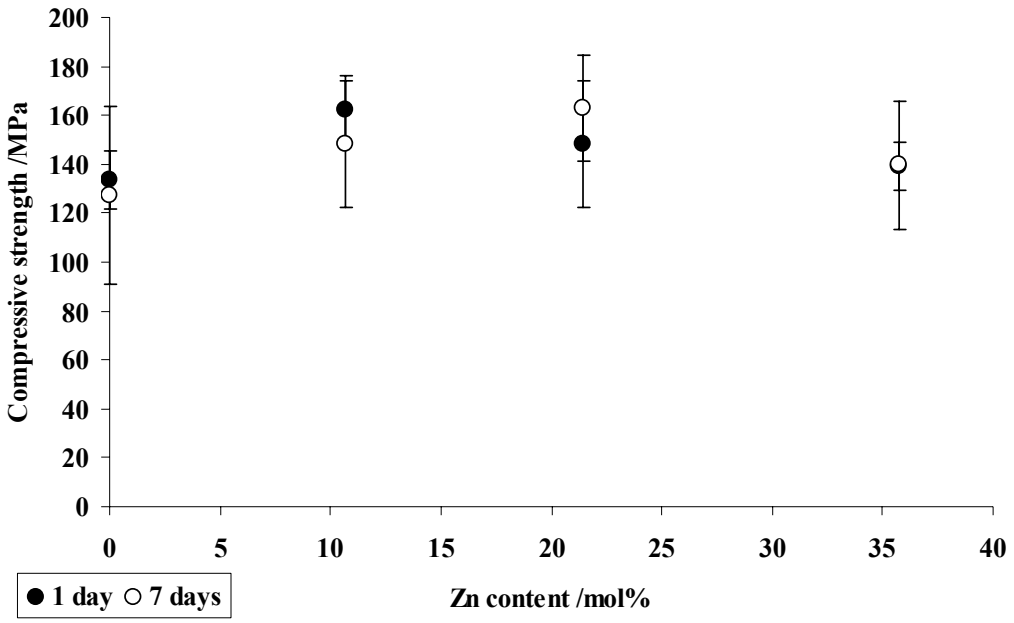


Figure 5.65. Compressive strengths of the cements formed using the glasses in the Ca-Zn series [4.5SiO_2. 3.0Al_2O_3. 1.5P_2O_5. (3.0-x)CaO. xZnO. (2.0-y)CaF_2. yZnF_2] measured at 1 and 7 days. Error bar – 1 s.d.

The compressive strengths of the cements having the same content of magnesium and zinc in the Ca-Mg and the Ca-Zn series measured at 1 and 7 days are shown in Figure 5.66 and Figure 5.67 respectively. It seems that in both 1 and 7 days, the compressive strengths of the cements in the Ca-Zn series are slightly higher than the Ca-Mg series, and this may be because of the differences in the behaviour of Mg^{2+} and Zn^{2+} in glass structures. The ^{31}P MAS-NMR spectra of the glasses in the Ca-Zn series (Figure 5.13) showed that Zn^{2+} seems to replace the charge balancing role of Ca^{2+} in the glass

structure, and NBOs on phosphorus in Al-O-PO_3^{3-} species are charge balanced by Zn^{2+} in glass LG26Zn. However, Mg^{2+} seems to form magnesium pyrophosphate (Figure 5.8) and F-Mg(n) species in glass LG26Mg (Figure 5.4), and as has been mentioned earlier, there seems a preferential release of Mg^{2+} over Al^{3+} in LG26Mg cements.

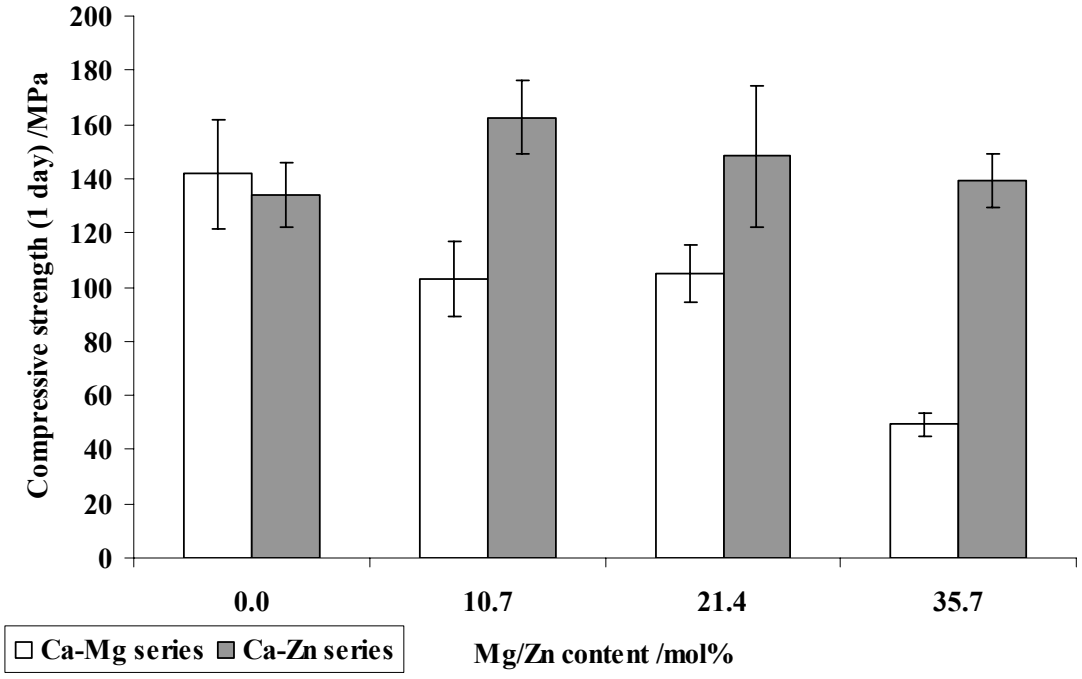


Figure 5.66. Compressive strengths of the cements formed using the glasses in the Ca-Mg [$4.5SiO_2$. $3.0Al_2O_3$. $1.5P_2O_5$. (3.0-x)CaO. xMgO. (2.0-y)CaF_2. yMgF_2] and the Ca-Zn series [$4.5SiO_2$. $3.0Al_2O_3$. $1.5P_2O_5$. (3.0-x)CaO. xZnO. (2.0-y)CaF_2. yZnF_2] measured at 1 day. Error bar – 1 s.d.

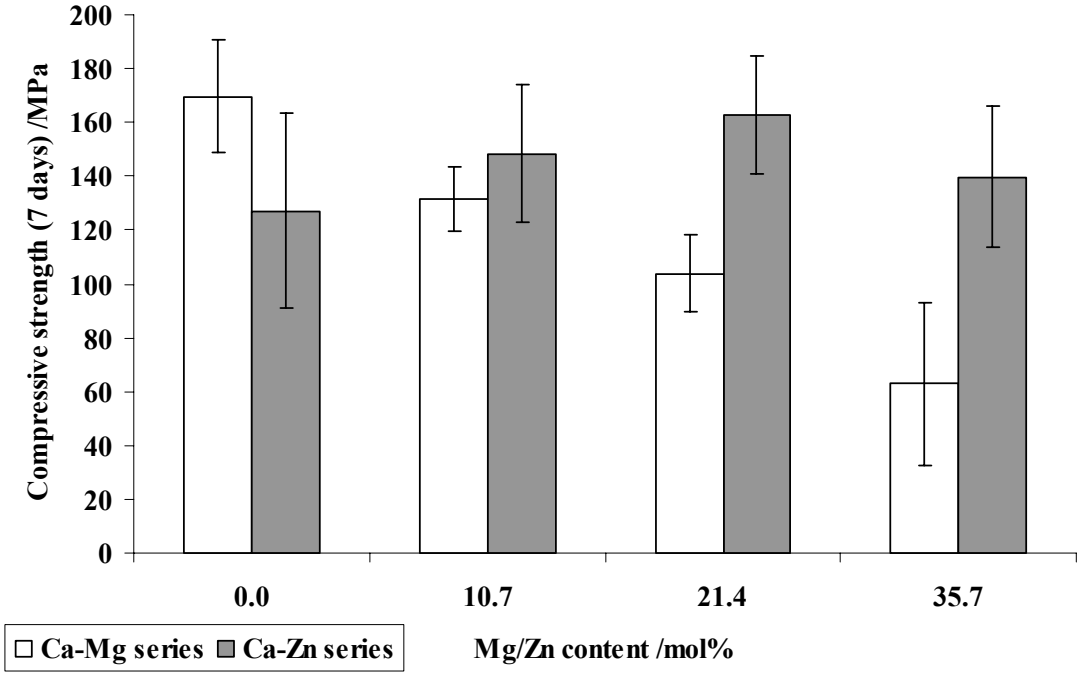


Figure 5.67. Compressive strengths of the cements formed using the glasses in the Ca-Mg [$4.5SiO_2$. $3.0Al_2O_3$. $1.5P_2O_5$. (3.0-x)CaO. xMgO. (2.0-y)CaF_2. yMgF_2] and the Ca-Zn series [$4.5SiO_2$. $3.0Al_2O_3$. $1.5P_2O_5$. (3.0-x)CaO. xZnO. (2.0-y)CaF_2. yZnF_2] measured at 7 days. Error bar – 1 s.d.

5.12. Fluoride Release

The fluoride release was measured for the cements in the Ca-Mg and the Sr-Mg series for 1, 3, 7, 14, 21, 28, 42, and 56 days. The glass compositions were selected so that the fluoride release of only the glass compositions, whose aged cements were also studied on MAS-NMR spectroscopy, was studied. This was to determine if there are some relationships between the setting chemistry of the cements and their fluoride release.

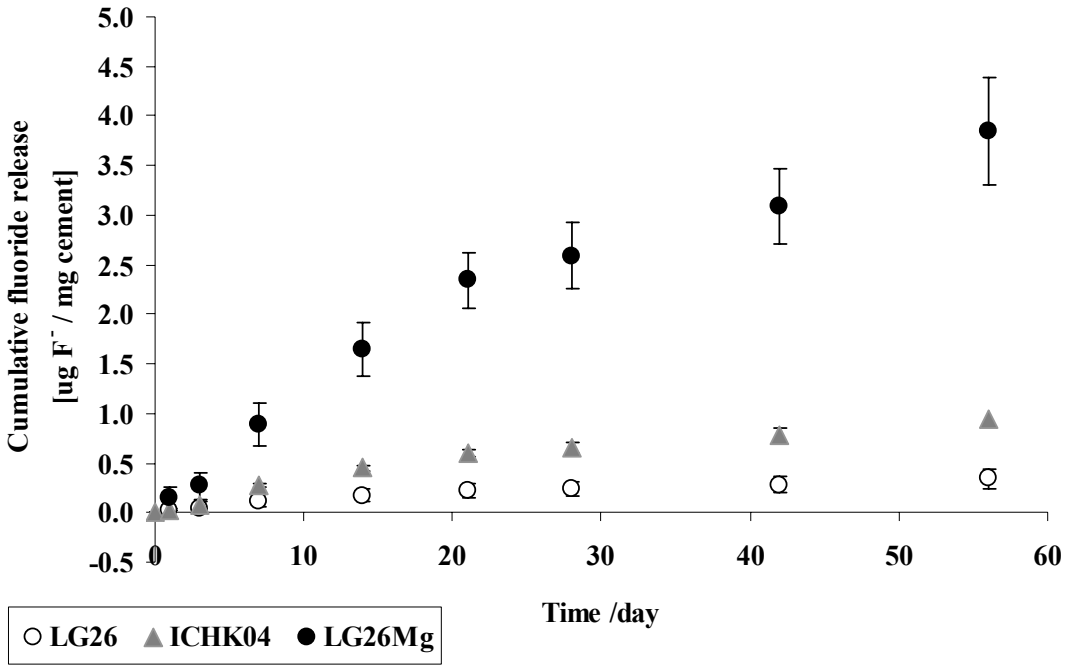


Figure 5.68. Cumulative fluoride release against time for the cements made with glasses in the Ca-Mg series [4.5SiO_2. 3.0Al_2O_3. 1.5P_2O_5. (3.0-x)CaO. xMgO. (2.0-y)CaF_2. yMgF_2]. Error bar – 1 s.d.

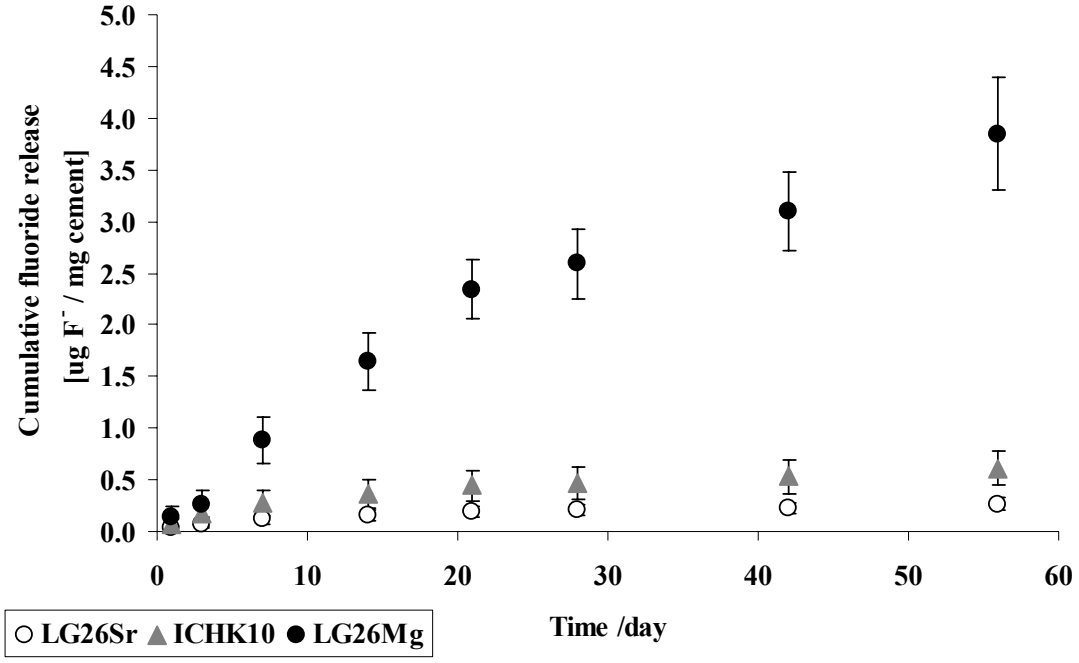


Figure 5.69. Cumulative fluoride release against time for the cements made with glasses in the Sr-Mg series [4.5SiO_2. 3.0Al_2O_3. 1.5P_2O_5. (3.0-x)SrO. xMgO. (2.0-y)SrF_2. yMgF_2]. Error bar – 1 s.d.

In both Ca-Mg and Sr-Mg series, there is an initial burst of fluoride release, and then the release rate decreases with time (Figure 5.68, Figure 5.69). This initial burst of fluoride release is from the surface of the cement, and the slow release occurs from the bulk of the cement [81].

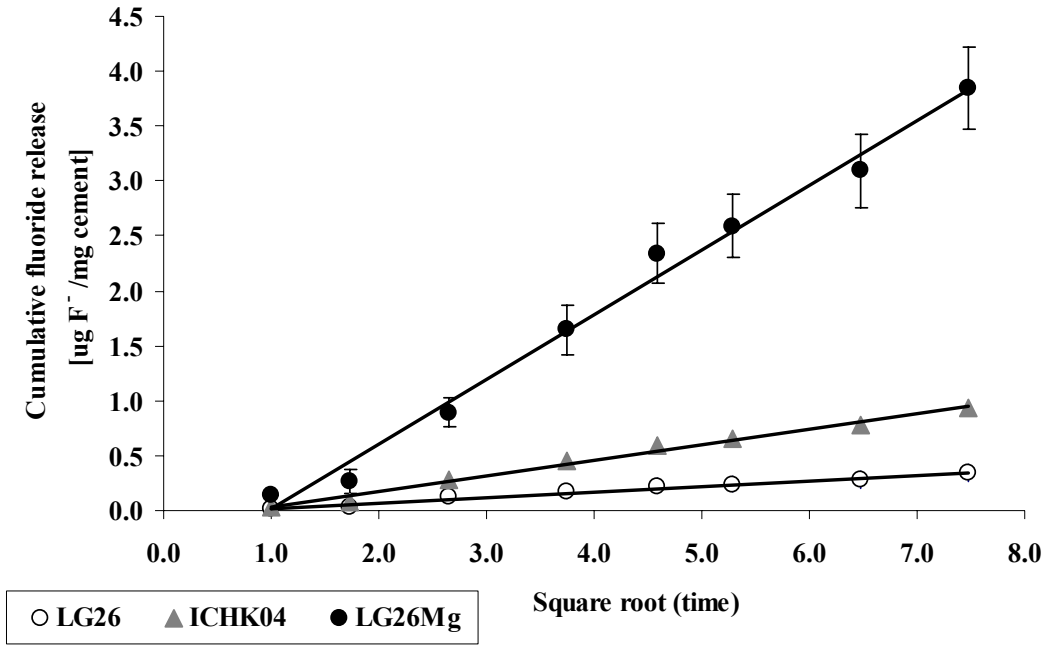


Figure 5.70. Cumulative fluoride release against square root of time for the cements made with glasses in the Ca-Mg series [4.5SiO_2. 3.0Al_2O_3. 1.5P_2O_5. (3.0-x)CaO. xMgO. (2.0-y)CaF_2. yMgF_2]. Lines are guide to eye only. Error bar – 1 s.d.

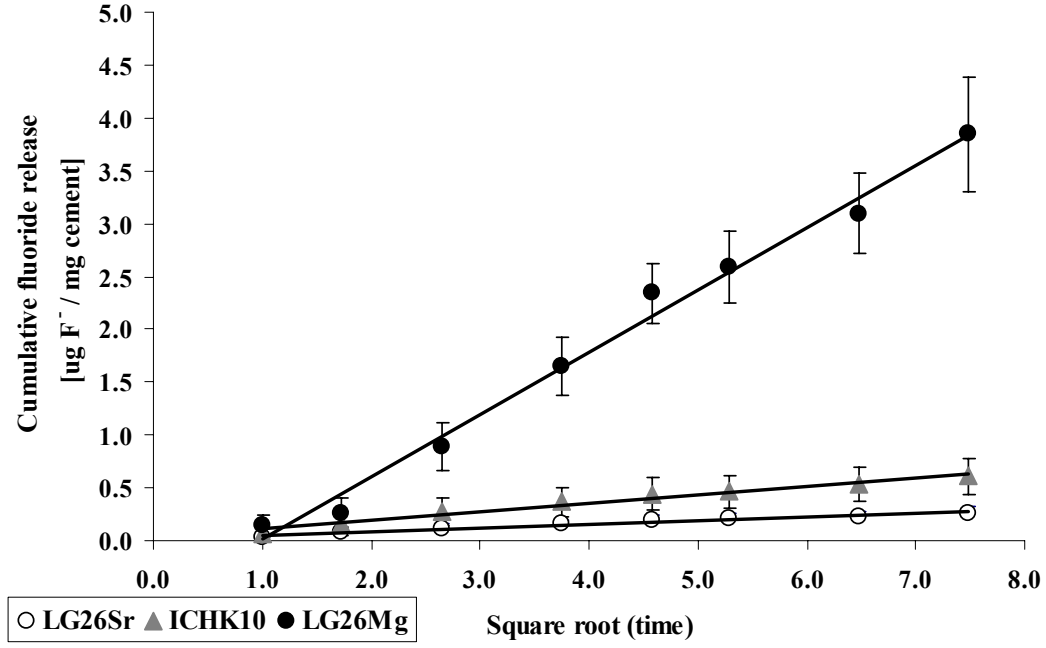


Figure 5.71. Cumulative fluoride release against square root of time for the cements made with glasses in the Sr-Mg series [4.5SiO_2. 3.0Al_2O_3. 1.5P_2O_5. (3.0-x)SrO. xMgO. (2.0-y)SrF_2. yMgF_2]. Lines are guide to eye only. Error bar – 1 s.d.

There is a linear relationship between the cumulative fluoride release and the square root of time (Figure 5.70, Figure 5.71). This shows that the fluoride release is diffusion controlled, rather than a surface dissolution process [1]. The highest amount of fluoride was released from LG26Mg cement. ^{19}F MAS-NMR spectrum of glass LG26Mg (Figure 5.4) has shown that fluorine is attached solely to magnesium forming F-Mg(n) species, and these species are not part of the glass network. Moreover, the ^{19}F MAS-NMR spectra of LG26Mg cements (Figure 5.35) have shown that these F-Mg(n) species are still present in the residual glass or the cement matrix. ICHK04 and ICHK10 cements, both containing 14.3mol% Mg, showed the next highest release of fluoride (Figure 5.70, Figure 5.71). The ^{19}F MAS-NMR spectra of glasses ICHK04 and ICHK10 showed the presence of Al-F-Ca(n) and Al-F-Sr(n) species, respectively, with a shoulder assigned to F-Mg(n) species (Figure 5.4, Figure 5.5). Therefore, the amount of fluoride released from the cements seems to be related to this F-Mg(n) species. The solubility of MgF_2, CaF_2, and SrF_2, in 100g water at $20^oC \pm 5^oC$ are 12.0mg, 2.5mg, and 11.7mg respectively [52]. The fluoride released from LG26 and LG26Sr cements are the lowest in each of the series (Figure 5.70, Figure 5.71). In both cements, F-Ca(n) and F-Sr(n) species are consumed in cement formation, and the other fluoride species present in these cements are Al-F-Ca(n) and Al-F-Sr(n) species respectively (Figure 5.33, Figure 5.37). These species are part of the glass network and are not readily released. Therefore, this study could indicate that the presence of magnesium can increase the amount of fluoride released from the cements.

In summary, the aging cements of the selected cements were studied on the MAS-NMR. F-Ca(n) and F-Sr(n) species were consumed in the cement formation.

Irrespective of the original glass compositions, Q^1 pyrophosphate Al-O-PO_3^{3-} species was still present in all cements. The Al(VI):Al(IV)+Al(V) ratio kept increasing with the fully magnesium substituted cements whereas the ratio for the non/partially substituted cements became plateau. The magnesium substitution decreased the compressive strengths with the fully magnesium substituted cement showing the lowest compressive strength. This may be related to the more polymerised silicate network of the glass shown on ^{29}Si MAS-NMR earlier. Apart from the increased fluoride release, the magnesium substitution did not improve the cement properties and therefore may not be beneficial for making GPCs.

Part III. Characterisation of Fluoro-Aluminosilicate Glasses containing Sr, Zn and Lower Phosphate

A new series of glasses, the Sr-Zn series [$4.5SiO_2$. $3.0Al_2O_3$. $0.75P_2O_5$. (3.0-x)SrO. xZnO. $2.0SrF_2$], was produced for cement formation with poly (γ-glutamic acid), PgGA. The glasses in this series contain a half amount of phosphate compared to the glasses used for the PAA based cements (the Ca-Mg, Sr-Mg, and Ca-Zn series). This is simply to increase the reactivity of glasses to be used with PgGA as PgGA is less acidic than PAA. The increase in the reactivity upon the reduction in the phosphate content results from a less number of Al-O-P bonds formed and a more number of Al^{3+} next to SiO_4, forming Al-O-Si bonds. These Al-O-Si bonds are susceptible to acid attack during the cement formation, but not Al-O-P bonds [7].

5.13. XRD Analysis

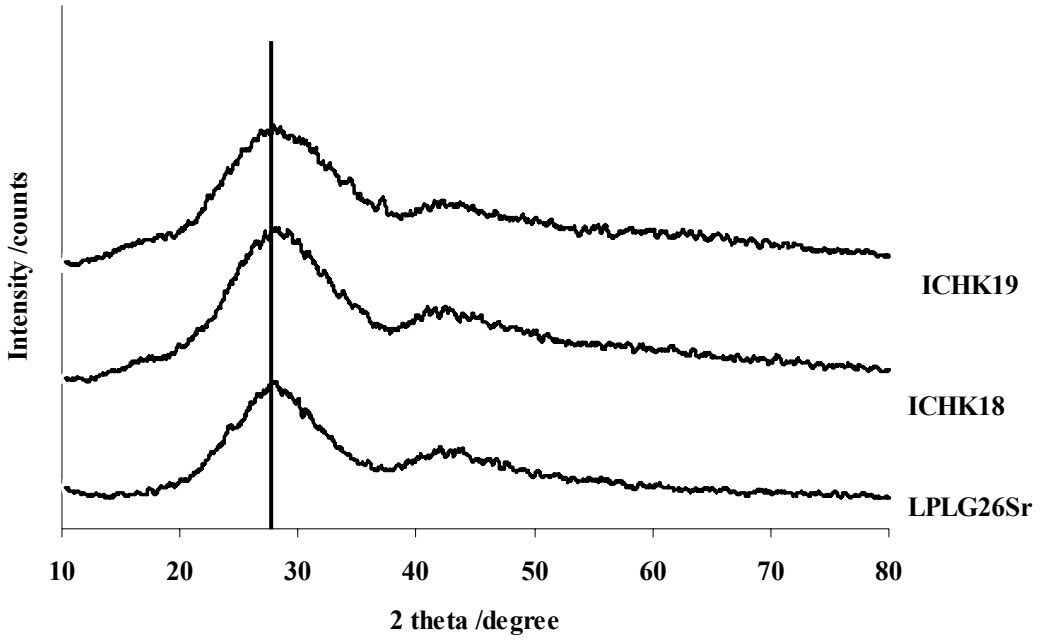


Figure 5.72. XRD patterns for the glasses in the Sr-Zn series [4.5SiO_2. 3.0Al_2O_3. 0.75P_2O_5. (3.0-x)SrO. xZnO. 2.0SrF_2]. The vertical line is a guide to eye only.

The XRD pattern showed a typical amorphous halo (Figure 5.72), and therefore the three glasses in the Sr-Zn series are amorphous. The position of the amorphous halo does not change upon the zinc substitution for strontium.

5.14. ^{31}P MAS-NMR Spectroscopy

The chemical shift for glass LPLG26Sr was observed at -6ppm (Figure 5.73) for Q^1 pyrophosphate Al-O-PO_3^{3-} species with NBOs on the phosphorus charge balanced by Sr^{2+} [8]. The formation of Al-O-P linkages results from the charge compensation of Al^{3+} by P^{5+} [62]. The chemical shift for glasses ICHK18 and ICHK19, in which strontium was gradually substituted by zinc, did not vary (Figure 5.73), and therefore zinc substitution for strontium seems to have not affected the phosphorus environment, and Zn^{2+} is simply replacing Sr^{2+} to charge balance NBOs on phosphorus.

The chemical shift for glass LPLG26Sr, -5.5ppm, is slightly less negative than glass LG26Sr, -7ppm (Figure 5.11). LPLG26Sr [$4.5SiO_2$. $3.0Al_2O_3$. $0.75P_2O_5$. 3.0SrO. $2.0SrF_2$] contains less P_2O_5 than LG26Sr [$4.5SiO_2$. $3.0Al_2O_3$. $1.5P_2O_5$. 3.0SrO. $2.0SrF_2$], and therefore, there would be less Al-O-PO_3^{3-} species in the glass. Stamboulis and co-workers [23] have also observed the changes in the phosphorus environment in the ^{31}P chemical shift increasing when phosphate content was decreased.

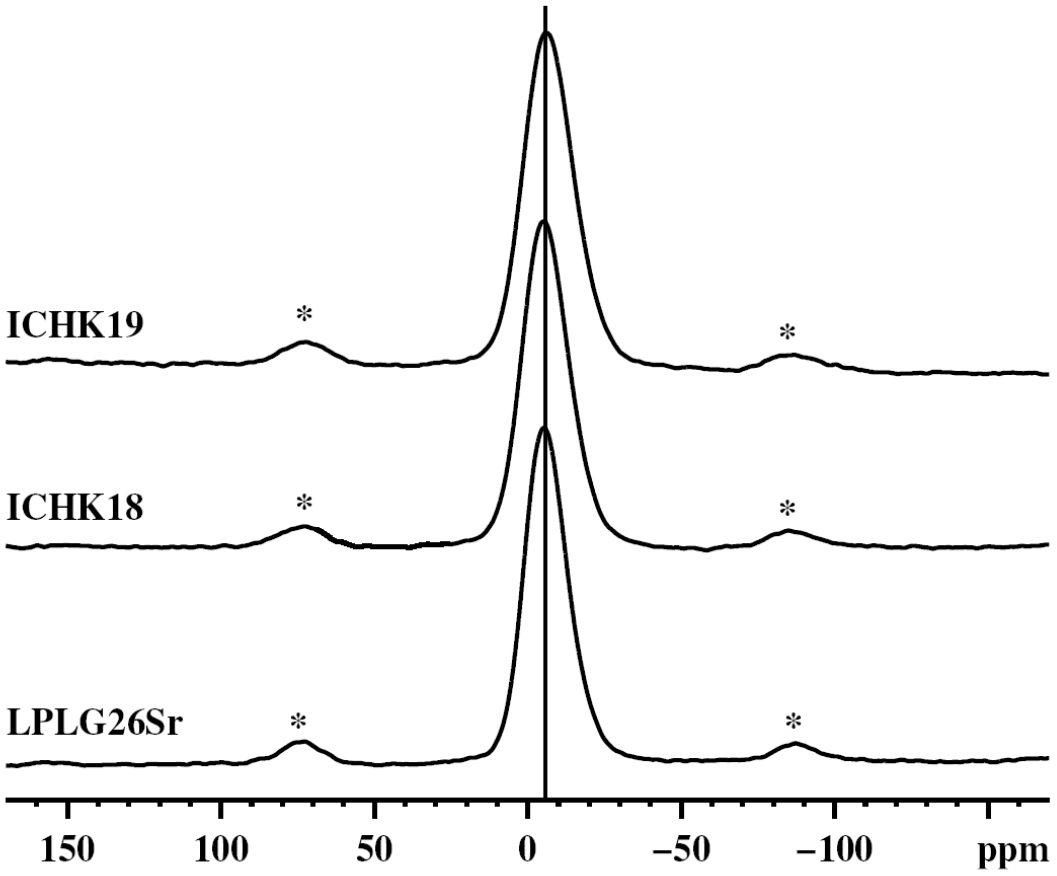


Figure 5.73. ^{31}P MAS-NMR spectra for the glasses in the Sr-Zn series [$4.5SiO_2$. $3.0Al_2O_3$. $0.75P_2O_5$. (3.0-x)SrO. xZnO. $2.0SrF_2$]. Spinning sidebands are marked by asterisks, and the vertical line is a guide to eye only.

5.15. ^{27}Al MAS-NMR Spectroscopy

Glass LPLG26Sr exhibited a chemical shift at 56ppm (Figure 5.74), and this chemical shift is in a region for Al in tetrahedral coordination, Al(IV) [28]. This chemical shift is higher than the Al(IV) peak for glass LG26Sr, 52ppm (Figure 5.17). The phosphate content in LPLG26Sr [$4.5SiO_2$. $3.0Al_2O_3$. $0.75P_2O_5$. 3.0SrO. $2.0SrF_2$] is a half of LG26Sr [$4.5SiO_2$. $3.0Al_2O_3$. $1.5P_2O_5$. 3.0SrO. $2.0SrF_2$]. The reduction in the phosphate content would result in the less number of Al-O-P bonds being formed, and therefore, the chemical shift would increase, towards 60ppm, which is Al(IV) for a simple aluminosilicate glass containing no P_2O_5 [28]. The ^{31}P MAS-NMR spectrum (Figure 5.73) has also shown the reduced number of Al-O-P bonds in LPLG26Sr. Stamboulis and co-workers [23] found a similar trend and concluded that this is because of the decrease in the P_2O_5 content resulting in a less number of Al-O-P bonds.

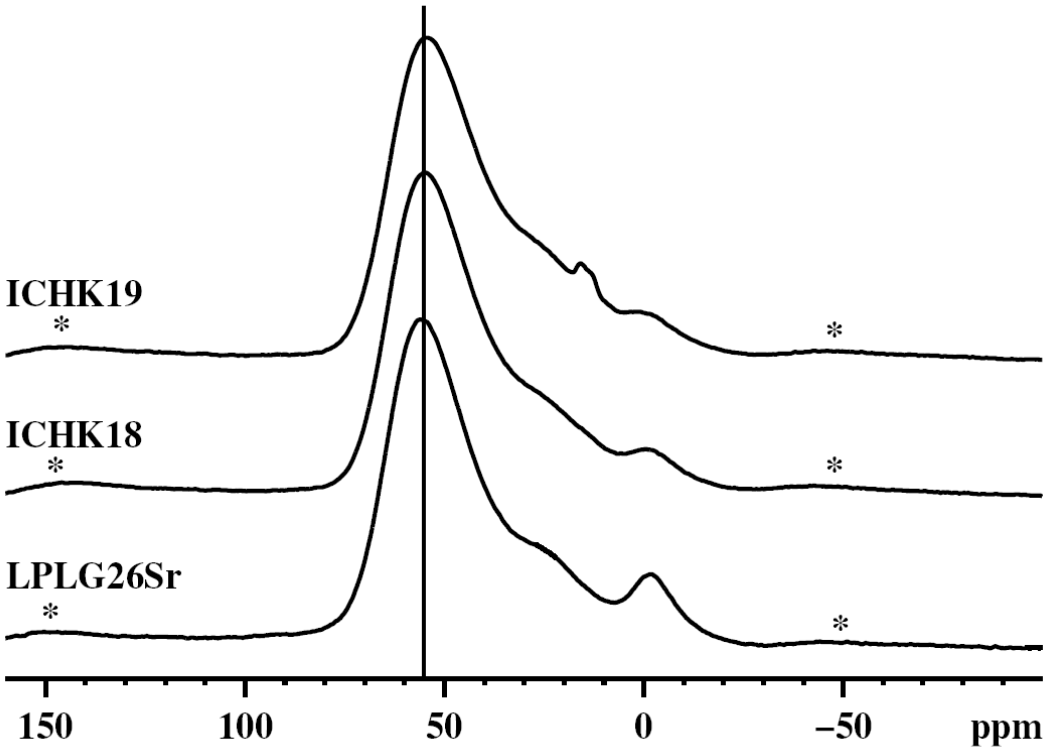


Figure 5.74. ^{27}Al MAS-NMR spectra for the glasses in the Sr-Zn series [4.5SiO_2. 3.0Al_2O_3. 0.75P_2O_5. (3.0-x)SrO. xZnO. 2.0SrF_2]. Spinning sidebands are marked by asterisks, and the vertical line is a guide to eye only.

The chemical shift for Al(IV) slightly decreased as zinc substituted strontium (Figure 5.74). This reduction in the chemical shift is similar to the trend seen with the ^{27}Al MAS-NMR spectra for the glasses in the Ca-Zn series containing calcium and zinc (Figure 5.18). Hill and co-workers [20] showed that the strontium substitution for calcium showed no change on ^{27}Al MAS-NMR. Therefore, it is possible to assume that Ca^{2+} in the Ca-Zn series and Sr^{2+} in the Sr-Zn series are behaving similarly in the aluminosilicate glasses studied here, and this could indicate that zinc in the Sr-Zn series is replacing strontium in the glass structure, that is, charge balancing Al in Al(IV) coordination, as was seen with the glasses in the Ca-Zn series.

5.16. ^{29}Si MAS-NMR Spectroscopy

Glass LPLG26Sr [$4.5SiO_2$. $3.0Al_2O_3$. $0.75P_2O_5$. 3.0SrO. $2.0SrF_2$] exhibited a peak at -87ppm (Figure 5.75), and this chemical shift shows that this glass consists of a mixture of Q structures, namely Q^4(4Al) and Q^3(3Al) [28]. The chemical shift for glass LG26Sr [$4.5SiO_2$. $3.0Al_2O_3$. $1.5P_2O_5$. 3.0SrO. $2.0SrF_2$] was observed at -90ppm (Figure 5.20). A less negative chemical shift, towards 0ppm, with a decrease in phosphate content was also observed by Zainuddin [19], and Stamboulis and co-workers [23]. Kirkpatrick and Brow [62] mentioned that phosphorus tends to remove cations from the silicate network to charge balance NBOs on phosphorus. This will increase the polymerisation of the silicate network. Therefore, LPLG26Sr may contain a lower proportion of Q^4(4Al) species than LG26Sr.

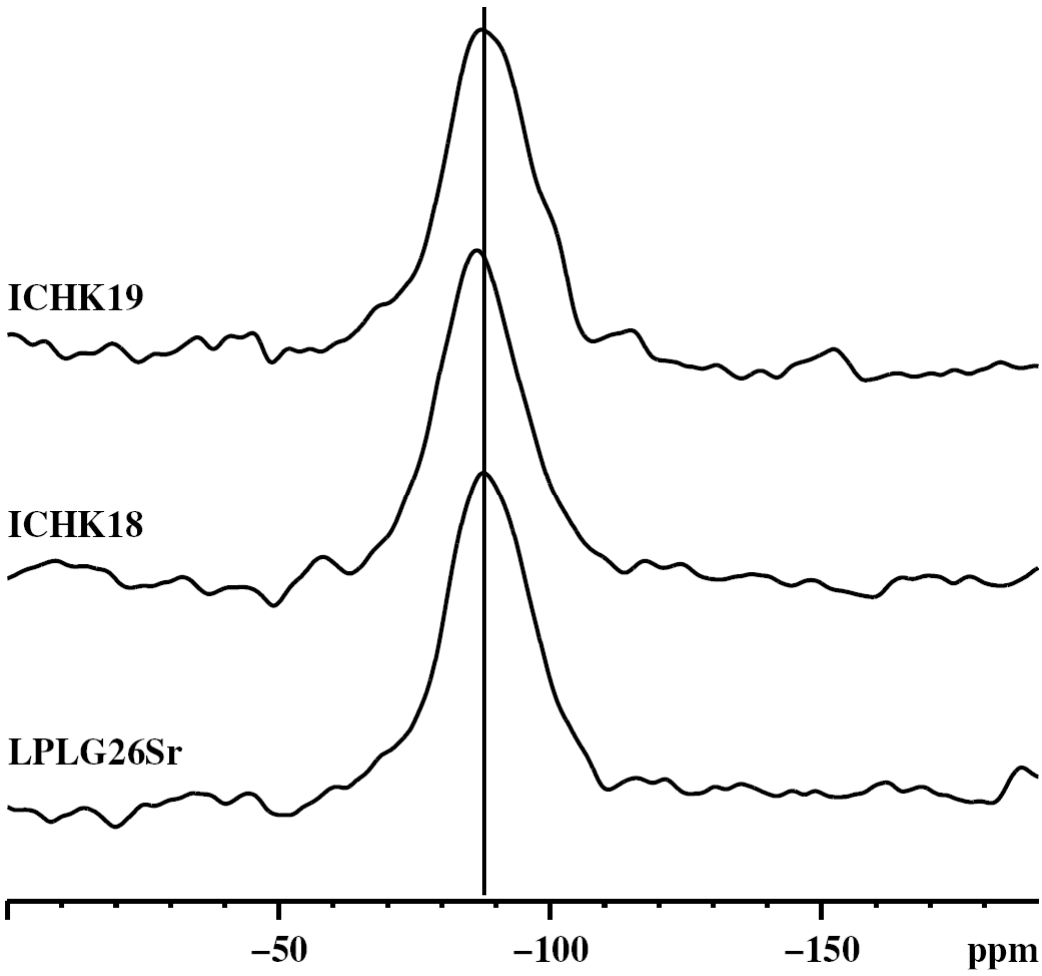


Figure 5.75. ^{29}Si MAS-NMR spectra for the glasses in the Sr-Zn series [4.5SiO_2. 3.0Al_2O_3. 0.75P_2O_5. (3.0-x)SrO. xZnO. 2.0SrF_2]. The vertical line is a guide to eye only.

The chemical shifts for glasses ICHK18 and ICHK19 were observed at -88ppm and -87ppm respectively. The change in the chemical shift is quite small when both strontium and zinc are present, and therefore, this substitution seems unlikely to have affected the Q structure of the silicate network up to the substitution studied here.

5.17. DSC Analysis

DSC was run on the glasses in the Sr-Zn series [4.5SiO_2. 3.0Al_2O_3. 0.75P_2O_5. (3.0-x)SrO. xZnO. 2.0SrF_2] to determine their glass transition temperatures, T_g, and the first crystallisation temperature, T_{c1} (Table 5.9).

Table 5.9. Glass transition temperatures, T_g, and first crystallisation temperatures of the glasses, T_{c1}, measured with particle sizes <38µm and >38µm, in the Sr-Zn series [4.5SiO_2. 3.0Al_2O_3. 0.75P_2O_5. (3.0-x)SrO. xZnO. 2.0SrF_2]. The error is +/- 10°C.

Glass	T_g /°C	T_{c1} /°C	
		<38µm	>38µm
LPLG26Sr	582	690	693
ICHK18	582	733	744
ICHK19	576	771	747

T_g did not vary much with zinc substitution for strontium (Table 5.9). The ^{31}P, ^{27}Al, and ^{29}Si MAS-NMR spectra of the glasses in the Sr-Zn series have already shown that the substitution of strontium by zinc affected the glass structures very slightly (Figures 5.73-5.75). This is reflected on the small variation in T_g upon the substitution. The change in the T_{c1} when measured with <38µm and >38µm is very small indicating that the crystallisation has most likely to have occurred *via* bulk nucleation.

In conclusion, this study showed that the effect of the zinc substitution for strontium on the structure of fluoro-aluminosilicate glasses was minimal. However, the reduction in the phosphate content resulted in a small structural change, such as a less number of Al-O-PO_3^{3-} species being formed and a lower proportion of Q^4(4Al)

species. These glasses will be used to make GPCs with a copolymer of PgGA and TCA in the next section.

Part IV. Characterisation of GPCs with PgGA and Fluoro-Aluminosilicate Glasses containing Sr, Zn, and Lower Phosphate

The Sr-Zn series [$4.5SiO_2$. $3.0Al_2O_3$. $0.75P_2O_5$. (3.0-x)SrO. xZnO. $2.0SrF_2$], whose structures have been characterised in the Part III, were used in the formation of the hybrid cements. Three polymeric acids were used: poly (γ-glutamic acid), PgGA, co-polymer of poly (but-3-ene 1,2,4-tricarboxylic acid), TCA, and poly (acrylic acid), PAA. This co-polymer is an aqueous solution containing 45wt% TCA and 55wt% PAA. Three types of conditions were tested: 0wt% PgGA (only TCA/PAA), 25wt% PgGA-75wt% TCA/PAA, and 50wt% PgGA-50wt% TCA/PAA. The co-polymer of TCA/PAA was used as it was not possible to form water cements with PgGA on its own.

5.18. Working and Setting Time

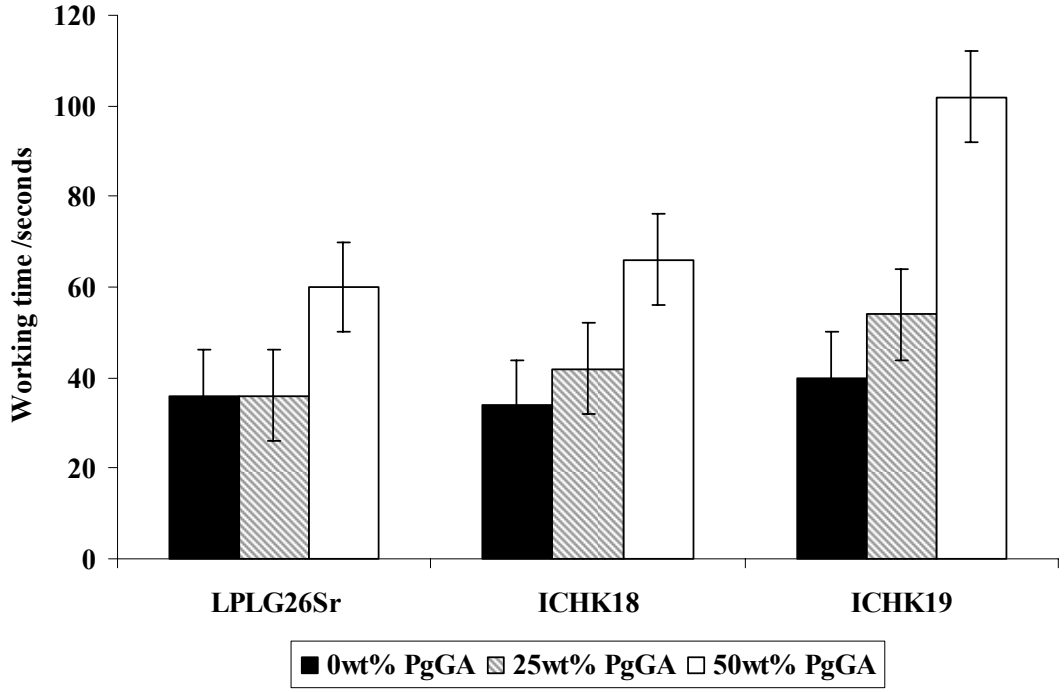


Figure 5.76. Working time of the PgGA-TCA/PAA hybrid cements for the glasses in the Sr-Zn series [4.5SiO_2. 3.0Al_2O_3. 0.75P_2O_5. (3.0-x)SrO. xZnO. 2.0SrF_2] where x=0.0 for LPLG26Sr, x=1.5 for ICHK18, and x=3.0 for ICHK19. Error bar – 10 seconds.

There is a slight increase in the working and the setting times when PgGA content is increased from 0wt% to 25wt%. More increase was observed with 50wt% PgGA (Figure 5.76, Figure 5.77). It is worth to point out that, although the PgGA content is varied, the number of carboxylate groups was kept constant. Therefore, this increase in the working time as the PgGA content was increased may result from the less acidic and less reactive nature of the PgGA than the TCA/PAA co-polymer.

Glass ICHK19 [4.5SiO_2. 3.0Al_2O_3. 0.75P_2O_5. 3.0ZnO. 2.0SrF_2] contains the highest amount of zinc in the Sr-Zn series. Its working time and setting time, with various

amount of PgGA, was measured to be the highest in the series. The substitution of zinc for calcium in the Ca-Zn series also resulted in a slight increase in the working and setting times in the PAA based cements (Figure 5.58). This may be caused by the bigger size of Sr^{2+} than Zn^{2+} or Ca^{2+}, and therefore Sr^{2+} can modify the glass network more effectively resulting in a more reactive glass. The more reactive glass would react with the polymeric acid more efficiently than the less reactive glass which would decrease the working and setting times of the cements.

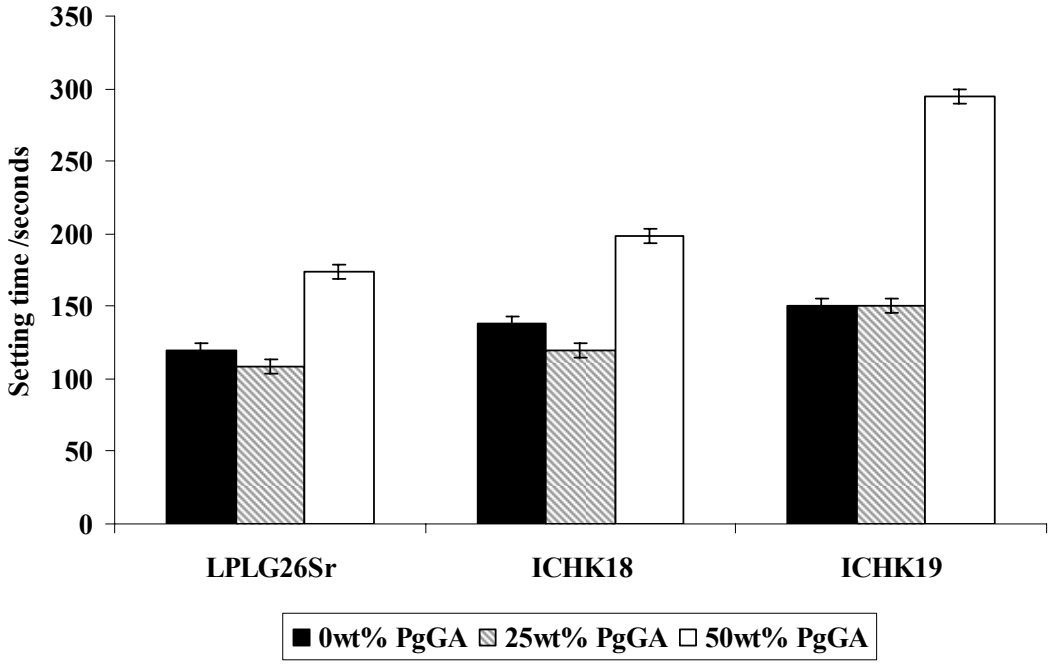


Figure 5.77. Setting time of the PgGA-TCA/PAA hybrid cements for the glasses in the Sr-Zn series [4.5SiO_2. 3.0Al_2O_3. 0.75P_2O_5. (3.0-x)SrO. xZnO. 2.0SrF_2] where x=0.0 for LPLG26Sr, x=1.5 for ICHK18, and x=3.0 for ICHK19. Error bar – 10 seconds.

The ISO standard for dental luting cements states that the working time should be a minimum of 60 seconds and the setting time a minimum of 90 seconds and a maximum of 600 seconds [80, 82]. Therefore, only the cements containing 50wt% PgGA comply with ISO standard. It is, however, possible to manipulate the working

and the setting times of the cements, such as, by acid treating the glass powder to reduce the reactivity of the glass.

5.19. Compressive Strength

The compressive strengths of the cements containing 0wt%, 25wt%, and 50wt% PgGA were measured at 1, 7, 28, and 56 days (Figures 5.78-5.80).

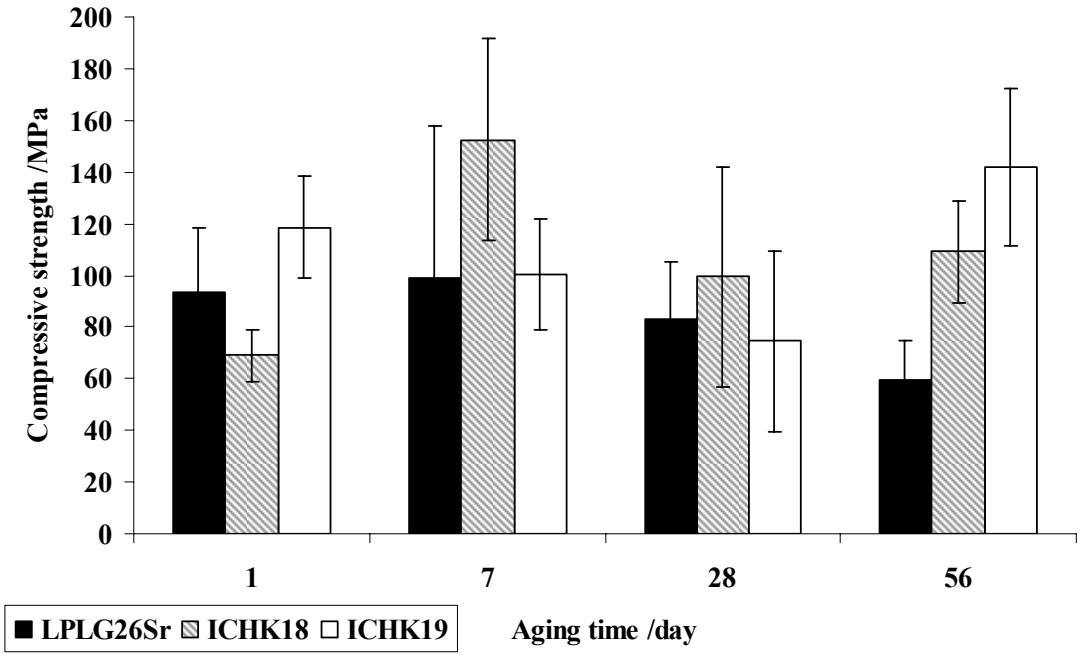


Figure 5.78. Compressive strengths of the cements formed with the glasses in the Sr-Zn series [4.5SiO_2. 3.0Al_2O_3. 0.75P_2O_5. (3.0-x)SrO. xZnO. 2.0SrF_2] where x=0.0 for LPLG26Sr, x=1.5 for ICHK18, and x=3.0 for ICHK19. No PgGA was used. Error bar – 1 s.d.

The effect of different glass compositions on the compressive strengths was not clearly observed with the cements containing no PgGA (Figure 5.78). This might have been caused by the short working time of these cements that there was not enough time to mix the glass and polymeric acid properly during cement formulation. Also,

the time needed to pour the cement paste into the mould was restricted due to the short working time.

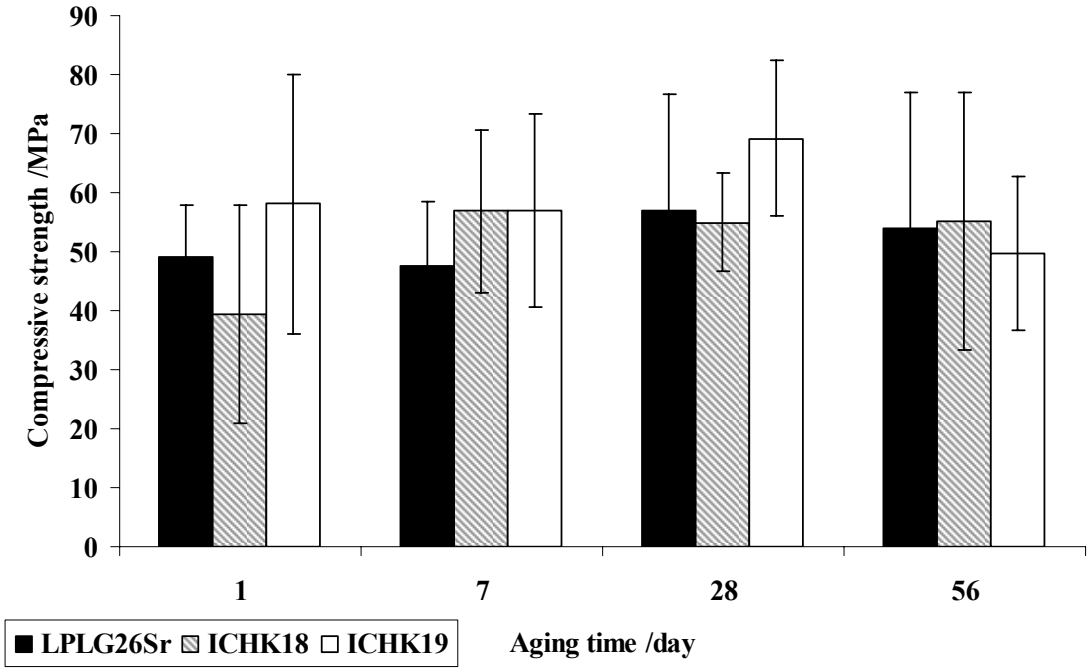


Figure 5.79. Compressive strengths of the cements formed with the glasses in the Sr-Zn series [4.5SiO_2. 3.0Al_2O_3. 0.75P_2O_5. (3.0-x)SrO. xZnO. 2.0SrF_2] where x=0.0 for LPLG26Sr, x=1.5 for ICHK18, and x=3.0 for ICHK19. A hybrid of 25wt% PgGA and 75wt% TCA/PAA co-polymer was used. Error bar – 1 s.d.

The incorporation of PgGA in the cement formulation showed a better relationship between the glass compositions and the compressive strengths. At most of the aging time points, ICHK19 cements showed slightly higher compressive strengths than the other cements (Figure 5.79). This may have resulted from the fact that carboxylate groups have been shown to crosslink well with Zn^{2+} [9], and glass ICHK19 contains the highest amount of zinc in the Sr-Zn series.

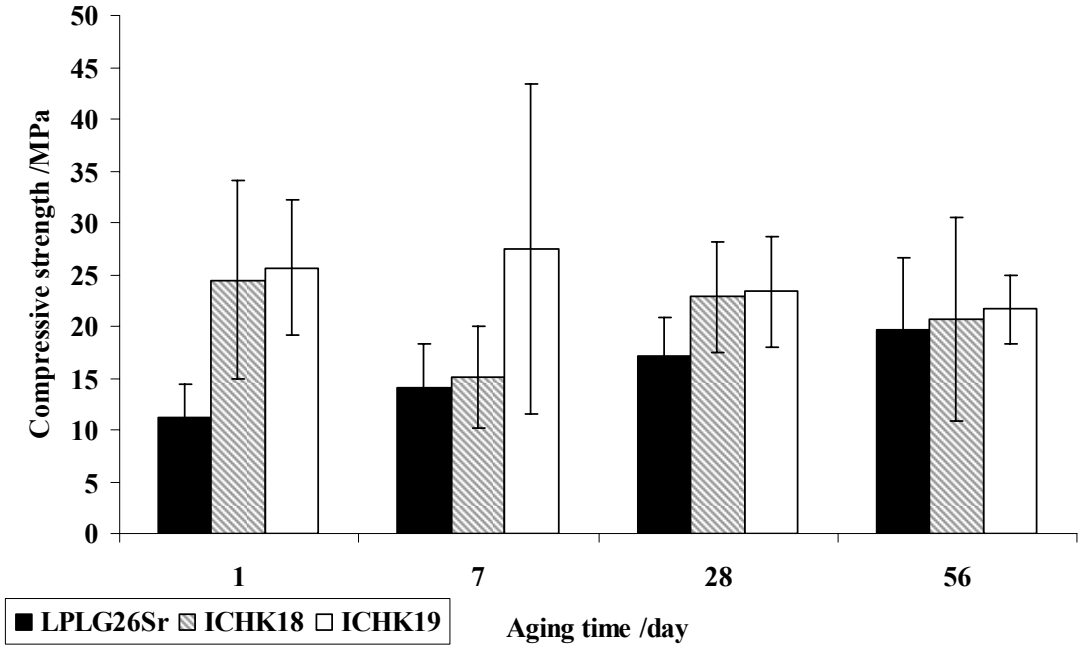


Figure 5.80. Compressive strengths of the cements formed with the glasses in the Sr-Zn series [4.5SiO_2. 3.0Al_2O_3. 0.75P_2O_5. (3.0-x)SrO. xZnO. 2.0SrF_2] where x=0.0 for LPLG26Sr, x=1.5 for ICHK18, and x=3.0 for ICHK19. A hybrid of 50wt% PgGA and 50wt% TCA/PAA co-polymer was used. Error bar – 1 s.d.

Increasing the PgGA content from 0wt%, 25wt% and to finally 50wt% resulted in a large decrease in the compressive strength. For example, LPLG26Sr cement at 1 day with no PgGA showed about 100MP compressive strength (Figure 5.78), but the same glass with 50wt% PgGA showed about 10MPa (Figure 5.80). This decrease in the compressive strengths may be due to the less reactive nature of PgGA than the TCA/PAA co-polymer, and therefore, the cement matrix could be less crosslinked.

There was no significant trend between the aging time and the compressive strength. It has been shown that the compressive strengths of PAA cements generally increase with time. The increased compressive strengths are likely to be due to the continued crosslinking process between the ions from the glass and the carboxylate groups from

the polymeric acid [5]. However, there are some studies which showed no significant trend between the compressive strengths and the aging time [6, 34].

ISO standard for the compressive strengths for luting cements is 50MPa minimum after 1 day of aging. The cements containing 25wt% PgGA seem to fulfil the requirement for the ISO standard. However, their working and setting times were too short for the standard. Therefore, the cement formulation needs to be manipulated to meet the standard by, such as, acid treating the glass particle beforehand, using glasses with slightly larger particle size, and increasing the acid concentration.

5.20. Fluoride Release

The fluoride release from the PgGA-TCA/PAA hybrid cements were measured at 1, 3, 7, 14, 21, 28, 42, and 56 days with different content of PgGA. There was an initial burst of fluoride release from all the cements up to 7 days, and after that, the release rate decreased (Figures 5.81-5.83). A similar trend was seen by published studies [81, 83]. Verbeeck and co-workers [81] suggested that there are two processes in fluoride release: an initial burst of fluoride from the surface followed by a slow release of fluoride from the bulk of the cement.

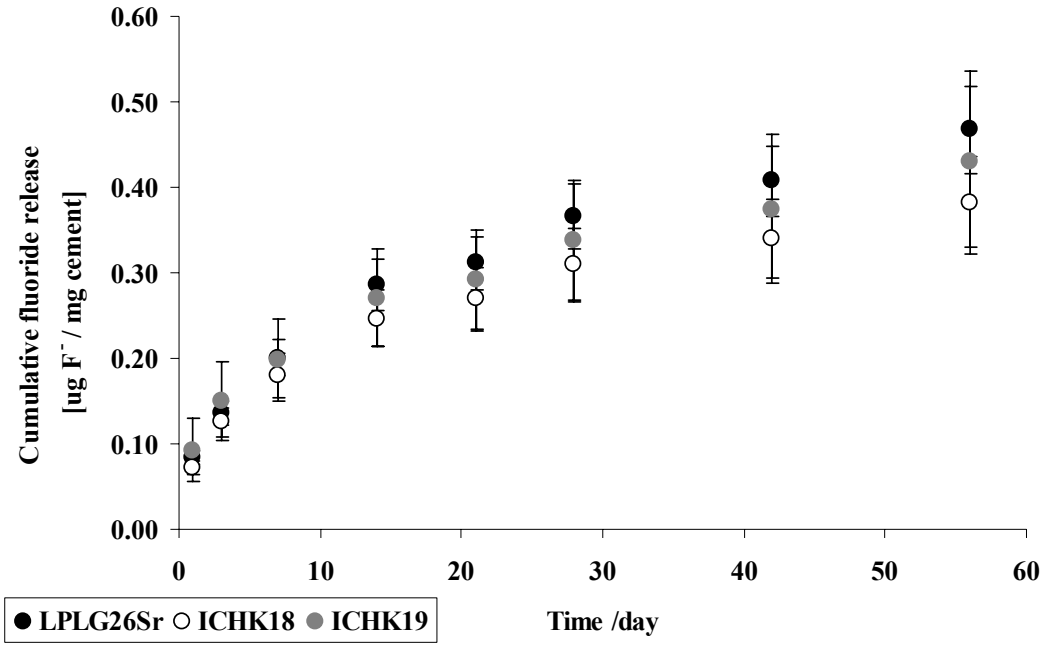


Figure 5.81. Fluoride release profile of the cements containing no PgGA and the glasses in the Sr-Zn series [4.5SiO_2. 3.0Al_2O_3. 0.75P_2O_5. (3.0-x)SrO. xZnO. 2.0SrF_2] where x=0.0 for LPLG26Sr, x=1.5 for ICHK18, and x=3.0 for ICHK19. Error bar – 1 s.d.

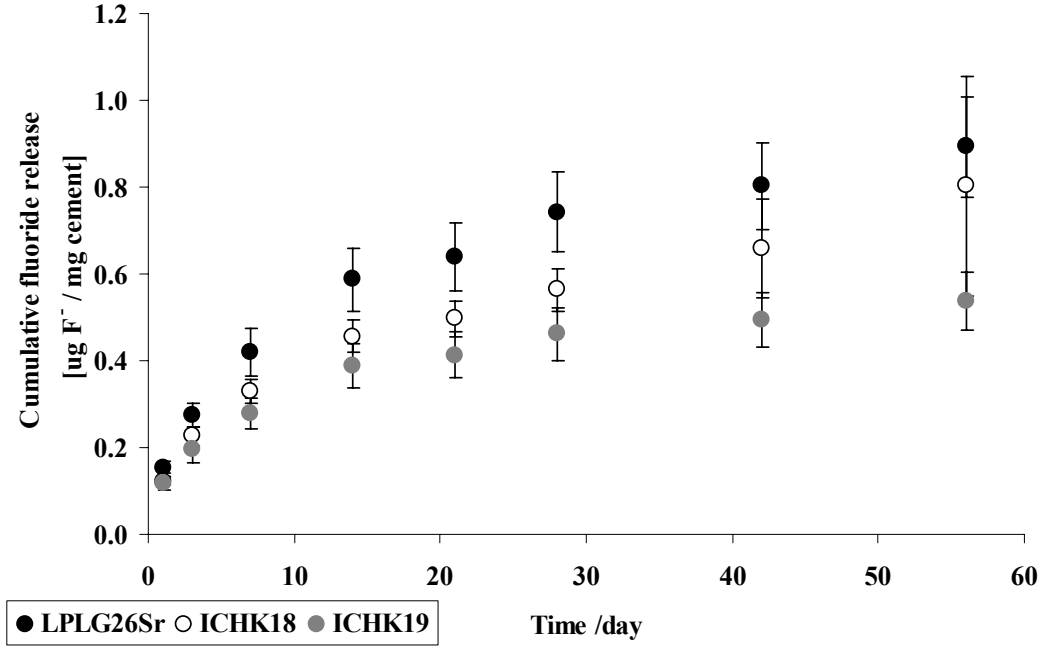


Figure 5.82. Fluoride release profile of the cements containing 25wt% PgGA and the glasses in the Sr-Zn series [4.5SiO_2. 3.0Al_2O_3. 0.75P_2O_5. (3.0-x)SrO. xZnO. 2.0SrF_2] where x=0.0 for LPLG26Sr, x=1.5 for ICHK18, and x=3.0 for ICHK19. Error bar – 1 s.d.

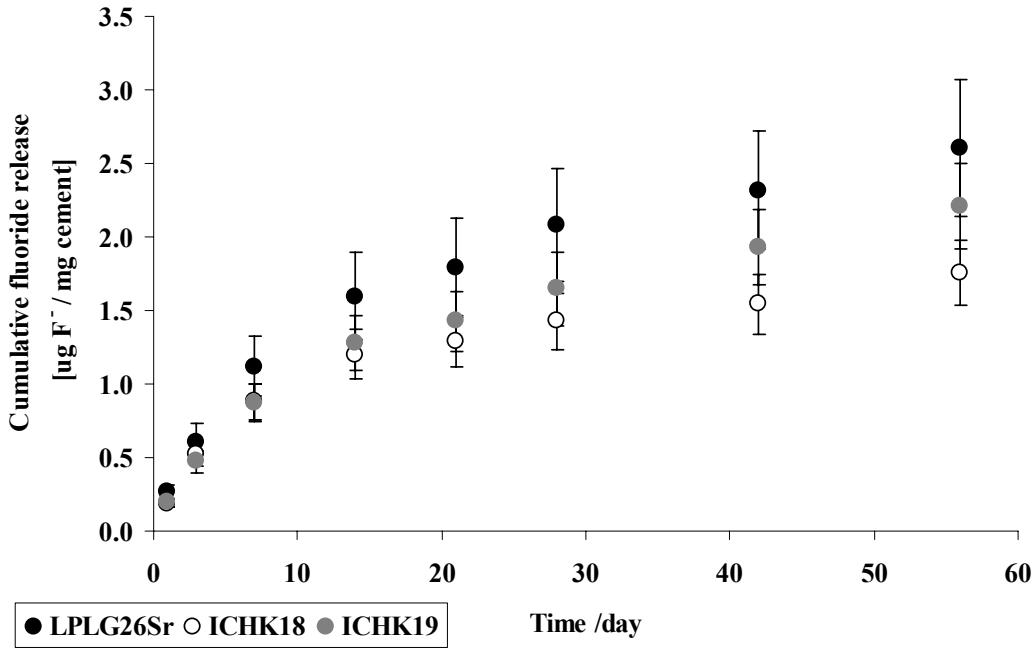


Figure 5.83. Fluoride release profile of the cements containing 50wt% PgGA and the glasses in the Sr-Zn series [4.5SiO_2. 3.0Al_2O_3. 0.75P_2O_5. (3.0-x)SrO. xZnO. 2.0SrF_2] where x=0.0 for LPLG26Sr, x=1.5 for ICHK18, and x=3.0 for ICHK19. Error bar – 1 s.d.

Figures 5.84-5.86 show almost a linear relationship between the cumulative fluoride release in μg F^- per mg of cement and the square root of days with all the cements containing different amount of PgGA. This indicates that the fluoride release is diffusion controlled [1].

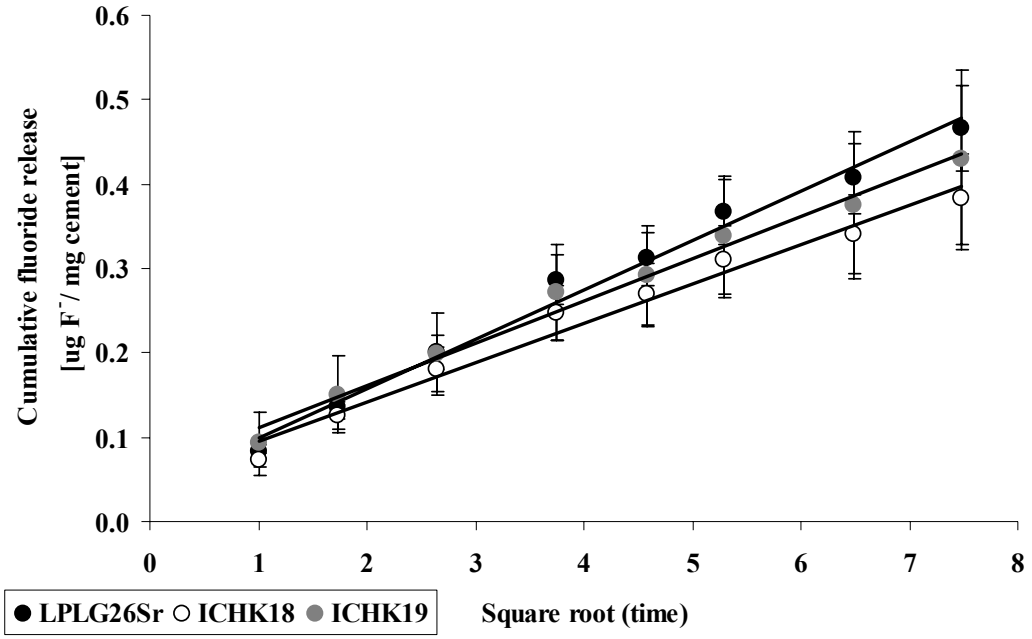


Figure 5.84. Fluoride release profile of the cements containing no PgGA and the glasses in the Sr-Zn series [4.5SiO_2. 3.0Al_2O_3. 0.75P_2O_5. (3.0-x)SrO. xZnO. 2.0SrF_2] where x=0.0 for LPLG26Sr, x=1.5 for ICHK18, and x=3.0 for ICHK19. Lines are guide to eye only. Error bar – 1 s.d.

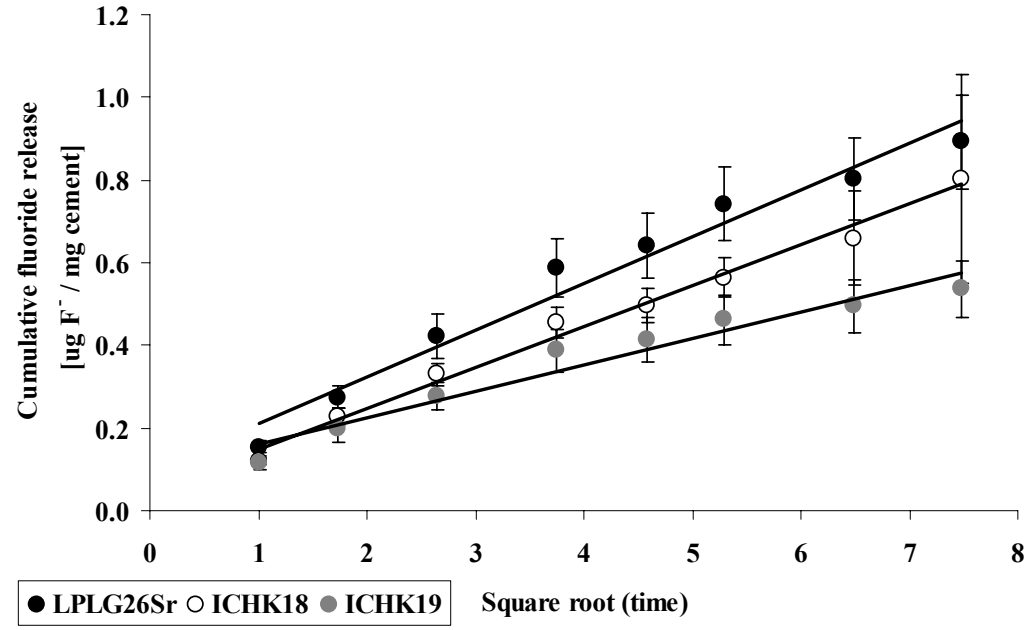


Figure 5.85. Fluoride release profile of the cements containing 25wt% PgGA and the glasses in the Sr-Zn series [4.5SiO_2. 3.0Al_2O_3. 0.75P_2O_5. (3.0-x)SrO. xZnO. 2.0SrF_2] where x=0.0 for LPLG26Sr, x=1.5 for ICHK18, and x=3.0 for ICHK19. Lines are guide to eye only. Error bar – 1 s.d.

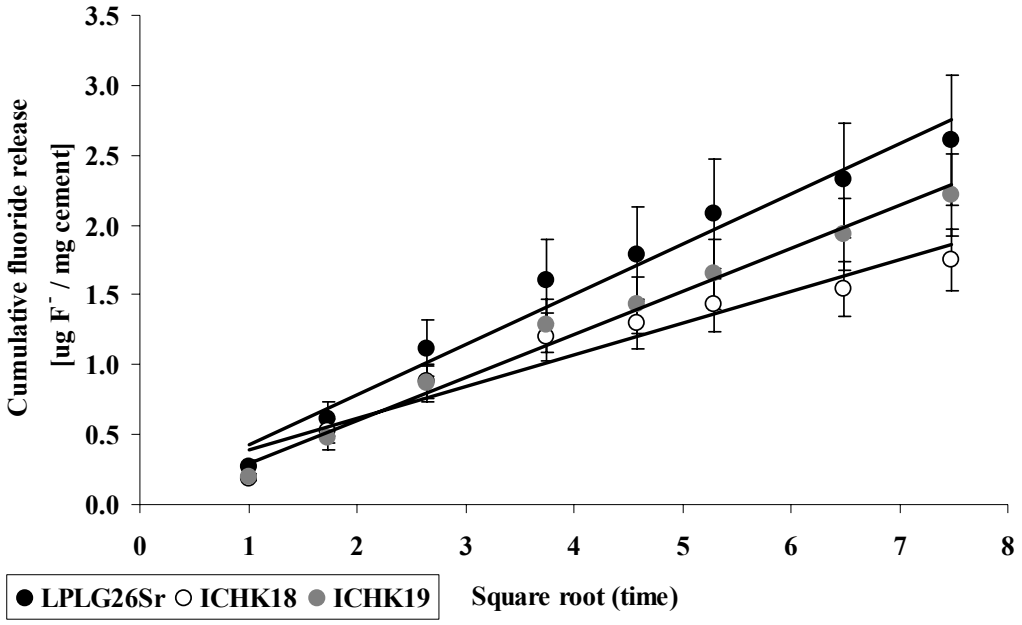


Figure 5.86. Fluoride release profile of the cements containing 50wt% PgGA and the glasses in the Sr-Zn series [4.5SiO_2. 3.0Al_2O_3. 0.75P_2O_5. (3.0-x)SrO. xZnO. 2.0SrF_2] where x=0.0 for LPLG26Sr, x=1.5 for ICHK18, and x=3.0 for ICHK19. Lines are guide to eye only. Error bar – 1 s.d.

Among the three compositions in the Sr-Zn series, it seems that LPLG26Sr cements containing the highest amount of strontium in the series, released the highest amount of fluoride with all the PgGA content (Figures 5.84-5.86). The fluoride concentration in all glass compositions in the Sr-Zn series is the same, and the number of ions in each cement was also kept constant for cement formulation. This indicates that the cement matrix in LPLG26Sr cement is less crosslinked, and this finding correlates well with the compressive strengths data which showed that LPLG26Sr cements exhibited the lowest compressive strength in the series (Figures 5.78-5.80). Xiaoming and Burgess [84] also found that the cements releasing the most fluoride had the lowest compressive strengths.

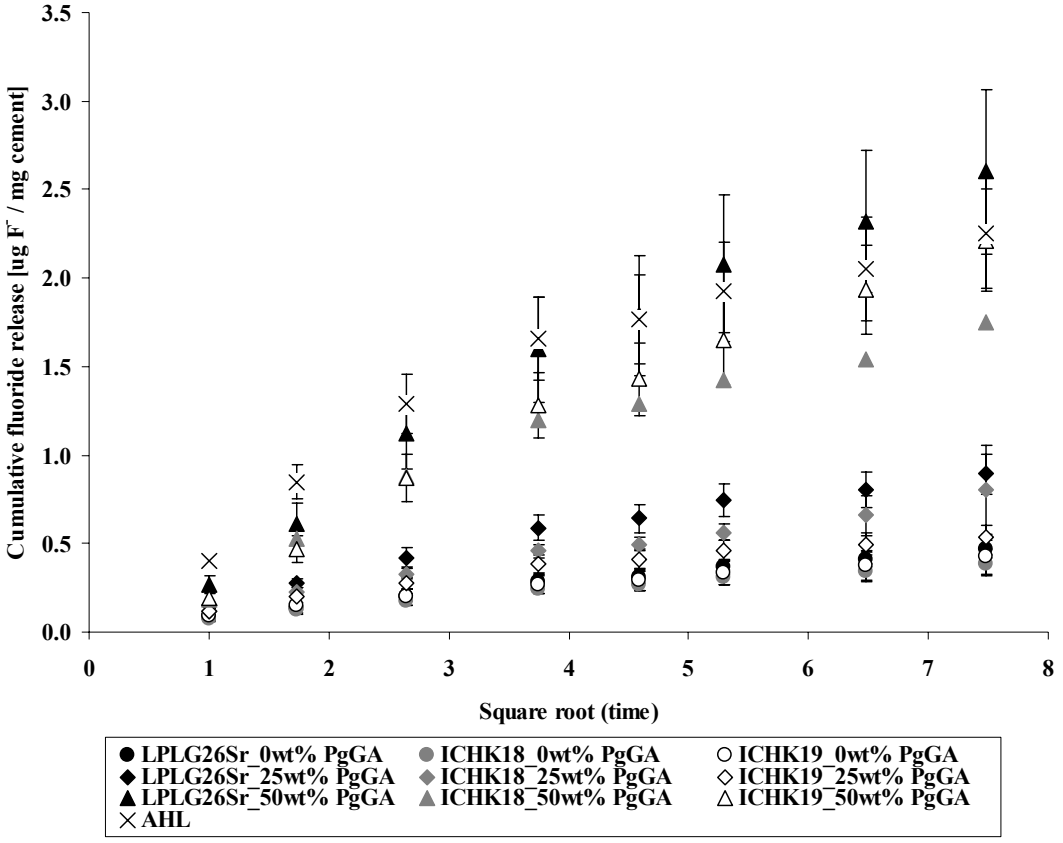


Figure 5.87. Fluoride release profile of the cements containing 0wt% PgGA, 25wt% PgGA, and 50wt% PgGA and the glasses in the Sr-Zn series [4.5SiO_2. 3.0Al_2O_3. 0.75P_2O_5. (3.0-x)SrO. xZnO. 2.0SrF_2] where x=0.0 for LPLG26Sr, x=1.5 for ICHK18, and x=3.0 for ICHK19. AHL is the standard luting cement provided from Advanced Healthcare Ltd (UK). Error bar – 1 s.d.

The fluoride release profile with different PgGA content is shown in Figure 5.87, and it is clear that the increase in the PgGA content resulted in more fluoride being released. Again, this result correlates well with the compressive strength study, which showed that increasing the PgGA content decreased the compressive strengths of the cements (Figure 5.78-5.80).

5.21. Adhesion

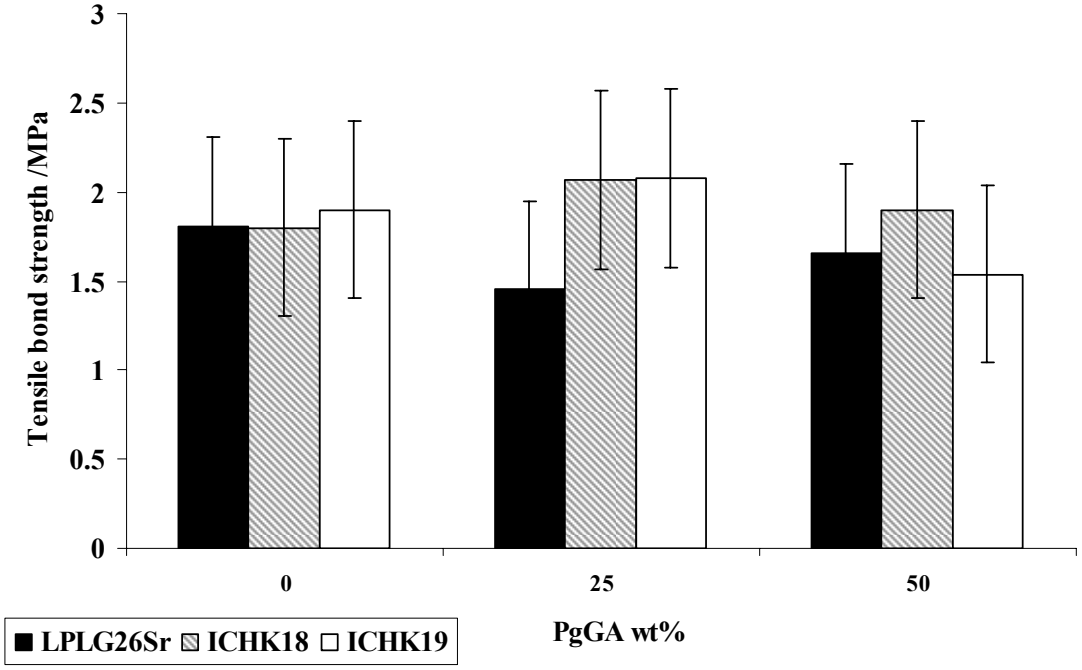


Figure 5.88. Tensile bond strengths to bovine dentine measured 1 day after mixing. The glasses in the Sr-Zn series [4.5SiO_2. 3.0Al_2O_3. 0.75P_2O_5. (3.0-x)SrO. xZnO. 2.0SrF_2] where x=0.0 for LPLG26Sr, x=1.5 for ICHK18, and x=3.0 for ICHK19 and a hybrid of PgGA and TCA/PAA co-polymer were used for cement formation. Error bar – 1 s.d.

An increase in the PgGA content, from 0wt% to 25wt%, showed a very slight increase in the tensile bond strength of the cements to the bovine dentine with most of the glass compositions in the Sr-Zn series. However, a further increase in the PgGA content, to 50wt%, decreased the tensile bond strength (Figure 5.88). The main mechanism of adhesion to tooth is the ionic crosslinking between the COO^- from the polyacid chain and Ca^{2+} from the tooth enamel. There is an extra mechanism of adhesion, for dentine, and this is the hydrogen bonding between the collagen in the dentine and the polymer in the cement matrix [85]. Therefore, it was originally postulated that the NH groups in PgGA would give hydrogen bonding for adhesion increasing the tensile bond

strength to the dentine compared to commercially available PAA based GPCs. An increase in the tensile bond strength observed with the increased amount of PgGA may have resulted from the NH contribution from PgGA, but the increase is quite small. The decrease, on the other hand, when PgGA was further increased, may have resulted from these cements exhibiting longer setting times than the cements containing less PgGA (Figure 5.77). Therefore, cements were more liquid, and when the 100g weight was placed on the orthodontic brackets on the cement, some cement was pushed out forming a thinner layer of cement underneath the bracket. Akinmade and Hill [86] studied the relationship between the cement layer thickness and the shear bond strength. They concluded that the shear bond strength is highly dependent on the cement layer thickness. In this experiment, tensile bond strength was measured rather than shear bond strength, but cement layer thickness may also play a significant role in tensile bond strength.

There were no significant differences in the tensile bond strengths with different glass compositions. The tensile bond strength was also measured on the commercial standard luting cements, AHL, provided by Advanced Healthcare Ltd (UK). This commercial cement showed the tensile bond strength of 4.1MPa, which is higher than the PgGA based cements.

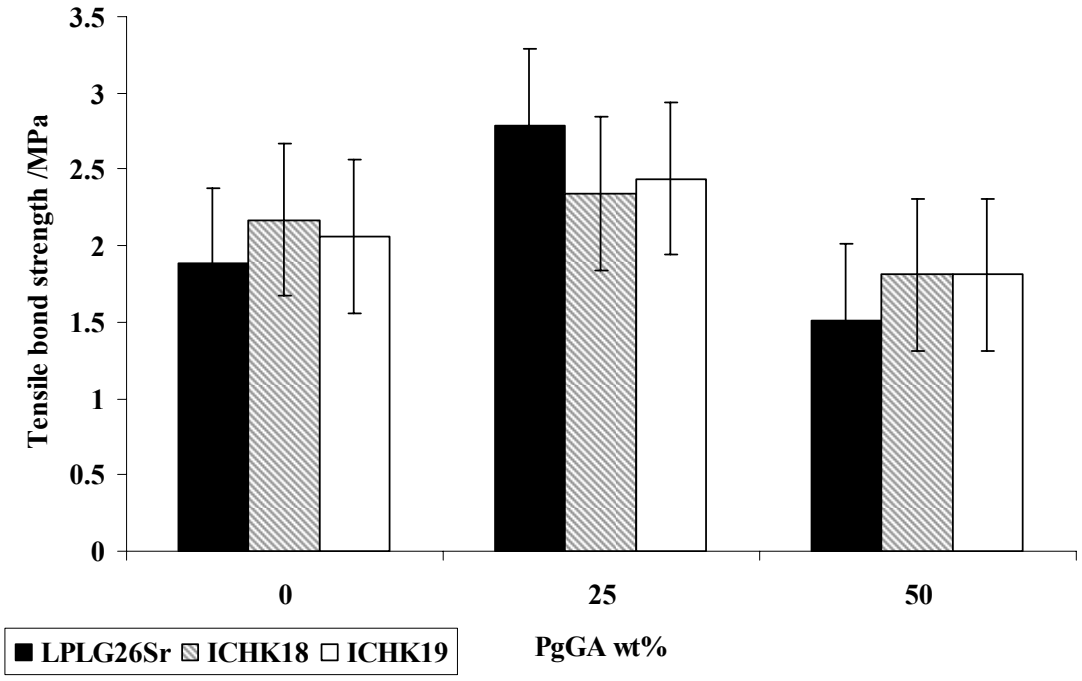


Figure 5.89. Tensile bond strength to bovine enamel measured 1 day after mixing. The glasses in the Sr-Zn series [4.5SiO_2. 3.0Al_2O_3. 0.75P_2O_5. (3.0-x)SrO. xZnO. 2.0SrF_2] where x=0.0 for LPLG26Sr, x=1.5 for ICHK18, and x=3.0 for ICHK19, and a hybrid of PgGA and TCA/PAA co-polymer were used for cement formation. Error bar – 1 s.d.

Similar to the tensile bond strength to dentine, there was a slight increase in the tensile bond strength to the enamel when PgGA content was increased from 0wt% to 25wt% and a decrease when PgGA content was further increased to 50wt%. The slight increase in the tensile bond strength may have resulted from PgGA contribution, but the increase is quite small. The decrease in the tensile bond strength may have resulted from these cements having longer setting times (Figure 5.77), as was seen with the tensile bond strength to dentine (Figure 5.88).

The tensile bond strength to enamel was measured to be higher than the tensile bond strength to dentine. There is more hydroxyapatite in the tooth enamel, 97%, than in

the tooth dentine, 69% [87]. Therefore, there would be more Ca^{2+} to ionically crosslink with the COO^- groups from the polyacid chains.

Once again, the tensile bond strength to the tooth enamel seems to be independent on the glass compositions. The tensile bond strength of AHL cement, was measured to be 5.5MPa.

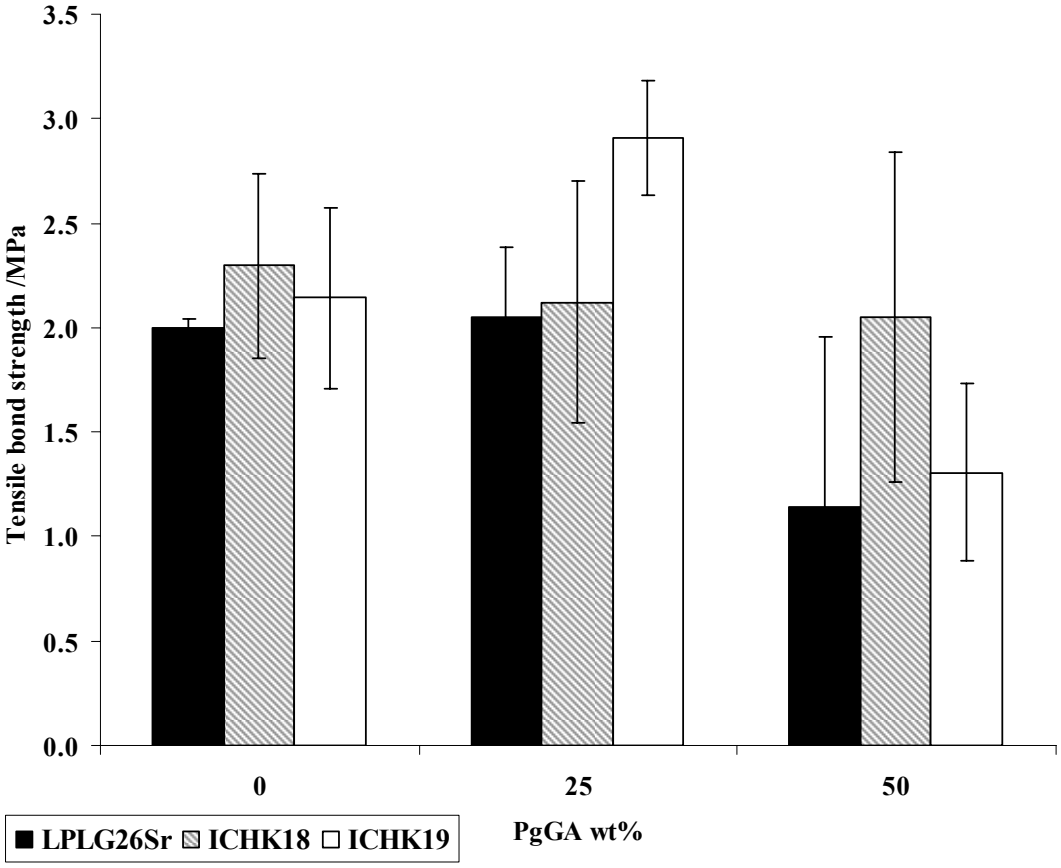


Figure 5.90. Tensile bond strength to stainless steel measured 1 day after mixing. The glasses in the Sr-Zn series [$4.5SiO_2$. $3.0Al_2O_3$. $0.75P_2O_5$. (3.0-x)SrO. xZnO. $2.0SrF_2$] where x=0.0 for LPLG26Sr, x=1.5 for ICHK18, and x=3.0 for ICHK19, and a hybrid of PgGA and TCA/PAA co-polymer were used for cement formation. Error bar – 1 s.d.

The tensile bond strength of ICHK19 cement when the PgGA content was increased from 0wt% to 25wt% increased while the other two cements did not show much difference in the tensile bond strength to the stainless steel (Figure 5.90). The adhesion mechanism to stainless steel is the chemical bonding between the oxide layer in the stainless steel and the carboxyl groups in the cement [1]. Therefore, the effect of PgGA on the tensile bond strength should be minimal. The increase in the tensile bond strength with ICHK19 cement containing 25wt% PgGA may be related to its higher compressive strengths than the other cements (Figure 5.79).

The tensile bond strength to the stainless steel for the standard luting cements, AHL, was measured to be 4.4MPa. Akinmade and Nicholson [88] discussed that the adhesion is very closely related to how the cement can wet the surface of the substrate. The wetting characteristics are highly dependent on the viscosity of the cements. If the working and setting times are too short, the viscosity of the cement increases rapidly, which reduces the polymer chain movement. The working and setting times of the cements from the Sr-Zn series are much shorter than AHL cement. This may have resulted in the difference in the tensile bond strength between the experimental and the commercial cements.

In summary, the zinc substitution for strontium affected the cement properties slightly. More importantly, an increase in the PgGA content for GPC formation decreased the cement properties, such as working and setting times and compressive strengths. More fluoride was released from the cements containing more PgGA due to less crosslinking in the cement matrix. However, a slight increase in the tensile bond strengths to bovine dentine and enamel was observed with an increase in the PgGA

content. Therefore, it may be beneficial to use PgGA for GPCs, but further investigation is required to improve the setting and the mechanical properties.

6. Conclusion

6.1. Characterisation of Mg, Sr, and Zn containing Fluoro-Aluminosilicate Glasses

Three series of glasses were produced by substituting calcium by magnesium and zinc in the base glass composition, LG26 [$4.5SiO_2$. $3.0Al_2O_3$. $1.5P_2O_5$. 3.0CaO. $2.0CaF_2$], and these glasses were characterised by XRD, ^{19}F, ^{31}P, ^{27}Al, and ^{29}Si MAS-NMR spectroscopy, and DSC. Apart from the fully zinc substituted glass LG26Zn, all the glasses were shown to be amorphous on the XRD. The mixed cation effect on glass transition temperatures for the glasses in all three series was observed on the DSC.

The MAS-NMR spectra have shown significant structural changes upon the substitution of calcium by magnesium in the Ca-Mg series. The ^{19}F MAS-NMR spectra showed the formation of F-Mg(n) species starting in the middle of the series. The ^{31}P and ^{27}Al MAS-NMR spectra both showed the formation of Al-O-PO_3^{3-} species. The gradual substitution of calcium by magnesium resulted in the steady change of the chemical shift in the ^{31}P MAS-NMR spectra indicating the replacement of charge balancing cations on NBOs of phosphorus from Ca^{2+} to Mg^{2+}. In addition, the ^{31}P MAS-NMR spectrum of the fully magnesium substituted glass LG26Mg exhibited a possible formation of magnesium pyrophosphate, $Mg_2P_2O_7$, as well as Al-O-PO_3^{3-} species. The ^{27}Al MAS-NMR spectra showed an increase in the formation of Al(V) with magnesium substitution. The chemical shift in the ^{29}Si MAS-NMR spectra decreased with the substitution which indicated the decrease in the number of Al around each SiO_4 tetrahedra and the increase in the number of BOs on Si. Similar

findings were observed in the Sr-Mg series as a result of Ca^{2+} and Sr^{2+} behaving similarly in fluoro-aluminosilicate glasses.

The characterisation of the glasses in the Ca-Zn series showed that zinc and magnesium behave differently in fluoro-acluminosilicate glasses studied here although they have a similar charge to size ratio. The ^{19}F MAS-NMR spectra showed the presence of F-Ca(n) and Al-F-Ca(n) species in the mixed Ca/Zn glasses. The ^{19}F MAS-NMR analysis for glass LG26Zn would be interesting to determine the fluorine environment in the fully zinc substituted glass. The ^{31}P and ^{27}Al MAS-NMR spectra both showed the formation of Al-O-PO_3^{3-} species. In addition, the ^{31}P MAS-NMR spectra showed the gradual replacement of the charge balancing cations, from Ca^{2+} to Zn^{2+}, on NBOs of phosphorus in Al-O-PO_3^{3-} species. The ^{27}Al MAS-NMR spectra exhibited the steady decrease in the chemical shift for Al(IV) with more substitution which seemed to have resulted from the increase in the Al(V). The ^{29}Si MAS-NMR spectra for the mixed Ca/Zn glasses showed no significant change, but the ^{29}Si MAS-NMR spectrum for the fully zinc substituted glass showed an increase in the number of BOs around Si and/or decrease in the number of Al next to SiO_4 tetrahedra.

6.2. Characterisation of GPCs with Mg, Sr, and Zn containing Fluoro-Aluminosilicate Glasses

The setting chemistry of selected cements from the Ca-Mg and the Sr-Mg series was studied by ^{19}F, ^{31}P, and ^{27}Al MAS-NMR spectroscopy. F-Ca(n) species were shown to be consumed during the cement formation. The Al-F-Ca(n) peak shifted to a more positive value, indicating a possible formation of new fluorine species. The new fluorine species may result from the change in the ligands on Al(VI) in the cement

matrix. For example, there may be originally two carboxylate groups, one hydroxyl group from water, and one fluorine from the glass on Al(VI) in the cement matrix. Over a long period of time, the hydroxyl group and fluorine may be released, and a new carboxylate group may be attached to this Al(VI). This will not change the Al coordination, but the fluorine environment will change, which may be the reason for the shift in the peak to a more positive value in the ^{19}F MAS-NMR spectra. The change in the ^{19}F MAS-NMR spectra takes place over a period of a long time, and it is highly possible that the release of fluorine from the Al(VI) takes a long time. Moreover, a continuous increase in the mechanical properties, usually observed with GPCs, may result from this increased number of carboxylate groups crosslinking with Al^{3+}. F-Mg(n) species were still present in the ^{19}F MAS-NMR spectra of LG26Mg cements. It was assumed that F-Mg(n) species participate in the cement formation, but as it was the only fluorine species in LG26Mg cements, the release of F-Mg(n) species during the cement formation was difficult to determine. The ^{31}P MAS-NMR spectra showed that Q^1 pyrophosphate Al-O-PO_3^{3-} species do not participate in the cement formation. The peak in LG26Mg cements moved to a more positive value indicating that magnesium pyrophosphate, $Mg_2P_2O_7$, was released from the glass network during the setting of the cements. The deconvolution of ^{27}Al MAS-NMR spectra allowed to calculate the Al(VI):Al(IV)+Al(V) ratio to follow whether the setting reaction has completed. However, the experimental ratio was found to be higher than the theoretical ratio with all the cements studied, and this may have resulted from the L-(+)-tartaric acid responsible for the extra conversion of Al(IV) and Al(V) to Al(VI). The Al(VI):Al(IV)+Al(V) ratio of LG26Mg cements seemed to keep increasing, although the ratio of the other cements became plateau.

The partially magnesium substituted cements, in both Ca-Mg and Sr-Mg series, showed no significant trend in the working and the setting times. However, both working and setting times increased with the fully magnesium substituted glass LG26Mg. Similarly, the cements in the Ca-Zn series showed no significant change in the working and the setting times with zinc substitution, but LG26Zn cement showed the longest working and setting times because of the presence of crystalline phase in the glass.

The radiopacity decreased with magnesium substitution in both Ca-Mg and Sr-Mg series and increased with zinc substitution in the Ca-Zn series. Both are related to the change in the electron density of the material.

The compressive strengths decreased with magnesium substitution in both Ca-Mg and Sr-Mg series due to a fewer divalent cations available for crosslinking with polymeric acid. Generally, an increase in the compressive strengths with aging time was observed in both Ca-Mg and Sr-Mg series. Moreover, the cements in the Sr-Mg series showed slightly higher compressive strengths than the cements in the Ca-Mg series. A slight increase in the compressive strength with zinc substitution in the Ca-Zn series was observed resulting from Zn^{2+} being smaller in size than Ca^{2+} pulling the polymeric chains closer together.

The fluoride release was shown to be diffusion controlled. The highest fluoride release was observed with the fully magnesium substituted LG26Mg cements. A possible source of the high fluoride release from LG26Mg cements is F-Mg(n) species, which are not part of the glass network and therefore are readily released.

6.3. Characterisation of Fluoro-Aluminosilicate Glasses containing Sr, Zn and Lower Phosphate

Another series of glasses, the Sr-Zn series, containing a lower content of phosphate than the glasses used for PAA cements, was prepared. XRD showed all of them to be amorphous. The ^{31}P MAS-NMR spectra showed the formation of Al-O-PO_3^{3-} species. The ^{31}P chemical shift was more positive than the glasses in the Ca-Mg, the Sr-Mg, and the Ca-Zn series due to the decreased content of phosphate. The ^{27}Al MAS-NMR spectra showed a slight decrease in the chemical shift for Al(IV) with zinc substitution. The ^{29}Si MAS-NMR spectra showed a mixture of $Q^4(4Al)$ and $Q^3(3Al)$ structures.

6.4. Characterisation of GPCs with PgGA and Fluoro-Aluminosilicate Glasses containing Sr, Zn, and Lower Phosphate

The working and setting times increased with increasing the amount of PgGA. There was a slight increase in the working and setting times with zinc substitution due to a possible decrease in the reactivity of the glass.

No clear trend was observed in the compressive strengths between the different glass compositions. Also, the aging time did not affect the compressive strengths of the cements. However, the increase in the PgGA content resulted in the decrease in the compressive strength in all the glass compositions in the Sr-Zn series.

The fluoride release was shown to be diffusion controlled. The highest amount of fluoride was released from the cements containing the highest amount of PgGA

possibly due to the cements being less crosslinked which reflected also on the decreased compressive strengths.

A very slight increase in the tensile bond strength for adhesion to the bovine dentine, enamel, and stainless steel, was observed with increasing the PgGA content. A further increase in the PgGA content resulted in the decrease in the tensile bond strength to all these substrates possibly because of the decrease in the cement layer thickness resulting from the increased working and setting times of the cements.

6.5. Recommendations for Future Work

This study has given a new insight to the structures of magnesium, strontium, and zinc containing fluoro-aluminosilicate glasses and their cements with PAA and PgGA. However, there are still more work which need to be done for further investigation.

1. It may be useful to identify the crystal phases of the magnesium containing fluoro-aluminosilicate glasses studied here to compare with the MAS-NMR analysis. The heat treated samples can be run on the XRD. Especially, the identification of the unknown peak observed at around 15ppm in the ^{27}Al MAS-NMR spectrum may benefit from the XRD analysis of the heat treated samples.
2. The ^{19}F MAS-NMR spectra of the aging cements showed that the peak for Al-F-Ca(n) species for the original glasses moved to a more positive value. This was assumed to be a formation of new species, possibly resulting from the exchange in the ligands on the Al(VI) in the cement matrix. The cross-polarisation MAS, CPMAS, can give information on which nuclei are close in contact. CPMAS of $^{19}F \rightarrow ^{27}Al$ or $^{1}H \rightarrow ^{27}Al$ could provide useful information

about the Al environment in the aged cements. Alternatively, ^{17}O labelled water can be used instead of distilled water for cement formulation, and ^{17}O MAS-NMR can be run on the aged cements. By doing so, if hydroxyl group attached to Al(VI) is exchanged with carboxylate groups over a period of a long time, the change in the ^{17}O environment can be observed.

3. The ^{29}Si MAS-NMR analysis on the magnesium containing aging cements may be useful as it will give information on any changes in the Q structures as the cements age.

4. In this study, the Al(VI):Al(IV)+Al(V) ratio obtained from the deconvolution of the ^{27}Al MAS-NMR spectra was found to be higher than the theoretical ratio. The cause of this was assumed to be the presence of L-(+)-tartaric acid which may have involved in the conversion of aluminium. To determine whether that is the case, it may be useful to make cements without L-(+)-tartaric acid and perform aging study on the ^{27}Al MAS-NMR spectroscopy.

5. The setting reaction of the hybrid cements of poly (γ-glutamic acid) with the co-polymer of poly (acrylic acid) and poly (but-3-ene 1,2,4-tricarboxylic acid) may give a new insight to why the water stable cements with only poly (γ-glutamic acid) were not possible to form. The setting reaction can be compared with the cements formed with pure co-polymer of poly (acrylic acid) and poly (but-3-ene 1,2,4-tricarboxylic acid). In this study, the setting reaction of the PAA cements was followed only by the ^{19}F, ^{31}P, and ^{27}Al MAS-NMR spectroscopy. It may also be interesting to perform the ^{13}C MAS-NMR spectroscopy for PgGA cements.

References

1. Wilson, A. D. and McLean, J. W., *Glass-Ionomer Cement*, Quintessence Publishing Co, 1988.

2. Craig, R. G., O'Brien, W. J., and Powers, J. M., *Dental Materials: Properties and Manipulation*, Mosby-Year Book, 1979.

3. Body, M., Silly, G., Legein, C., and Buzare, J., Cluster models and *ab initio* calculations of F-19 NMR isotropic chemical shifts for inorganic fluorides, Journal of Physical Chemistry B 2005, 109, 10270-10278.

4. Guida, A., Preliminary work on the antibacterial effect of strontium in glass ionomer cements, Journal of Materials Science Letters 2002, 22, 1401-1403.

5. Griffin, S. G. and Hill, R. G., Influence of glass composition on the properties of glass polyalkenoate cements. Part I: Influence of aluminium to silicon ratio, Biomaterials 1999, 20, 1579-1586.

6. De Barra, E. and Hill, R. G., Influence of glass composition on the properties of glass polyalkenoate cements. Part III: Influence of fluorite content, Biomaterials 2000, 21, 563-569.

7. Griffin, S. G. and Hill, R. G., Influence of glass composition on the properties of glass polyalkenoate cements. Part II: Influence of phosphate content, Biomaterials 2000, 21, 399-403.

8. Dollase, W. A., Merwin, L. H., and Sebald, A., Structure of $Na_{3-3x}Al_xPO_4$, X = 0 to 0.5, Journal of Solid State Chemistry 1989, 83, 140-149.

9. Wilson, A. D., The chemistry of dental cements, Chemical Society Reviews 1978, 7, 265-296.

10. Loewenstein, W., The distribution of aluminum in the tetrahedra of silicates and aluminates, American Mineralogist 1954, 39, 92-96.

11. Fayon, F., Massiot, D., Suzuya, K., and Price, D. L., P-31 NMR study of magnesium phosphate glasses, Journal of Non-Crystalline Solids 2001, 283, 88-94.

12. Gervais, F., Blin, A., Massiot, D., Coutures, J. P., Chopinet, M. H., and Naudin, F., Infrared reflectivity spectroscopy of silicate glasses, Journal of Non-Crystalline Solids 1987, 89, 384-401.

13. Merzbacher, C. I. and White, W. B., The structure of alkaline earth aluminosilicate glasses as determined by vibrational spectroscopy, Journal of Non-Crystalline Solids 1991, 130, 18-34.

14. Shih, I. L. and Van, Y. T., The production of poly (γ-glutamic acid) from microorganisms and its various applications, Bioresource Technology 2001, 79, 207-225.

15. Ledezma-Perez, A. S., Romero-Garcia, J., Vargas-Gutierrez, G., and Arias-Marin, E., Cement formation by microbial poly (γ-glutamic acid) and fluoro aluminosilicate glass, Materials Letters 2005, 59, 3188-3191.

16. Zarzycki, J., *Glasses and the Vitreous State*, Cambridge University Press, 1991.

17. Hore, P. J., *Nuclear Magnetic Resonance*, Oxford University Press Inc., 1995.

18. MacKenzie, K. J. D. and Smith, M. E., *Multinuclear Solid-State NMR of Inorganic Materials*, Pergamon, 2002.

19. Zainuddin, N., "Structural and Setting Reaction Studies of Glass Polyalkenoate Cements by MAS-NMR Spectroscopy", Ph.D.Thesis, Imperial College London, 2009.

20. Hill, R. G., Stamboulis, A., and Law, R. V., Characterisation of fluorine containing glasses by F-19, Al-27, Si-29 and P-31 MAS-NMR spectroscopy, Journal of Dentistry 2006, 34, 525-532.

21. Stamboulis, A., Hill, R. G., and Law, R. V., Characterisation of the structure of calcium alumino-silicate and calcium fluoro-alumino-silicate glasses by magic angle spinning nuclear magnetic resonance (MAS-NMR), Journal of Non-Crystalline Solids 2004, 333, 101-107.

22. Stamboulis, A., Law, R. V., and Hill, R. G., Characterisation of commercial ionomer glasses using magic angle nuclear magnetic resonance (MAS-NMR), Biomaterials 2004, 25, 3907-3913.

23. Stamboulis, A., Hill, R. G., and Law, R. V., Structural characterisation of fluorine containing glasses by F-19, Al-27, Si-29 and P-31 MAS-NMR spectroscopy, Journal of Non-Crystalline Solids 2005, 351, 3289-3295.

24. Hill, R. G., Stamboulis, A., Law, R. V., Clifford, A., Towler, M. R., and Crowley, C., The influence of strontium substitution in fluorapatite glasses and glass-ceramics, Journal of Non-Crystalline Solids 2004, 336, 223-229.

25. Matsuya, S., Stamboulis, A., Hill, R. G., and Law, R. V., Structural characterisation of ionomer glasses by multinuclear solid state MAS-NMR spectroscopy, Journal of Non-Crystalline Solids 2007, 353, 237-243.

26. Zeng, Q and Stebbins, J. F., Fluoride sites in aluminosilicate glasses: High-resolution F-19 NMR results, American Mineralogist 2000, 85, 863-867.

27. Stebbins, J. F., Kroeker, S., Lee, S. K., and Kiczenski, T. J., Quantification of five- and six-coordinated aluminum ions in aluminosilicate and fluoride-containing glasses by high-field, high-resolution Al-27 NMR, Journal of Non-Crystalline Solids 2000, 275, 1-6.

28. Engelhardt, G., Noftz, M, Forkel, K., Wishmann, F. G., Magi, M., Samson, A., and Lippma, E., Structural studies of calcium aluminosilicate glasses by high resolution solid state Si-29 and Al-27 magic angle spinning nuclear magnetic resonance, Physics and Chemistry of Glasses 1985, 26, 157-165.

29. Crisp, S. and Wilson, A. D., Reactions in glass ionomer cements: I. Decomposition of the powder, Journal of Dental Research 1974, 53, 1408-1413.

30. Crisp, S., Pringuer, M. A., Wardleworth, D., and Wilson, A. D., Reactions in glass ionomer cements: II. An infrared spectroscopic study, Journal of Dental Research 1974, 53, 1414-1419.

31. Matsuya, S., Maeda, T., and Ohta, M., IR and NMR analyses of hardening and maturation of glass-ionomer cement, Journal of Dental Research 1996, 75, 1920-1927.

32. Pires, R., Nunes, T. G., Abrahams, I., Hawkes, G., Morais, C. M., and Fernandez, C., Stray-field imaging and multinuclear magnetic resonance spectroscopy studies on the setting of a commercial glass-ionomer cement, Journal of Materials Science: Materials in Medicine 2004, 15, 201-208.

33. Stamboulis, A., Matsuya, S., Hill, R. G., Law, R. V., Udoh, K., Nakagawa, M., and Matsuya, Y., MAS-NMR spectroscopy studies in the setting reaction of glass ionomer cements, Journal of Dentistry 2006, 34, 574-581.

34. De Barra, E. and Hill, R. G., Influence of alkali metal ions on the fracture properties of glass polyalkenoate (ionomer) cements, Biomaterials 1998, 19, 495-502.

35. Zainuddin, N., Karpukhina, N., Hill, R. G., and Law, R. V., A long-term study on the setting reaction of glass ionomer cements by Al-27 MAS-NMR spectroscopy, Dental Materials 2009, 25, 290-295.

36. Clifford, A. and Hill, R., Apatite-mullite glass-ceramics, Journal of Non-Crystalline Solids 1996, 196, 346-351.

37. Griffin, S. G. and Hill, R. G., Influence of glass composition on the properties of glass polyalkenoate cements. Part IV: Influence of fluorine content, Biomaterials 2000, 21, 693-698.

38. Hill, R. and Wood, D., Apatite-mullite glass-ceramics, Journal of Materials Science: Materials in Medicine 1995, 6, 311-318.

39. Hill, R., Trimethylsilylation analysis of the silicate structure of fluoro-alumino-silicate glasses and the structural role of fluorine, Journal of Materials Science 1999, 34, 1767-1774.

40. De Barra, E., Influence of poly (acrylic acid) content on the fracture behaviour of glass polyalkenoate cements, Journal of Materials Science 1998, 33, 5487-5497.

41. Griffin, S. and Hill, R., Influence of poly (acrylic acid) molar mass on the fracture properties of glass polyalkenoate cements, Journal of Materials Science 1998, 33, 5383-5396.

42. Hill, R., The influence of poly(acrylic acid) molecular weight on the fracture toughness of glass-ionomer cements, Journal of Materials Science 1989, 24, 363-371.

43. Wilson, A. D., Hill, R. G., Warrens, C. P., and Lewis, B. G., The influence of polyacid molecular weight on some properties of glass-ionomer cements, Journal of Dental Research 1989, 68, 89-94.

44. Crisp, S., Lewis, B. G., and Wilson, A. D., Characterisation of glass-ionomer cements: I. Long term hardness and compressive strength, Journal of Dentistry 1976, 4, 162-166.

45. Wasson, E. A. and Nicholson, J. W., New aspects of the setting of glass-ionomer cements, Journal of Dental Research 1993, 72, 481-483.

46. Hanby, W. E. and Rydon, H. N., The capsular substance of *Bacillus anthracis*, Biochemical Journal 1946, 40, 297-309.

47. Steinbuchel, A., *Biopolymers. Polyamides and Comprex Proteinaceous Materials I*, Wiley-VCH, 2003.

48. Kubota, H, Matsunobu, T, Uotani, K, Takebe, H, Satoh, A, Tanaka, T, and Taniguchi, M., Production of poly (γ-glutamic acid) by *Bacillus subtilis* F-2-01, Bioscience, Biotechnology and Biochemistry 1993, 57, 1212-1213.

49. Troy, F. A., Chemistry and biosynthesis of the poly(γ-d-glutamyl) capsule in *Bacillus licheniformis*. II. Characterisation and structural properties of the enzymatically synthesised polymer, Journal of Biological Chemistry 1973, 248, 316-324.

50. Cromwick, A. M. and Gross, R. A., Effects of manganese (II) on *Bacillus licheniformis* ATCC 9945A physiology and γ-poly (glutamic acid) formation, International Journal of Biological Macromolecules 1995, 17, 259-267.

51. Atkins, P. W., *Physical Chemistry*, Oxford University Press, 1998.

52. Sidgwick, N. V., *The Chemical Elements and Their Compounds*, Oxford University Press, 1950.

53. Fechtelkord, M., Behrens, H., Holtz, F., Bretherton, J. L., Fyfe, C. A., Groat, L. A., and Raudsepp, M., Influence of F content on the composition of Al-rich synthetic phlogopite: Part II. Probing the structural arrangement of aluminium in tetrahedral and octahedral layers by Al-27 MQMAS and H-1/F-19 - Al-27 HETCOR and REDOR experiments, American Mineralogist 2003, 88, 1046-1054.

54. Hill, R. G., Stamboulis, A., Law, R. V., Hawes, J., and Henry, J., A MAS-NMR study of the crystallisation process of barium fluorphlogopite glass-ceramics, Glass Technology 2004, 45, 121-126.

55. Labouriau, A., A F-19 nuclear magnetic resonance study of natural clays, Clays and Clay Minerals 1995, 43, 697-704.

56. Stebbins, J. F. and Zeng, Q., Cation ordering at fluoride sites in silicate glasses: A high-resolution F-19 NMR study, Journal of Non-Crystalline Solids 2000, 262, 1-5.

57. Bureau, B., Silly, G., Buzare, J. Y., and Emery, J., Superposition model for F-19 isotropic chemical shift in ionic fluorides: From basic metal fluorides to transition metal fluoride glasses, Chemical Physics 1999, 249, 89-104.

58. Karpukhina, N., Law, R. V., and Hill, R. G., *Unpublished results*, 2009.

59. Brow, R. K., Phifer, C. C., Turner, G. L., and Kirkpatrick, R. J., Cation effects on P-31 NMR chemical shifts of metaphosphate glasses, Journal of American Ceramic Society 1991, 74, 1287-1290.

60. Roling, B. and Ingram, M. D., Mixed alkaline-earth effects in ion conducting glasses, Journal of Non-Crystalline Solids 2000, 265, 113-119.

61. Sadiq, M., Bensitel, M., Lamonier, C., and Leglise, J., Influence of the nature of precipitating basic agent on the synthesis of catalytic magnesium phosphate materials, Solid State Sciences 2008, 10, 434-437.

62. Kirkpatrick, R. J. and Brow, R. K., Nuclear magnetic resonance investigation of the structures of phosphate and phosphate-containing glasses: A review, Solid State Nuclear Magnetic Resonance 1995, 5, 9-21.

63. Kelsey, K. E., Allwardt, J. R., and Stebbins, J. F., Ca-Mg mixing in aluminosilicate glasses: An investigation using O-17 MAS and 3QMAS and Al-27 MAS NMR, Journal of Non-Crystalline Solids 2008, 354, 4644-4653.

64. Libourel, G., Geiger, C. A., Merwin, L., and Sebald, A., Si-29 and Al-27 MAS-NMR spectroscopy of glasses in the system $CaSiO_3$-1b$MgSiO_3$-1bAl_2O_3, Chemical Geology 1992, 96, 387-397.

65. Kohn, S. C., Dupree, R., Mortuza, M. G., and Henderson, C. M. B., NMR evidence for 5- and 6-coordinated aluminum fluoride complexes in F-

bearing aluminosilicate glasses, Americane Mineralogist 1991, 76, 309-312.

66. Massiot, D., Fayon, F, Capron, M., King, I., Le Calve, S., Alonso, B., Durand, J., Bujoli, B., Gan, Z., and Hoatson, G., Modelling one- and two-dimensional solid-state NMR spectra, Magnetic Resonance in Chemistry 2002, 40, 70-76.

67. Lee, S. K., Cody, G. D., and Mysen, B. O., Structure and the extent of disorder in quaternary (Ca-Mg and Ca-Na) aluminosilicate glasses and melts, American Mineralogist 2005, 90, 1393-1401.

68. Neuville, D. R., Cormier, L., and Massiot, D., Al coordination and speciation in calcium aluminosilicate glasses: Effects of composition determined by Al-27 MQ-MAS NMR and Raman spectroscopy, Chemical Geology 2006, 229, 173-185.

69. O'Dell, L. A., Savin, S. L. P., Chadwick, A. V., and Smith, M. E., A 27Al MAS NMR study of a sol-gel produced alumina: Identification of the NMR parameters of the [theta]-Al2O3 transition alumina phase, Solid State Nuclear Magnetic Resonance 2007, 31, 169-173.

70. Merzbacher, C. I., Sherriff, B. L., Hartman, J. S., and White, W. B., A high-resolution Si-29 and Al-27 NMR study of alkaline earth aluminosilicate glasses, Journal of Non-Crystalline Solids 1990, 124, 194-206.

71. Boyd, D, Towler, M. R., Watts, S, Hill, R. G., Wren, A. W., and Clarkin, O. M., The role of Sr^{2+} on the structure and reactivity of SrO-CaO-ZnO-SiO_2 ionomer glasses, Journal of Materials Science: Materials in Medicine 2008, 19, 953-957.

72. Boyd, D., Towler, M. R., Law, R. V., and Hill, R. G., An investigation into the structure and reactivity of calcium-zinc-silicate ionomer glasses using MAS-NMR spectroscopy, Journal of materials science.Materials in medicine 2002, 17, 397-402.

73. Bovo, N and Hill, R. G., *Unpublished results*, 2006.

74. Shriver, D. F. and Atkins, P. W., *Inorganic Chemistry*, Oxford University Press, 1999.

75. Lang, D. P., Alam, T. M., and Bencoe, D. N., Solid-state P/Al and P/Na TRAPDOR NMR investigations of the phosphorus environments in sodium aluminophosphate glasses, Chemistry of Materials 2001, 13, 420-428.

76. Matsuya, S., Maeda, T., and Ohta, M., Na-23, Al-27, Si-29 and P-31 MAS NMR spectroscopy of setting reaction of the glass-ionomer cement, Bioceramics 1996, 9, 461-464.

77. Billington, R. W., Williams, J. A., and Pearson, G. J., Ion processes in glass ionomer cements, Journal of Dentistry 2006, 34, 544-555.

78. Hill, R. G. and Wilson, A. D., A rheological study of the role of additives on the setting of glass-ionomer cements, Journal of Dental Research 1988, 67, 1446-1450.

79. Tang, H. M., "Investigating the Role of Al:Si Ratio in Model Anorthite-based Glass Polyalkenoate Cements", Final Year Project, Imperial College London, 2009.

80. International Standards Organisation ISO4049., "Dentistry - Polymer-based filling, restorative and luting materials", 2000.

81. Verbeeck, R. M. H., de Moor, R. J. G., van Even, D. F. J., and Martens, L. C., The short-term fluoride release of a hand-mixed vs. capsulated system of a restorative glass-ionomer cement, Journal of Dental Research 1993, 72, 577-581.

82. International Standards Organisation ISO9917-1., "Dentistry - water-based cements - Part 1: Powder/liquid acid-base cements", 2003.

83. Vermeersch, G., Leloup, G., and Vreven, J., Fluoride release from glass-ionomer cements, compomers, and resin composites, Journal of Oral Rehabilitation 2001, 28, 26-32.

84. Xu, X. and Burgess, J. O., Compressive strength, fluoride release and recharge of fluoride-releasing materials, Biomaterials 2003, 24, 2451-2461.

85. McCabe, J. F. and Walls, A. W. G., *Applied Dental Materials*, Blackwell Publishers, 2008.

86. Akinmade, A. O. and Hill, R. G., Influence of cement layer thickness on the adhesive bond strength of polyalkenoate cements, Biomaterials 1992, 13, 931-936.

87. Nicholson, J. W., Adhesive dental materials: A review, International Journal of Adhesion and Adhesives 1998, 18, 229-236.

88. Akinmade, A. O. and Nicholson, J. W., Effect of adhesive layer thickness on the bond strength of a zinc polycarboxylate dental cement, Biomaterials 1995, 16, 149-154.

Appendices

Appendix Ia: Glass compositions in the Ca-Mg series [4.5SiO_2. 3.0Al_2O_3. 1.5P_2O_5. (3.0-x)CaO. xMgO. (2.0-y)CaF_2. yMgF_2] in mole percentages.

Glass	SiO_2	Al_2O_3	P_2O_5	CaO	MgO	CaF_2	MgF_2
LG26	32.1	21.4	10.7	21.4	---	14.3	---
ICHK02	32.1	21.4	10.7	16.1	5.4	14.3	---
ICHK03	32.1	21.4	10.7	10.7	10.7	14.3	---
ICHK04	32.1	21.4	10.7	21.4	---	---	14.3
ICHK05	32.1	21.4	10.7	---	21.4	14.3	---
ICHK06	32.1	21.4	10.7	10.7	10.7	---	14.3
LG26Mg	32.1	21.4	10.7	---	21.4	---	14.3

Appendix Ib: Glass compositions in the Sr-Mg series [4.5SiO_2. 3.0Al_2O_3. 1.5P_2O_5. (3.0-x)SrO. xMgO. (2.0-y)SrF_2. yMgF_2] in mole percentages.

Glass	SiO_2	Al_2O_3	P_2O_5	SrO	MgO	SrF_2	MgF_2
LG26Sr	32.1	21.4	10.7	21.4	---	14.3	---
ICHK08	32.1	21.4	10.7	16.1	5.4	14.3	---
ICHK09	32.1	21.4	10.7	10.7	10.7	14.3	---
ICHK10	32.1	21.4	10.7	21.4	---	---	14.3
ICHK11	32.1	21.4	10.7	---	21.4	14.3	---
ICHK12	32.1	21.4	10.7	10.7	10.7	---	14.3
LG26Mg	32.1	21.4	10.7	---	21.4	---	14.3

Appendix Ic: Glass compositions in the Ca-Zn series [4.5SiO_2. 3.0Al_2O_3. 1.5P_2O_5. (3.0-x)CaO. xZnO. (2.0-y)CaF_2. yZnF_2] in mole percentages.

Glass	SiO_2	Al_2O_3	P_2O_5	CaO	ZnO	CaF_2	ZnF_2
LG26	32.1	21.4	10.7	21.4	---	14.3	---
ICHK14	32.1	21.4	10.7	10.7	10.7	14.3	---
ICHK15	32.1	21.4	10.7	---	21.4	14.3	---
LG26Zn	32.1	21.4	10.7	---	21.4	---	14.3

Appendix Id: Glass compositions of three fluoro-aluminosilicate glasses obtained from Schott AG (Germany) in mole percentages.

Glass	SiO_2	Al_2O_3	P_2O_5	CaO	Na_2O	SrO	ZnO	F
GM35429	23.7	14.5	2.9	9.5	7.7	---	---	41.7
G018-090	26.4	12.9	1.6	---	2.0	12.1	6.5	38.4
G018-117	29.8	12.2	1.6	---	2.2	12.9	6.2	35.0

Appendix Ie: Glass compositions in the Sr-Zn series [4.5SiO_2. 3.0Al_2O_3. 0.75P_2O_5. (3.0-x)SrO. xZnO. 2.0SrF_2] in mole percentages.

Glass code	SiO_2	Al_2O_3	P_2O_5	SrO	ZnO	SrF_2
LPLG26Sr	34.0	22.6	5.7	22.6	---	15.1
ICHK18	34.0	22.6	5.7	15.1	7.6	15.1
ICHK19	34.0	22.6	5.7	7.6	15.1	15.1

Appendix II: MAS-NMR chemical shifts (ppm) for the glasses studied here.

	^{29}Si	^{27}Al /Al(IV)	^{31}P	^{19}F	
LG26	-88.1	50.6	-7.9	-97.8	-159.0
ICHK02	-89.1	50.2	-8.3	-96.9	-157.8
ICHK03	-89.1	49.6	-8.6	---	-158.1
ICHK04	-90.4	48.4	-8.7	---	-159.3
ICHK05	-87.7	48.6	-10.2	---	-176.2
ICHK06	-92.0	47.1	-10.9	---	-181.8
LG26Mg	-94.8	45.8	-18.7	---	-178.5
LG26Sr	-89.7	51.9	-6.7	-62.0	-155.8
ICHK08	-88.8	50.5	-8.4	---	-158.0
ICHK09	-88.8	50.9	-9.3	---	-158.4
ICHK10	-87.4	50.4	-7.9	---	-158.0
ICHK11	-87.2	48.9	-10.6	---	-175.0
ICHK12	-92.6	47.5	-12.1	---	-177.0
ICHK14	-90.9	49.2	-8.8	---	-151.0
ICHK15	-90.9	48.5	-10.8	---	-153.4
LG26Zn	-95.2	46.5	-14.5	---	---
LPLG26Sr	-87.2	56.1	-5.5		
ICHK18	-87.4	54.8	-5.4	Not performed	
ICHK19	-86.5	54.4	-6.1		

Appendix III: MAS-NMR chemical shifts (ppm), various ratios calculated for the glasses from Schott AG (Germany), and their glass transition temperatures, T_g. The error for the T_g is taken as +/- 10^{o}C.

	GM35429	G018-090	G018-117
^{19}F	-146.8	-143.3	-139.9
	-193.5	-195.2	-194.5
^{27}Al /Al(IV)	48.3	51.2	51.4
^{31}P	-16.8	-6.2	-4.0
^{29}Si	-92.0	-92.3	-93.0
Al:P	5 : 1	8 : 1	8 : 1
Al:(Si+P)	0.99	0.87	0.74
P:(Ca/Sr + Na)	1 : 6	1 : 7	1 : 7.5
Si:Al	1 : 0.61	1 : 0.49	1 : 0.41
T_g /^{o}C	430	486	497

Appendix IV: Particle sizes (μm) of the glasses used for the GPC formation.

Ca-Mg series					
Glass	Test No.	10% distribution	50% distribution	90% distribution	Mean diameter
LG26	1	0.91	4.51	22.72	8.54
	2	0.97	5.16	27.62	10.12
	3	0.91	4.71	24.61	9.21
	Average	0.93	4.79	24.98	9.29
ICHK02	1	1.08	5.51	22.11	5.59
	2	1.01	5.22	20.89	8.46
	3	1.00	5.37	21.95	8.77
	Average	1.03	5.37	21.65	7.61
ICHK03	1	0.91	4.44	18.59	7.49
	2	0.90	4.41	18.58	7.45
	3	0.98	4.60	19.27	7.76
	Average	0.93	4.48	18.81	7.57
ICHK04	1	1.04	4.47	19.86	7.74
	2	1.09	4.93	22.27	8.69
	3	1.07	4.81	21.90	8.52
	Average	1.07	4.74	21.34	8.32
ICHK05	1	1.16	5.57	24.59	9.68
	2	1.19	6.13	31.03	11.89
	3	1.16	5.49	24.43	9.65
	Average	1.17	5.73	26.68	10.41
ICHK06	1	1.10	4.82	19.59	7.93
	2	0.98	4.58	20.03	7.89
	3	1.08	4.77	19.83	7.98
	Average	1.05	4.72	19.82	7.93
LG26Mg	1	1.14	4.92	20.01	8.09
	2	1.15	5.01	19.88	8.14
	3	1.02	4.76	19.96	7.93
	Average	1.10	4.90	19.95	8.05

Sr-Mg series					
Glass	Test No.	10% distribution	50% distribution	90% distribution	Mean diameter
LG26Sr	1	1.01	4.79	24.66	9.93
	2	0.96	4.39	22.57	8.75
	3	0.97	4.51	23.04	8.89
	Average	0.98	4.56	23.42	9.19
ICHK08	1	0.96	5.45	23.89	9.29
	2	0.95	5.31	23.77	9.19
	3	0.97	5.44	23.71	9.24
	Average	0.96	5.40	23.79	9.24
ICHK09	1	0.99	4.24	19.89	7.73
	2	1	4.37	20.69	8.03
	3	1.01	4.86	25.42	10.31
	Average	1.00	4.49	22.00	8.69
ICHK10	1	0.93	4.18	19.89	7.57
	2	0.87	4.14	21.33	7.94
	3	0.86	4.36	22.71	8.59
	Average	0.89	4.23	21.31	8.03
ICHK11	1	1.05	4.22	19.09	7.44
	2	1.05	4.35	21.1	8.07
	3	1.07	4.42	20.53	7.95
	Average	1.06	4.33	20.24	7.82
ICHK12	1	0.96	4.02	19.31	7.36
	2	0.87	3.77	18.8	7.1
	3	0.86	3.73	18.87	7.08
	Average	0.90	3.84	18.99	7.18

Ca-Zn series					
Glass	Test No.	10% distribution	50% distribution	90% distribution	Mean diameter
ICHK14	1	1.03	4.64	23.67	8.96
	2	1.10	5.15	28.77	11.17
	3	1.08	4.97	26.9	10.18
	Average	1.07	4.92	26.45	10.10
ICHK15	1	1.01	4.82	26.68	9.71
	2	1.10	4.90	26.50	9.70
	3	0.98	4.68	26.00	9.50
	Average	1.03	4.80	26.39	9.64
LG26Zn	1	1.06	5.23	21.75	8.88
	2	1.00	5.20	22.84	7.55
	3	1.10	5.60	22.00	9.00
	Average	1.05	5.34	22.20	8.48

Sr-Zn series					
Glass	Test No.	10% distribution	50% distribution	90% distribution	Mean diameter
LPLG26Sr	1	0.97	3.77	19.33	7.24
	2	0.97	3.92	21.62	7.96
	3	0.97	3.88	21.58	8.13
	Average	0.97	3.86	20.84	7.78
ICHK18	1	0.82	3.81	20.16	7.49
	2	0.79	3.79	20.2	7.48
	3	0.73	4.03	23.21	8.6
	Average	0.78	3.88	21.19	7.86
ICHK19	1	0.87	3.59	24.37	9.23
	2	0.86	3.37	19.91	7.17
	3	0.77	3.28	22.87	8.35
	Average	0.83	3.41	22.38	8.25

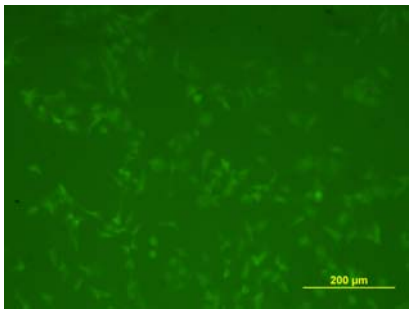
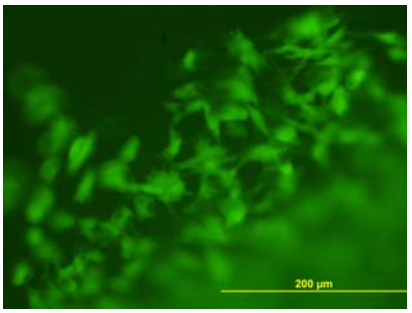
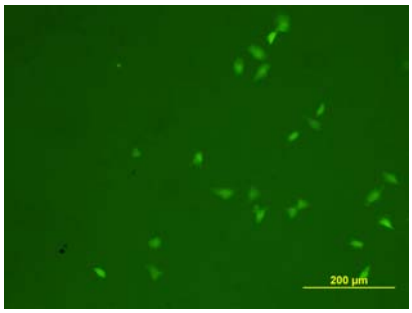
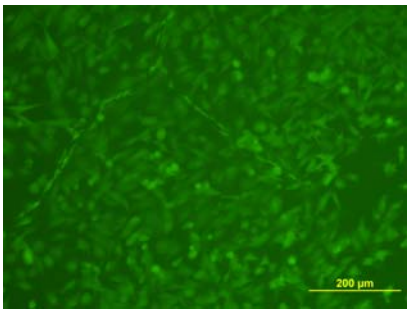
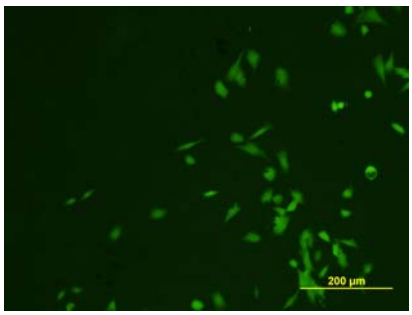
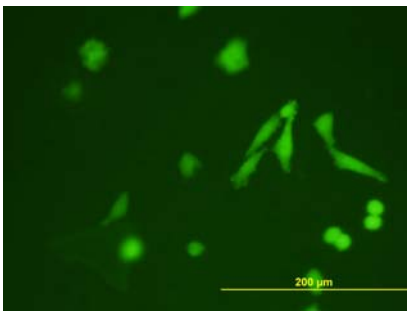
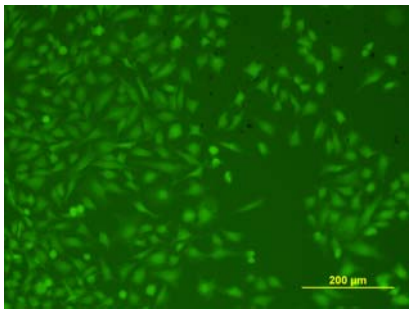
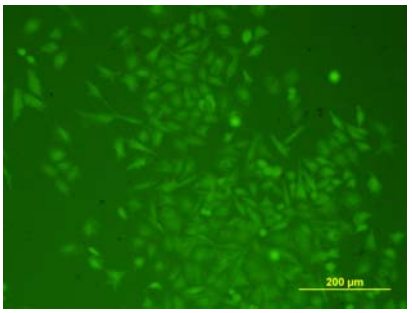
Appendix V: Percentages of Al species and the Al(VI):Al(IV)+Al(V) ratio calculated using the *dmfit* Cz software.

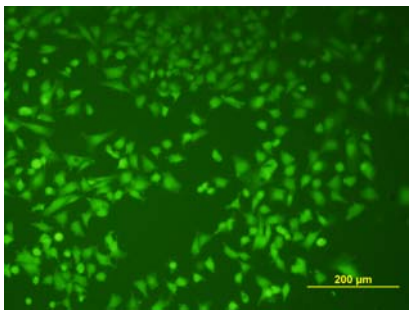
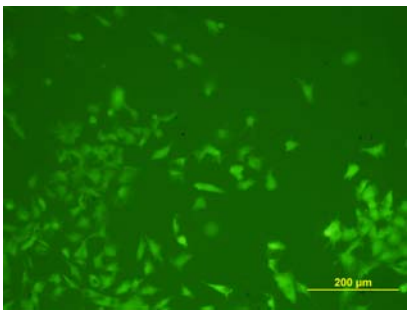
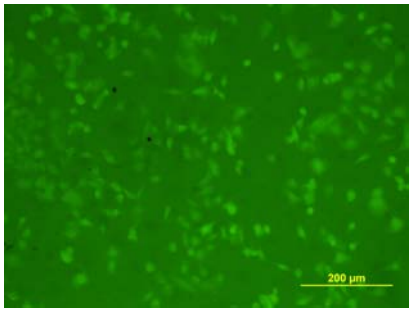
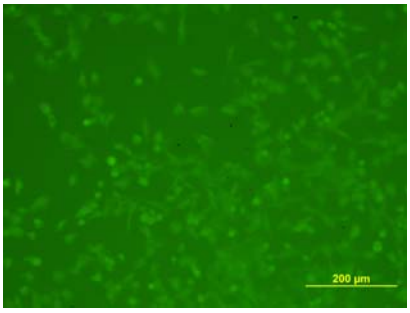
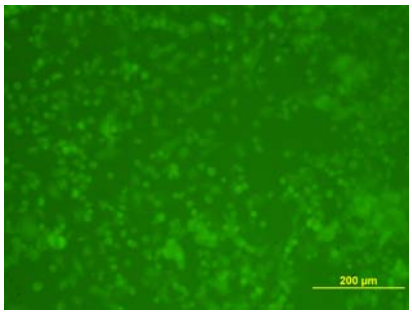
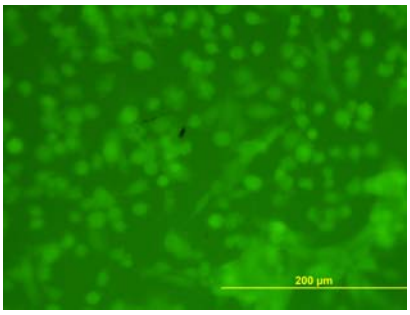
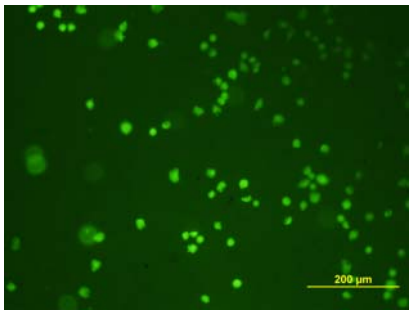
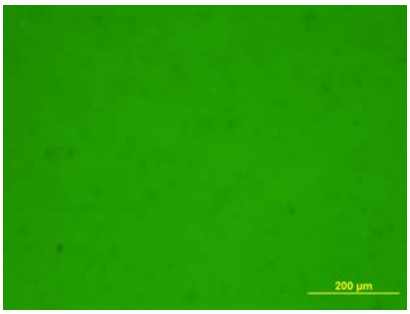
Glass	Aging time	Al sites / %			Al(VI):Al(IV)+Al(V)
		Al (IV)	Al(V)	Al(VI)	
LG26	Glass	72	22	5	0.06
	5 minutes	61	17	22	0.28
	30 minutes	58	17	24	0.32
	1 hour	59	17	24	0.32
	6 hours	57	17	26	0.35
	1 day	57	16	26	0.36
	1 week	57	16	27	0.38
	1 month	56	15	29	0.41
	2 months	56	15	30	0.42
	4 months	47	18	35	0.54
ICHK04	Glass	67	26	7	0.07
	5 minutes	56	19	25	0.33
	30 minutes	59	19	22	0.28
	1 hour	57	18	25	0.33
	6 hours	57	18	25	0.32
	1 day	57	18	25	0.34
	1 week	56	17	27	0.37
	1 month	55	16	29	0.41
	2 months	54	17	28	0.4
	4 months	54	17	29	0.41

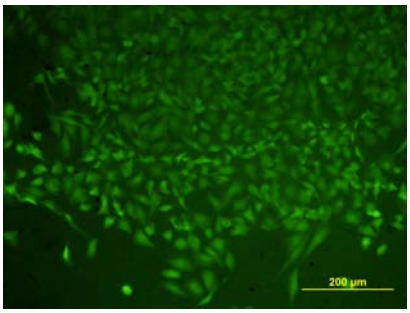
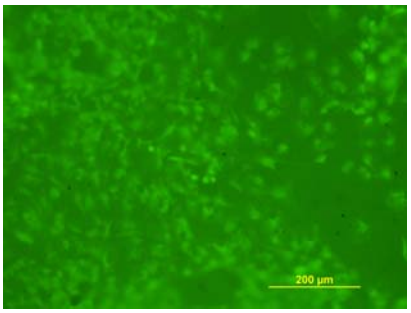
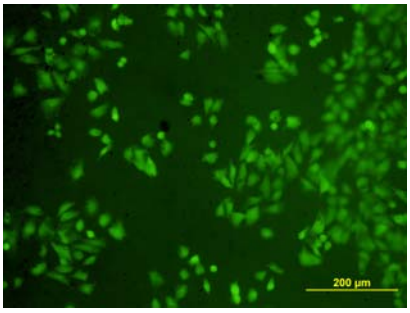
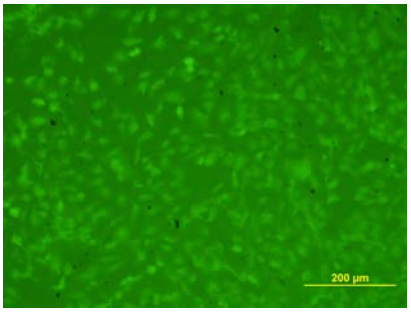
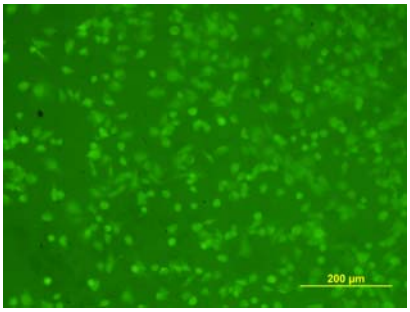
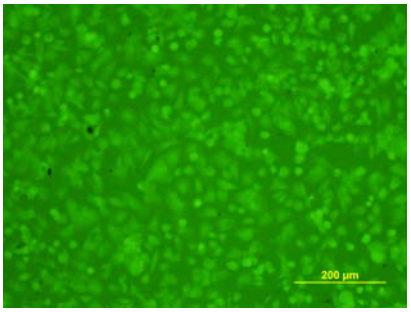
Glass	Aging time	Al sites / %			Al(VI):Al(IV)+Al(V)
		Al (IV)	Al(V)	Al(VI)	
LG26Mg	Glass	65	29	6	0.06
	5 minutes	61	27	11	0.13
	30 minutes	58	26	17	0.20
	1 hour	57	25	18	0.22
	6 hours	53	23	24	0.31
	1 day	51	21	28	0.39
	1 week	49	20	31	0.45
	1 month	47	19	34	0.52
	2 months	47	18	35	0.53
	4 months	46	18	36	0.56

Glass	Aging time	Al sites / %			Al(VI):Al(IV)+Al(V)
		Al (IV)	Al(V)	Al(VI)	
ICHK10	Glass	71	24	6	0.06
	5 minutes	66	23	11	0.13
	30 minutes	62	21	16	0.20
	1 hour	62	21	18	0.21
	6 hours	60	19	21	0.27
	1 day	58	18	23	0.31
	1 week	57	18	25	0.34
	1 month	56	17	27	0.37
	2 months	56	17	27	0.37
	4 months	56	17	27	0.36
LG26Sr	Glass	73	21	7	0.07
	5 minutes	66	21	13	0.15
	30 minutes	64	19	17	0.21
	1 hour	62	18	20	0.25
	6 hours	60	17	23	0.30
	1 day	59	17	24	0.32
	1 week	58	16	26	0.34
	1 month	56	16	17	0.36
	2 months	58	16	27	0.36
	4 months	58	15	27	0.37

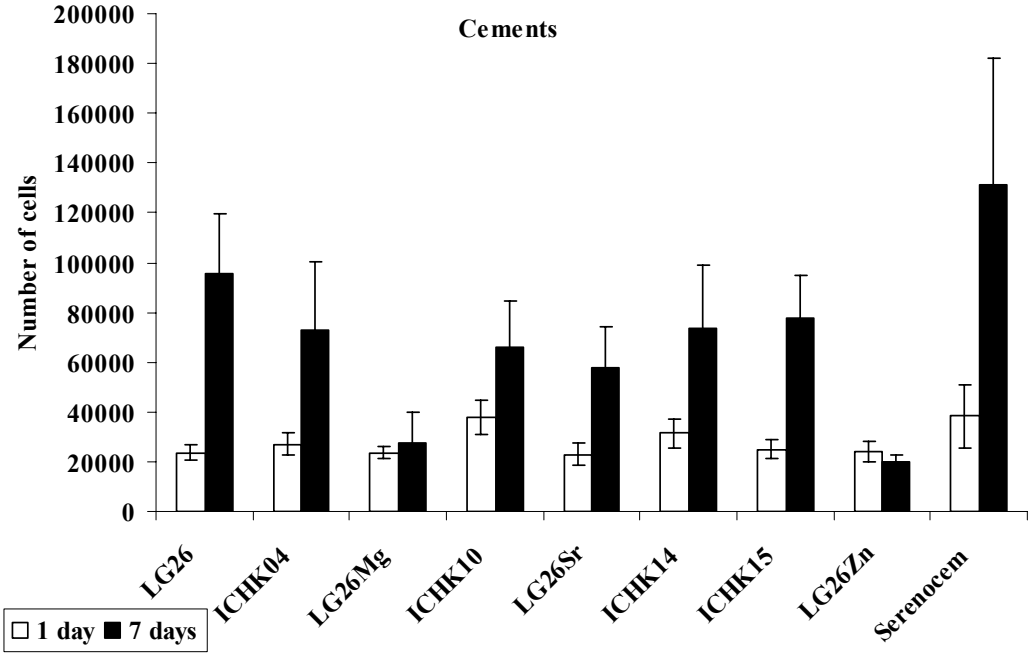
Appendix VI: Live/Dead staining of Saos-2 cells on the selected cements after 1 and 7days.

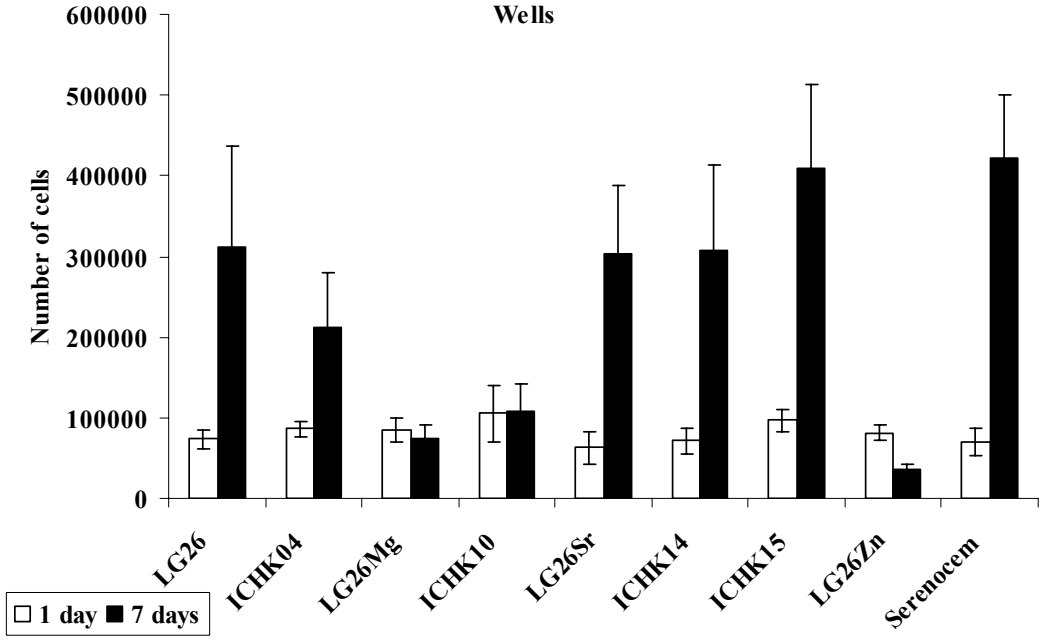
Cements	1 day	7 days
LG26		
ICHK04		
LG26Mg		
ICHK10		

Cements	1 day	7 days
LG26Sr		
ICHK14		
ICHK15		
LG26Zn		

Cements	1 day	7 days
LPLG26Sr		
ICHK18		
ICHK19		

Appendix VII: Total cell quantification by measuring LDH activity of Saos-2 cultured on the selected cements after 1 and 7 days in culture.





Appendix VIII: Alkaline phosphatase activity normalised to cell number in Saos-2 cultured on the selected cements for 1 and 7 days.

